Representation Theory of Dynamical Systems

A Thesis

Submitted to the Faculty

of

Drexel University

by

Daniel J. Cross

in partial fulfillment of the

requirements for the degree

of

Doctor of Philosophy

August 2010

Dedications

I dedicate this work to my late grandfather, Walter Ferraris. Ever since he first let me create great ~~messes~~ structures of pipe and wire in his garage, he fostered in me a great love and wonder for making, for understanding, for science.

Acknowledgments

I must first acknowledge the immense contributions of all those who have worked before me. While a lengthy list of laborers may be found in the bibliography, I would like to especially highlight the contributions of J. S. Birman, R. Gilmore, M. Lefranc, C. Letellier, H. Poincaré, N. Romanazzi, S. Smale, F. Takens, T. D. Tsankov, H. Whitney, and R. F. Williams.

I thank my adviser, Robert Gilmore, for guiding me throughout my many years of study. While he led me on occasion to both oases and deserts, without him I would certainly have gone nowhere at all. The questions he set to me were always worthy of answering; whether or not I found the answer to any particular question, it was always an honor and a joy to search.

There are many others who have helped refine my thinking and my writing in both physics and mathematics. I thank my colleagues Greg Naber, Tim Jones, Nicola Romanazzi, Aruna Nishtala, Ben Coy, and Ryan Michaluk for all their helpful conversations and correspondences.

Each staff member of the department of physics has been a tremendous help in tasks large and small throughout my stay at Drexel. I thank Laura D'Angelo, Lisa Ferrara, Maryann Fitzpatrick, Janice Murray, Wolf Nadler, and Jackie Sampson for all that they have done for me and for every other student.

I thank Jorge Cham, not for making graduate school sane, but for allowing me to accept its insanity through laughter.

I thank my parents, Jim and Lynn Cross, for nurturing me in body, mind, and soul throughout all my life. They have provided me every opportunity to grow and to pursue that which I love.

Finally, I thank my wife, Karin, for her overwhelming love, support, and encouragement that has seen me through all the extrema of my graduate career.

Table of Contents

List of Tables

List of Figures

Abstract

Representation Theory of Dynamical Systems
Daniel J. Cross
Robert Gilmore, Ph.D.

In physics, experiments form the bridge connecting theory to reality. This bridge is often quite narrow: one typically only records one of the myriad variables responsible for generating a complicated dynamical behavior. Nevertheless, every variable can usually be "reconstructed" from that single observation. Such a reconstruction provides an embedding of the original phase space into some Euclidean space. However, this reconstruction or embedding is not unique. Most analyses of experimental data from complex dynamical systems depend on these reconstructions, and they could, in principle, depend on the choice of reconstruction. It is the purpose of this thesis to establish a framework suitable to address this dependence on reconstruction: a representation theory for dynamical systems.

This dynamical representation theory is constructed in analogy with the well known representation theory for groups. We regard reconstructions or embeddings as *representations* of dynamical phase spaces. Different embeddings may or may not be equivalent under smooth deformations. The program of representation theory is to work out all inequivalent representations in Euclidean spaces of various dimension and to identify the topological obstructions preventing equivalence between distinct representations.

Our main result is the complete representation theory for three dimensional dynamical systems. This is possible because the theory of three dimensional systems is rather well understood. In contrast, higher dimensional systems are much less thoroughly understood, so we offer only preliminary results for the representation theory of a certain class of dynamical systems that exist in every dimension. We also present some results for equivariant dynamical systems. While not a part of representation theory proper, these investigations were motivated by a problem that manifests only when viewing reconstructions of the Lorenz system from the perspective of representation theory.

Chapter 1: Introduction and Background

In the physical world, things change with time. Dynamical systems are abstract, mathematical models of such time-dependent realities. More precisely, they are sets of ordinary differential equations $dx^i/dt = f^i(x)$, $i = 1, \ldots, N$. The most fundamental example is Newton's second law. Though these equations are second order, following Hamilton, they can be transformed into first order equations. However, we are not primarily concerned with any particular dynamical system or the physics it describes, but rather with developing a framework capable of handling a wide range of dynamical systems that could ultimately describe a wide range of physics.

There is a definite and useful distinction between those dynamical systems which are linear and those which are non-linear. The mathematics necessary to thoroughly analyze and understand linear systems is classical, and it now comes standard in every physicist's toolbox. In stark contrast, the mathematics necessary to thoroughly analyze and understand non-linear systems is not yet fully developed. We can appreciate this lack of complete understanding if we grasp the sheer magnitude of all possible non-linear behaviors, and how different each is from the other. As Bob Gilmore paraphrases Tolstoy: all linear systems are alike; each non-linear system is non-linear in its own way.

The pioneering days on this non-linear frontier were characterized by the study of individual systems. Much as in biology, one must begin with a catalog of creatures. Eventually, similarities between different systems became apparent, including certain types of universality shared among wide classes of systems. Moving beyond these observations to a theoretical understanding came at a price: great mathematical sophistication.

Owing to the complexity of the problems we study, complex mathematics is unavoidable. The main purpose of this chapter is to review some of those mathematical structures that have been developed to aid our understanding of non-linear dynamical systems. This review will be rather abstract and quickly paced. Most applications of this mathematical edifice are deferred to later chapters. The reader may prefer to skip directly to Chap. 2 and then refer back here as the need arises.

In Chap. 2 we motivate, introduce, and discuss the central idea of this thesis: a representation theory

for dynamical systems. In Chaps. 3 and 4 we work out this theory for (essentially all) three dimensional dynamical systems. We retreat from generality in Chap. 5 to discuss in detail a question that our theory raises concerning the Lorenz dynamical system. Some of these results depend on the symmetry of the Lorenz system. In Chap. 6 we extend this analysis to all systems with discrete symmetries. We then make some steps into higher dimensions in Chap. 7 by working out the representation theory for a certain class of dynamical systems that exists in every dimensions, generalizing those systems studied in Chap. 3. Finally, we conclude in Chap. 8.

We now lay the foundation upon which this thesis will build. This foundation consists of material drawn from three central areas: differential topology, knot theory, and dynamical systems theory. Differential topology is the general mathematical setting in which all other material is embedded. Knot theory concerns how many different ways a string may be knotted in space and how to distinguish one knotting from another. Some results here are fundamental to the theory of dynamical systems, which is the immediate setting of this thesis. Our review of dynamical systems theory will be focused on building up to the Birman-Williams theorem and the classification of three dimensional dynamical systems. Of course, not everything can be presented in this introduction. In particular, we assume the reader is familiar with basic notions and results from point-set topology.

1.1 Differential Topology

1.1.1 Manifolds

Consider a smooth surface in three dimensional space. On this surface, one may define smooth functions or mappings, introduce a notion of distance (metric), and quantify its shape through curvature. A smooth manifold is a generalization of these smooth surfaces to objects of arbitrary dimension and without reference to an ambient space. Standard references for the material in this chapter are [7, 17, 31, 36, 39].

A smooth surface "looks" locally like a subset of the plane $\mathbb{R}^2$. More specifically, about any point p in the surface, there is an open neighborhood homeomorphic to an open set in $\mathbb{R}^2$. The idea of space looking locally like Euclidean space (that is, having topologically equivalent neighborhoods) is the central notion defining a manifold. A topological space is called *locally Euclidean* if every point has a neighborhood U homeomorphic to an open subset V of $\mathbb{R}^n$ for some n. The homeomorphism $\varphi : U \to V$ is called an n-dimensional

coordinate chart. We can envision the inverse φ^{-1} as covering U with the coordinate system of $\mathbb{R}^n$. A *topological manifold* is a second countable[1] Hausdorff[2] space that is locally Euclidean.

Now that we have an appropriate topological space, the next step is to introduce smoothness so that we can do calculus. Let (U, φ) and (U', φ') be two coordinate charts about p. If we consider the two charts as introducing two separate coordinate systems into the overlap $U \cap U'$, then we have the coordinate change function $\varphi' \circ \varphi^{-1}$. This is a map from one subset of Euclidean space to another, $\varphi(U \cap U') \to \varphi'(U \cap U')$ (see Fig. 1.1). It certainly makes sense to ask whether maps such as this are differentiable in the usual calculus sense. A mapping is C^r, $1 \leq r < \infty$ if all partial derivatives through order r exist and are continuous, and it is C^∞ or smooth if all partials of all orders and type exist. For completeness, a function is C^0 if it is continuous. A C^r *differentiable manifold* is a topological manifold such that all coordinate change functions are C^r, $r \in \{1, 2, \cdots, \infty\}$. A C^0 manifold is a topological manifold. Unless otherwise noted, the term manifold will always mean a smooth (C^∞) manifold.

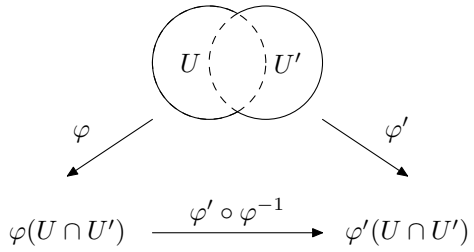

Figure 1.1: Overlap maps for a manifold.

The set of charts covering a manifold is called an *atlas*. The atlas is C^r if all transition maps are C^r. A chart is *admissible* to a C^r-atlas if all coordinate change maps between this new chart and all those in the atlas are C^r. An atlas determines a unique maximal atlas by adding all admissible charts. This maximal atlas is called a C^r *differentiable structure*. A differentiable structure is determined by specifying any admissible atlas.

An atlas is called *oriented* if the Jacobians of all overlap maps have positive determinants. A manifold is *orientable* if it possesses an oriented atlas, and it is *oriented* if an oriented atlas has been chosen. An orientable manifold always possesses two distinct orientations.

[1] *Second countable* means that the topology has a countable basis. This prevents the space from being too big and ensures embeddability in Euclidean space (Whitney's theorem, Thm. 1.2).

[2] *Hausdorff* means that pairs of points may be separated by neighborhoods, a desirable non-local property.

Once manifolds M and N are endowed with differentiable structures, it is possible to do calculus. A real valued function $f : M \to \mathbb{R}$ is defined to be smooth at a point p if for any[3] chart (U, φ) about p, the local expression $f_{\text{loc}} \equiv f \circ \varphi^{-1}$ is smooth (in the calculus sense). We may represent these mappings in the diagram

$$\begin{array}{ccc} U \subseteq M & \xrightarrow{f} & \mathbb{R} \\ {\scriptstyle\varphi}\downarrow & \nearrow_{f_{\text{loc}}} & \\ \mathbb{R}^m & & \end{array} \tag{1.1}$$

More generally a map $f : M \to N$ of manifolds is smooth at p if in charts (U, φ) of p and (V, ψ) of $f(p)$, the local expression $f_{\text{loc}} \equiv \psi \circ f \circ \varphi^{-1}$ is smooth (in the calculus sense), which is expressed by the diagram

$$\begin{array}{ccc} U \subseteq M & \xrightarrow{f} & V \subseteq N \\ {\scriptstyle\varphi}\downarrow & & \downarrow{\scriptstyle\psi} \\ \mathbb{R}^m & \xrightarrow{f_{\text{loc}}} & \mathbb{R}^n \end{array} \tag{1.2}$$

The former case is a special version of the latter by considering $\mathbb{R}$ as a smooth manifold with the standard atlas $(\mathbb{R}, \mathrm{id})$. If $f : M \to N$ is a homeomorphism which is smooth and has a smooth inverse, we say f is a *diffeomorphism* and we write[4] $M \cong N$.

Many spaces of interest carry natural differentiable structures. For example, the single chart atlas $(\mathbb{R}^n, \mathrm{id})$ defines the standard or usual differentiable structure on $\mathbb{R}^n$. It is a classical result that this structure is unique (up to diffeomorphism) when $n \leq 3$. Smale [75] was able to confirm that this structure is unique for every $n \geq 5$. However, the theory developed by Smale fails catastrophically in dimension four: as first shown by Freedman [18], $\mathbb{R}^4$ supports more than one smooth structure. Even worse, we have the following remarkable theorem [80]:

Theorem 1.1 (Taubes). *There exists uncountably infinitely many* $(2^{\aleph_0})$ *distinct differentiable structures on* $\mathbb{R}^4$.

Interestingly, many of these *exotic* $\mathbb{R}^4$s may be embedded in the usual $\mathbb{R}^4$, that is, there are subsets of usual

[3] We note that by the chain rule and the requirement of smooth coordinate changes, these compositions are smooth in one chart if and only if they are smooth in all charts.

[4] There are different standards in use in the literature to denote various equivalences between objects. We will write $X \sim Y$ to denote that X and Y are homologous, $X \simeq Y$ to denote that they are homotopic, and $X \cong Y$ to denote that they are homeomorphic, diffeomorphic, or isomorphic, depending on context. We will also use $\sim$ to denote a generic equivalence relation.

$\mathbb{R}^4$ that are homeomorphic to $\mathbb{R}^4$, but the differentiable structure they inherit is not the usual one [14].

The unit sphere S^n inherits a natural differentiable structure[5] from the usual structure on $\mathbb{R}^{n+1}$. One may ask whether spheres support alternative differentiable structures. In many cases the answer is yes, as Milnor [48] first showed in 1959 for S^7. This was the first example of an exotic smooth structure. We will discuss this point further in Chap. 7.

Let M be a manifold and $\gamma : \mathbb{R} \to M$ a smooth curve with $\gamma(0) = p$. If U is a neighborhood of p and $f : U \to \mathbb{R}$ a smooth function, then the *directional derivative* of f along γ is

$$D_\gamma(f) = \left.\frac{d}{dt}\right|_0 f(\gamma(t)), \tag{1.3}$$

and the operator D_γ is the *tangent vector* to γ at p. In other words, we define tangent vectors to curves on a manifold as first order differential operators on functions. Two tangent vectors D_γ and $D_{\gamma'}$ are equal if they take the same value at p on every function f. The collection of all tangent vectors at p is the *tangent space* to p, denoted T_pM. The collection of all tangent spaces fit together smoothly to yield a manifold of twice the dimension of M called the tangent bundle, TM.

If $x^1, \ldots, x^n$ are local coordinates, then writing $\gamma(t) = (\gamma^1(t), \ldots, \gamma^n(t))$ (where we define $\gamma^i = x^i(\gamma)$ as the local coordinates of γ), we find that

$$D_\gamma(f) = \left.\frac{\partial f}{\partial x^i}\right|_p \left.\frac{d\gamma^i}{dt}\right|_0, \tag{1.4}$$

so that we can identify $D_\gamma = a^i\partial_i$. Here, $a^i = d\gamma^i/dt$ are the components of the vector in the (coordinate) basis spanned by the partial derivatives $\partial_i|_p$ at p. Under a coordinate change $x \to x'$ these quantities transform as

$$a'^i = \left.\frac{\partial f}{\partial x'^i}\right|_p = a^j \frac{\partial x^j}{\partial x'^i}, \tag{1.5}$$

by the chain rule. This is the defining transformation of a (contravariant) vector. Local coordinates for the tangent bundle are then given by (x^i, a^j).

For any smooth map $f : M \to N$ of manifolds there is an induced map of tangent spaces $f_* = df$:

[5] This smooth structure is the same as the smooth structure defined by stereographic projection charts.

$T_pM \to T_pN$, defined by $(f_*v)(g) = v(g \circ f)$ for any function g. In local coordinates, f_* is just the Jacobian matrix. There is therefore an induced map of tangent bundles $TM \to TN$ given by the pair (f, f_*) at each point. For a mapping f of manifolds, if f_* is injective we say that f is an *immersion*, and if f_* is surjective we say that f is a *submersion*. Note that in these definitions it is f_* and not f that is injective or surjective. In some contexts a *submanifold* is defined as the image of an injective immersion (that is, when both f and f_* are injective). However, the topology of the image as a subset need not be the same as the original topology, i.e. f may fail to be a homeomorphism (topological embedding). In such cases, a submanifold need not be a manifold at all (see Fig 1.2). When f is additionally a homeomorphism, the image is called an *embedded submanifold*, which is in fact a manifold. For us, submanifold will always mean an embedded submanifold.

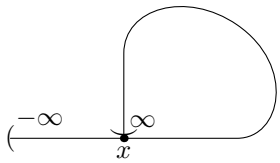

Figure 1.2: Injective immersion of $\mathbb{R}$ into $\mathbb{R}^2$, which is not an embedding. This mapping does not preserve the topology of $\mathbb{R}$ since points near ∞ accumulate at x.

This brings us the notion of an embedding. An *embedding* of a manifold M into another manifold N is a diffeomorphism $f : M \to f(M) \subseteq N$. Equivalently, it is a smooth homeomorphism of M onto a submanifold of N. Embeddings are always one-to-one: they possess no self intersections. Our definition of manifold is an intrinsic one that makes no reference to an ambient space, whereas our initial motivation was considering surfaces in space. We recover the idea of surfaces in space by considering embeddings. An important question is whether our notion of manifold is more general than that of submanifolds of Euclidean space. Put another way, is every manifold embeddable into some $\mathbb{R}^N$. Using genericity arguments, Whitney [87] showed that the notion of manifold is no more general than that of submanifold:

Theorem 1.2 (Whitney Embedding). *Every m-dimensional manifold M embeds in $\mathbb{R}^{2m+1}$.*

This result says that, generically, a collection of $2m + 1$ functions on any m-manifold may be used as coordinates defining an embedding into Euclidean space. The essential idea is that given an arbitrary mapping of M into $\mathbb{R}^{2m+1}$, any self intersections may be pulled apart by small perturbations (the self-intersections are necessarily non-transverse. See Pg. 11). Thus, if a given set of functions does not provide an embedding, then

another arbitrarily close set does. Whitney improved this result to $2m$ (though genericity is lost) and showed that this is the optimal linear bound on the minimum dimension of the embedding space[6].

Consider a smooth surjection of manifolds $\pi : E \to M$. We say that E has the structure of a *fiber bundle* over M with fiber F if it satisfies the following triviality condition: E is locally a product of F over M. More specifically, if $p \in M$ then there is some neighborhood U of p in M for which we have the diagram

$$\begin{array}{ccc} \pi^{-1}(U) & \xrightarrow{\varphi} & U \times F \\ \downarrow{\scriptstyle \pi} & \swarrow{\scriptstyle \pi_1} & \\ U, & & \end{array} \tag{1.6}$$

where π_1 is projection onto the first factor and φ is a diffeomorphism. A pictorial representation of this diagram is given in Fig. 1.3. This bundle is sometimes written $F \hookrightarrow E \xrightarrow{\pi} M$ to emphasize the fiber. The global structure of the bundle is implicit in π. If the fiber $F \cong \mathbb{R}^n$ is a vector space and in the local trivialization the association $v \mapsto \varphi^{-1}(x, v)$ is a vector space isomorphism, then $\pi : E \to M$ is a *vector bundle*.

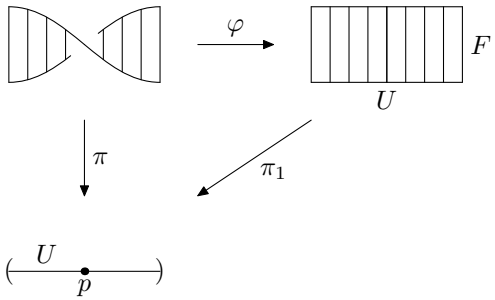

Figure 1.3: Local product structure of a fiber bundle.

For example, the cylinder and the Möbius strip are both line ($\mathbb{R}$) bundles over S^1. The cylinder is just the product $\mathbb{R} \times S^1$, and thus a trivial bundle. The Möbius strip cannot be a product since it is not orientable. Up to diffeomorphism, these are the only two line bundles over S^1.

An important class of vector bundles is provided by the tangent bundle to any manifold. A manifold is called *parallelizable* if the tangent bundle is trivial, $TM \cong M \times \mathbb{R}^n$. The only parallelizable spheres are those supporting a division algebra structure: S^1, S^3, and S^7, which are the unit complex numbers, quaternions,

[6]This bound is saturated for each m a power of two by the real projective spaces $\mathbb{R}P^m$: these spaces do not embed in $(2n-1)$-space.

and octonians respectively. When a metric g is present on a vector bundle we may consider two new bundles. The first is the *unit tangent bundle*, the sub-bundle consisting of all vectors v with $g(v,v) = 1$, and the second is the *unit disk bundle*, the sub-bundle consisting of all vectors v with $g(v,v) \leq 1$.

For any bundle $\pi : E \to M$, a *(global) section* σ is a smooth mapping $\sigma : M \to E$ such that $\pi \circ \sigma = \mathrm{id}_M$. In other words, for each $x \in M$, σ picks out a unique member $\sigma(x)$ out of the fiber over x, $F|_x \cong \pi^{-1}(x)$, and this selection varies smoothly with x. A section of the tangent bundle $v : M \to TM$ is the smooth selection of a tangent vector at each point of M, or a smooth (tangent) vector field. A vector bundle always possesses a section (take $v(x) = 0$), but a general bundle need not.

The fundamental characteristic of a manifold was that every point have a Euclidean neighborhood. This means that while the sphere S^2 is a manifold, the three-ball D^3 is not, since in the latter case the points of the boundary $\partial D^3 = S^2$ do not have Euclidean neighborhoods in D^3. This leads us the more general notion of a *manifold with boundary*, which is the same as a manifold, but now every point has a neighborhood homeomorphic with an open set of the half-space $\mathbb{R}^n_+ = \{(x^1, \ldots, x^n) \in \mathbb{R}^n \mid x^n \geq 0\}$. The set of points of M that do not possess Euclidean neighborhoods are the boundary points, denoted ∂M. The boundary is itself a manifold (without boundary) of codimension one in M (all points in the boundary have neighborhoods in the boundary homeomorphic to subsets of $\mathbb{R}^{n-1}$). We will use the term manifold to refer to a manifold with or without boundary. If we wish to emphasize that $\partial M = \emptyset$, we will say that M is boundaryless or *closed*[7].

If M and N are closed manifolds, then the product space $M \times N$ inherits a natural smooth structure from M and N. The product manifold is also closed. If M has boundary and N is closed, then $M \times N$ is a manifold with boundary $\partial(M \times N) = \partial M \times N$. If both M and N have boundary, then $M \times N$ cannot be given the structure of a smooth manifold. It is a more general *manifold with corners* (see Fig. 1.4).

Manifolds of dimension at most two have been classified. Since the disjoint union of manifolds forms a new manifold in a trivial way, we assume in the following that all manifolds are connected. A zero dimensional manifold is simply a one point space. For one dimensional manifolds we have the following [31]:

Theorem 1.3 (Classification of one-manifolds). *Every one dimensional manifold is diffeomorphic to one of the following: the real line* $\mathbb{R}$*, the half line* $[0, \infty)$*, the interval* $[0, 1]$*, or the circle* S^1*.*

[7] Note that some authors define a closed manifold as being both boundaryless and compact.

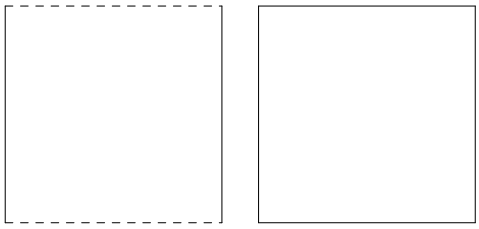

(a) $[0,1] \times (0,1)$ **(b)** $[0,1] \times [0,1]$

Figure 1.4: The product $[0,1] \times (0,1)$ is a manifold with boundary $\{0,1\} \times (0,1)$, while the product $[0,1] \times [0,1]$ is a manifold with corners.

The second and third have non-empty boundary and the last two are compact. There is only one closed compact one-manifold: S^1. Every one-manifold is orientable. If in the two dimensional case we restrict our attention to connected compact orientable closed two-manifolds, i.e. closed surfaces, then have the following [31, 39]:

Theorem 1.4 (Classification of Surfaces). *Every connected compact orientable closed two-manifold is diffeomorphic to a genus-g surface: the 2-sphere, the torus, and more generally a torus with g holes, $g \in \mathbb{N}$ (see Fig. 1.5).*

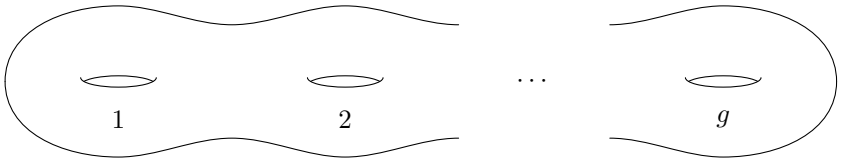

Figure 1.5: Genus g surface.

In a sense, a torus with g holes is composed of g tori that are smoothly patched together. This procedure is described by the process of *connected sum*, or the joining of two manifolds by a tube. Naïvely, one would cut out the interiors of a disk from each surface, then glue the ends (boundaries) of a tube $S^1 \times [0,1]$ to the boundaries left in the surfaces from where the disks were removed. Alternatively, the tube may be dispensed with and the two boundaries of the manifolds identified directly (Fig. 1.6). This procedure yields a topological manifold, but not a smooth manifold. While we could turn this topological manifold into a smooth one by some smoothing procedure, it is advantageous to define a smooth gluing procedure directly.

The idea is to throw away a distinguished point (rather than a disk) of each manifold and then smoothly

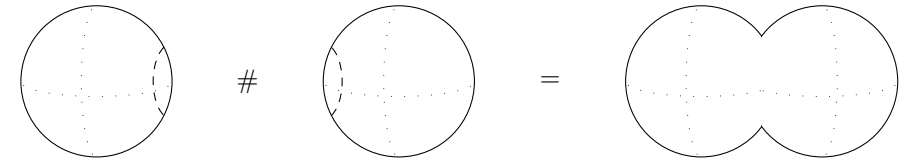

(a) Topological construction.

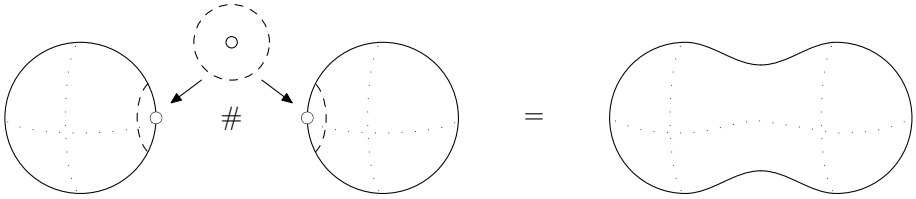

(b) Smooth construction.

Figure 1.6: Connected sum of manifolds.

identify Euclidean neighborhoods of those points with each other (Fig. 1.6). It is this smooth identification of neighborhoods which immediately yields a smooth construction. Moreover, this procedure agrees with the topological one described above; that is, it yields a homeomorphic topological manifold. Let $\alpha : (0, \infty) \to (0, \infty)$ be an arbitrary orientation *reversing* diffeomorphism and define $\alpha_n : \mathbb{R}^n - \{0\} \to \mathbb{R}^n - \{0\}$ by

$$\alpha_n(v) = \alpha(||v||)\frac{v}{||v||}, \tag{1.7}$$

where $|| \cdot ||$ is the Euclidean norm. Let $h_i : \mathbb{R}^n \to M_i$, $i = 1, 2$ be two arbitrary embeddings of $\mathbb{R}^n$. If M is oriented, let h_1 preserve orientation and h_2 reverse orientation. The connected sum $M_1 \# M_2$ of two n-manifolds M_1 and M_2 is the space obtained by removing $h_i(0)$ from M_i and then identifying $h_1(v)$ in $M_1 - h_1(0)$ with $h_2(\alpha_n(v))$ in $M_2 - h_2(0)$. The connected sum of two manifolds is always itself a smooth manifold. For connected manifolds, the connected sum is independent of the choices of h_1, h_2, and α [39].

For manifolds with boundary there is an analogous construction called *boundary connected sum*. It is essentially the connected sum of the boundary manifolds, appropriately extended into the interiors. Specifically, let $h_i : \mathbb{R}^{n-1} \to \partial M_i$ be embeddings (h_1 orientation reversing and h_2 preserving) and $\bar{h}_i : \mathbb{R}^n_+ \to M$ arbitrary embeddings extending the h_i. The boundary connected sum $M_1 \#_\partial M_2$ is obtained from $M_1 - h_1(0)$ and $M_2 - h_2(0)$ by identifying $\bar{h}_1(v)$ with $\bar{h}_2(\alpha_n(v))$. As before, the result is a manifold (with boundary) independent of α, h_i, or the extensions $\bar{h}_i$ (assuming connected boundaries).

The connected sum may be thought of as a binary algebraic operation on the set of connected closed n-manifolds. Thought of in this way, we obtain a commutative monoid[8] with the n-sphere (with usual differentiable structure) as the identity element:

1. $M_1 \# M_2 = M_2 \# M_1$,
2. $(M_1 \# M_2) \# M_3 = M_1 \# (M_2 \# M_3)$,
3. $M \# S^n = M$.

We may now describe or rather construct a genus g surface as the connected sum of g tori, $T^2 \underbrace{\# \cdots \#}_{g} T^2$. If we remove the restriction of orientability, we may rephrase and extend Thm. 1.4 as follows [39]:

Theorem 1.5 (Classification of compact two-manifolds). *The monoid of compact connected closed two-manifolds is generated by the torus T^2 and the projective plane $\mathbb{R}P^2$ and has a single relation: $\mathbb{R}P^2 \# \mathbb{R}P^2 \# \mathbb{R}P^2 = T^2 \# \mathbb{R}P^2$.*

This classification is essentially topological: it only depends on the structure of these spaces as topological manifolds. Since every topological manifold of dimension at most three admits a unique smooth structure, this classification passes to the smooth case as well. We note that the Klein bottle is constructed as the sum $\mathbb{R}P^2 \# \mathbb{R}P^2$. Hence, attaching either a torus or a Klein bottle to $\mathbb{R}P^2$ results in the same manifold.

The final concept we introduce in this section is *transversality*. This captures the intuitive notion of two submanifolds intersecting in a stable fashion: no (sufficiently small) perturbation of either submanifold can remove the intersection. Let $f_1 : M_1^{m_1} \to N^n$ and $f_2 : M_2^{m_2} \to N^n$ be embeddings of M_1 and M_2 into N. Suppose that the submanifolds intersect at $p = f_1(x_1) = f_2(x_2)$. Then M_1 and M_2 intersect *transversely* at p, $M_1 \pitchfork_p M_2$ if $df_1(T_{x_1}) \oplus df_2(T_{x_2}) = T_p N$. In other words, the images of the tangent spaces span the tangent space of the image point. If the submanifolds intersect transversely at every point of intersection (or if they never intersect), we write $M_1 \pitchfork M_2$. Some examples of transverse and non-transverse intersections are given in Fig. 1.7.

Non-transverse intersections are unstable against perturbations. In particular, an arbitrarily small perturbation can change a non-transverse intersection into a transverse intersection. On the other hand, transverse

[8] A *monoid* may be thought of as a group lacking inverses or as a semi-group with identity.

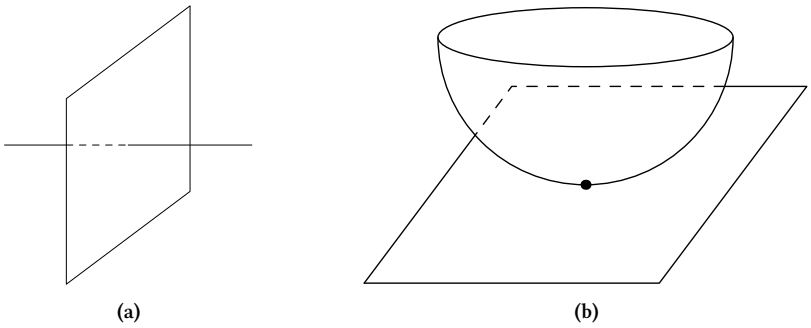

Figure 1.7: Example of a transverse (a) and a non-transverse (b) intersection in $\mathbb{R}^3$.

intersections are stable against arbitrary small perturbations, and the intersection set itself has the structure of a smooth manifold with $\operatorname{codim} M_1 \cap M_2 = \operatorname{codim} M_1 + \operatorname{codim} M_2$. It is immediate that in order for two manifolds to intersect transversely at p, the sum of their dimensions must at least equal the dimension of the ambient space, or else there is no way for their tangent spaces to span the image tangent space: $m_1 + m_2 \geq n$. Of course, this condition is not sufficient.

1.1.2 Algebraic Topology and Homotopy

The ultimate goal of topology is the classification of all spaces up to homeomorphism, though this is quite impossible. Nevertheless, it is useful to have some criteria by which spaces may be distinguished. This means developing certain properties that are invariants of homeomorphism, so that spaces which do not share this property cannot possibly be homeomorphic. The theory of algebraic topology associates groups (or other algebraic structures) to topological spaces as homeomorphism invariants. It follows that spaces may be distinguished if their associated groups are distinct. Moreover, the topology of a manifold can be an obstruction to the existence of certain vector fields, and this topological obstruction is measured by these groups (Thm. 1.6). The particular groups we will discuss here are the fundamental and homology groups.

The association of groups to spaces is a *functor* from the *category* of topological spaces and continuous maps (Top) to the category of groups and homomorphisms (Grp). The functor $F : \mathrm{Top} \to \mathrm{Grp}$ associates to every topological space X a group $F(X)$ and to every continuous map $f : X \to Y$ of topological spaces a group homomorphism $F(f) : F(X) \to F(Y)$ in a way that preserves the structure of the categories: that is, we require that F preserve identities and compositions: $F(\mathrm{id}_X) = \mathrm{id}_{F(X)}$ and $F(f \circ g) = F(f) \circ F(g)$. All

of this may be summarized by demanding that F take commutative diagrams to commutative diagrams:

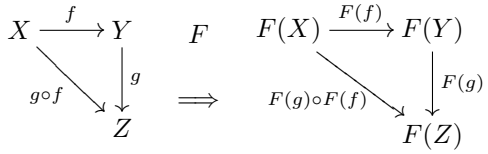

(1.8)

Given two continuous mappings $f_0, f_1 : X \to Y$, we say that f_0 and f_1 are *homotopic*, $f_0 \simeq f_1$, if there exists a continuous mapping $F : X \times [0,1]$ with $F(x,0) = f_0(x)$ and $F(x,1) = f_1(x)$. In other words, f_0 may be deformed into f_1 through continuous mappings. Note that none of these maps is required to be injective. Two spaces X and Y are said to be *homotopy equivalent* or have the same *homotopy type*, $X \simeq Y$, if there are continuous maps $f : X \to Y$ and $g : Y \to X$ such that $g \circ f \simeq \mathrm{id}_X$ and $f \circ g \simeq \mathrm{id}_Y$. The maps g and f are called *homotopy inverses* of each other. Note that these maps are not true inverses: their compositions need only be homotopic to the identity, which is far weaker than being the identity.

Spaces that are homotopy equivalent share certain (though not all) topological properties, such as path or simple connectedness, and have many of the same algebraic invariants[9]. A space is *contractible* if it is homotopy equivalent to a one-point space. Each $\mathbb{R}^n$, and more generally any convex or star-shaped space, is contractible. In particular, all Euclidean spaces are homotopy equivalent to a single point and therefore to each other: $\mathbb{R}^n \simeq \mathbb{R}^m$ for every n, m. On the other hand, no sphere S^n is contractible and $S^n \simeq S^m$ if and only if $n = m$.

A *loop* γ at $p \in X$ is a continuous mapping $\gamma : [0,1] \to X$ with $\gamma(0) = \gamma(1) = p$, or a path beginning and ending at p. We say that p is the *base point* of γ. Two loops are *homotopic*, $\gamma_0 \simeq \gamma_1$ if they are homotopic as maps and if the homotopy preserves base points. In other words, if F is the homotopy, we require that $F(0,t) = F(1,t) = p$ for all $t \in [0,1]$. Homotopy is an equivalence relation on the set of maps or loops preserving base points. Denote by $[\gamma]$ the homotopy class of γ.

A loop is *contractible* or *homotopically trivial*, $\gamma \simeq p$, if it is homotopic to the constant loop $\gamma(t) = p$.

[9] It is not necessary that an algebraic homeomorphism invariant be a homotopy invariant, but since the algebraic constructions considered here use homotopy or weaker notions to define them, they will be homotopy invariants.

Given two loops, γ_1 and γ_2, the product $\gamma_1\gamma_2$ of two loops can be made into a loop by defining

$$\gamma_1\gamma_2(t) = \begin{cases} \gamma_1(2t), & 0 \leq t \leq \frac{1}{2}, \\ \gamma_2(2t-1), & \frac{1}{2} \leq t \leq 1. \end{cases} \tag{1.9}$$

Moreover, if $\gamma_1 \simeq \gamma_1'$ and $\gamma_2 \simeq \gamma_2'$ then $\gamma_1\gamma_2 \simeq \gamma_1'\gamma_2'$. In other words, given $[\gamma_1]$ and $[\gamma_2]$, the product $[\gamma_1][\gamma_2] = [\gamma_1\gamma_2]$ is well-defined, independent of representative. With concatenation as multiplication, the homotopy classes of loops at p becomes a group, where the identity is the class of the constant loop $1 = [p]$. This group is Poincaré's *fundamental* or *first homotopy group*, denoted $\pi_1(X, p)$. If X is path-connected[10], then changing the base point merely changes π_1 by inner-automorphism [7], hence it makes sense to speak of the fundamental group of X forgetting base points, which is denoted by $\pi_1(X)$.

As was mentioned, the fundamental group is a functor from Top to Grp. If $f : X \to Y$ and γ is a loop at p in X, then $f \circ \gamma$ is a loop in Y at $f(p)$. There is an induced map $f_\sharp : \pi_1(X, p) \to \pi_1(Y, f(p))$. If $f, g : X \to Y$ are homotopic, then the induced maps are equal, $f_\sharp = g_\sharp$. Finally, the induced map of a composition is the composition of the induced maps, $(f \circ g)_\sharp = f_\sharp \circ g_\sharp$.

The fundamental group of a space is generally non-abelian, difficult to compute, and difficult to compare with other groups given a presentation. We may obtain a simpler, though less sensitive, invariant by taking its abelianization, $\pi_1/[\pi_1, \pi_1]$. A theorem of Hurewicz states that this group is in fact isomorphic to another group constructed in algebraic topology: the *first homology group*, H_1. Loosely speaking, homology groups identify "holes" in a space. For instance, there is a sense in which each sphere S^n has a central hole, and this is reflected in a non-trivial homology group (the n-th). Homology groups detect such holes, or rather give precise meaning to the intuitive concept of a hole. While there are many different homology theories, they are all constructed in essentially the same way. We will discuss *singular homology* theory below.

Given any topological space X, a *singular simplex* is a continuous (not necessarily injective) mapping $\sigma : \Delta^p \to X$ of the standard p-simplex into X. The standard p-simplex is the convex hull of the unit vectors $\{e_0, \ldots e_p\}$ in $\mathbb{R}^{p+1}$ and is denoted by $[e_o, \ldots e_p]$. The boundary $\partial_p\sigma$ is essentially the restriction of σ to the boundary of Δ^p, but with an alternating sign to account for orientation. Specifically,

[10] A connected manifold is always path-connected, though this is not necessarily true of an arbitrary topological space.

$\partial\sigma([e_o, \dots e_p]) = \sum_i (-1)^i \sigma([e_o, \dots, \hat{e}_i, \dots, e_p])$, where the hat indicates a missing term (see Fig. 1.8). A *singular chain* is a finite formal sum of singular simplexes. Taking all singular simplexes as generators, the set of all singular chains in X, $C_p(X)$, becomes a free abelian group. The boundary map extends to chains and yields a homomorphism $\partial_p : C_p \to C_{p-1}$. One can verify that the composition $\partial_{p-1} \circ \partial_p \equiv 0$, thus (C_p, ∂_p) forms a chain complex called the *singular chain complex*. The *singular homology groups* are given by the "homology" of this complex. Specifically, if we let $Z_p(X) = \ker \partial_p$ denote the kernel of ∂_p (the set of p-cycles or closed p-chains) and $B_p(X) = \operatorname{im} \partial_{p+1}$ denote the image of ∂_{p+1} (the set of p-boundaries), then the n-th singular homology group is the quotient of cycles modulo boundaries,

$$H_p(X) = \frac{\text{cycles}}{\text{boundaries}} = \frac{Z_p(X)}{B_p(X)} = \frac{\ker \partial_p}{\operatorname{im} \partial_{p+1}}. \tag{1.10}$$

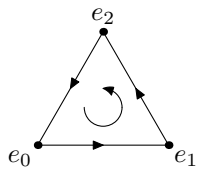

Figure 1.8: Boundary of a simplex. $\partial[e_0, e_1, e_2] = [e_1, e_2] - [e_0, e_2] + [e_0, e_1]$.

Non-triviality of some H_p indicates a cycle which is not a boundary, which captures the idea of a hole: if there were no holes[11], every cycle would be a boundary. We can also say that two p-cycles z_1 and z_2 are *homologous*, $z_1 \sim z_2$, if they differ by a boundary, $z_1 - z_2 = b = \partial c$. We say that z_1 and z_2 have the same homology class, $[\![z_1]\!] = [\![z_2]\!]$, and the homology groups are just these homology classes of p-cycles. For a manifold M of dimension n, the groups $H_p(M)$ for $p > m$ are always trivial. If M is compact, then all of the homology groups are finitely presented. This is why H_p is used as an invariant rather than Z_p and B_p – the latter two are generally far too large to be useful.

Being a quotient of abelian groups, each H_p is abelian. When an abelian group G is finitely generated, the fundamental theorem of abelian groups says that such a group always has the form $G \cong \mathbb{Z}^r \oplus \mathbb{Z}_{q_1} \cdots \oplus \mathbb{Z}_{q_s}$. The integer r is an isomorphism invariant called the *rank* of G, and the finite cyclic part is called the *torsion*. The rank[12] of the n-th homology group is sometimes called the n-th *Betti number*. The *Euler characteristic* is

[11] We are speaking very loosely here. Homology groups can contain elements of finite order (torsion), which represent topological features that cannot be regarded as holes – what kind of hole vanishes if traversed a finite number of times?

[12] If chains are defined using real coefficients rather than integer coefficients, then the groups C, Z, and H become real vector spaces

defined to be the alternating sum of Betti numbers,

$$\chi(X) = \sum_i (-1)^i \operatorname{rank} H_i(X). \tag{1.11}$$

The group H_0 never has torsion, and its rank indicates the number of connected components in the space.

As an example, the torus $T^2 = S^1 \times S^1$ has the homology groups $H_0 \cong \mathbb{Z}$, $H_1 \cong \mathbb{Z}^2$, and $H_2 \cong \mathbb{Z}$, which have ranks 1, 2, and 1 respectively, and $\chi(T^2) = 1 - 2 + 1 = 0$. That $H_0 \cong \mathbb{Z}$ just means that T^2 is connected. Each $\mathbb{Z}$ factor in H_1 is generated by one of the circles defining T^2 as a product (a longitude and a meridian). The generator of H_2 is the torus surface itself[13]. The surface can be written as the sum of singular 2-simplexes, has no boundary, and does not bound any singular 3-chain inside of T^2 (the boundary of any $n+1$-chain in an n-manifold is zero).

If X is triangulated[14], this quantity may be calculated as the alternating sum of the number of simplexes used in its construction in various dimensions. This comes from developing a simplicial homology theory, analogous to the singular theory discussed above, and showing that for triangulated spaces (simplicial complexes), the resulting homology groups are isomorphic. If X is a polyhedron, this yields the famous formula $\chi(X) = V - E + F$, where V, E, and F are the number of vertices, edges, and faces in the triangulation, respectively.

One notable use of homology theory is restricting the structure of vector fields on a compact manifold. This restriction is related to the indices of the vector field at its singularities. If a vector field v on an n-manifold M has a singularity at p, we say that the singularity is *isolated* if there exists a neighborhood U of p such that p is the only singularity in U. Let U be a small neighborhood of the isolated singularity p. The *index* of v at p is the degree of a map to S^{n-1},

$$\operatorname{ind} v \equiv \deg \frac{v(x)}{||v(x)||}, \tag{1.12}$$

and rank is replaced by dimension. Moreover, the rank of H_p computed with integer coefficients is equal to the dimension of H_p computed with real coefficients. Torsion information, however, is lost.

[13] The top homology of a compact and closed manifold is $\mathbb{Z}$ iff it is oriented. The generator is the manifold itself, with a choice of orientation.

[14] Loosely, a triangulation of a space X is a decomposition of X in terms of a number of embedded simplexes glued together along faces.

defined on a small $(n-1)$-sphere about p contained in U. The degree of a map measures the number of times (counting orientation) that the map wraps the domain around the range[15]. In this situation, the degree measures the number of times the vector field "goes around" the singularity, counting direction. A degree may be defined at a non-singular point, but it will always have the value zero.

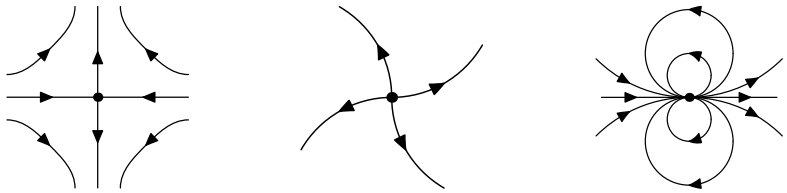

(a) Index -1. **(b)** Index $+1$. **(c)** Index $+2$.

Figure 1.9: Indexes of vector fields. The first two are non-degenerate while the last is degenerate.

A zero of v at p is *non-degenerate* if $dv_p : T_p(M) \to T_p(M)$ is bijective. Non-degenerate zeros are always isolated and they correspond to transverse intersection of v with the zero section of TM. The index of a non-degenerate zero may be calculated as the sign of the determinant of dv_p, or equivalently as $(-1)^q$, where q is the number of unstable directions at p, which is given by the number of eigenvalues of dv_p with negative real part. It follows that a non-degenerate zero can only have index ± 1. A degenerate zero corresponds to a non-transverse intersection of v with the zero section of TM and may thus be split through an arbitrarily small perturbation into a number of non-degenerate zeros, with the sum of the indices of the new zeros equal to the index of the original degenerate zero.

The link between the topology of a manifold and the structure of its vector fields is given by the following:

Theorem 1.6 (Poincaré-Hopf Index Theorem). *Let M be an oriented compact manifold and $v : M \to TM$ a smooth vector field on M with finitely many singularities. If M has boundary we assume the flow is strictly outward on ∂M. Then the global sum of the indices of v is equal to the Euler characteristic of M, $\sum \operatorname{ind} v = \chi(M)$.*

If, on the other hand, the vector field flows inward on ∂M, we have the following [61]:

Theorem 1.7 (Relative Poincaré-Hopf Index Theorem). *Let M be an oriented compact manifold with boundary and $v : M \to TM$ a smooth vector field on M with finitely many singularities, which flows inward on ∂M.*

[15] A map f of oriented, closed, and compact n-manifolds induces a homomorphism on $H_n \cong \mathbb{Z}$. This map must be multiplication by an integer. This integer is the degree of f.

Then the global sum of the indices of v is equal to the Euler characteristic of M relative to its boundary, $\sum \operatorname{ind} v = \chi(M, \partial M) = \chi(M) - \chi(\partial M)$.

In fact, Pugh [61] has proven a generalization of this theorem valid for essentially arbitrary behavior of the vector field on the boundary, including tangencies. He must assume a certain niceness condition on the boundary behavior, but this is satisfied by almost all[16] vector fields. However, we have no need of this generalization here.

The relative Euler characteristic is the alternating sum of the ranks of the relative homology groups $H_p(M, \partial M)$. Consider a pair of spaces (X, A) with $A \subset X$. A relative p-cycle in X is a p-chain whose boundary (if non-empty) lies in A; it is a cycle "mod" A. Similarly, a relative p-boundary is a chain of the form $\partial c + a$, where c is a chain in X and a is a chain in A; it is a boundary "mod" A. Two relative cycles are considered homologous if their difference is a relative p-boundary. The relative homology groups $H_p(X, A)$ are the relative p-cycles modulo relative p-boundaries. The relative homology groups fit into a long exact[17] sequence [7]

$$\cdots \to H_p(A) \to H_p(X) \to H_p(X, A) \to H_{p-1}(A) \to \cdots . \tag{1.13}$$

Since the alternating sum of the ranks of the groups in an exact sequence is zero [33] (assuming there are all finitely presented, as they are for compact manifolds), we see that

$$0 = \sum_i (-1)^i \left(\operatorname{rank} H_i(A) - \operatorname{rank} H_i(X) + \operatorname{rank} H_i(X, A)\right) = \chi(A) - \chi(X) + \chi(X, A), \tag{1.14}$$

which verifies the last line of Thm. 1.7 with $X = M$ and $A = \partial M$.

Clearly a non-vanishing vector field has index zero. The converse of this fact is also true: a non-zero Euler characteristic is the only obstruction for a compact oriented manifold to possess a nowhere vanishing vector field [31].

[16] An open and dense set in the C^r-topology on the space of all vector fields.
[17] A sequence is exact when the image of each map (arrow) is equal to the kernel of the next.

1.2 Knot Theory

Knots arise naturally in the context of dynamical systems as periodic orbits of flows. As Poincaré observed [59], periodic orbits "yield solutions so precious, that is to say, they are the only breach through which we can penetrate into a place, which up to now has been reputed to be inaccessible." As we will investigate further in a later section, periodic orbits are ubiquitous in non-linear systems. Generally, these orbits are unstable so they are not directly seen. A typical trajectory of a system (experimental time series) will not be strictly periodic, but will often come close to exhibiting periodic behavior when the system state comes sufficiently near one of the unseen periodic solutions. In a very real sense, these unstable periodic orbits organize the dynamics of the entire system. The Birman-Williams theorem (Sec. 1.3.2) yields a nice fundamental picture of how these orbits arise, behave, and influence the dynamics. We therefore take this opportunity to understand these orbits (knots) abstractly. Standard references for this section are [13, 64].

By a *knot* K we mean an embedding $K : S^1 \to M$ of the circle into a three-dimensional manifold M. Very often M will be $\mathbb{R}^3$ or a submanifold of $\mathbb{R}^3$. An m-component *link* L is an embedding $L : S^1 \times \cdots \times S^1 \to M$ of m copies of the circle as disjoint subsets of M. A knot is therefore a link with one component. An *oriented* knot or link is defined the same way, but all copies of the circle are endowed with orientations. We are generally interested in oriented knots since the periodic orbits of a flow inherit an orientation from the flow direction.

We want to consider a pair of knots or links as equivalent if they can be smoothly deformed one into the other. In some cases knots and links are defined to be these equivalence classes. This equivalence is formalized by the notion of ambient isotopy. An *ambient isotopy* of a manifold M is a smooth map $H : M \times [0, 1] \to M$, such that $H(x, 0) = x$ and $H_t(x) = H(x, t)$ is a diffeomorphism for each fixed t. In other words, it is a sequence of diffeomorphisms of M to itself, or a smooth deformation of M. Two knots K_1 and K_2 are considered equivalent if there exists an ambient isotopy H_t of M such that $H_1(K_1) = K_2$. If the knots are oriented then they must not only agree as subsets, but they must have equivalent orientations. Two links L_1 and L_2 are equivalent if there is an ambient isotopy H of M such that $H_1(L_1) = L_2$, that is, each component knot of L_1 is taken onto a component knot of L_2. If the link is oriented, the ambient isotopy must respect orientations.

A somewhat weaker relation is that of *isotopy*. Given two embeddings $f, g : X \to M$, a (smooth) isotopy of f to g is a smooth map $h : X \times [0,1] \to M$ such that $h(x,0) = f(x)$, $h(x,1) = g(x)$, and $h_t(x) = h(t,x)$ is an embedding for each fixed t. In other words, it is a smooth deformation of one embedding into another through embeddings. Clearly an ambient isotopy of M taking f to g induces an isotopy of f to g. One simply defines the isotopy h by setting $h(t,x) = H(t, f(x))$. On the other hand, though it seems reasonable, it is not clear whether every isotopy may be extended to an ambient isotopy. As it turns out, not every isotopy can be extended [39]. However, this is always possible when X is compact and M closed [9, 39, 53]:

Theorem 1.8 (Isotopy Extension). *Let $f : X \to M$ be an embedding of compact X into closed M. If $h : X \times [0,1] \to M$ is an isotopy of f, then there exists an ambient isotopy $H : M \times [0,1] \to M$ such that $H(f(x), t) = h(x,t)$ for all $x \in X$ and $t \in [0,1]$.*

Thus, for embeddings of compact manifolds, there is no distinction between isotopy and ambient isotopy, so the two notions may be used interchangeably. In particular, knot equivalence may be established using either type of deformation.

We note that in the topological category, even for compact objects, these notions are distinct. In particular, *any* (continuous) knot in $\mathbb{R}^3$ (a topological embedding of S^1) is continuously isotopic to the trivial knot ($S^1 \subset \mathbb{R}^2 \hookrightarrow \mathbb{R}^3$). The process essentially involves "pulling tightly" on the knot, shrinking the knotted parts until they become infinitesimally small and finally disappear. This is called Bachelor's unknotting (Fig. 1.10) [13]. During this unknotting, the space around the knot is essentially torn, and this isotopy cannot be extended to an ambient one. This unknotting trick fails for smooth embeddings since the change in direction of the tangent vectors of the knot would increase without bound as the knotted portions are shrunk. Though isotopy is a trivial equivalence relation for continuous knots and links, ambient isotopy remains non-trivial, and this is often the equivalence relation used in practice. It turns out that continuous and smooth knot theory are equivalent, that is, the continuous ambient isotopy classes of knots are in bijective correspondence with the smooth ambient isotopy classes of knots [18]. This is, however, a low dimensional coincidence – the continuous and smooth knot theories for embeddings of k-spheres, $k > 1$, into higher dimensional Euclidean spaces are generally distinct. This distinction is relevant to our investigations in Chap. 7.

[18] Actually, for this to be true we must ignore "wild knots". These are topological embeddings of S^1 that do not extend to embeddings of $D^2 \times S^1$ and are not ambient isotopic to any smooth knot. Such knots exhibit pathological properties.

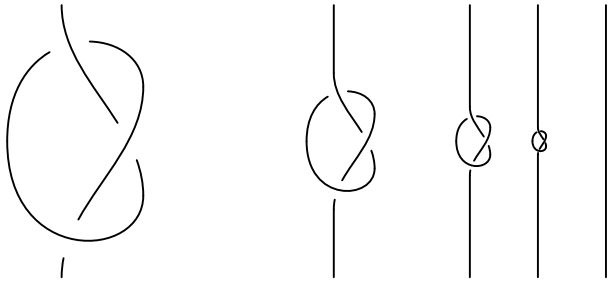

Figure 1.10: Bachelor's unknotting.

There are many useful invariants of knots and links. These are quantities that are invariants of isotopy and computable given a description of a knot or link. Since we regard isotopic knots as equivalent, these quantities help distinguish one equivalence class from another. The knot complement is one such invariant. In fact, for knots, the complement is a complete invariant – two knots are equivalent if and only if they have homeomorphic complements[19]. This is the Gordon-Luecke theorem [27]. This is not, however, a practical scheme for determining knot equivalence in general, since the homeomorphism problem for three manifolds is intrinsically more difficult. The most important open problem in knot theory is to find a complete set of "easily" computable invariants that distinguish any two non-isotopic knots. Most known invariants take the form of numbers, polynomials, or other algebraic quantities [64] that are algorithmically computable given a description of a knot or link.

For links in $\mathbb{R}^3$, a useful and readily computable invariant is the Gauss linking number. There are many different and equivalent means of defining this quantity [64]. The most common is through the linking integral. Let $\gamma_1, \gamma_2 : S^1 \to \mathbb{R}^3$ be a pair of disjoint knots or a two component link. Then the linking number $\mathrm{lk}(\gamma_1, \gamma_2)$ of the pair is given by the integral

$$\mathrm{lk}(\gamma_1, \gamma_2) = \frac{1}{4\pi} \oint_{\gamma_1} \oint_{\gamma_2} \frac{\gamma_2 - \gamma_1}{||\gamma_2 - \gamma_1||^3} \cdot (d\gamma_1 \times d\gamma_2) \tag{1.15}$$

$$= \frac{1}{4\pi} \int \det\left(\gamma_2 - \gamma_1, \frac{\partial \gamma_1}{\partial s}, \frac{\partial \gamma_2}{\partial t}\right) \frac{ds\, dt}{||\gamma_2 - \gamma_1||^3}, \tag{1.16}$$

where the matrix in parenthesis is built by interpreting each entry as a column vector in its components. This

[19] This is not true of links in general. Two inequivalent links may have homeomorphic complements.

expression is equivalent [17] to the degree of a map $S^1 \times S^1 \to S^2$,

$$\mathrm{lk}(\gamma_1, \gamma_2) = \deg \frac{\gamma_2 - \gamma_1}{||\gamma_2 - \gamma_1||}. \tag{1.17}$$

The degree of a map is an invariant of any continuous deformations of γ_1 and γ_2 so long as the map remains well defined, that is, so long as the two curves remain disjoint[20]. Since the linking integral can be expressed as the degree of a map, it is necessarily integer valued. Finally, in practice it is usually simplest to compute the linking number by adding the signed number crossings in a two-dimensional projection rather than using the above formulas. If in a projection the (oriented) segment a crosses above segment b, then the sign of the crossing is positive if the cross product $a \times b$ points toward the observer and negative if it points away (see Fig. 1.11).

Figure 1.11: Positive (a) and negative (b) crossings.

Finally, we note that while a non-trivial linking number $\mathrm{lk}(\gamma_1, \gamma_2) \neq 0$ between two curves indicates that they are non-trivially linked, the converse is not true. A simple example is provided by the Whitehead link, shown in Fig. 1.12. In addition to having zero linking number, both component knots of this link are actually unknots. To show that this link is non actually trivial one must resort to other invariants, such as the Jones polynomial [64].

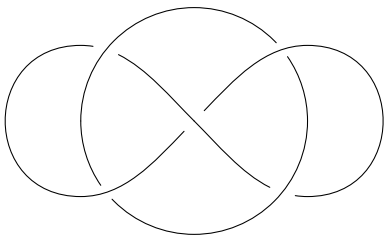

Figure 1.12: The Whitehead link is non-trivial, but it has linking number zero.

[20] The degree of a map is actually a *homotopy* invariant. It's value is invariant under any continuous deformation of the knots γ_1 and γ_2, even if they fail to remain embeddings (they may self-intersect).

1.3 Dynamical Systems

This section provides a selected review of the theory of dynamical systems with the goal of stating the Birman-Williams theorem, Thm. 1.13. Canonical references for this section are [15, 20, 25, 26, 30, 82]. Let M be a smooth manifold. An (autonomous) *dynamical system* on M is a set of time-independent first order ordinary differential equations, or equivalently, a smooth vector field on M. If $v : M \to TM$ is a smooth vector field then we can write

$$\dot{x} = v(x), \tag{1.18}$$

as the dynamical system on M. No generality is lost in considering only the autonomous case, since a non-autonomous dynamical system can always be made autonomous through a standard trick. Specifically, if $\dot{x} = v(x,t)$ is the non-autonomous dynamical system, introduce the new variable $s = t$ and consider the new system $\dot{x} = v(x,s),\ \dot{s} = 1$. This new system is autonomous and equivalent to the original system, though it lives in a manifold of one higher dimension.

The unique solution $\varphi : M \times \mathbb{R} \to M$ of Eq. (1.18) is called the *flow* associated to v. We often write $\varphi_t(x) = \varphi(x,t)$. As a solution of Eq. (1.18), φ satisfies

$$\frac{d}{dt}\varphi_t(x)\Big|_{t=\tau} = v(\varphi_\tau(x)), \tag{1.19}$$

for every time $\tau \in \mathbb{R}$ for which $\varphi_\tau(x)$ is defined. In general the solution Eq. (1.19) need only exist locally and thus may not be defined for all time. If the vector field becomes arbitrarily large, solutions may wander off of M in finite time. This behavior is prevented if M is compact. In this case, a global solution always exists. A manifold M equipped with a dynamical system or flow will be called a *phase space*[21].

For any fixed $x_0 \in M$, $\varphi_t(x_0)$ is a curve in M giving the solution of Eq. (1.18) starting at x_0, called the trajectory of x_0. If $\varphi_t(x_0) = x_0$ for all t, then x_0 is a *fixed point* of the flow. Fixed points correspond to zeros of the vector field, $v(x_0) = 0$. If x_0 is not a fixed point, but there exists some $T > 0$ such that $\varphi_T(x_0) = x_0$, then the solution $\gamma_t = \varphi_t(x_0)$ is a simple closed curve, which we call a *periodic orbit*. If T is the least time

[21] This terminology is consistent with, but distinct from, that used in mechanics, where the fundamental equations are of second order. Solutions are not unique in configuration space, the position manifold, but on the phase space, which is the cotangent bundle. This is where the first order Hamilton equations are defined. If the phase space is defined to be the minimal manifold for unique solutions, then both usages are consistent.

such that $\varphi_T(x_0) = x_0$, that is, $\varphi_t(x_0) \neq x_0$ for any $0 < t < T$, we say that the orbit has (least) period T. A period T orbit masquerades as an orbit of period qT for every $q \in \mathbb{Z}^+$. In certain contexts it is advantageous to consider masquerading orbits among the periodic orbits of a given period. Where it is important, we will be explicit about whether the period of an orbit is to be considered the minimal period.

Let γ be some periodic orbit of the flow with period T. A *local Poincaré section* is a codimension one hypersurface $\Sigma \subset M$ transverse to the flow and intersecting γ (Fig. 1.13). If $p = \gamma \cap \Sigma$, then for points x sufficiently close to p there is a Poincaré or first return map defined by $f(x) = \varphi_\tau(x)$, where τ is the first return time for the trajectory of x to intersect Σ. As $x \to p$, $\tau \to T$, but in general $\tau \neq T$. If Σ may be chosen to intersect all solution curves $\varphi_t(x)$, then Σ is a *global Poincaré section.* We note that Σ need not be connected.

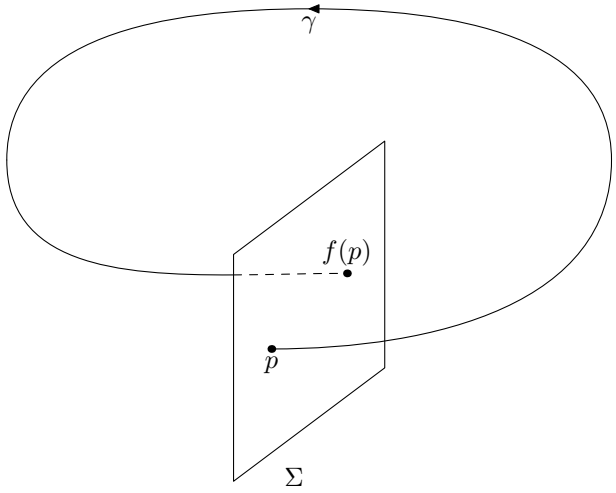

Figure 1.13: Local Poincaré section Σ about orbit γ and first return map f.

Given a diffeomorphism $f : \Sigma \to \Sigma$ of a manifold Σ, one may construct a flow that "suspends" f by taking the trivial flow on the mapping torus of f. The mapping torus Σ_f is the quotient space $\Sigma \times \mathbb{R}/\sim$, where $(f(x), s) \sim (x, s+1)$ (see Fig. 1.14). This may also be thought of as the cylinder $\Sigma \times [0,1]$ with the ends glued together via f (and appropriately smoothed). This space is equipped with the trivial flow $\varphi_t(x, s) = (x, s+t)$. Thus the point $(x, 0)$ flows to $(x, 1)$, but this is identified with $(f(x), 0)$. Thus we see that the flow φ_t creates a smooth analogue of the discrete mapping f. This *suspension flow* has f as a a global Poincaré map on Σ. We note that when f is isotopic to the identity then $\Sigma_f \cong \Sigma \times S^1$, the "torus" of Σ. On the other hand, if f is not isotopic to the identity, then Σ_f need not be a product. For example, the suspension

of the map $f : [0,1] \to [0,1]$, $x \mapsto -x$ yields the Möbius strip, which is distinct from the cylinder $[0,1] \times S^1$. In general, the space Σ_f will be a fiber bundle over S^1 with fiber Σ.

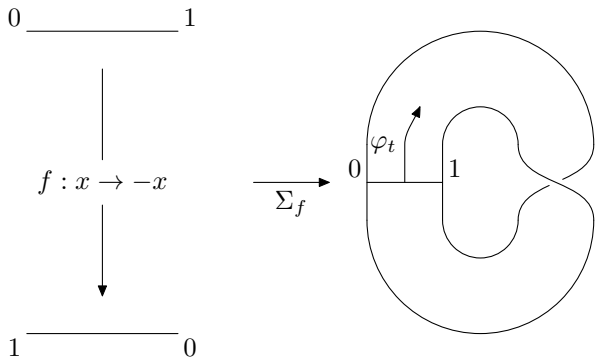

Figure 1.14: Suspension of a diffeomorphism.

The suspension construction is essentially the inverse of the global Poincaré map as the suspended map becomes the Poincaré map of the suspension flow. A great deal of information about a flow is contained in its Poincaré map. For example, periodic orbits of the flow become (discrete) periodic orbits of the map (period one orbits of the flow become fixed points of the map). The stability properties of the continuous orbits are equivalent to the stability properties of the corresponding discrete orbits.

We now define some important sets for flows. There are analogous notions for maps which may be defined with obvious modifications. For any flow φ_t on M, an *invariant set* Λ is any subset that is invariant under the flow, that is, $\varphi_t(x) \in \Lambda$ for all $x \in \Lambda$ and $t \in \mathbb{R}$. The individual points of Λ may move around under the flow, but they are confined to Λ. Fixed points and periodic orbits are obviously invariant sets. More generally, any solution curve $\varphi_t(x_0)$ is invariant.

A point p is an *ω-limit point* if some orbit $\varphi_t(x)$ converges to p, that is, if there exists a sub-sequence $\varphi_{t_1}(x), \varphi_{t_2}(x), \ldots$ such that $\varphi_{t_i}(x) \to p$ as $t_i \to \infty$. The ω-limit set of x, $\omega(x)$ is the set of all ω-limit points of the orbit through x and may be expressed as (see Fig. 1.15)

$$\omega(x) = \bigcap_{\tau \in \mathbb{R}} \overline{\{\varphi_t(x) \mid t > \tau\}}. \tag{1.20}$$

An *α-limit point* is defined similarly, but with $t_i \to -\infty$. They are ω-limit points of the time-reversed flow. A closed invariant set $\Lambda \subset M$ is an *attracting set* if there is a neighborhood U of Λ such that for every $x \in U$,

$\varphi_t(x) \in U$ for every $t \geq 0$ and $\varphi_t(x) \to \Lambda$ as $t \to \infty$. The union of all such U, $\cup_{t \leq 0} \varphi_t(U)$ is the *domain of attraction* of Λ. A repelling set is defined by replacing $t \to -t$.

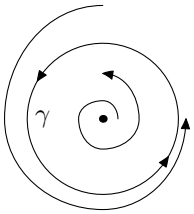

Figure 1.15: The periodic orbit γ is the ω-limit set for the indicated flow in $\mathbb{R}^2$.

The definition of attracting set appears to be too restrictive to always encapsulate the idea of attraction [30]. The reason is that a set does not need to attract every nearby orbit in order to appear as an attractor. It is therefore reasonable to define an *(measure) attractor* Λ_μ as a closed invariant set such that every neighborhood U of Λ_μ contains a subset V of positive (Lebesgue) measure, $\mu(V) > 0$, such that for every $x \in V$, $\omega(x) \in \Lambda_\mu$. In other words, sufficiently close points are attracted to Λ_μ with positive probability. In particular, if $\mu(V) = \mu(U)$, the set of orbits not attracted to Λ_μ will be negligible, and in practice, all observed orbits will converge to Λ_μ.

We note in passing that with this more general definition, complicated situations can emerge: intermingling basins of attraction. Here, points in an open set have positive probability of being attracted to multiple attractors. For example, consider the discrete dynamical system on the cylinder $S^1 \times [0, 1]$ given by the mapping

$$f(\theta, x) = (2\theta, x + \tfrac{1}{2} x(x-1) \cos\theta). \tag{1.21}$$

This system has two attractors: the two boundary circles $S^1 \times \{0, 1\}$, and their basins of attraction are intermingled: every non-empty open set in $S^1 \times [0, 1]$ intersects each basin in a set of positive measure [37]. Hence, one cannot know to which attractor an initial condition will converge, unless that initial condition is known exactly. A graphical approximation of the intermingled basins may found on Scholarpedia [49].

A more complicated invariant set is the *non-wandering set* Λ_{NW}, which is roughly the set of all points that are arbitrary close to being periodic. Specifically, a point p is called *non-wandering* if for any neighborhood U of p there exists a $t > 1$ such that $\varphi_t(U) \cap U \neq \emptyset$. Notice that p itself need not return to U. If p does return to U then p is said to be *recurrent*. The non-wandering set is the collection of all non-wandering points.

Note that wandering (the opposite of non-wandering) is an open condition: if there exists a neighborhood U of p such that $\varphi_t(U) \cap U = \emptyset$, then every point of U is wandering. Hence Λ_{NW} is closed and, since it contains all fixed points and periodic orbits, it must also contain their closure. It also contains all recurrent points and the α- and ω-limit sets of every point in phase space. One deficit of the non-wandering set is that it is not invariant under iteration, meaning that in general $\Lambda_{NW}(\Lambda_{NW}) \neq \Lambda_{NW}$.

One of the most general and useful invariant sets is the chain-recurrent set defined as follows. A point $x \in M$ is called *chain-recurrent* if it is part of a sequence of trajectories that together are arbitrarily close to being periodic. More specifically, x is chain-recurrent if for every distance $\epsilon > 0$ and time $T > 0$ there exists a sequence of points $x = x_0, x_1, \ldots, x_n = x$ and times $t_0, t_1, \ldots, t_{n-1}$, all greater than T, such that $d(\phi_{t_i}(x_i), x_{i+1}) < \epsilon$ for all $0 \leq i \leq n-1$ (see Fig. 1.16). Since for any $\epsilon > 0$ $\varphi_t(x)$ is within ϵ of x for all sufficiently small t, the restriction on T in the definition is to prevent choosing the next point in the sequence from the immediate trajectory (i.e. T can be arbitrary large). The chain-recurrent set, Λ_{CR}, is the set of all chain-recurrent points. This set is closed and invariant under the flow, and thus compact if M is compact.

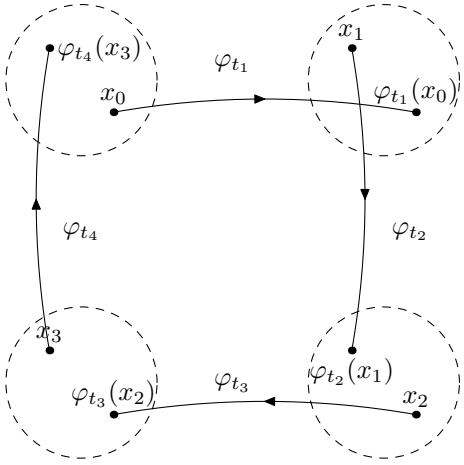

Figure 1.16: Illustration of chain recurrence.

The chain recurrent set includes all recurrent points, since these are just chain-recurrent with a chain of length one. However, the chain-recurrent set also includes the non-wandering set, and therefore all periodic orbits and their closure. Unlike the non-wandering set, the chain-recurrent set is closed under iteration: $\Lambda_{CR}(\Lambda_{CR}) = \Lambda_{CR}$. The importance of the chain-recurrent set will be seen when we discuss the Birman-Williams theorem.

We are often interested in the dynamics on these invariant sets, especially when the dynamics is sufficiently complicated or chaotic. When the invariant set possesses chaotic dynamics, its attractor is called *strange*. While there is no universally accepted definition of chaos, Devaney [15] has suggested the following three essential characteristic to describe chaotic behavior. A map or flow on an invariant set Λ is *chaotic* if it:

- Displays sensitivity to initial conditions;
- Is topologically transitive;
- Has periodic orbits that are dense in Λ.

These characteristics correspond to instability, irreducibility, and regularity, respectively. We say that a flow on a manifold M is chaotic if its restriction to some invariant set Λ is chaotic. Note that the dynamics need not be chaotic on all of M. We now define these conditions.

A flow φ_t on Λ has *sensitive dependence on initial conditions* if there exists a $\delta > 0$ such that for any $x \in \Lambda$ and neighborhood U of x, there is some $y \in U$ and $t > 0$ such that $d(\varphi_t(x), \varphi_t(y)) > \delta$. In other words, given any point there are certain other points that, no matter how close initially, will eventually separate by the finite distance δ. This is the source of future unpredictability, also known as the weather man is always wrong – predictions diverge in finite time unless the current conditions are known *exactly*, which is of course impossible. There are two things to note. The first is that this does *not* require that *all* nearby trajectories diverge in finite time. Second, there is no required lower bound on the rate of separation, though in practice the separation rate is often exponential (as it is for the hyperbolic systems studied later).

Topological transitivity is a generalization of the non-wandering property. A flow φ_t is *topologically transitive* if for every pair of open sets $U, V \subset \Lambda$ there exists a $T > 0$ such that $\varphi_T(U) \cap V \neq \emptyset$. This condition says that the dynamics are irreducible – points from any one arbitrarily small neighborhood map inside any other, so the two cannot be dynamically separated. This condition is equivalent to having Λ possess a dense orbit. If an invariant set is *reducible*, then it may be decomposed into smaller, disjoint pieces.

The periodic orbits have the nicest behavior possible and they are dense in Λ – any point is arbitrarily close to behaving nicely. This also means that the structure of the periodic orbits determines to a great extent the structure of the flow on a neighborhood of the invariant set and perhaps the entire system. These solutions

determine the short term behavior of typical solutions as they come sufficiently close to some periodic solution. This idea forms the basis of the method of close returns for determining periodic orbits in a system.

1.3.1 Symbolic Dynamics

A fortunate and tremendously simplifying property available to many chaotic systems is a description in terms of symbolic dynamics. This is an abstract dynamics defined in terms of sequences of letters in some alphabet. An *alphabet* is just a set (of letters) $\mathcal{A} = \{x_1, \ldots, x_N\}$. These letters can be thought of, for example, as labeling regions in phase space. An *itinerary* is a bi-infinite (infinite in both directions) sequence of letters $\cdots a_{-1}a_0a_1 \cdots$, where $a_i = x_j \in \mathcal{A}$ for each $i \in \mathbb{Z}$. The set of all itineraries

$$\Sigma_{\mathcal{A}} = \{\cdots a_{-1}a_0a_1 \cdots : \ a_i \in \mathcal{A}\} \cong \mathcal{A}^{\mathbb{Z}}, \tag{1.22}$$

is the same as the set of all mappings $\mathbb{Z} \to \mathcal{A}$ (in other words, any such mapping f is a bi-infinite sequence of letters in $\mathcal{A}$ defined by $a_i = f(i)$). This is the space on which the dynamics will be defined.

This space of all itineraries $\Sigma_{\mathcal{A}}$ may be endowed with a natural metric. Two itineraries are considered close if they share many common iterates. Specifically, given two itineraries $a = (a_i)$ and $b = (b_i)$, we define the distance $d(a, b)$ between them by

$$d(a,b) = \sum_{n=-\infty}^{\infty} \frac{\delta(n)}{2^{|n|}}, \ \delta(n) = \begin{cases} 0 : a_n = b_n \\ \\ 1 : a_n \neq b_n \end{cases}. \tag{1.23}$$

The space $\Sigma_{\mathcal{A}}$ is complete with respect to this metric. With the topology induced by this metric, $\Sigma_{\mathcal{A}}$ is homeomorphic to a Cantor set.

We can now define a dynamical system on $\Sigma_{\mathcal{A}}$ by iterating the itineraries. We define the *shift map* $\sigma : \Sigma_{\mathcal{A}} \to \Sigma_{\mathcal{A}}$ by

$$\sigma(\cdots a_{-2}a_{-1}.a_0a_1 \cdots) = (\cdots a_{-1}a_0.a_1a_2 \cdots), \tag{1.24}$$

where we have introduced a decimal point for clarity. The shift map shifts the sequence one iterate to the left, it sends the letter $a_i \to a_{i-1}$ for every i. It is a homeomorphism. The dynamical system $(\Sigma_{\mathcal{A}}, \sigma)$ is called a

full N-shift.

Sometimes we want a subset of this full dynamics. If the pair of letters $x_i x_j$ occur in some sequence a, then there is an itinerary that goes from x_i to x_j. There may be situations when we want to prohibit or restrict certain transitions. Perhaps x_i and x_j represent states of a system which never makes the transition $x_i \to x_j$. Allowing certain transitions and prohibiting others can be encoded in a *transition matrix*, M. This is an $N \times N$ matrix of zeros and ones defined by

$$M_{ij} = \begin{cases} 1 : x_i \to x_j \\ 0 : x_i \nrightarrow x_j \end{cases} \tag{1.25}$$

M encodes which pair of letters may or may not appear in itineraries. The sequence $x_i x_j$ may appear if and only if $M_{ij} = 1$. An itinerary is *admissible* with respect to M if whenever $a_k a_{k+1} = x_i x_j$, $M_{ij} = 1$, i.e. the itinerary makes only allowed transitions. Obviously, this property is preserved under the shift map σ. If we denote by $\Sigma_M \subset \Sigma_{\mathcal{A}}$ the set of all itineraries admissible to M, then the pair (Σ_M, σ) is also a dynamical system, called a *subshift (of finite type)*. Much information of interest concerning the dynamical system may be extracted directly from the matrix M, such as the structure of periodic orbits and the topological entropy[22] (the natural logarithm of the Perron-Frobenius eigenvalue [1, 19, 58]).

While shifts are easy enough to define, their dynamics are often enormously complicated. Notice that if a is periodic with period p, then it has the form $a = (\cdots a_0 a_1 \cdots a_{p-1} a_0 a_1 \cdots a_{p-1} \cdots)$ and $\sigma^p(a) = a$. Consider the full shift on the alphabet $\mathcal{A} = \{0, 1\}$. There are 2^p distinct symbol sequences of length p. This implies that σ has 2^p periodic orbits for each p, though many of these are masquerading orbits. A periodic itinerary can be defined by giving the repeated word that defines it. For instance, $a_0 a_1 \cdots a_{p-1}$ will denote a periodic itinerary with period p. The set of all periodic sequences is dense in $\Sigma_{\mathcal{A}}$. To see this, let $a = (\cdots a_{-1} a_0 a_1 \cdots)$ be an arbitrary itinerary, and consider the sequence of periodic trajectories $b_0 = a_0$, $b_1 = a_{-1} a_0 a_1$, and so on. It is apparent that in the metric Eq. (1.23), the sequence converges to a, $(b_i) \to a$. We see that a is in the closure of the set of periodic orbits, hence the latter is dense in $\Sigma_{\mathcal{A}}$.

A dense orbit can be constructed by successively concatenating all strings of all lengths. Consider the orbit

[22] Topological entropy is a measure of complexity. A positive entropy indicates chaotic dynamics [25].

$$a^* = (\cdots \underbrace{0\ 1}_{1}\ \underbrace{00\ 01\ 10\ 11}_{2}\ \underbrace{000\ 001\ \cdots}_{3}\ \cdots), \tag{1.26}$$

(its definition for places to the left of 0 is inconsequential). For any itinerary a, some iterate $\sigma^q(a^*)$ will agree with a in an arbitrarily large number of places about the zeroth, hence these two orbits become arbitrarily close, hence a^* is dense in $\Sigma_{\mathcal{A}}$.

Finally, let a and b be two itineraries that first differ in the $|k|$-th place. Then $d(a,b) \leq 2^{-|k-1|}$. However, after k iterations the itineraries differ in the zeroth place, and $1/2 \leq d(\sigma^k(a), \sigma^k(b))$. In other words, any two distinct itineraries, no matter how close, are eventually separated by at least a distance of $1/2$, thus shift dynamics display sensitivity to initial conditions. In summary, according to our definition (Pg. 1.3), shift dynamics are chaotic. Subshifts are often chaotic, but it depends on the transition matrix. For example, if the only allowed transition is $x_i \to x_i$, then there is only one orbit, and therefore no sensitivity to initial conditions.

1.3.2 The Theorem of Birman and Williams

Let φ_t be a flow on M. Assume that M is compact and equipped with a metric d. We have seen that there are a number of closed sets invariant under the flow that are of dynamical interest, such as the set of fixed points, periodic orbits, the non-wandering set, and the chain-recurrent set. An invariant Λ set is said to have a *hyperbolic structure* if the restriction of the tangent bundle of M to Λ may be written as a continuous sum $TM = E_S \oplus E_U \oplus E_C$ of sub-bundles, the stable, unstable, and center bundles respectively. Each of these bundles must be invariant under the flow (specifically, under the differential $D\varphi_t$). The center bundle E_C is spanned by the vector field tangent to the flow (and hence one-dimensional). The stable and unstable bundles are defined by the following exponential growth conditions. There are constants $C, \lambda > 0$ such that for all $t \geq 0$ we have

$$||D\varphi_t(v)|| \leq Ce^{-\lambda t}||v|| \qquad v \in E_S \tag{1.27}$$

$$||D\varphi_t(v)|| \geq Ce^{\lambda t}||v|| \qquad v \in E_U. \tag{1.28}$$

If all of M is hyperbolic, the corresponding flow is said to be *Anosov*.

For a subset X of a hyperbolic set Λ we have the stable $W_S(X)$ and unstable $W_U(X)$ manifolds of X, which given by

$$W_S(X) = \{y \mid d(\varphi_t(y), \varphi_t(X)) \to 0, \text{ as } t \to \infty\} \tag{1.29}$$

$$W_U(X) = \{y \mid d(\varphi_t(y), \varphi_t(X)) \to 0, \text{ as } t \to -\infty\}. \tag{1.30}$$

Intuitively, the stable manifold is the set of all points that approach X asymptotically into the future, while the unstable manifold is the set of all points that approach X asymptotically into the past. Contrary to what their names might imply, these sets are not generally *embedded* submanifolds of M. In the most interesting cases they wind around M densely. When $X = \{x\}$ is a single point, we have the following [34]:

Theorem 1.9 (Stable Manifold Theorem). *The sets $W_S(x)$ and $W_U(x)$ are smooth injective immersions of the spaces E_S and E_U respectively. Moreover, they are tangent to these spaces at x, $T|_x W_S(x) = E_s|_x$ and $T|_x W_U(x) = E_U|_x$.*

When the chain-recurrent set is hyperbolic, Smale [74] has shown that it possesses a finite "prime" decomposition:

Theorem 1.10. *Given a flow φ_t on M having a hyperbolic chain-recurrent set $\Lambda_{CR}(\varphi_t)$, Λ_{CR} decomposes as the disjoint union of a finite number of basic sets $\mathcal{B}_i$. Each $\mathcal{B}_i$ is closed, invariant, and contains a dense orbit. The set of periodic orbits within each $\mathcal{B}_i$ is also dense within $\mathcal{B}_i$.*

Another condition worth mentioning, but not necessary for the Birman-Williams theorem, is strong transversality. A flow is said to satisfy the *strong transversality condition* if the stable and unstable manifolds of each pair of points in Λ_{CR} intersect transversely: $W_S(x) \pitchfork W_U(y)$ for all $x, y \in \Lambda_{CR}$. An important consequence of a flow φ satisfying this condition is that all nearby flows are conjugate to φ, so that they all possess the same dynamics. This is called *structural stability*. We thus have the following theorem of Robinson [63]:

Theorem 1.11. *Any flow φ on M having a hyperbolic chain recurrent set and satisfying the strong transversality condition is structurally stable.*

The corresponding theorem for diffeomorphisms was proven earlier by Robbin [62].

Let $\mathcal{B}$ be a basic set as in Smale's theorem and suppose that its topological dimension[23] is $\dim \mathcal{B} = 1$. Bowen [5] has shown that under this hypothesis the flow always has a Poincaré section Δ. Moreover, this section can always be taken to be a finite union of disjoint disks, Δ_i. The flow induces a diffeomorphism of the section Δ. This induced diffeomorphism turns out to be very nice – it is essentially a subshift of finite type [6]:

Theorem 1.12. *Let $F : N \to N$ be a diffeomorphism with hyperbolic chain-recurrent set Λ_{CR} and $\mathcal{B} \subset \Lambda_{CR}$ a basic set. There exists a semi-conjugacy $h : \Sigma_A \to \mathcal{B}$ of a subshift of finite type Σ_A onto $\mathcal{B}$. Specifically, h is a continuous surjection that satisfies $h \circ \sigma = f \circ h$.*

This implies that on $\mathcal{B}$ the flow φ_t is a suspended subshift of finite type and admits a description in symbolic dynamics.

The essential step in the proof of Thm. 1.12 is the construction of a *Markov partition.* A Markov partition is built up from (generally non-geometric) "rectangles". A closed set R is a *rectangle* if its interior is dense in R and the stable and unstable manifolds of every pair of points in R intersect at a single point, also in R. A Markov partition for an invariant set Λ is a finite union $\Lambda = \cup R_i$ of rectangles with disjoint interiors. If $x \in \operatorname{int} R_i$ and $f(x) \in \operatorname{int} R_j$, then f preserves stable and unstable manifolds. In other words, $f(W_S(x) \cap R_i) \subset W_S(f(x)) \cap R_j$ and $(W_U(f(x)) \cap R_j) \subset f(W_U(x) \cap R_i)$. Once a Markov partition has been established the shift is easily defined. If there are N rectangles, the $N \times N$ shift matrix A is defined by

$$A_{i,j} = \begin{cases} 1 : f(R_i) \cap R_j \neq \emptyset \\ 0 : f(R_i) \cap R_j = \emptyset \end{cases} . \tag{1.31}$$

Figure 1.17 shows a Markov partition with two rectangles for Arnold's "cat map". This is a linear map of

[23] Also known as the Lebesgue covering dimension, the topological dimension is defined to be the minimum value of $n \in \mathbb{Z}$ such that every open cover of the set has a refinement in which no point is covered by more than $n + 1$ elements. The covering dimension of $\mathbb{R}^n$ is n. For example, any open covering of the real line by intervals may be refined so that no point is contained in more than two intervals.

the torus[24] given by

$$\begin{pmatrix} x \\ y \end{pmatrix} \mapsto \begin{pmatrix} 2 & 1 \\ 1 & 1 \end{pmatrix} \begin{pmatrix} x \\ y \end{pmatrix}. \tag{1.32}$$

Linear maps of $\mathbb{R}^n$ are never dynamically complex, but the compactness of T^2 allows for complexity: the stable and unstable manifolds of each point wrap densely around T^2. In this case the rectangles are geometric squares, and their axes align with the stable and unstable directions of the map, which are just the eigen-directions of the defining matrix. The stretching and squeezing rates are given by the eigenvalues of the matrix, which are $(3 \pm \sqrt{5})/2$. The figure demonstrates that both rectangles are mapped across both rectangles. The corresponding transition matrix represents a full shift

$$A := \begin{pmatrix} 1 & 1 \\ 1 & 1 \end{pmatrix}, \tag{1.33}$$

which has eigenvalues 2 and 0, and thus an entropy of $\ln 2$.

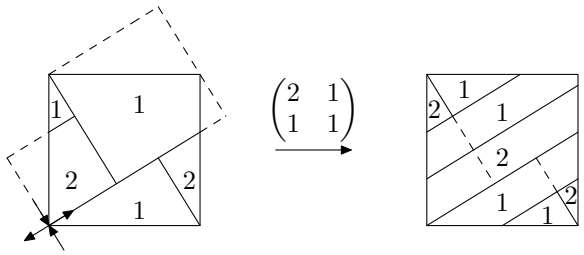

Figure 1.17: Markov partition for Arnold's cat map.

Going back to our general discussion, the Markov partition of the basic sets in the Poincaré section may be extended into *Markov flowboxes* in the flow. This is a sort of suspension of the Markov partition. The flow boxes have two types – in-going and out-going. Projecting out the stable directions, one is left with essentially a two-dimensional object carrying only the flow and unstable directions. This "Birman-Williams" projection of the stable manifold may be described in terms of an equivalence relation: two points are identified if they

[24] Think of T^2 as the unit square in $\mathbb{R}^2$ with identifications. This linear map acts on $\mathbb{R}^2$ and takes lattice points to lattice points, hence descends to T^2.

share the same asymptotic future (Fig. 1.18)

$$x \sim y \text{ iff } \lim_{t\to\infty} ||\varphi_t(x) - \varphi_t(y)|| \to 0. \tag{1.34}$$

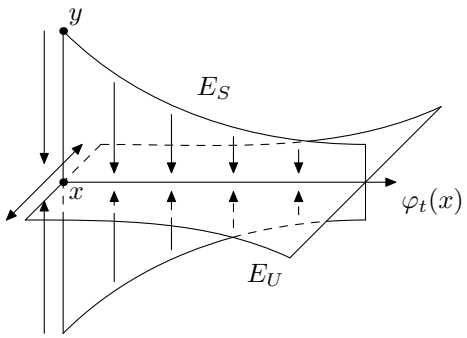

Figure 1.18: Projection of stable manifolds.

This quasi two-dimensional object is called a *branched two-manifold* or *template* (see Fig. 1.19). A branched manifold is a manifold with a finite number of singular regions. These take the form of line singularities (joining charts) and point singularities (splitting charts). The in-going and out-going flow boxes project onto the joining and splitting charts respectively. It is customary to collapse the middle lower boundary region of the splitting chart to a point (see Fig. 1.20).

Since this collapse may be done smoothly, it induces an an ambient isotopy of all periodic orbits in the flow. This is called the Birman-Williams projection. Collecting these results we have the Birman-Williams theorem [4]:

Theorem 1.13 (Birman and Williams). *Given a flow φ_t on a three-dimensional manifold M having a hyperbolic chain-recurrent set, there is a smooth projection of the flow onto a semi-flow on an embedded branched manifold $\mathcal{T} \subset M$, which is a suspension of a subshift of finite type. The link of all periodic orbits in M is in bijective correspondence with the link of periodic orbits in $\mathcal{T}$. On any finite sublink, this correspondence is via ambient isotopy.*

Note that, in agreement with Thm. 1.12, the projection induces only a semi-conjugacy, and the flow on the template is only a semi-flow. This means that it is only defined for forward time. The reason is that when the stable manifolds are collapsed, distinct orbits are identified if they share the same asymptotic future (they may

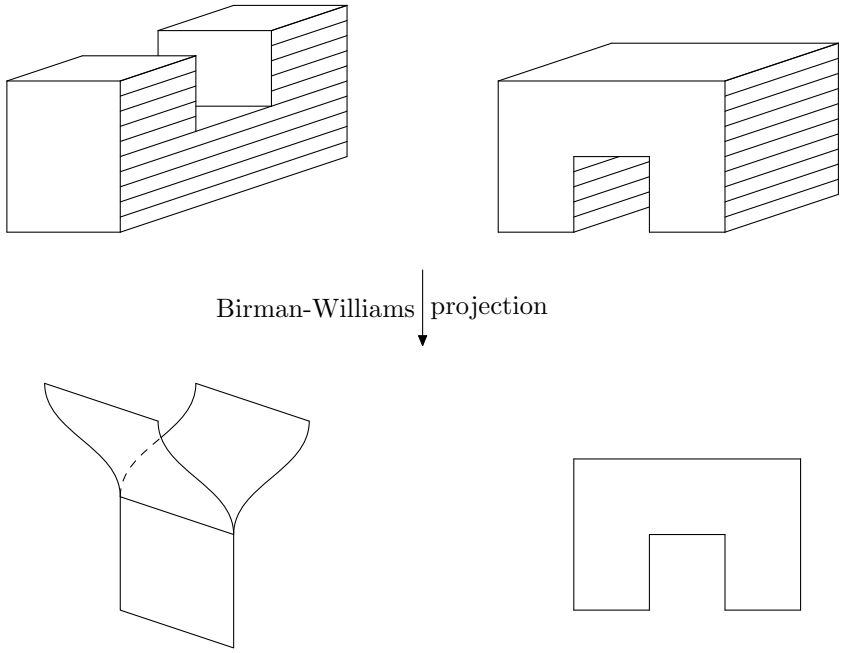

Figure 1.19: Birman-Williams projection. On the left is the projection of an in-going Markov flowbox to a joining chart, and on the right is the projection of an out-going Markov flowbox to a splitting chart. The flow direction is from top to bottom and the parallel lines represent the stable foliation, which is projected out.

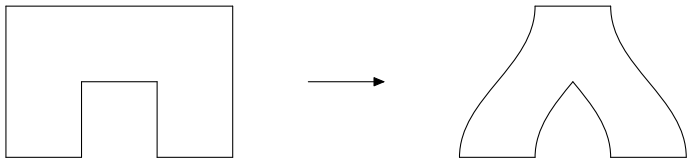

Figure 1.20: Modification of the splitting chart.

have wildly different pasts). This occurs at the line singularity or *branchline* on the joining charts (Fig. 1.19). Flowing backward through a branchline requires a choice and is not unique.

So far we have assumed that $\dim \mathcal{B} = 1$. The problem with the case $\dim \mathcal{B} > 1$ is that, while the Birman-Williams projection may be carried out, the resulting object need not be a template. In particular, when the stable manifolds are dense in the space (e.g., suspensions of Anosov diffeomorphisms such as Arnold's cat map), the quotient space fails even to be Hausdorff, so is certainly not a template. Nevertheless, this more general case may be reduced to the case already considered by first perturbing the chain recurrent set through a process called DA (*derived from Anosov* [4], also called *Smale surgery* [74] or *orbit splitting*). The purpose of this perturbation is to disrupt the density of the stable manifolds. The construction is as follows (see Fig. 1.21).

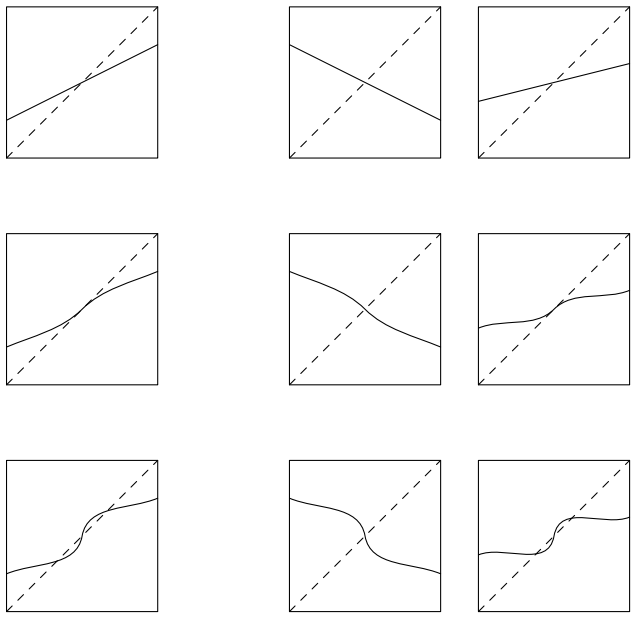

Figure 1.21: The DA. Shown is the first return map of the stable direction of the periodic orbit as the control parameter δ is varied (from top to bottom). Fixed points are given by intersections of the map with the diagonal. The orientable case (a) results in a pitchfork bifurcation, while the non-orientable case (b) results in a period doubling bifurcation. In (b) both the first and second iterate of the first return map are shown in order to show clearly the period doubling. The second iterate undergoes a pitchfork bifurcation.

First suppose $\dim \mathcal{B} = 3$. Let γ be a periodic orbit in $\mathcal{B}$. There is a well-defined coordinate frame (e_S, e_U, e_C) along γ based on the stable, unstable, and center manifolds according to hyperbolicity. This frame can be extended to a coordinate system within a small tubular neighborhood N_ϵ of γ. Let X be a vector field supported in N_ϵ, vanishing along γ, but pointing "outward" along the stable direction. For instance, if $x = (x_S, x_U, x_C)$ is a point in N_ϵ, then $X(x) = (x_S, 0, 0)$, inside a smaller tubular neighborhood, will suffice. One then replaces the original flow by

$$\frac{d\varphi}{dt} \to \frac{d\varphi}{dt} + \delta X, \tag{1.35}$$

where $\delta > 0$ is a parameter. For δ sufficiently small the qualitative features of the flow are the same as the stable direction will still dominate over X. But, when δ is sufficiently large to overcome the stability, γ will bifurcate from a saddle to a source and one or two new saddle orbits will be created within N_ϵ. The stable

manifold of each point along γ is a line ($\mathbb{R}$) by Thm. 1.9, so the stable manifold of γ is a line bundle over S^1, which can either be a cylinder (orientable) or a Möbius strip (not orientable). Whether one orbit or two gets created depends on whether the stable manifold of γ was orientable (two orbits) or not (one).

Remarkably, this preserves hyperbolicity while having the effect of reducing the dimension of the basic set by one. The DA procedure may then be repeated to reduce the dimension from two to one. Note that in this case one dimension of the basic set belongs to the flow direction. The basic set contains either the stable or the unstable direction, but not both. The other direction will be transverse to the set. Assume it contains the stable direction so that it is a repeller (the unstable direction being transverse). Then one can split an orbit along the stable direction as before. If it is an attractor, then it becomes a repeller under time-reversal and one can then split the same way. Either way the dimension of $\mathcal{B}$ is reduced to one and the general result follows. Pictures illustrating the application of the DA to the chain recurrent set of Arnold's cat map (which has the structure of a Cantor set times an interval) may be found in [11].

There are two major problems with the Birman-Williams theorem. The first is that it is only formulated for three dimensional systems, and the second is the requirement of hyperbolicity. The first problem relates to the failure of orbit splitting to preserve invariant sets [4], thus not every higher dimensional flow is necessarily well-represented by a template (at least not one obtainable through the DA procedure). However, there is no reason why the Birman-Williams projection cannot be carried out in general, especially when the chain-recurrent set is already one dimensional. Of course, in general the projection may not yield a reasonable object, but for one dimensional chain-recurrent sets, a higher-dimensional branched manifold (with, perhaps, higher dimensional singular sets) is possibly attainable.

Restricting our attention to three dimensional systems, the assumption of hyperbolicity is overly strong. In practice, attractors are never hyperbolic. Nevertheless, for systems such as Rössler's, a template description is essentially obvious just from looking at the attractor[25] (compare Figs. 1.24 and 2.1). Global hyperbolicity fails when it is not possible to distinguish the stable and unstable directions at a point, a so-called *homoclinic tangency*.

For "folding maps" of the plane, the existence of such points distinguishes between hyperbolic maps and

[25] That is, looking at a typical numerically integrated trajectory, which yields a visual approximation to the underlying attracting set.

non-hyperbolic ones (see Fig. 1.22). An example of a hyperbolic map is Smale's horseshoe, which is a simple stretch and fold of the plane. One example of a non-hyperbolic map is the Hénon map, defined by

$$\begin{aligned} x' &= y + 1 - ax^2 \\ y' &= bx, \end{aligned} \tag{1.36}$$

and has folding-like properties. Another example is given by the Poincaré map of the Rössler dynamical system, which is the flow defined by the equations

$$\begin{aligned} \dot{x} &= -y - z \\ \dot{y} &= x + ay \\ \dot{z} &= b + z(x - c). \end{aligned} \tag{1.37}$$

Away from the fixed points, this flow resembles a suspension of the Hénon map.

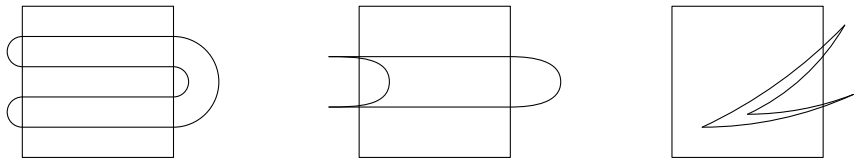

Figure 1.22: Comparison of folding maps of the plane: the Smale horseshoe (a), the Hénon map (b), and the Rössler system Poincaré map (c). The Hénon map was iterated with $(a, b) = (1.4, 0.3)$. The Rössler Poincaré map was taken as a subset of the plane $y = -0.528$ (through the central fixed point) and was found by numerical integration with $(a, b, c) = (0.398, 2.0, 4.0)$. The thickness of the image under this map is greatly exaggerated for clarity.

In the latter two cases, the folding area becomes part of the attracting set, and a homoclinic tangency is forced somewhere along this bent region. This phenomenon introduces a breakdown in the symbolic dynamics analogous to the breakdown in unimodal interval maps when iterates of the critical point need to be taken into account. In fact, the Rössler system is so highly dissipative its return map is "practically" one-dimensional. A symbolic dynamics can be recovered by utilizing the so-called *kneading theory* [15, 25]. A good discussion of this phenomenon in the case of the Hénon map may be found in Sec. 2.11.2 of [25].

In any case, hyperbolic systems are stable under small perturbations since they are defined in terms of

transversality conditions. This implies that the underlying templates are also stable. Real non-hyperbolic attractors are typically not invariant under small perturbations. As control parameters are varied, families of solutions can be created or destroyed (exhibited in a bifurcation diagram). This can imply violent changes for the underlying template, with entire branches being grafted or pruned. The symbolic dynamics on these templates can fail to be finite subshifts – they can require an infinite number of symbols (or an infinite number of entries in the appropriate transition "matrix").

For many real systems there seems to be a related hyperbolic system and associated template into which the dynamics can be embedded. Since the real flow only occupies a subset of this new flow, it will not fully represent the dynamics of the latter. In particular, there will be periodic sequences in the new flow that do not represent sequence in the actual flow. However, under small parameter changes, the dynamics may bifurcate and change, but always within the confines of the fixed larger system. This suggests an extension of the Birman-Williams theorem to families of dynamical systems.

1.3.3 The Classification of Three Dimensional Systems

The Birman-Williams theorem yields a classification of dynamical systems at the level of branched two-manifolds. The essential elements of any three dimensional dynamical may be constructed by gluing together joining and splitting charts. Recall that these charts and the branched manifold arose from the Birman-Williams projection applied to the Markov flowboxes. The union of these flowboxes determines the fundamental phase space in which all of the important dynamics takes place. In particular, this is where the chain recurrent set lives. In this section we look at the classification of dynamical systems at the level of phase spaces.

Each flowbox is, up to continuous isotopy, a trinion (see Fig. 1.23). These are essentially three dimensional balls, D^3, with three distinguished disks in the boundary. The flow is transverse to the boundary only along these disks where they enter or leave the trinion. Trinions are the fundamental regions where the flow is mixed or split and chaotic behavior is created. The out-going flowboxes correspond to splitting trinions and contain splitting charts in the branched manifold. Likewise, in-going flowboxes correspond to joining trinions and contain joining charts.

Our smooth trinions enclose the Markov flowboxes. The output disks on the joining trinions correspond

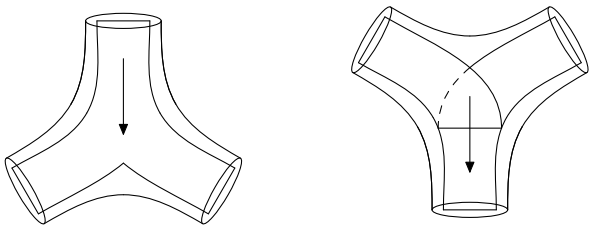

Figure 1.23: Fundamental trinions and included charts – splitting (a) and joining (b).

to the component disks Δ_i of the Poincaré section in Bowen's theorem [5]. The union of all these trinions, matching each out-going port of a trinion to an in-going port of another and leaving no free ends, results in a handlebody. A *handlebody* is a three dimensional manifold whose boundary is a closed, orientable surface. A handlebody is said to have genus g if its boundary has genus g. Just as a genus g surface may be created as the connected sum of g tori, a genus g handlebody may be created as the boundary connected sum of g solid tori. From the trinion viewpoint, a genus g handlebody is composed of $2(g-1)$ trinions: $g-1$ splitting and $g-1$ joining.

These handlebodies are the natural phase spaces for flows with one-dimension chain recurrent sets. There are, however, two exceptional cases. The first is the genus one handlebody or solid torus, $D^2 \times S^1$. This handlebody is unique in that it cannot be decomposed into trinions. The solid torus is the natural phase space for driven (suspensions of) two dimensional oscillators and certain other autonomous three dimensional flows, such as the Rössler dynamical system [66]. These systems are created by a continuous "stretch and fold" process, which does not have a well-defined splitting region. In practice, this is generally related to lack of hyperbolicity [25]. For example, the Rössler system can be described by the "template" shown in Fig. 1.24, which can be thought of as one squeezing and one joining chart connected to each other, but with the spurious hold "zipped up".

The second exceptional case is the genus two handlebody, which never occurs as a phase space. A genus two handlebody must be composed of two trinions: one joining and one splitting. The two possible ways to distribute the flow directions in a genus two handlebody are shown in in Fig. 1.25. The first possibility was already dealt with above, viz. the flow is actually genus one and the second hole is spurious. The second

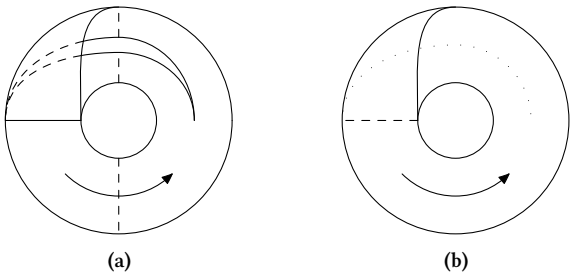

Figure 1.24: Template (a) for Rössler attractor with one joining chart (left) and one splitting chart (right) and the template-like object that results from zipping up the spurious hole (b). The arrow indicates the flow direction.

possibility indicates that the flow is really of one higher genus – rather than having a spurious hole, one is missing. Discussing this point further requires some preparation.

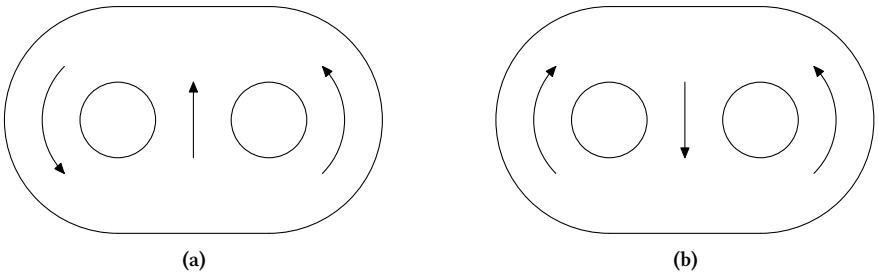

Figure 1.25: The two possibilities for genus two flow. Either the flow is parallel in two adjacent branches and a genus one flow is obtained by removing the right hole (a) or the flow is always contrary in adjacent branches and a genus three flow is obtained by adding a central hole (b).

The boundary of a handlebody is a closed surface of genus g. We may restrict the flow to this surface and obtain a two-dimensional vector field, $v_{||}$. By the Poincaré-Hopf theorem (Thm. 1.6), the sum of the indices of this vector field is equal to the Euler characteristic of the surface, which we investigate next.

The genus zero surface is the sphere S^2, which has homology groups $H_0 \cong \mathbb{Z}$, $H_1 \cong 0$, and $H_2 \cong \mathbb{Z}$. The Euler characteristic is thus $\chi(S^2) = 1 - 0 + 1 = 2$. The genus one surface is the torus, which has homology groups $H_0 \cong H_2 \cong \mathbb{Z}$ and $H_1 \cong \mathbb{Z}^2$, so that $\chi(T^2) = 0$. A surface of genus $g > 1$ is constructed from the connected sum of g tori. One can show[26] that for compact, closed, oriented manifolds, the homology of a connected sum is the sum of the homology groups except in dimensions zero and n, where they remain $\mathbb{Z}$. Hence it follows that for $T^2 \# T^2$, $H_0 \cong H_2 \cong \mathbb{Z}$ and $H_1 \cong \mathbb{Z}^2 \oplus \mathbb{Z}^2 \cong \mathbb{Z}^4$. For g summands it follows by

[26] see Appendix A.

induction that $H_0 \cong H_2 \cong \mathbb{Z}$ and $H_1 \cong \mathbb{Z}^{2g}$. The $2g$ generators of H_1 are the g longitudes and g meridians from the tori in the sum. Finally, we see that the Euler characteristic of a genus g surface is $\chi = 2 - 2g$.

Thus, for a genus-g surface, we have $\sum \operatorname{ind} v_{||} = 2(1-g)$. While the flow never has singularities inside the handlebody, the induced flow on the surface may. In fact, for $g \neq 1$, it must. We may adjust the boundary surface by isotopy to ensure that these singularities are isolated. At these isolated singularities the flow is perpendicular to the surface, so by hyperbolicity, the induced flow in a neighborhood of the singular point is dominated by the stable and unstable manifolds of the trajectory. In other words, there is a contracting and an expanding direction to the induced flow. Hence, the singular point is necessarily a saddle, which has index -1. We may rephrase the Poincaré-Hopf result as

$$\#\text{saddles} = 2(g-1). \tag{1.38}$$

We note that this result automatically eliminates S^2 as a possible phase space since it has genus zero, and would have to support a negative number of saddle points.

We now return to our genus two case with contrary flow directions in adjacent branches. In this case we have a pair of saddle singularities on the boundary. By consulting Fig. 1.25, one can easily add the boundary singularities, yielding Fig. 1.26. There is a trajectory from the top singularity to the bottom singularity, which is not a part of the "interior flow". Removing or "drilling out" this trajectory increases the genus by one. This phenomenon is apparent in the Lorenz system (see Fig. 1.27), where the pruned trajectory is the stable manifold of the central fixed point [25, 83].

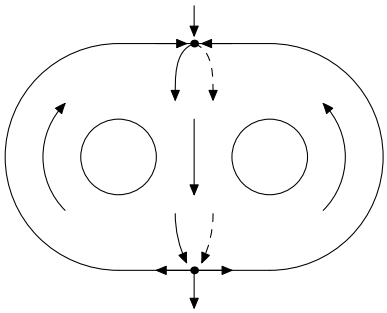

Figure 1.26: Surface singularities for a genus two flow. "Drilling out" the trajectory connecting the boundary singularities results in a genus three flow.

This relationship between the holes of a handlebody and the singularities of the original flow is quite general [25, 83]. These singularities provide the lowest level of structure organizing the dynamics. For example, consider the singular structure of the Lorenz flow (branched manifold) indicated in Fig. 1.27. The two symmetry related foci organize the outward rotational motion, while the central saddle tears the flow, sending "half" toward each saddle. At the next level, connecting curves seem to extend this organization around one dimensional sets [22]. The structure of branched manifolds and bounding tori, together with this organization by singular points, leads to the introduction of canonical forms, which describe the different ways a genus g torus may be dressed with a flow. This theory is developed elsewhere [25, 26, 83] and is not needed here. We conclude that the fundamental phase spaces for three dimensional flows are genus g handlebodies, where $g \in \mathbb{Z}^+ - \{2\}$.

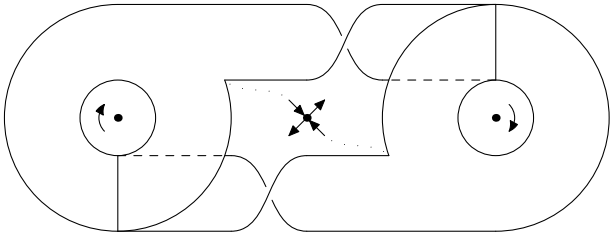

Figure 1.27: Organization of the Lorenz flow by its singular structure. The splitting of the flow by the central saddle is evident.

1.3.4 Observation Functions and Reconstructions

Since each point of a manifold M dressed with a flow represents some particular state of a dynamical system, a smooth real valued function on M, $f : M \to \mathbb{R}$ may be regarded as giving the values of some state-dependent property of the dynamical system. For instance, if the dynamical system Eq. (1.18) models laser activity, then f could measure laser intensity as a function of the state variables x (population inversion, etc.). In this context such a function is called an *observation function*. Data recorded during an experiment are the values of some observation function f sampled along the trajectory of the system as it evolves in time. In other words, the composition

$$f(\phi_t(x_0)), \tag{1.39}$$

is recorded as a function of time t, usually discretely sampled at regular intervals.

In a typical experiment, only one such time series is recorded. It would seem that most of the information contained in the original multi-dimensional dynamics is irretrievably lost. Surprisingly, this is not so, as the following theorem shows [79]:

Theorem 1.14 (Takens). *Let M be an n-dimensional smooth manifold. If v is a vector field on M with flow φ_t and f is an observation function on M, then for generic choices of v and f, the map $\Phi : M \to \mathbb{R}^m$ defined by*

$$x \mapsto \left(f(x), \left.\frac{d}{dt}\right|_0 f(\varphi_t(x)), \ldots, \left.\frac{d^{m-1}}{dt^{m-1}}\right|_0 f(\varphi_t(x)) \right), \tag{1.40}$$

is an embedding when $m = 2n + 1$.

This theorem is best understood as a generalization of Whitney's first embedding theorem [87]. Whitney showed that, generically, any set of $2n + 1$ functions on M provide coordinates defining an embedding. Takens showed that a single function and its first $2n$ derivatives sampled along a trajectory fulfill this rôle. Takens [79] also proved alternative versions of the same theorem valid for discrete sampling intervals and for finite sample times.

A mapping of the form of Eq. (1.40) is called a *differential mapping*. It is called a *differential embedding* when it provides an embedding (which it does, generically, when $m \geq 2n + 1$). Since in actual experiments data are discretely sampled, typically at even intervals, it is important to consider the discretized version of Eq. (1.40). This is called a *time delay mapping* as is given by

$$x \mapsto \left(f(x), f(\varphi_\tau(x)), \ldots, f(\varphi_{(m-1)\tau}(x)) \right), \tag{1.41}$$

where τ is some multiple of the experimental sampling time. We note that for minimal time delay, linear combinations of delay coordinates may be used to approximate derivatives, and therefore a differential mapping may be approximated using delay coordinates.

Differential embeddings have four attractive features: (i) Each embedding coordinate is the derivative of the previous coordinate ($X_{i+1} = \dot{X}_i$); (ii) Attempts to model the dynamics using the embedding coordinates involve construction of only one unknown source function [43], for the last time derivative $\dot{X}_N = h(X_1, X_2, \ldots, X_N)$; (iii) An explicit expression for the source function h may be constructed when the differ-

ential equations are known; and (iv) In three dimensions it is a simple matter to determine the topological organization of all unstable periodic orbits simply by inspection of their projection onto the $(X_1, X_2) = (X_1, \dot{X}_1)$ subspace. In this projection all crossings in the upper half plane have sign -1 while all crossings in the lower half plane have sign $+1$. The linking number of two periodic orbits is half the number of crossings in the lower half plane minus half the number of crossings in the upper half plane [21, 25].

The principal drawback of differential embeddings of scalar time series is the signal to noise problem. As a rough rule of thumb, there is an order of magnitude loss of S/N ratio for each derivative (or integral) that is taken. A differential embedding of the type $x \to (x, \dot{x}, \ddot{x})$ generally suffers two orders of magnitude reduction in this ratio. One way around this problem is to use an integral-differential embedding $x \to (\int x, x, \dot{x})$. In this case the integral and differential each lose about one order of magnitude. The three coordinates remain differentially related. Care must be taken that secular terms be removed from the scalar time series before the integral is taken. The subtle points involved in such embeddings have been described in the first topological analysis of experimental data that was carried out [50]. These points were amplified on in [21, 25].

Briefly, in the first topological analysis, the data set under consideration behaved like a relaxation oscillator, with a slow linear change over about half a cycle. The differential embedding $(x, \dot{x}, \ddot{x})$ collapsed to a straight line, as can be seen in Fig. 4 of Ref. [50]. Spline fits [60] were unable to lift this degeneracy, as indeed no data processing method based on local fitting methods could succeed. More recently, newer data processing methods have been developed to treat problems of this type [46].

This concludes our review of foundational material. We now turn our attention to defining and carrying out the representation theory for dynamical systems, which will occupy us for the remainder of this thesis.

Chapter 2: The Program of Representation Theory

The idea of a representation theory for dynamical systems is a natural for anyone familiar with the theory of groups. The classical groups are groups of transformations acting on vector spaces by means of certain matrices. There is an abstract group isomorphic to this transformation group of matrices, and the latter may be regarded as a representation of the former. One may then ask if there are other ways this abstract group may act on the same vector space, or if it may act on other vector spaces. In other words, what are all the representations of the group? Representation theory aims to enumerate all of the inequivalent ways the a given abstract group may be represented as a group of matrices acting on various vector spaces.

More specifically, an (n-dimensional) *representation* of a group G is a mapping $\Gamma : G \to \mathrm{Mat}_n(F)$ (the set of $n \times n$ matrices over a field F) which preserves the group structure. That is

$$\begin{array}{ccccc} g & \cdot & h & = & gh \\ \downarrow & & \downarrow & & \downarrow \\ \Gamma(g) & \cdot & \Gamma(h) & = & \Gamma(gh) \end{array} , \tag{2.1}$$

for $g, h \in G$. When the mapping Γ is injective the representation is called *faithful*. Let V denote the n-dimensional vector space on which the representation Γ acts. Two representation Γ_1 and Γ_2 of G are equivalent if there exists an isomorphism $M : V \to V$ such that the following diagram commutes

$$\begin{array}{ccc} V & \xrightarrow{M} & V \\ {\scriptstyle \Gamma_1}\downarrow & & \downarrow{\scriptstyle \Gamma_2} \\ V & \xrightarrow{M} & V \end{array} \tag{2.2}$$

This essentially says that the two representations have the same action as seen from two different coordinate systems that are related by M. Thus, we do not regard them as distinct.

A familiar example in physics is the Lie group $SO(3)$, consisting of all rotations of $\mathbb{R}^3$. Equivalently, these are all of the orientation preserving isometries of geometrically flat Euclidean space that preserving the

origin. The usual representation is in terms of 3×3 orthogonal matrices R, which satisfy $R^\top R = I_3$ and $\det R = 1$. The most well known representations are given by the scalars (trivial), vectors (usual) and second rank tensors:

scalar: $f \to (1)f$;

vector: $v^\mu \to R^\mu{}_\alpha v^\alpha$

tensor: $t^{\mu\nu} \to R^\mu{}_\alpha R^\nu{}_\beta t^{\alpha\beta} \Rightarrow t^{(\mu\nu)} \to R^{(\mu\nu)}{}_{(\alpha\beta)} t^{(\alpha\beta)}$.

Notice that by grouping indices appropriately, second rank tensors form a vector space of dimension $3^2 = 9$, and the two rotation matrices become a single 9×9 matrix. The mathematical problem of enumerating all of the representations of this group is important for physics – it yields the theory of angular momentum in quantum mechanics.

The corresponding theory for dynamical systems begins with the following observation. When studying a physical system, one does not have direct access to the underlying dynamics. Experiments yield only indirect access through measured data. Quite often this data is a scalar time series. As was observed in Chap. 1, in order to study the dynamics of the system, one must attempt to "reconstruct" the original dynamics through some embedding technique applied to that scalar data.

The term "reconstruction" implies that the dynamics obtained through an embedding is in some sense unique. This is not the case: many different embeddings are possible (see Fig. 2.1). It is therefore more appropriate to call the result of such a procedure a *representation* rather than a *reconstruction*, as the former term connotes non-uniqueness.

These considerations raise three very important questions.

1. For any analysis methodology, which results depend on the representation and which are representation independent?

2. For an experimental attractor, what is its spectrum of inequivalent representations and how are they distinguished?

3. As the embedding dimension increases, which representations remain inequivalent?

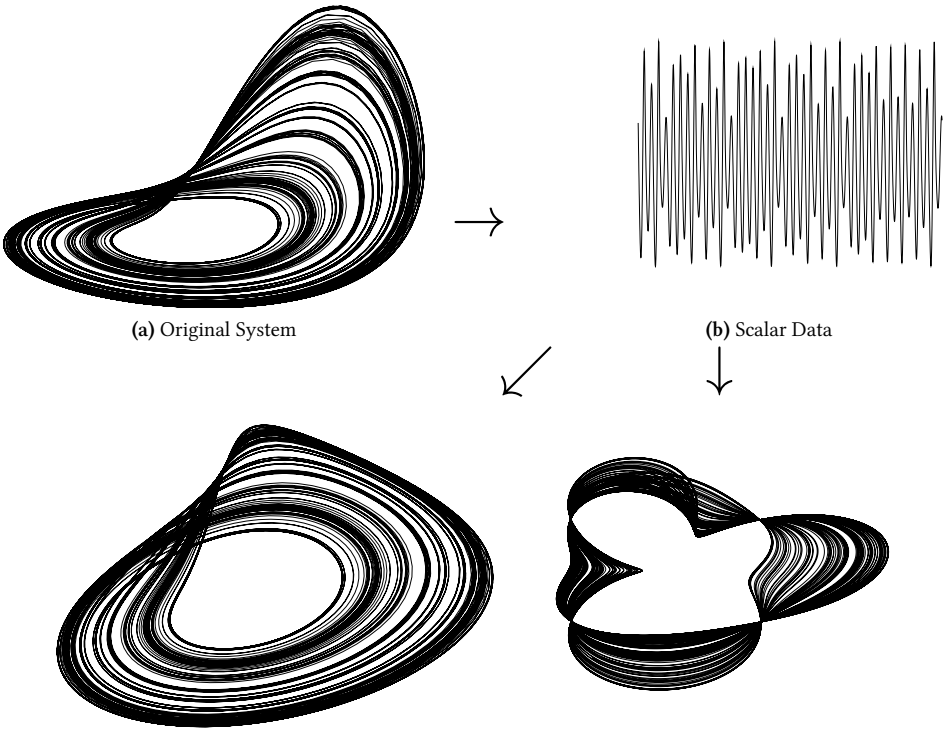

Figure 2.1: Illustration of reconstruction procedure for the Rössler attractor (a). Many different reconstructions (c and d) are possible from time series (b).

Question (1) has a precise answer. All geometric measures (e.g., spectrum of fractal dimensions[1] [25, 54] are diffeomorphism invariants. All dynamical measures (e.g., spectrum of Lyapunov exponents[2] [25, 30]) are also embedding invariants, except that care must be taken to account for the extra or "spurious" Lyapunov exponents[3] [68]. As a result, these measures should be independent of the particular representation used to compute them. This means that the second and third questions are not important when the objectives of an analysis are restricted to computation of geometric and dynamical invariants. Unfortunately, such analyses do not provide information about the *mechanism* responsible for generating chaotic behavior [65, 24]. By mechanism, we mean an understanding of how different regions of the phase space are brought together and compressed under the flow, generating complicated dynamical behavior. In terms of the branched

[1]For example, if chaotic dynamics are created by a repeated "stretch and fold", the chain-recurrent set will have a layered fractal structure, often a Cantor set. (Think of an infinitely folded pastry.)

[2]A flow on an n-manifold has n Lyapunov exponents λ_i, giving the average stretching ($\lambda_i > 0$) and squeezing ($\lambda_i < 0$) rates over the whole dynamics. There is always at least one zero exponent corresponding to the flow direction itself.

[3]If a dynamical system is n-dimensional there are n Lyapunov exponents, but if an embedding has codimenion $p > 0$, there will be p spurious Lyapunovs implying relaxation onto the embedded submanifold. These are artifacts of the embedding process.

manifolds describing a three-dimensional flow, mechanism describes how the separate branches, each coded by a separate symbol, are joined together at branch lines, rather than how they wrap around each other when situated in $\mathbb{R}^N$.

Topological measures depend on the particular representation [21]. For three-dimensional representations, the spectrum of the linking numbers of unstable periodic orbits depends in a well-defined way on the representation. Indeed, their link type is determined by the particular embedding. However, the mechanism responsible for generating chaotic behavior is representation independent [65, 24]. It is naturally an intrinsic property of the abstract flow. For topological analyses, the second and third questions are of paramount importance.

The goal of representation theory is therefore to answer the second and third questions.

A time series represents the image under some unknown observation function of a solution to the dynamics in the original phase space, staring from some unknown initial condition. This phase space is some differentiable manifold, and one may speak of differential embeddings of this manifold into Euclidean spaces. An embedding in this sense is a mapping of the manifold into some $\mathbb{R}^N$, which is a diffeomorphism onto its image. Such an embedding induces an embedding of any particular trajectory or indeed any subspace of the phase space manifold onto an image in $\mathbb{R}^N$. For trajectories or attracting sets, this induced mapping is an embedding in the sense of the previous paragraph. We intend to study the representation problem for dynamical systems by studying the embeddings of the phase space manifolds.

Let (M, ψ) be an abstract dynamical system. A *representation* (N, ϕ) of (M, ψ) is a smooth surjective mapping $f : (M, \psi) \to (N, \phi)$, $N \subset \mathbb{R}^n$. The mapping f takes the flow ψ onto ϕ, i.e. f is a semi-conjugacy. More explicitly, we have $\phi(f(x), t) = f \circ \psi(x, t)$ for every x and t. This is summarized by the commutative diagram

$$\begin{array}{ccc} M & \xrightarrow{f} & N \\ {\scriptstyle\psi}\downarrow & & \downarrow{\scriptstyle\phi} \\ M & \xrightarrow{f} & N. \end{array} \tag{2.3}$$

We have not required that f be injective. If f is injective, then it is a diffeomorphism and we say, in analogy with the group case, that (N, ϕ) provides a *faithful representation* of (M, ψ). Since we are concerned primarily with faithful representations, hereafter the word representation will imply faithful, unless otherwise

indicated.

To make the enumeration of representations tractable we require an appropriate notion of equivalence. We wish to regard two representations $f_i : (M, \psi) \to (N_i, \phi_i)$, $i = 0, 1$, of a dynamical systems as equivalent if one is smoothly deformable into the other. The intuitive notion of a smooth deformation is made precise though the notion of isotopy. This is the same notion used to define knot equivalence in Chap. 1. Two embeddings f_0 and f_1 of M are isotopic if there exists a smooth map $F(x, t) : M \times [0, 1] \to \mathbb{R}^n$ such that $F(x, 0) = f_0(x)$, $F(x, 1) = f_1(x)$ and $f_t(x) = F(x, t)$ is an embedding for each fixed t. An isotopy is a smoothly varying family of embeddings indexed by t. Non-isotopic embeddings provide inequivalent representations of a dynamical system since one is not deformable into the other without self-intersection.

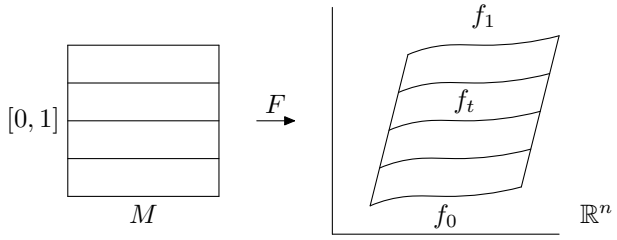

Figure 2.2: Illustration of an isotopy. The embedding f_0 is isotoped into the embedding f_1 through the family f_t.

As also mentioned in Chap. 1, there is another closely related notion called an ambient isotopy. Two embeddings f_0 and f_1 are ambient isotopic if there exists a smooth map $F(x, t) : \mathbb{R}^n \times [0, 1] \to \mathbb{R}^n$ such that $G(x, 0) = x$ and $G(f_0(x), 1) = f_1(x)$. Since the phase space manifolds we shall deal with we always compact, the Isotopy Extension Theorem [39] guarantees that the notions of isotopy and ambient isotopy are equivalent. We will thus use these two notions interchangeably.

When two embeddings are non-isotopic there is some topological obstruction preventing the isotopy. Such obstructions are the topological indices that distinguish representations. In the representation theory of groups there exists an infinite number of representations on vectors spaces of arbitrarily high dimension. By contrast, we expect that in the dynamical systems case the number of inequivalent representations to be a decreasing function of embedding dimension. This is because we may induce a representation in $\mathbb{R}^{n+1}$ from one in $\mathbb{R}^n$ by the natural inclusion $\mathbb{R}^n \hookrightarrow \mathbb{R}^{n+1}$, and generally the greater ambient room will allow some of topological obstructions to be surmounted and the previously distinct representations to become equivalent under isotopy.

This creates a tower of fewer and fewer representations in higher and higher dimensions. One might expect to eventually reach a summit in some $\mathbb{R}^N$ in which there is only one representation up to isotopy. In fact, this summit always exists. Wu has shown that for $n \geq 2$, any two embeddings of an n-manifold into R^N are isotopic when $N = 2n + 1$ [88]. We call this unique representation the *universal* representation. While Wu guarantees that this universal representation exists in $2n + 1$ dimensions, in all of the cases we consider it exists in a lower dimension. Once the existence of a universal representation has been established, all of the various inequivalent representations in lower dimensions may be regarded as inequivalent projections or shadows of the one universal form. This Platonic perspective emphasizes the unity of all representations.

The problem of enumerating all inequivalent embeddings of a manifold M may be roughly partitioned into an extrinsic and an intrinsic part. The extrinsic part consists of enumerating, up to isotopy, all of the different subsets of $\mathbb{R}^n$ that M can map onto. The subsets are considered setwise rather than pointwise, so one does not keep track of which points of M are mapped onto which points in the subset.

The intrinsic part consists of describing for a given subset of $\mathbb{R}^N$ how many different ways M may be mapped into that subset, up to isotopy. This intrinsic part is intimately related to the *mapping class group* of M, $\mathrm{MCG}(M)$. Since diffeomorphisms may be composed and inverted, the set of all diffeomorphisms of M, $\mathrm{Diff}(M)$ has a natural group structure. We may introduce a natural equivalence relation on $\mathrm{Diff}(M)$ by regarding two diffeomorphisms f and g as equivalent if and only if they are isotopic. Such an equivalence relation is in perfect keeping with our present ambitions. Moreover, while diffeomorphism groups are formidable objects, mapping class groups are far simpler and often quite tractable.

The mapping class group is defined as the quotient of $\mathrm{Diff}(M)$ by this equivalence relation: $\mathrm{MCG}(M) \equiv \mathrm{Diff}(M)/\sim$, where $f \sim g$ iff f and g are isotopic. An isotopy from f to g yields a smooth sequence of diffeomorphisms connecting f to g, hence yields a path in $\mathrm{Diff}(M)$ from f to g. Thus, the equivalence relation collapses path components, and the mapping class group enumerates the path components of $\mathrm{Diff}(M)$. We therefore have the isomorphism[4] $\mathrm{MCG}(M) \cong \pi_0(\mathrm{Diff}(M))$. As we shall see, it is often useful to determine the mapping class group of a manifold before attempting to find its representations.

Since the phase spaces we consider are oriented, and orientation reversal is never isotopic to the identity[5],

[4] π_0 is the 0-th homotopy group, which counts the path components of a space. It is not generally a group, though it is when the original space is a group.

[5] A smooth change of orientation implies a smooth change in sign of the Jacobian determinant, which implies that it must pass through

we will often consider only those diffeomorphisms that preserve orientation. The subspace of orientation preserving diffeomorphisms is often denoted $\mathrm{Diff}^+(M) \subset \mathrm{Diff}(M)$. The isotopy classes of orientation preserving diffeomorphisms, $\mathrm{Diff}^+(M)/\sim$, is in many contexts the group to which the term mapping class group refers. In other contexts this group is referred to as the *restricted mapping class group*. We will follow the former practice, so that mapping class group for us will refer to the isotopy classes of orientation preserving diffeomorphisms. Orientation reversing diffeomorphisms will be handled separately.

On occasion we wish diffeomorphisms to leave a certain subset of M pointwise invariant. If $X \subset M$, then the subset of $\mathrm{Diff}(M)$ fixing X is written $\mathrm{Diff}(M; X)$. This is sometimes denoted $\mathrm{Diff}(M \text{ fix } X)$ in the literature. The mapping class group of M fixing X is denote similarly by $\mathrm{MCG}(M; X)$.

Finally, by replacing smooth with continuous we can discuss the homeomorphism group, $\mathrm{Hom}(M)$, and the (continuous) mapping class group $\mathrm{MCG}(M) \cong \mathrm{Hom}(M)/\sim$. Clearly $\mathrm{Diff}(M) \subset \mathrm{Hom}(M)$. In dimension at most two they have the same arc components, so that the two mapping class groups are identical. More generally, these two groups always have the same homotopy type up to dimension two. This will simplify the discussion in the following chapters. On the other hand, $\mathrm{Diff}(M)$ and $\mathrm{Hom}(M)$ generally have different homotopy types in higher dimensions. Specifically, the smooth and continuous mapping class groups are generally different. This distinction will be important in Chap. 7.

zero. But then the mapping fails to be an immersion, and hence fails to be an embedding.

Chapter 3: Representations of Genus One Systems

The simplest three dimensional systems are the genus one systems – those whose natural phase space is the solid torus. Familiar examples of this class of systems includes periodically driven non-linear oscillators such as the Duffing and van der Pol oscillators as well as autonomous dynamical systems such as the Rössler system. We begin in Sec. 3.1 with an overview of results without justification. We provide the justification over the next four sections; we work out the mapping class group in Sec. 3.2, and then determine the spectrum of representations in three, four, and five dimensions in Secs. 3.3, 3.4, and 3.5 respectively. Finally, we conclude in Sec. 3.6.

3.1 Overview of Results

A genus one system is a flow inside of the solid torus, $\mathcal{T} = D^2 \times S^1$. Three labels are required to distinguish inequivalent representations in $\mathbb{R}^3$. These are oriented knot type $\mathcal{K}$, parity $\mathbb{Z}_2$, and global torsion $\mathbb{Z}$. The knot type of the representation is the knot type of the center-line or core circle of the torus. This core circle may be obtained by simultaneously shrinking[1] each disk D^2 in $\mathcal{T} = D^2 \times S^1$ to their centers, yielding the circle $\{0\} \times S^1$. This circle inherits an orientation determined by the direction of the original flow. This core may be thought of as describing the fundamental flow direction of the dynamical system. This fundamental flow direction may be mapped onto any oriented knot in $\mathbb{R}^3$. We denote by $\mathcal{K}$ the set of all oriented knots. Different knots will determine different (inequivalent) representations.

The parity of the representation is its handedness or orientation. The orientation reversing diffeomorphism $(x, y, z) \mapsto (x, y, -z)$ of $\mathbb{R}^3$ changes the handedness of the representation. There are exactly two orientations ($\mathbb{Z}_2 = \{\pm 1\}$). Different orientations determine different representations.

Global torsion is more subtle [78]. A genus one system has a global Poincaré section consisting of a disk D transverse to the flow. Imagine cutting $\mathcal{T}$ open along this disk, rotating one side of the cut q turns, then reconnecting. If the number of rotations is an integer, the flow will always match up smoothly afterward. This integer $q \in \mathbb{Z}$ is the global torsion. Different global torsions determine different representations.

[1] Technically, this is known as a deformation retraction and is a type of homotopy. The solid torus is homotopy equivalent to a circle.

If an embedding with representation labels $(\mathcal{K}, \mathbb{Z}_2, \mathbb{Z})$ in $\mathbb{R}^3$ is mapped into $\mathbb{R}^4$, there are fewer obstructions to isotopy, hence fewer representation labels and fewer distinct representations. It is well known that knots fall apart in $\mathbb{R}^4$: any two simple closed curves are isotopic. Since these curves represented the fundamental flow direction for the dynamical system, any two choices are equivalent in $\mathbb{R}^4$, and knot type disappears as a representation label. Parity also disappears. Global torsion is more complicated. Representations with different global torsions fall into two classes in $\mathbb{R}^4$ – all those with q even are equivalent to each other, all those with q odd are equivalent to each other, and the first class is inequivalent to the second. In short, the global torsion reduces to an integer mod 2. This phenomenon is related to the Dirac belt and Feynman plate tricks [16]. As a result, there is only a single label needed to distinguish representations in $\mathbb{R}^4$, and it has only two values ($\mathbb{Z}_2 = \{0, 1\}$). There are exactly two distinct representations of a genus one system in $\mathbb{R}^4$.

Finally, in $\mathbb{R}^5$ the single remaining representation label from $\mathbb{R}^4$ is lost and all representations are equivalent. There is an explicit isotopy taking the single remaining Dehn twist to the identity. The universal representation lives in this dimension. This progressive diminution of the rich structure of inequivalent representations with increasing dimension is summarized in Tab. 3.1.

Table 3.1: Representation labels for genus one systems. For parity $\mathbb{Z}_2 = \{\pm 1\}$, while for global torsion $\mathbb{Z}_2 = \{0, 1\}$. $\mathcal{K}$ denotes the set of oriented knots.

Representation	Obstructions to Isotopy		
Labels	$\mathbb{R}^3$	$\mathbb{R}^4$	$\mathbb{R}^5$
Global Torsion	$\mathbb{Z}$	$\mathbb{Z}_2$	-
Parity	$\mathbb{Z}_2$	-	-
Knot Type	$\mathcal{K}$	-	-

3.2 Mapping Class Group of the Solid Torus

The solid torus $\mathcal{T} = D^2 \times S^1$ is a three dimensional manifold whose boundary is the two dimensional torus, $\partial\mathcal{T} = S^1 \times S^1 = T^2$. A flow in $\mathcal{T}$ may be regarded as the the suspension of a map from the disk D^2 to itself, the Poincaré map. This manifold is to be considered abstractly and not as embedded in some Euclidean space.

Next we define some important simple closed curves in $\mathcal{T}$. The *core* of $\mathcal{T}$ in represented by the curve $\{0\} \times S^1$. Such a curve has no intrinsic dynamical meaning. If we denote the Poincaré map by ϕ, then the

Brouwer Fixed Point Theorem [7] guarantees that ϕ possesses a fixed point. The suspension of this fixed point is a period one orbit of the flow. If we so desired, we could define a *dynamical core* of the torus as this (or some other) period one orbit, though this is not necessary.

A simple closed curve γ in any surface S is called *essential* if it is non-separating in S, i.e. removing γ from S does not decompose the surface into two disjoint sub-surfaces. A *meridian* $\gamma \in \mathcal{T}$ is an essential curve in the boundary $\partial\mathcal{T}$ that bounds a disk $D \subset \mathcal{T}$ that is properly embedded in $\mathcal{T}$, i.e. such that $D \cap \partial\mathcal{T} = \partial D = \gamma$. This disk is called a *meridional disk*.

A *longitude* is a simple closed curve in $\partial\mathcal{T}$ that intersects some meridian transversely in a single point. A longitude represents a generator of $\pi_1(\mathcal{T})$ (and of H_1) and therefore cannot[2] bound a disk in $\mathcal{T}$. Longitudes and meridians are therefore distinct (See Fig. 3.1).

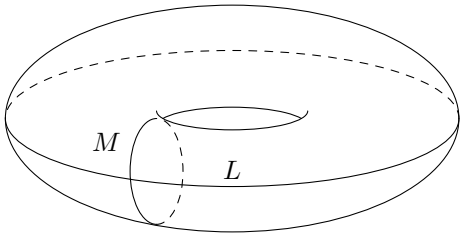

Figure 3.1: Longitude (L) and meridian (M) on T^2.

Any diffeomorphism of $\mathcal{T}$ induces a diffeomorphism of its boundary. However, a diffeomorphism of the boundary need not extend to all of $\mathcal{T}$. A necessary and sufficient condition for it to extend is that it preserve meridians (up to isotopy) [64]. Using this property, we will determine the mapping class group for $\mathcal{T}$ from the mapping class group of the torus, T^2.

To describe the mapping class groups we introduce a particular diffeomorphism called a *Dehn twist*. Let γ be a simple closed curve in an oriented surface S. A Dehn twist about γ is the isotopy class of a map determined as follows. Cut the surface along γ, twist one side 2π to the right and then reconnect along γ (see Fig. 3.2). This makes sense since S is assumed oriented. Note than a Dehn twist is obvious trivial if γ is separating.

If S is the boundary of a 3-manifold M and γ bounds a disk properly embedded in M (γ is homotopically trivial), then a Dehn twist about γ may be extended to a diffeomorphism of M. Consider a cylindrical

[2]Deforming through such a disk would provide a homotopy to the constant path.

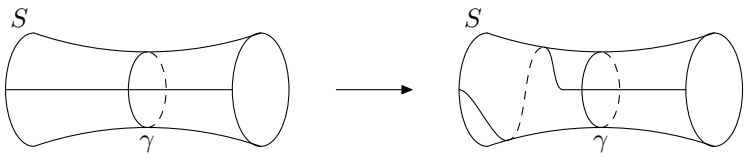

Figure 3.2: Illustration of a Dehn twist on a surface.

neighborhood of such a disk (the disk times an interval) and parametrize it by $(re^{i\theta}, s)$, with $s \in [0,1]$, where the disk is the set $(re^{i\theta}, 1/2)$. Then a Dehn twist about γ can be written as the map

$$(re^{i\theta}, s) \mapsto (re^{i(\theta+2\pi s)}, s). \tag{3.1}$$

We are essentially foliating the solid cylinder $D^2 \times [0,1]$ with parallel hollow cylinders $S^1 \times [0,1]$ and applying simultaneous Dehn twists to each leaf of the foliation. This map is continuous and smooth except for the edges. It may easily be smoothed by suitably damping the rotation with a bump function, defining a diffeomorphism which is the identity outside of this set.

The mapping class group of the torus, $\mathrm{MCG}(T^2)$, is linear and isomorphic the matrix group $GL(2,\mathbb{Z})$ [64]. This group acts as matrices on the first homology group $H_1(T^2) \cong \mathbb{Z} \oplus \mathbb{Z}$ with basis (L, M) consisting of a longitude and a meridian, respectively. An arbitrary element of this group can be written as a product of the three matrices

$$D_L = \begin{pmatrix} 1 & 1 \\ 0 & 1 \end{pmatrix}, \quad D_M = \begin{pmatrix} 1 & 0 \\ 1 & 1 \end{pmatrix}, \quad \text{and } S = \begin{pmatrix} 0 & 1 \\ 1 & 0 \end{pmatrix}, \tag{3.2}$$

and their powers. The first operation D_L is a Dehn twist about L, which preserves L and maps $M \to M + L$. The second operation D_M is a Dehn twist about M, which preserves M and maps $L \to L + M$. The third operation S interchanges M and L, has determinant -1, and thus reverses orientation. Since S swaps L and M, the first two operations are conjugate: $SD_MS^{-1} = D_L$. Thus D_M and S may be taken as generators.

In order for one of these diffeomorphisms to extend to the solid torus, it must preserve a meridian. This is equivalent to preserving the vector $(0,1)$ up to sign, since this homology element represents a meridional curve. Restricting attention to orientation preserving maps, it is easy to show that such a matrix must have

the form

$$\begin{pmatrix} \pm 1 & 0 \\ c & \pm 1 \end{pmatrix} = \begin{pmatrix} \pm 1 & 0 \\ 0 & \pm 1 \end{pmatrix} \begin{pmatrix} 1 & 0 \\ c & 1 \end{pmatrix} = \begin{pmatrix} 1 & 0 \\ c & 1 \end{pmatrix} \begin{pmatrix} \pm 1 & 0 \\ 0 & \pm 1 \end{pmatrix}, \tag{3.3}$$

where $c \in \mathbb{Z}$ and the signs are coherent. We see that the resulting subgroup is commutative and isomorphic[3] to $\mathbb{Z} \oplus \mathbb{Z}_2$. The first subgroup is generated by a Dehn twist about M, and the second is generated by an operation that simultaneously reverses the orientation of both M and L. Both operations preserve the orientation of T^2, and thus of $\mathcal{T}$ (when extended).

The second generator we call an *inversion* and can be visualized as followed. Embed $\mathcal{T}$ the standard way into $\mathbb{R}^3$ with rotational symmetry about the z-axis. Perform a π rotation about the x-axis taking $\mathcal{T}$ onto itself. It is apparent that this preserves longitudes and meridians setwise, but reverses their orientation. Both generators are illustrated in Fig. 3.3. Since a meridional disk represents a Poincaré section in $\mathcal{T}$, this group has the dynamical significance of describing all of the inequivalent (non-isotopic) suspensions of a given Poincaré map of D^2.

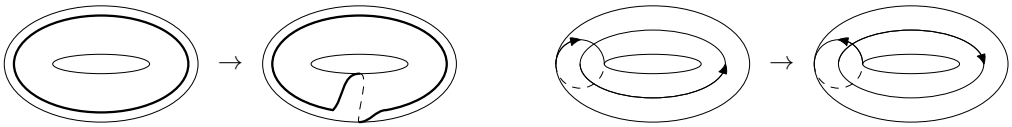

(a) Dehn Twist **(b)** Inversion

Figure 3.3: Generators of the torus mapping class group: Dehn twist (a) and inversion (b).

3.3 Three Dimensional Representations

Here we will describe in detail the spectrum of representations of genus one systems in dimension three. It is useful to parametrize points in $\mathcal{T} \cong D^2 \times S^1$ by $(re^{i\phi}, s)$. For the disk, $0 \leq r \leq 1$, $0 \leq \phi < 2\pi$ and $\phi = 0$ is identified with $\phi = 2\pi$, while for the circle $0 \leq s < 2\pi$ and $s = 0$ is identified with $s = 2\pi$. The mapping class group acts in this parameterization as follows:

$$\begin{array}{cccc} \mathbb{Z} & \text{Global Torsion} & (re^{i\phi}, s) & \rightarrow & (re^{i(\phi+ns)}, s) \\ \mathbb{Z}_2 & \text{Inversions} & (re^{i\phi}, s) & \rightarrow & (re^{-i\phi}, 2\pi - s) \end{array}. \tag{3.4}$$

[3] This same result was found in [86] through different means.

The global torsion n from the mapping class group represents one of the topological indices distinguishing the inequivalent representations of flows on a torus in $\mathbb{R}^3$. It is an invariant of embeddings into $\mathbb{R}^3$ since it may be calculated as the Gauss linking number of the core ($r = 0$ in the parametrization above) of the solid torus with a longitude in its boundary, and the linking number is invariant under ambient isotopy of the curves. In practice, global torsion appears as a systematic change in linking numbers between pairs of periodic orbits of an attractor [78, 65, 21].

It is clear that the operation of inversion is isotopic to the identity for the standardly embedded torus. Indeed, we represented its action on $\mathcal{T}$ through an ambient isotopy of $\mathbb{R}^3$. However, it is not immediately clear whether or not this operation is isotopic to the identity for an arbitrary embedding. Before describing inversion further, we must first describe the extrinsic embeddings.

There are two extrinsic indices that describe how the torus sits in $\mathbb{R}^3$ under the embedding. The first is knot-type, which arises as follows. The torus can be mapped into $\mathbb{R}^3$ so that its core follows any smooth closed curve. Each different knot in $\mathbb{R}^3$ provides a different embedding of the torus in $\mathbb{R}^3$. Actually, each knot provides *two* embeddings, which may or may not be equivalent. The argument is as follows. Position along a knot can be described by a real scalar parameter d that is periodic: d and $d + 2\pi m$ describe the same point on the knot ($m \in \mathbb{Z}$). The torus can be mapped along any knot in two opposite senses, with $s = d$ or $s = 2\pi - d$ (s here is the same as in Eq. (3.1)).

This degree of freedom is clearly related to the inversion degree of freedom ($\mathbb{Z}_2$) in the mapping class group, since $(2\pi - s = d) \leftrightarrow (s = 2\pi - d)$. When the two oriented knots obtained from an unoriented one are isotopic, they are called *inversion symmetric* [13]. Inversion symmetric knots provide equivalent representations of a torus in $\mathbb{R}^3$, while inversion asymmetric knots provide two inequivalent representations of a torus in $\mathbb{R}^3$. It is somewhat challenging to demonstrate inversion asymmetric knots. The simplest, 8_{17}, has eight crossings and is shown in Fig. 3.4 [13].

Oriented knot type provides the second topological index distinguishing inequivalent representations of a torus in $\mathbb{R}^3$. Note the interaction between the intrinsic (inversion) and extrinsic (knot type) parts of the problem, which leads to an absorption of the former into the latter. The intrinsic inversion index merges with extrinsic knot type to produce oriented knot type. On the other hand, since Dehn twists are trivial on the core

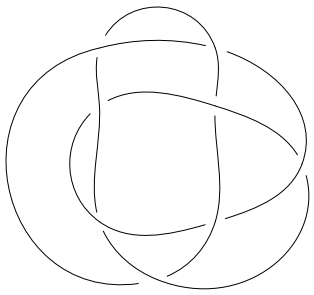

Figure 3.4: The simplest inversion asymmetric knot, 8_{17}.

knot, there is no interaction between twists and knot type. It is remarkable that the action of the mapping class group splits so cleanly.

The third and final index is parity, obtained under the isometry $(x^1, x^2, x^3) \rightarrow (x^1, x^2, -x^3)$ of $\mathbb{R}^3$. Unlike the previous operations, this one reverses the handedness of the torus as the Jacobian determinant for this diffeomorphism is negative. As was mentioned previously, this mapping cannot be isotopic to the identity, since the identity preserves orientation.

We conclude that the complete set of representation labels required to distinguish inequivalent embeddings into $\mathbb{R}^3$ are parity $\mathbb{Z}_2$, oriented knot type $\mathcal{K}$, and global torsion $\mathbb{Z}$. These labels represent the topological obstructions to isotopy in dimension three. These results are summarized in Tab. 3.1.

3.4 Four Dimensional Representations

When we increase the embedding dimension to four, we expect the extra room available for isotopy to overcome some of the obstructions to isotopy in dimension three. The result is fewer distinct representations. First, we show that the three dimensional representations with different parity or knot type are isotopic in this larger space. Consequently, these indices are no longer obstructions to isotopy, and the corresponding representations become equivalent in $\mathbb{R}^4$.

We change parity by lifting from $\mathbb{R}^3$ into $\mathbb{R}^4$, performing a rotational isotopy on the x^3-x^4 axes, then

projecting back down into $\mathbb{R}^3$ using the first three coordinates:

$$\begin{pmatrix} x^1 \\ x^2 \\ x^3 \end{pmatrix} \overset{\text{Inject}}{\longrightarrow} \begin{pmatrix} x^1 \\ x^2 \\ x^3 \\ 0 \end{pmatrix} \overset{\text{Isotopy}}{\longrightarrow} \begin{pmatrix} x^1 \\ x^2 \\ x^3\cos\theta \\ x^3\sin\theta \end{pmatrix} \overset{\text{Project}}{\underset{\theta=\pi}{\longrightarrow}} \begin{pmatrix} x^1 \\ x^2 \\ -x^3 \end{pmatrix}. \tag{3.5}$$

This operation has reversed the orientation of the z-axis in $\mathbb{R}^3$ through a smooth deformation in $\mathbb{R}^4$. The analogous operation for reversing the orientation of $\mathbb{R}^2$ in $\mathbb{R}^3$ is demonstrated in Fig. 3.5. The formula for this analogous operation may be found by setting either x^1 or x^2 to zero in Eq. (3.5). Notice that the projection is necessarily singular for some value of θ ($\pi/2$ in our parameterization).

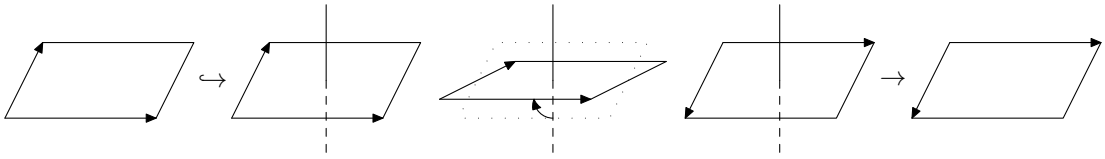

Figure 3.5: Reversing the orientation of $\mathbb{R}^2$ via isotopy in $\mathbb{R}^3$.

Next we consider equivalence in $\mathbb{R}^4$ of representations with different oriented knot type. It is well known that knots "fall apart" in $\mathbb{R}^4$ [64]. An analogous result holds for thickened knots or solid tori. First consider the knot defined by the core of the solid torus. By perturbing the embedding [64] it is possible to ensure that under planar projection $\pi : \mathbb{R}^3 \to \mathbb{R}^2$, the image has only a finite number of double points, each representing a single transverse intersection of the projected knot with itself. This result of transversality theory is sometimes called general position. These double points are called crossings. Choose any one of these crossings. Above it are two sections of the embedded solid torus (core), one above the other. We will show that the handedness of the solid torus crossing can be changed by isotopy in $\mathbb{R}^4$.

In the neighborhood of this projected crossing, the embeddings in the upper (U) and lower (L) tubular regions can be parametrized by

$$\begin{aligned} U:\ (x,y,z) &= (s_1, y_1, z_1 + g(s_1)) \\ L:\ (x,y,z) &= (x_2, s_2, z_2 - g(s_2)). \end{aligned} \tag{3.6}$$

The variables s_1 and s_2 parametrize the flow in the upper and lower tubes, respectively. The flow in the upper tubular region is in the x direction with $y_1^2 + z_1^2 \leq 1$, and the core of this tube is defined by $y_1 = z_1 = 0$. The flow in the lower tubular region is in the y direction with $x_2^2 + z_2^2 \leq 1$ and the core of this tube is defined by $x_2 = z_2 = 0$. The cores cross in the projection into $\mathbb{R}^2$ at $(x, y) = (0, 0)$. The two tubular regions miss by a large margin because of the offset in the z direction. The function $g(s)$ is a *bump function*[4] that is $+2$ in the neighborhood of the crossing (at $s_1 = s_2 = 0$) and drops to 0 before other double points are reached. The use of the bump function allows to localize the crossing to a small neighborhood while preserving the smoothness of the embedding.

Next we embed into $\mathbb{R}^4$ (x, y, z, w) by

$$\begin{aligned} U: &\quad (s_1, y_1, z_1 + g(s_1)\cos\theta, +g(s_1)\sin\theta) \\ L: &\quad (x_2, s_2, z_2 - g(s_2)\cos\theta, -g(s_2)\sin\theta) \end{aligned} \quad . \tag{3.7}$$

This mapping is an isotopy in $\mathbb{R}^4$ and has the effect of replacing right handed crossings in $\mathbb{R}^3$ (first three coordinates) by left handed crossings in $\mathbb{R}^3$ as θ varies from 0 to π as indicated in Fig. 3.6. One may think of this parameterization and mapping as foliating the cylinders U and L by streamlines or arcs. Each pair of arcs in U and in L defines a crossing in the sense of a knot, and each such crossing is swapped by rigidly moving the two foliations rigidly around each other in $\mathbb{R}^4$. By swapping appropriate crossings through this process, every embedded knotted torus can be isotoped in $\mathbb{R}^4$ to a torus that projects to the standard unknotted torus in $\mathbb{R}^3$, which is inversion symmetric. This eliminates knot type as a representation label in four dimensions.

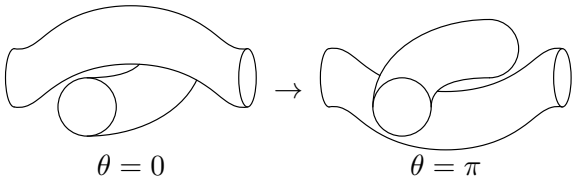

Figure 3.6: Projection of the knot type isotopy into $\mathbb{R}^3$.

This leaves only global torsion as a possible index to distinguish inequivalent embeddings of $\mathcal{T}$ into $\mathbb{R}^4$. We prove the rather surprising result that global torsion remains a partial invariant of embeddings into $\mathbb{R}^4$.

[4]Generally speaking, a bump function is any smooth, real valued function with compact support.

Specifically, we show that global torsion in $\mathbb{R}^4$ is defined mod 2; a pair of Dehn twists is isotopic to the identity, though a single Dehn twist is not. We do this by demonstrating a correspondence between the embeddings of $\mathcal{T}$ into $\mathbb{R}^4$ and the fundamental group of the Lie group $SO(3)$, which is isomorphic to $\mathbb{Z}_2$. We first introduce the technique by revisiting the global torsion in $\mathbb{R}^3$.

3.4.1 Global Torsion in $\mathbb{R}^3$ Revisited

Before discussing global torsion in four dimensions, we return to the situation in three dimensions in order to introduce a useful technique. We previously detected global torsion in $\mathbb{R}^3$ by computing the Gauss linking number of the core of $\mathcal{T}$ with a longitude in the boundary. This approach is difficult to generalize. The global torsion describes how many times the longitude in the boundary wraps around the core. Instead of using linking theory, we will calculate this quantity utilizing group theory. While these two approaches are essentially equivalent in $\mathbb{R}^3$, the latter permits a straightforward generalization to higher dimensions. We will now describe this latter approach in detail.

Let $\mathcal{T}$ be a solid torus embedded in the standard way into $\mathbb{R}^3$ (centered at the origin with rotational symmetry about the z-axis). Denote by γ the core of $\mathcal{T}$ and by δ the standard longitude in the boundary defined by the intersection of the xy-plane with $\mathcal{T}$. Note that δ and γ do not link. If we apply a single Dehn twist to $\mathcal{T}$, the image of δ is still a longitude in the boundary, but now it rotates around the core, completing one full rotation (see Fig. 3.7). If n Dehn twists are applied, the image of δ will make n full rotations. This n represents the global torsion.

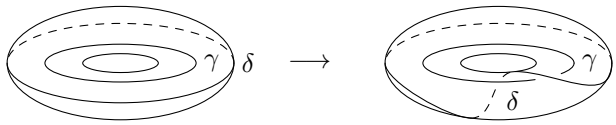

Figure 3.7: Dehn twist on the standard embedding.

We now make this idea more precise and in the process cast it in a form that applies to general embeddings. Again, start with the standard embedding of $\mathcal{T}$ with core γ and longitude δ in the boundary lying radially outward from γ. Instead of considering the longitude directly, we construct a vector field along γ that indicates how δ is twisting about γ. Begin with the unit vector field t that is tangent to γ at each point. Next, adjoin a unit vector field u that points radially outward from γ to δ. Finally, add a third unit vector field v orthogonal

to both t and u so that we have a positively oriented orthonormal basis of $\mathbb{R}^3$ at each point along γ (see Fig. 3.8).

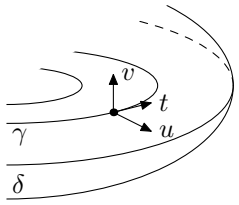

Figure 3.8: Orthonormal triad along γ.

Now consider an arbitrary embedding h of $\mathcal{T}$ into $\mathbb{R}^3$. Since an embedding is an immersion, it will carry the triad (t, u, v) at each $x \in \gamma$ onto a new triad $(\tilde{t}, \tilde{u}, \tilde{v})$ at $h(x)$ that is still linearly independent. However, the new triad need not be orthonormal. This may be remedied by applying the Gram-Schmidt process to the triad. First, normalize $\tilde{t}$ to obtain t'. This vector is still tangent to $h(\gamma)$. Next, remove the projection of $\tilde{u}$ onto t' and normalize to obtain u'. This only removes any shearing of $\tilde{u}$ into $\tilde{t}$ and not any twisting of $\tilde{u}$ about $\tilde{t}$. Finally, v' is obtained by removing the shearing of $\tilde{v}$ into u' and t' and normalizing. While this process is abrupt as described, it is possible to smoothly deform[5] the triad $(\tilde{t}, \tilde{u}, \tilde{v})$ into (t', u', v') [39].

Now we have three orthonormal vector fields along $h(\gamma)$ that describe the twisting of $h(\delta)$ about $h(\gamma)$. Notice that the vector field u' need not "point" directly to $h(\delta)$ because of distortions induced by the embedding. However, it does indicate the location of $h(\delta)$ in a more general sense which can be seen as follows. In the original standard embedding of $\mathcal{T}$ one can connect γ to δ with a ribbon (annulus) so that the vector fields t and u are tangent to the ribbon and v is normal. The image of this ribbon under h is a ribbon connecting $h(\gamma)$ to $h(\delta)$ with tangents t' and u' and normal v' along γ. Therefore, u' describes the direction one would start out on in the ribbon to reach $h(\delta)$. The twisting of $h(\delta)$ about $h(\gamma)$ is equivalent to the twisting of this attached ribbon.

We now desire a way to extract the global torsion from these vector fields. This can be done by calculating the total accumulated twisting in the fields as one traverses $h(\gamma)$. To do this, we need a way of comparing the triads at different points in a standard way. This is accomplished by *parallel transport* along $h(\gamma)$, which is a way to push vectors along $h(\gamma)$ that keeps initially parallel vectors parallel and normal vectors normal, but

[5] $SO(3)$ is a deformation retraction of $GL^+(3)$ and the two are homotopy equivalent.

otherwise does not alter them. Parallel transport does not here mean with respect to the ambient Euclidean space, but rather along the submanifold $h(\gamma)$. Equivalently, this means parallel transporting tangent vectors through the tangent bundle of $h(\gamma)$ and normal vectors through through the normal bundle of $h(\gamma)$ [17].

Of course, t' is always tangent by construction so we need not consider it further. Now, let n be some normal vector field along $h(\gamma)$. It is parallel transported if it obeys the equation

$$\dot{n} - \langle \dot{n}, t' \rangle t' = 0, \tag{3.8}$$

where the dot indicates differentiation with respect to arc length and the angle brackets indicate the inner product in the ambient Euclidean space. Essentially, to keep the vector field normal, one must remove any tangential component during the translation. This construction makes sense in any dimension. For further details see [17].

Now that we have a means of moving triads around $h(\gamma)$, it is possible to compare the frames at different points by transporting them all to a common location. Choose a reference point $x_0 \in h(\gamma)$. Parallel translate the triad at x_0 along $h(\gamma)$ to x. As mentioned above, the tangent vectors t' always coincide. Thus we need only compare the pair of vectors (u', v') in the space normal to t', which is an isomorphic copy of $\mathbb{R}^2$ (the fiber of the normal bundle above x_0). The transformation between a pair of orthonormal bases is an orthogonal transformation, which is an element of $SO(2)$. The transformation at x_0 (sending the frame at x_0 into itself) is the identity, and the transformations to the frames at each x vary continuously with x. So, for each $x \in h(\gamma)$, an element of $SO(2)$ is determined. All together, these elements determine a closed path in $SO(2)$ starting from and ending at the identity element.

We have succeeded in associating with an embedding h of $\mathcal{T}$ a loop through the identity in $SO(2)$ that encodes the global torsion. However, this path is not unique. We know that an embedding h_1 isotopic to $h_0 = h$ has the same global torsion, but this new embedding will determine a different curve in $SO(2)$. As may be guessed, these two curves are related by homotopy. Denote by h_s the isotopy from h_0 to h_1. Fix a point $p \in \gamma$ and let the image point $x_s = h_s(p)$ under each embedding be the reference point for comparing frames in each embedding h_s. We thus obtain a family of loops in $SO(2)$ through the identity that vary continuously in s, but this just says the curves are homotopic. We see that isotopic embeddings determine

homotopic loops in $SO(2)$. We conclude that global torsion depends only on the homotopy class of the loop in $SO(2)$.

It is known that $\pi_1 SO(2) \cong \mathbb{Z}$. Assuming that each of these classes is realized by some embedding, we have recovered the global torsion of $\mathbb{Z}$ in $\mathbb{R}^3$. To show that each class has some realization by an embedding, it is sufficient to consider the standard embedding of $\mathcal{T}$ into $\mathbb{R}^3$ with n Dehn twists applied. The original triad field on the untwisted $\mathcal{T}$ is given by (e_ϕ, e_r, e_z) and it is easy to see that these fields are parallel transported along γ. Thus the corresponding path in $SO(2)$ is the constant path at the identity which represents the trivial element $0 \in \mathbb{Z} \cong \pi_1 SO(2)$. If n Dehn twists are applied, the normal frame fields may be written concisely in complex notation by $e^{in\phi}(e_r, e_z)$. We have chosen representatives frames that twist around the core at a constant rate. The corresponding loop in $SO(2)$ makes n full rotations and represents the element $n \in \mathbb{Z}$. We conclude that global torsion is represented by an integer $(\mathbb{Z})$ in $\mathbb{R}^3$.

3.4.2 Global Torsion in $\mathbb{R}^4$

We now apply the method described in the previous section in order to determine the global torsion of embeddings in $\mathbb{R}^4$. Begin again with the standard $\mathcal{T}$ in $\mathbb{R}^3$ with core γ, standard longitude δ, and frame fields (t, u, v). Now let h be an arbitrary embedding of $\mathcal{T}$ into $\mathbb{R}^4$. This carries the orthonormal triad (t, u, v) onto a non-orthonormal triad $(\tilde{t}, \tilde{u}, \tilde{v})$, and the Gram-Schmidt process may be applied again to obtain an orthonormal triad (t', u', v'). Now adjoin the unique unit vector field w' which completes this triad to a positively oriented orthonormal basis of $\mathbb{R}^4$ at every point along $h(\gamma)$.

Choose a base point $x_0 \in h(\gamma)$, and parallel translate the frame at x_0 to every other $x \in h(\gamma)$ to compare frames. As before, the tangents are always identical, so we need only compare the vectors (u', v', w') in the space orthogonal to t', which is now a copy of $\mathbb{R}^3$. The transformations between triads is now an element in $SO(3)$, and by comparing the frames at every point along $h(\gamma)$ we obtain a loop in $SO(3)$ through the identity.

As before, the homotopy class of this path is an invariant under isotopy. The fundamental group in this case[6] is $\pi_1 SO(3) \cong \mathbb{Z}_2$, so that there are at most only two classes of global torsion in $\mathbb{R}^4$. It remains to show that each is represented by some embedding. To this end it is sufficient to lift the standard $\mathcal{T}$ in $\mathbb{R}^3$

[6]This says that two rotations of 3-space is continuously deformable to no rotation. Fundamentally, this is the reason for the existence of exactly two kinds of particle in physics – fermions and bosons.

with n Dehn twists applied into $\mathbb{R}^4$. The frame fields normal to t' are now given by $(e^{in\phi}(e_r, e_z), e_w)$ and the loops determined in $SO(3)$ describe n full rotations about the w-axis, which determines the element $n \mod 2 \in \mathbb{Z}_2$. A homotopy deforming a loop traversing $SO(3)$ "twice" to the constant loop is illustrated explicitly in Fig. 3.9, utilizing the homeomorphism $SO(3) \cong \mathbb{R}P^3$, the latter represented as the cube with identifications. We conclude that global torsion is represented by an integer mod 2 ($\mathbb{Z}_2$) in $\mathbb{R}^4$. Since we already know that knot-type and parity are no longer obstructions to isotopy in $\mathbb{R}^4$ this shows that there are exactly two representations in this dimension, and they differ by a single Dehn twist.

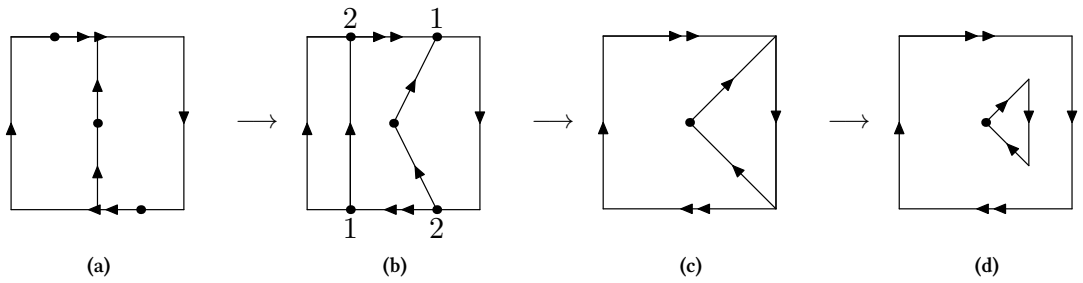

Figure 3.9: A loop traversing $\mathbb{R}P^3$ twice is homotopic to the constant loop. It is sufficient to perform the deformation in $\mathbb{R}P^2 \subset \mathbb{R}P^3$, represented as the square with identifications.

While the above proof was somewhat abstract, it is possible to see directly why two Dehn twists should be isotopic to the identity. Embed $\mathcal{T}$ in the standard way into $\mathbb{R}^3 \subset \mathbb{R}^4$. The xz-plane intersects the embedding along two disjoint disks, dividing $\mathcal{T}$ into two cylinders or handles. Cut open the embedding along these two disks and insert two Dehn twists, one at each disk, and reattach (see Fig. 3.10). Now, spinning the whole handle on one side of the xz-plane through one full turn converts the two Dehn twists into a writhe. Finally, the writhe may be removed by passing one part of the handle through another in $\mathbb{R}^4$ (c.f. Fig. 3.6), which results in the trivial embedding. This phenomenon is related to the well-known Dirac belt and Feynman plate tricks, which demonstrate that two rotations about an axis in $\mathbb{R}^3$ are isotopic to the identity[7] [16].

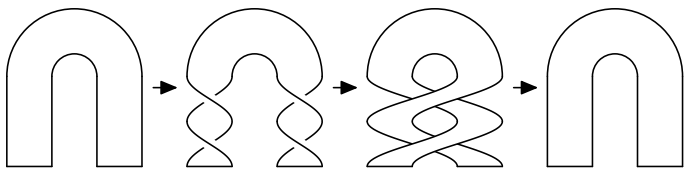

Figure 3.10: Isotopy of two Dehn twists to the identity in $\mathbb{R}^4$.

[7] It is also the reason for the existence of two types of particles in physics: Fermions and Bosons.

One may wonder whether a single Dehn twist is isotopic to the identity, but the preceding proof demonstrates that this is not the case. If two embeddings are isotopic, the curves determined in $SO(3)$ are homotopic, but the curves that correspond to zero and one Dehn twist belong to different classes in the fundamental group, so cannot be homotopic.

What makes this result so surprising is that γ and δ do not link in $\mathbb{R}^4$ when considered as just curves in $\mathbb{R}^4$. The fact that they are actually embedded within $\mathcal{T}$ provides the additional structure necessary to have them still "link" in a meaningful way. However, the triviality of the extrinsic embeddings does have an influence since it allows any two twists to annihilate, leaving a global torsion that is only defined mod 2. Incidentally, this shows why the linking number would be difficult to generalize. The linking number suggests an integer valued invariant rather than an integer mod 2.

The extra dimension obtained in passing from $\mathbb{R}^3$ to $\mathbb{R}^4$ allows a tremendous amount of freedom that overcomes almost every obstruction to isotopy existing in $\mathbb{R}^3$. Parity and knot-type are completely removed as obstacles to isotopy, and all these once separate representations become unified. By the exchange of twist and writhe, the triviality of knot-type allows for pairs of Dehn twists to become isotopic to the identity. The only obstruction remaining to isotopy in $\mathbb{R}^4$ is a single Dehn twist. We conclude that there are only two distinct representations in this dimension.

3.5 Five Dimensional Representations

There now only remains a one obstruction to isotopy - a single Dehn twist. However, the method utilized in the previous sections to analyze global torsion essentially fails in $\mathbb{R}^5$. Everything applies verbatim through the part when one arrives at the orthonormal frame (t', u', v') along $h(\gamma)$. At this point, there is no unique way to complete this frame to a frame of $\mathbb{R}^5$ since there is a two dimensional subspace to span. The pair of vectors may always be chosen so that the corresponding loop in $SO(4)$ the frames determine is represented by the trivial element in $\pi_1 SO(4) \cong \mathbb{Z}_2$.

This seems to indicate that the global torsion in $\mathbb{R}^5$ is trivial. This is in fact the case as we now verify directly. We construct an isotopy between representations that differ by a Dehn twist. First, lift $D^2 \times S^1$ into

$D^4 \times S^1$:

$$\begin{pmatrix} s \\ re^{i\phi} \end{pmatrix} \mapsto \begin{pmatrix} s \\ re^{i\phi} \\ re^{i(\phi+s)} \end{pmatrix}. \tag{3.9}$$

Now, define the isotopy by

$$\left(\begin{array}{c|cc} 1 & 0 & \\ \hline 0 & \cos\theta & \sin\theta \\ & -\sin\theta & \cos\theta \end{array}\right) \begin{pmatrix} s \\ re^{i\phi} \\ re^{i(\phi+s)} \end{pmatrix}. \tag{3.10}$$

This is in fact an isometry. This rotation effectively interchanges the two complex factors between $\theta = 0$ and $\theta = \pi/2$, so that the projection onto the first two components goes from an untwisted to a twisted torus. We see that global torsion is no longer an invariant in $D^4 \times S^1$ and, by the natural embedding, in $\mathbb{R}^5$.

Every degree of freedom has now been exhausted, and we have arrived at a *universal embedding* in $\mathbb{R}^5$. Every lower dimensional representation may be regarded as a non-singular projection of this universal attractor into the appropriate Euclidean space, where these representations are distinguished by the appropriate topological indices.

3.6 Résumé

We have worked out the program of representation theory for a restricted, but broad and important class of three dimensional dynamical systems: those whose natural phase space is the solid torus. Three topological indices are required to distinguish inequivalent embeddings into $\mathbb{R}^3$: parity, oriented knot type, and global torsion. Parity and knot type are extrinsic indices, while global torsion is an intrinsic index. When embeddings are lifted into $\mathbb{R}^4$, parity and knot type are no longer obstructions to isotopy, and the global torsion is reduced from $\mathbb{Z}$ to $\mathbb{Z}_2$. When the embedding space is further enlarged to $\mathbb{R}^5$, global torsion is also no longer an obstruction to isotopy. All embeddings into $\mathbb{R}^5$ are equivalent. This is the universal embedding. All distinct representations in lower dimensions are shadows or projections of this universal embedding. These results are summarized in Tab. 3.1.

Chapter 4: Representations of Higher Genus Systems

In this chapter we extend the program of representation theory to include all three dimensional dynamical systems. A dissipative three-dimensional dynamical system has a genus g handlebody as its natural phase space, $g \neq 2$. The representation theory for higher genus systems $g \geq 3$ consists in classifying the embeddings of handlebodies dressed with flows. As example of a higher genus system is the Lorenz system (with typical control parameter values), which lives inside a genus three handlebody, shown in Fig. 4.1. The caricature of this flow, its Birman-Williams projection or template [3, 4, 84], is also shown. This handlebody may be constructed as the union four trinions, two joining and two splitting. It is this decomposition of the genus three handlebody into four trinions that is shown in Fig. 4.1.

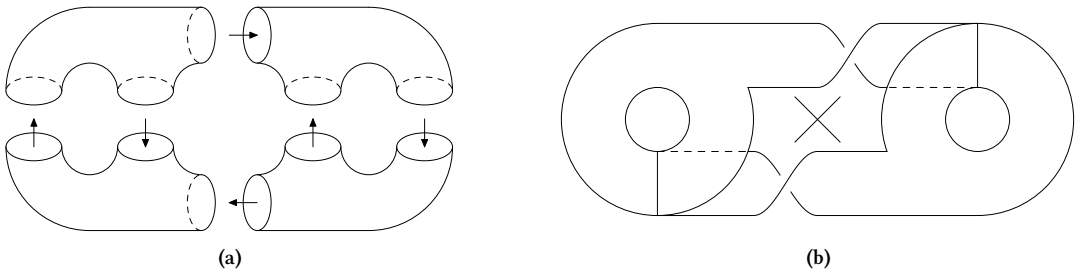

Figure 4.1: The Lorenz system: its genus three handlebody phase space (a) and template (b). The $\times$ denotes the central saddle.

As in the previous chapter, we begin with overview of results in Sec. 4.1, and then provide justification in Sec. 4.2. In Sec. 4.3 we use these results to make some observations on the links of periodic orbits. Sec. 4.4 is difficult. In it we provide a prescription for determining the fundamental groups of the complement of an embedded graph, which we then use to distinguish a few representations. We then make a few comments concerning cover and image systems in Sec. 4.5 and then conclude in Sec. 4.6.

4.1 Overview of Results

We now enumerate the representations of genus g systems in $\mathbb{R}^3$. The first representation label is oriented knot type $\mathcal{K}_g$, which is obtained as follows. A genus g handlebody has a core just as in the genus one case.

First, recall that the handlebody has a decomposition into $2(g-1)$ trinions. To obtain the core, shrink each of the $2(g-1)$ trinions onto a three legged graph or *dreibein* as illustrated in Fig. 4.2. Each leg of the dreibein inherits a flow direction or orientation from the flow directions through the ports of the trinion. The dreibein for a splitting (joining) trinion has 1 (2) inflowing leg and 2 (1) outflowing legs. The core of the handlebody is the union of the dreibein along common edges. This object is a directed graph of genus g with $2(g-1)$ trivalent vertices and $3(g-1)$ edges. This directed graph represents the fundamental flow directions of the dynamical system, just as the core circle did for genus one flows. The only difference is that the tearing in the system creates multiple flow directions, whereas when only folding is present there is just one. The collection of all oriented "knot types" $\mathcal{K}_g$ is the set of all embeddings of these directed genus g graphs into $\mathbb{R}^3$.

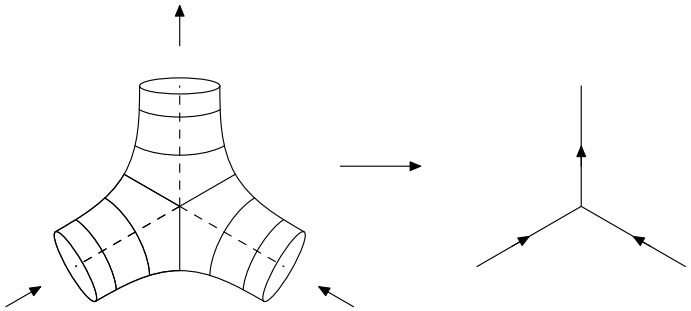

Figure 4.2: The core of a trinion (left) is a dreibein (right), obtained by collapsing the indicated disks onto points. Arrows indicate the flow directions. The pictured collapse is for a joining trinion. The collapse for a splitting trinion is obtained by reversing all arrows.

The second label is again parity. A handlebody has an orientation, and the mapping $(x, y, z) \mapsto (x, y, -z)$ reverses it. There are exactly two orientations $\mathbb{Z}_2 = \{\pm 1\}$, just as in the genus one case.

The last representation label is the analogue of global torsion. A genus g handlebody is constructed by gluing together $g-1$ splitting and $g-1$ joining trinions. All together, there are $3(g-1)$ such gluings (corresponding to the $3(g-1)$ graph edges above). The flow is always transverse to the port disks D_i where trinions are glued together. The union of these disks may be taken as a global Poincaré section for the flow, though for this purpose a smaller subset suffices [83]. The handlebody may be cut along any of these disks and one side rotated $q_i \in \mathbb{Z}$ turns before being reconnected. We thus obtain a spectrum of $3(g-1)$ *local* torsions $(q_1, \ldots, q_{3(g-1)}) \in \mathbb{Z}^{3(g-1)}$.

In three dimensions, in direct analogy with the genus one case, there is a triple of representation labels

$(\mathcal{K}_g, \mathbb{Z}_2, \mathbb{Z}^{3(g-1)})$: the oriented knot type, an orientation, and a spectrum of local torsions. We point out that the problem of distinguishing two knotted circles in $\mathbb{R}^3$ is difficult and still has no general solution. The corresponding problem for higher genus knotted graphs is correspondingly more difficult. Nevertheless, in simple cases it may be reasonable to distinguish embedded graphs "by inspection". Also, see Sec. 4.4 where we develop the fundamental group of the graph complement and use it to distinguish two embeddings.

In $\mathbb{R}^4$ many of these distinct representations become equivalent as obstructions to isotopy are lifted. Since graphs are essentially one dimensional objects, all of their embeddings in $\mathbb{R}^4$ are isotopic, just as all embedded closed curves are isotopic. Knotted graphs become unknotted just as knotted circles do. Oriented knot type is no longer a representation label. Parity also ceases to distinguish embeddings in the same way as before.

Once again, local torsion is more subtle. We anticipate that, in analogy with the genus one case, the local torsions at each of the $3(g-1)$ ports fall into two classes: q_i even and q_i odd. Thus the integer $\mathbb{Z}$ that characterized the torsion at each port is reduced to $\mathbb{Z}_2 = \{0, 1\}$. But this is not all. On any trinion, a single twist on any port can be translated into a pair of twists – one on each of the other two ports – at the expense of introducing a writhe or twisting of the legs near those ports. However, this writhing is easily pulled apart in $\mathbb{R}^4$ (see Fig. 4.3). This means that a single twist on any one port is fully interchangeable with a pair of twists, one on each of the other two ports. In other words, out of the three twists on each of the three ports of the trinion, only two are now independent. Instead of there being $3(g-1)$ $\mathbb{Z}_2$ local torsions, there are only $2(g-1)$. We conclude that in $\mathbb{R}^4$ there is only one representation label, a spectrum of $2(g-1)$ local torsions, $(q_1, \ldots, q_{2(g-1)}) \in \mathbb{Z}_2^{2(g-1)}$.

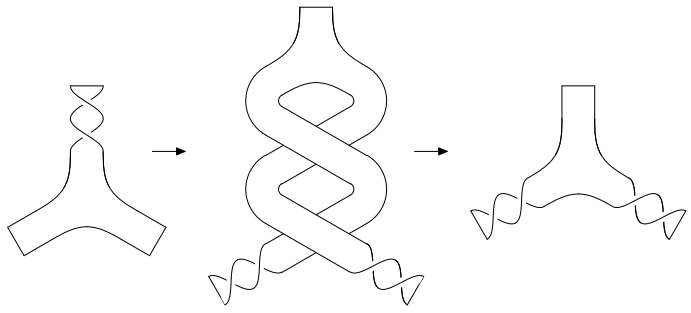

Figure 4.3: Conversion of a twist into two twists plus a writhe. The writhe is removed in $\mathbb{R}^4$ by an isotopy.

Finally, in $\mathbb{R}^5$ all representations become equivalent. The remaining local torsions become isotopic to

the identity exactly as in the genus one case. We arrive at a universal representation for genus g dynamical systems in five dimensions, which is two dimensions lower than that guaranteed by Wu ($2 \cdot 3 + 1 = 7$) [88]. The complete representation theory for genus g systems is summarized in Tab. 4.1.

Table 4.1: Representation labels for arbitrary genus systems. For parity $\mathbb{Z}_2 = \{\pm 1\}$, while for local torsion $\mathbb{Z}_2 = \{0, 1\}$. $\mathcal{K}_g$ denotes the set of oriented knotted graphs of genus g.

Representation	Obstructions to Isotopy		
Labels	$\mathbb{R}^3$	$\mathbb{R}^4$	$\mathbb{R}^5$
Local Torsion	$\mathbb{Z}^{3(g-1)}$	$\mathbb{Z}_2^{2(g-1)}$	-
Parity	$\mathbb{Z}_2$	-	-
Knot Type	$\mathcal{K}_g$	-	-

4.2 The Details

4.2.1 Mapping Class Group

We begin our justification of these results with a discussion of the mapping class group. The mapping class group for an arbitrary genus handlebody has been worked out [86]. Though the group is finitely presented, the list of defining relations is quite complicated. However, our concern is for handlebodies dressed with flows, and in this case the full mapping class group is unnecessary. We may forgo the full mapping class group for handlebodies by imposing the following dynamically natural constraint: we require that diffeomorphisms of the handlebody preserve the trinion decomposition. This *dynamical mapping class* group may be computed directly and is simple to describe. We first describe it. A handlebody is obtained by gluing trinions along distinguished disks, which are analogous to the meridional disk of $\mathcal{T}$. Just as in the genus once case, Dehn twists may be applied along each of these disks. There are three twists possible per trinion, but disks are identified in pairs when constructing the handlebody. This leaves $3(g-1)$ twists – one for every disk along which two trinions are glued. Each of these twists is independent. We conclude that the dynamical mapping class group of a handlebody of genus g, with a trinion decomposition, is $\mathbb{Z}^{3(g-1)}$, the abelian group generated by $3(g-1)$ Dehn twists.

While this dynamical mapping class group could be computed from the full mapping class group, it is easy to determine directly. The first step is to determine the mapping class group of one of the trinion units. Any diffeomorphism of the trinion must be fixed on the three distinguished disks that connect trinions to

each other. Hence we are to determine $\mathrm{MCG}(D^3;\partial)$. Consider the surface S defined as the boundary of the trinion with the interiors of the three attaching disks removed. The boundary of S consists of the boundaries ∂_i of the disks, $i \in \{1,2,3\}$. Any diffeomorphism of the trinion induces a diffeomorphism of S fixed on the boundaries ∂_i. On the other hand, any diffeomorphism of S (and fixed on the ∂_i), extends to the entire trinion. Moreover, since the mapping class group of a three-ball is trivial, this extension is unique (up to isotopy).

It therefore remains to determine the mapping class group of S, a sphere with n holes (fixed on the boundaries). This group is also known [86]. Define $I = \{1,2,\ldots,n\}$. Denote by d_i a Dehn twist about a curve surrounding (only) the i-th hole and by $d_{j,k}$ a Dehn twist about a curve surrounding (only) holes j and k. The generators of this group are d_i for $i \in I$ and $d_{j,k}$ for $j < k \in I$. The twists $d_{j,k}$ generate the pure braid group on n strands, considering the holes as braid strings.

We now specialize to the $n = 3$ case for writing down the relations satisfied by the generators. To simplify our notation we denote conjugation by $a * b = aba^{-1}$ and commutation by $[a,b] = aba^{-1}b^{-1}$. In this case we have generators d_i, $i \in I = \{1,2,3\}$ and $d_{j,k}$, for $(j,k) \in \{(1,2),(2,3),(1,3)\}$. The relations are

$$[d_i, d_j] = 1, \tag{4.1a}$$

$$[d_i, d_{j,k}] = 1, \tag{4.1b}$$

$$d_{1,2}^{-1} * d_{2,3} = d_{1,3} * d_{2,3}, \tag{4.1c}$$

$$d_{1,2}^{-1} * d_{1,3} = (d_{1,3}d_{2,3}) * d_{1,3}, \tag{4.1d}$$

$$\Delta^2 = d_1 d_2 d_3, \tag{4.1e}$$

$$d_k = d_{I_k}, \tag{4.1f}$$

where $I_k \equiv I - \{k\}$.

Relations (4.1a) and (4.1b) just say that hole twists mutually commute and commute with the pure braid generators. Relations (4.1c) and (4.1d) are the pure braid relations on three strings. In relation (4.1e), $\Delta^2 \equiv d_{1,2}d_{1,3}d_{2,3}$ is one full rigid rotation of all braid strings and is the generator of the center of the pure braid group. With this in mind, relation (4.1e) states that on S, the operation Δ^2 is isotopic to the identity modulo the twisting induced on each ∂_i. Finally, notice that the curve ∂_k is isotopic to the curve γ_k surrounding the

k-th disk, which in turn is isotopic to the curve γ_{I_k} surrounding the other two (see Fig. 4.4). We see then that the two operations d_k and d_{I_k} are both twists about this same curve. The only difference is which side of the curve is rotated by 2π. Since the two choices are equivalent, the two twists are isotopic, which is relation (4.1f).

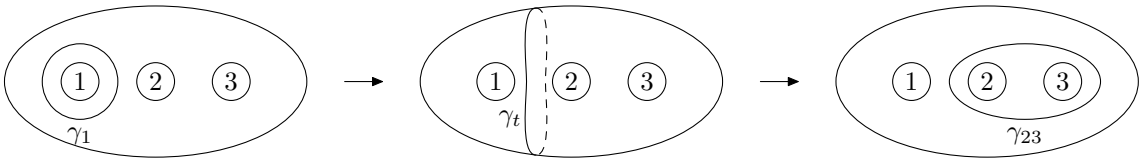

Figure 4.4: Isotopy of the curve γ_1 to γ_{23}.

We can use relation (4.1f) to eliminate the braid generators in favor of the boundary twists. This tremendously simplifying relation is unique to the $n = 3$ case. One can check that all the remaining relations (4.1b-4.1e) are then trivially satisfied. We conclude that the mapping class group of a trinion is $\mathbb{Z}^3$, the free abelian group generated by Dehn twists about each of the three boundaries, ∂_k.

Let us return to the handlebody decomposition. The $2(g-1)$ trinions are put together by connecting "in" and "out" ports between the them. Let ∂_i and ∂'_j be boundary curves on the ports of two distinct trinions. If these ports are identified, then twists about the two matched boundary curves must obey the relation $d_i^{-1} d'_j = 1$, since these two curves have been identified and are now the same curve. There are a total of $6(g-1)$ ports which are identified in pairs, each imposing an identification of twists. This leaves $3(g-1)$ generators. No additional constraints are imposed, and we conclude that the dynamical mapping class group of a handlebody of genus g, which respects the trinion decomposition, is $\mathbb{Z}^{3(g-1)}$. The independent twists could be taken on either all of the "in" ports or on all of the "out" ports.

We conclude that the spectrum of embeddings that lie in the same subset of $\mathbb{R}^3$ as the standard embedding are in one-to-one correspondence with $\mathbb{Z}^{3(g-1)}$. In other words, the dynamical mapping class group acts faithfully on the standard embedding. This gives us a spectrum of $3(g-1)$ locals torsion indices, one for each meridional disk between trinions.

4.2.2 The Core of a Manifold

One of the key steps in finding the three dimensional embeddings was the idea of mapping the handlebody along a graph or core. It is the purpose of this section to demonstrate how a core of a manifold may be used to help classify embeddings of that manifold. This will justify the conclusions of Sec. 4.1. We define the *core* N of a manifold M to be a subset (not necessarily a manifold) $N \subset M$ into which M may be deformed almost entirely through embeddings. More precisely, N is a core of M if there exists a smooth mapping $r : M \times [0,1] \to M$ which satisfies the following properties ($r_t(x) \equiv r(x,t)$):

1. $r_0 = \mathrm{id}$;
2. $r_1(M) = N$;
3. $r_t|_N = \mathrm{id}$ for every t;
4. $r_t(M - N) \cong \partial M \times (0, 1-t]$ for every $t \neq 1$.

We may summarize these properties by saying that r is a smooth strong deformation retraction of M into N that deforms M through embeddings for every $t \neq 1$.

The primary example is one we have already seen, viz. the core circle $N = \{0\} \times S^1$ of the torus $M = D^2 \times S^1$ (see Fig. 4.5). The retraction can be defined to be linear on each disk. If $y \in D^2$ then the retraction on each disk is $y \to (1-t)y$. For coordinates $x = (y, \theta)$ on $M = D^2 \times S^1$, the retraction is $(y, \theta) \mapsto ((1-t)y, \theta)$. We readily see that $r_0 = \mathrm{id}$, $r_1(x) = (0, \theta) \in N$, and $r_t|_N = \mathrm{id}$. For the last property, when $t \neq 1$ the mapping takes D^2 diffeomorphically onto a disk of radius $1-t$. But N intersects each disk at 0, and the image of $D^2 - \{0\}$ is the punctured disk of radius $1-t$, which we write as $\partial D^2 \times (0, 1-t]$. Since $\partial M = \partial D^2 \times S^1$ we have $r_t(M - N) = \partial M \times (0, 1-t]$.

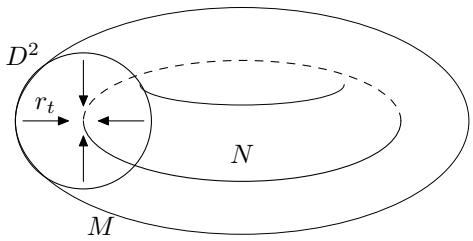

Figure 4.5: Core $N = \{0\} \times S^1$ of $M = D^2 \times S^1$.

Cores are not unique. It is helpful to choose a core that is as simple or minimal as possible. For the handlebodies considered here, N is a graph. There are many inequivalent graphs that could serve as a core, though they all have the same homotopy type. A unique graph is chosen by demanding that all vertices be trivalent.

Suppose that $f_i : (M, N) \to (M_i, N_i) \subset \mathbb{R}^n$, $i = 1, 2$, are two embeddings of the pair (M, N) into $\mathbb{R}^n$. We say that f_1 and f_2 are isotopic modulo $\mathrm{MCG}(M)$ if there exists a diffeomorphism g of M such that f_2 is isotopic to $f_1 \circ g$. The embeddings f_1 and f_2 thus determine the same subsets of $\mathbb{R}^n$ up to isotopy, but different permutations of the points of M within that subset unless g is isotopic to the identity. In other words, the same *extrinsic* embedding type.

We want to show that f_1 and f_2 are isotopic modulo $\mathrm{MCG}(M)$ if and only if N_1 and N_2 are isotopic. In other words, we wish to show that the extrinsic embedding type of f is determined by its restriction of the core, N. We will assume that the dimension of M is equal to n, the dimension of the Euclidean space into which it is being embedded.

First suppose that f_1 and f_2 are isotopic modulo $\mathrm{MCG}(M)$. Then the images N_1 and N_2 of N are isotopic. Specifically, N and $g(N)$ are isotopic, thus $f_1(N)$ and $f_2(N) = f_1 \circ g(N)$ are isotopic.

On the other hand, given the two embeddings f_i of M suppose that N_1 and N_2 are isotopic. Remove N from M to obtain embeddings of $M - N \cong \partial M \times [0, 1)$. We now "blow up" the hole where N used to be as follows. Define the smooth vector field $X = (0, h(t)\partial_t)$ on $\partial M \times [0, 1)$ where $h(t)$ is a smooth bump function that is zero for $t = 0$ and one for $t = 1$. Denote by X_i the image of X in $\mathbb{R}^n$ under f_i. Now deform the embeddings of $\partial M \times [0, 1)$ by flowing along X_i for time one. This process results in new embeddings which are isotopic to the original ones, respectively. Taking the closure of these embeddings yields embeddings of $\partial M \times [0, 1]$.

Since M has codimension zero in $\mathbb{R}^n$, $f_i(\partial M \times \{1\})$ may be regarded as the boundary of the blown up region. But then the sets $f_i(\partial M \times [0, 1])$ are *collars* of this boundary. The uniqueness of collars theorem (see e.g. Theorem 3.3 of [39]) states that there is an isotopy taking $f_1(\partial M \times [0, 1])$ onto $f_2(\partial M \times [0, 1])$ setwise, so that f_1 and f_2 agree up to an element of the mapping class group.

4.2.3 Local Torsion in $\mathbb{R}^4$

As in the genus one case, the Dehn twists generating the mapping class group are not all distinct in $\mathbb{R}^4$. We now examine this phenomenon in detail. Consider a trinion with boundary curves ∂_1, ∂_2, and ∂_3 about the distinguished disks, and consider the twist d_1 about ∂_1. As was shown in Fig. 4.3, an isotopy in $\mathbb{R}^3$ can undo this twist at the expense of braiding neighborhoods of the other two ports and inducing twists on them, and this braid may be undone by an isotopy in $\mathbb{R}^4$. The effect of this isotopy on the trinion mapping class group Eq. (4.1) is to modify the defining relation to the set

$$d_1 = d_2 d_3, \tag{4.2a}$$

$$d_2 = d_3 d_1, \tag{4.2b}$$

$$d_3 = d_1 d_2. \tag{4.2c}$$

We may therefore eliminate d_3 in favor of d_1 and d_2, whereupon the other two relations become equivalent to $d_1^2 = d_2^2 = 1$. Therefore, the mapping class group of a trinion is reduced from $\mathbb{Z}^3$ to $\mathbb{Z}_2^2$. Not only are the twists reduced mod 2, one entire twist is lost.

Since this isotopy fixes all ports, it readily extends to the whole handlebody. Each trinion has two ports of like type (both input or both output). Choose the independent twists to be about these two ports. Handlebodies are constructed by connecting trinions of alternating type: the output a splitting trinion goes to the input of a joining trinion, and *vice versa.* Since the independent twists were chosen on ports of like type, if the flow is from a joining trinion to a splitting trinion, neither identified port has a twist, and there are no relations imposed. On the other hand, if the flow is from a splitting trinion to a joining trinion, each of the identified ports has a twist. Only one is independent, and the total number of independent twists is reduced by half. There is therefore only one independent twist per trinion, and thus $2(g-1)$ independent twists in all. The embeddings into $\mathbb{R}^4$ are in one-to-one correspondence with the group $\mathbb{Z}_2^{2(g-1)}$.

4.3 Observations on Linking Theory in $\mathbb{R}^3$

Consider a handlebody with a trinion decomposition embedded into $\mathbb{R}^3$ in the standard way (cf. Fig. 4.6). Applying Dehn twists about the various meridional disks changes the linking numbers of various pairs of periodic orbits (simple closed curves). We can label periodic orbits by the sequence of meridional disks it passes through, in order. For example, consider the orbit aba, which circles hole 1, and $aedfaba$, which circles all holes, then hole 1. Both orbits move "clockwise." Dehn twists about a or b will alter the linking numbers of these two periodic orbits.

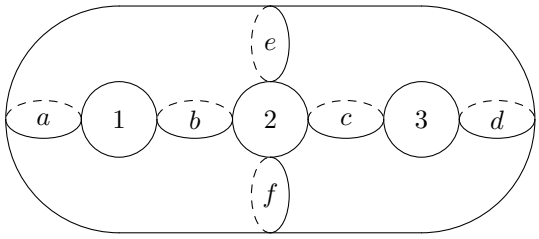

Figure 4.6: Genus three handlebody with holes labeled 1 through 3 and boundary curves defining Dehn twists labeled a through f.

The number of Dehn twists along disks a, b, c, and d can be determined uniquely by comparing the linking numbers of certain pairs of orbits. Curiously, this is not the case for the twists along e and f. For every time a periodic orbit passes through e it must also pass through f. This is because the union of e and f disconnect the handlebody, and each is a one-way door from one side to the other. As a result, linking numbers between orbits can only determine the sum of the twists along e and f, not each separately. Nevertheless, twists about e or f change the link type of certain pairs of periodic orbits in distinct ways, even if this cannot be measured by differences in linking numbers. Figure 4.7 shows the change of link type for a pair of orbits under a twist about e. If it were possible, within the handlebody, to move the twist to f, then by a π rotation of the entire handlebody this is equivalent to keeping twist at e, but having the orbit γ_1 that traverses the rightmost hole traversing the leftmost hold instead. The latter is not possible, since these two curves represent distinct elements of H_1. Note, moreover, that the curve γ_1, while an unknot in $\mathbb{R}^3$, is not trivial when confined to the handlebody. It is not isotopic to γ_2.

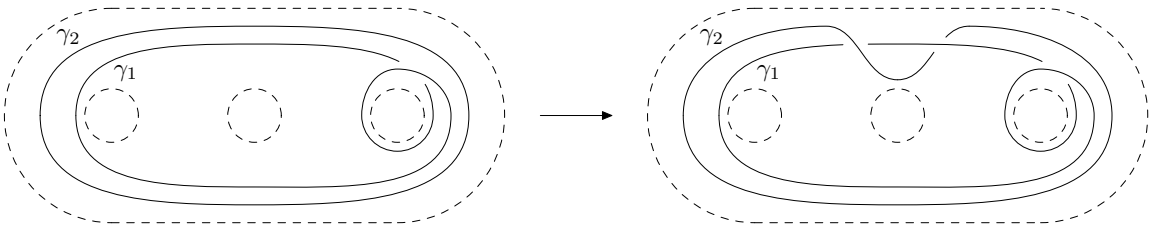

Figure 4.7: The change of the link type of two curves by a twist through e.

4.4 The Fundamental Group of a Graph Complement

For a knot $K : S^1 \to \mathbb{R}^3$, the fundamental group of the complement, $\pi_1(\mathbb{R}^3 - K)$, or *knot group* is a invariant of knot type. Given any knot, there is a standard algorithm providing a representation of the group, the *Wirtinger presentation* [64]. We slightly augment this algorithm so that it applies to any embedded graph.

Here is a brief summary of the result. Start by looking down upon a planar projection of the embedded graph and choose the base point to be the observation point (your eye). We then decompose the projected graph into a series of arcs (see Fig. 4.8). At each crossing, the lower arc is cut in two where the upper arc crosses it. The upper arc is not cut. At each trivalent vertex, all three arcs are cut at the vertex point. We may define non-trivial loops from the base point that "circle around" each of these arcs. These loops generate the fundamental group. At crossings and vertices there are certain obvious relations that hold among these generators (see Fig. 4.9). These relations are complete.

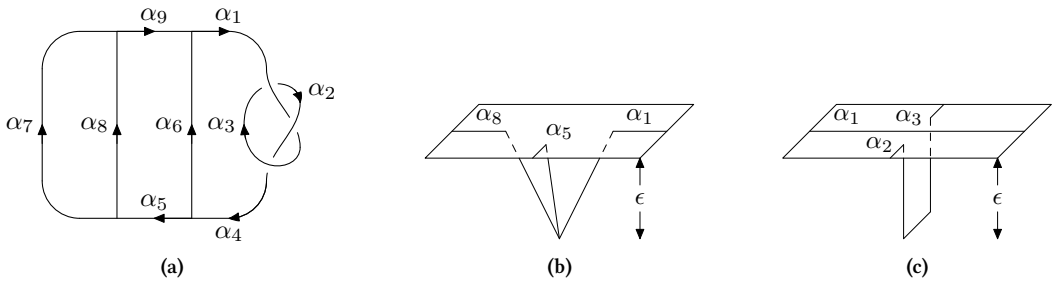

Figure 4.8: Graph embedding for π_1: planar projection (a) and the behavior in the neighborhood of vertices (b) and crossings (c).

We now proceed to justify this result. Denote the embedded graph of genus g by K, and construct a planar representation of it. This may be accomplished by projection into a generic plane, just as for knots. Decompose the planar graph into a series of n oriented arcs α_i, whose end points are determined by every

crossing and trivalent vertex. We can restore the crossings (and therefore an embedding) by connecting the appropriate arcs with line segments that dip down a distance ϵ below the plane (see Fig. 4.8). In much the same way we restore the trivalent vertices by adjoining line segments that meet at the vertex point, which is now placed as $-\epsilon$ as well. Note that the arcs on each side of a crossing and the three arcs about a vertex have distinct labels (in general).

To be definite, let $* = (0, 0, 1)$ be the base point. We can construct loops based at $*$ that run around each arc α_i as follows. Draw an arrow x_i passing from right to left beneath α_i (i.e. so that the crossing (α_i, x_i) is positive. See Fig. 4.9). The loop is the straight line segment from $*$ to the tail of x_i, then along x_i, and finally from the head of x_i straight back to $*$. We will use the same symbol x_i to denote the loop as denotes the arrow.

Each crossing yields an obvious relation among these loops. This relation takes one of two forms depending on the sign of the crossing. Suppose the upper arc is labeled α_k and the lower arc (which has been divided into two) is given by α_i on one side and α_j on the other (see Fig. 4.9). If the crossing is positive we have the relation

$$x_i x_k = x_k x_j, \tag{4.3}$$

and if it is negative we have the relation

$$x_k x_i = x_j x_k. \tag{4.4}$$

Finally, if arcs α_i, α_j and α_k meet at a vertex we have the relation (see Fig. 4.9)

$$x_j x_k = x_i, \tag{4.5}$$

or something similar, depending on the directions of the arcs at the intersection.

We wish to prove that this set of generators and relations is complete. In order to do this we will decompose the graph complement into simpler pieces. The tool which allows us to relate the fundamental groups of the simpler pieces to the whole is van Kampen's theorem [64]:

Theorem 4.1 (van Kampen). *Suppose that a space X may be written as the union $X = X_1 \cup X_2$, and further*

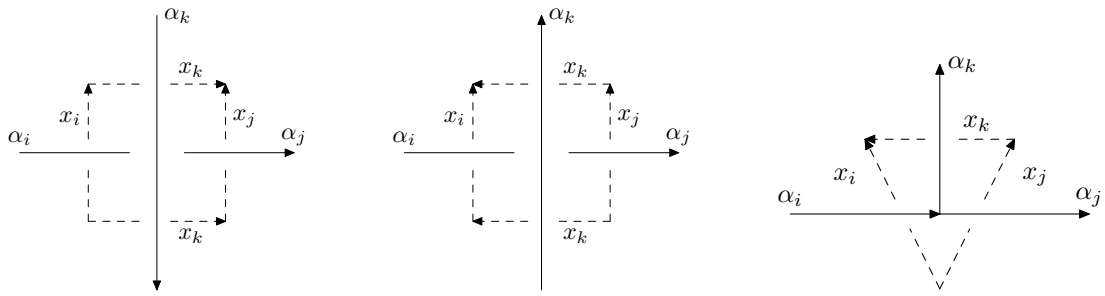

(a) $x_i x_k = x_k x_j$ **(b)** $x_k x_i = x_j x_k$ **(c)** $x_j x_k = x_i$

Figure 4.9: Arrows representing basic loops and the relations for positive crossings (a), for negative crossings (b), and for vertices (c).

suppose that X_1, X_2, and $X_0 = X_1 \cap X_2$ are each non-empty and path connected. Then, if we have the presentations

$$\pi_1(X_1) = (x_1, \ldots; r_1, \ldots) \tag{4.6}$$

$$\pi_1(X_2) = (y_1, \ldots; s_1, \ldots) \tag{4.7}$$

$$\pi_1(X_0) = (z_1, \ldots; t_1, \ldots), \tag{4.8}$$

then $\pi_1(X)$ has the presentation

$$\pi_1(X) = (x_1, \ldots, y_1, \ldots; r_1, \ldots, s_1 \ldots, \iota_{1\#}(z_1) = \iota_{2\#}(z_1), \ldots), \tag{4.9}$$

where $\iota_j : X_0 \hookrightarrow X_j$ are the inclusions. In other words, one combines the presentations for $\pi_1(X_1)$ and $\pi_1(X_2)$ and adds relations stating that the images of each generator of $\pi_1(X_0)$ in $\pi_1(X_1)$ and $\pi_1(X_2)$ are equal.

Now we may state and prove our

Theorem 4.2. *The fundamental group of $\mathbb{R}^3 - K$, $G(K)$ is generated by the loops $x_1, \ldots x_n$, one for each arc in the planar projection, and for each incidence of arcs one of the three relations 4.3, 4.4, or 4.5 depending on whether it is a positive crossing, negative crossing, or trivalent vertex, respectively.*

Proof. To begin, define the decomposition of $\mathbb{R}^3 - K$ as $A \cup B_1 \cup \cdots \cup B_n \cup C$ as follows. Recall that the

graph K lies in the region $\{0 \geq z \geq -\epsilon\}$. Let $A = \{z \geq -\epsilon\} - K$. The lower boundary of A is the plane $z = -\epsilon$ with m line segments $\beta_1, \ldots, \beta_m$ defining the under crossings and $2(g-1)$ points defining the trivalent vertices removed. Construct a solid rectangular box beneath each arc β_i and vertex point whose top coincides with the bottom of A. Since the number of crossings and vertices are finite, the boxes can be chosen small enough to be disjoint. Define B_i as the union of this box with a straight line segment from the top of the box to $*$ which misses K, (see Fig. 4.10). Finally, define C to be the closure of the complement of $A \cup B_1 \cup \cdots \cup B_n$, along with an arc running to $*$ (and missing K).

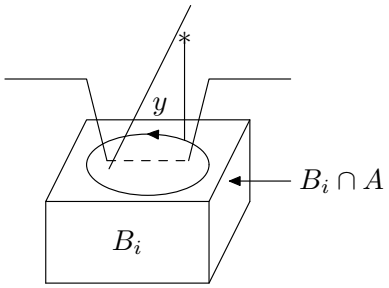

Figure 4.10: The sets B_i. The path y generates $\pi_1(B_i \cap A)$.

Now, A is an infinite slab with n arcs removed, each of whose endpoints are in the ∂A. There are also segments removed from ∂A associated with crossings. The interiors of these segments may be added back in, preserving the homotopy type of A. In the same way, the triples of arcs meeting at vertex points may be perturbed so that the arcs now meet in three distinct points in ∂A. Thus, we may replace A with a homotopically equivalent set consisting of an infinite slab with n arcs removed, where each arc has distinct end point in ∂A. By construction, none of these arcs knot any others. We may now deform (homotopy) A into a finite slab with n straight line segments removed, running from one boundary component to the opposite one. This slab may be retracted onto an n-punctured plane and finally to an n-petaled rose. It is thus apparent that $\pi_1(A) = F_n$, the free group with n generators. These generators can be taken to be $x_1, \ldots, x_n$, the curves that run about each arc. This sequence of alternations is presented in Fig. 4.11.

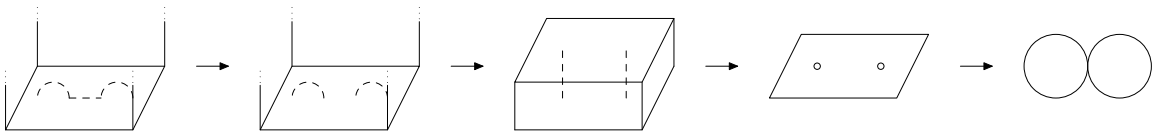

Figure 4.11: Sequence of homotopies to more easily compute $\pi_1(A)$.

Each B_i is simply connected. In the case of a crossing, the set $B_i \cap A$ is a planar rectangle missing the segment β_i with the line segment to $*$ attached. This intersection is homotopy equivalent to a circle, so that $\pi_1(B_i \cap A)$ is infinite cyclic with generator y (see Fig. 4.10). The case of a vertex is similar: $B_i \cap A$ is a planar rectangle missing a point with a line segment to $*$ attached. Again we see that $B_i \cap A \simeq S^1$ and π_1 is cyclic with generator y. By van Kampen's theorem $\pi_1(A \cup B_i)$ has generators $x_1, \ldots, x_n$ and the single relation expressing y in terms of the x_i, which is one of relations previously considered. Each B_i may be adjoined in the same way. Finally, the sets C and $C \cap (A \cup B_1 \cup \cdots \cup B_n)$ are simply connected, so adjoining C does not change π_1. □

As an example, consider the following three graphs representing genus three embeddings (Fig. 4.12). Applying the above theorem to K_1 we obtain the presentation

$$(x_1, \ldots, x_6 \mid x_1 = x_2x_6, x_1 = x_3x_2, x_6 = x_4x_5, x_2 = x_4x_5). \tag{4.10}$$

Using the relations, the generators x_1, x_2, and x_6 may be eliminated. The remaining relations become trivial and we have

$$G(K_1) \cong (x_3, x_4, x_5;) \cong F_3, \tag{4.11}$$

where F_k denotes the free group on k generators.

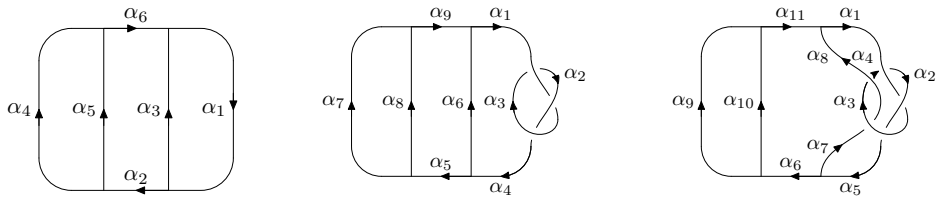

(a) K_1 **(b)** K_2 **(c)** K_3

Figure 4.12: Three genus three embeddings differing by knot type. K_1 (a) is the standard embedding, K_2 (b) has a trefoil in one branch, and K_3 (c) has a trefoil and two braided branches.

In fact, we can easily generalize this to arbitrary genus:

Theorem 4.3. *If K is the standard embedding of genus g graph, then $G(K) \cong F_g$, the free group on g generators.*

Proof. We proceed by induction. For the standard genus one embedding, or standard unknot, $G \cong \mathbb{Z} \cong F_1$ [64]. Now suppose we have the standard embedding of genus $g-1$, and we turn this into the standard embedding for genus g by adding a line segment (see Fig. 4.13). We can describe the group in the genus g case as F_{g-1} together with the new generators x_2, x_3, and x_4, as well as the two relations $x_3 = x_4 x_1$ and $x_2 = x_4 x_1$. Thus x_2 and x_3 may be eliminated, and we are left with $F_{g-1} * F_1 \cong F_g$ (the free product of free groups is free). □

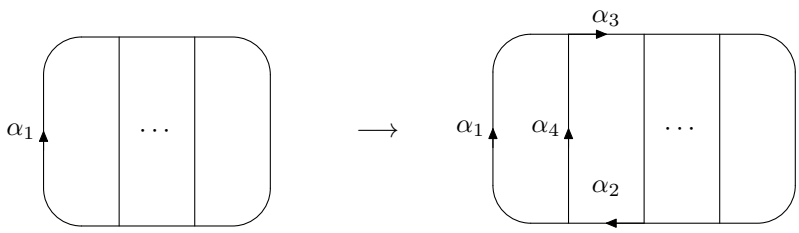

Figure 4.13: Induction step for Thm. 4.3.

Now consider K_2. From Fig. 4.12 we obtain the presentation

$$(x_1, \ldots, x_9;\, x_3x_1 = x_1x_2, x_1x_2 = x_2x_3, x_2x_3 = x_3x_4, \\ x_4 = x_6x_5, x_1 = x_6x_9, x_5 = x_8x_7, x_9 = x_8x_7). \tag{4.12}$$

We may use the last four relations to eliminate x_4, x_5, x_6, and x_9. This results in

$$(x_1, x_2, x_3, x_7, x_8;\; x_3x_1 = x_1x_2, x_1x_2 = x_2x_3, x_2x_3 = x_3x_1). \tag{4.13}$$

Eliminating x_3 leaves the presentation

$$(x_1, x_2, x_7, x_8;\; x_1x_2x_1 = x_2x_1x_2), \tag{4.14}$$

which is isomorphic to the free product of the group of the trefoil [64] and F_2: $\pi_1(K_2) \cong G(\text{trefoil}) * F_2$. By defining $a = x_1x_3$ and $b = x_1x_3x_1$, the trefoil group can be written in the perhaps more familiar form $G(\text{trefoil}) \cong (a, b;\; a^3 = b^2)$.

Finally, consider K_3. From Fig. 4.12 we obtain the presentation

$$\begin{aligned}(x_1,\ldots,x_{11};\, x_4x_1 = x_1x_2, x_1x_2 = x_2x_3, x_2x_3 = x_3x_5, x_8x_3 = x_3x_7, x_4x_8 = x_8x_3,\\ x_5 = x_7x_6, x_1 = x_8x_{11}, x_6 = x_{10}x_9, x_{11} = x_{10}x_9).\end{aligned} \tag{4.15}$$

Using the last four relations to eliminate x_5, x_6, x_8, and x_{11} yields

$$\begin{aligned}(x_1,x_2,x_3,x_4,x_7,x_9,x_{10};\, x_4x_1 = x_1x_2 = x_2x_3 = x_3x_7x_{10}x_9,\\ x_3x_7 = x_1x_9^{-1}x_{10}^{-1}x_3 = x_4x_1x_9^{-1}x_{10}^{-1}).\end{aligned} \tag{4.16}$$

The relations in the first row may be used to eliminate x_2 and x_4, while the relations in the bottom row may be used to eliminate x_7. This results in

$$(x_1,x_3,x_9,x_{10};\; x_1x_9^{-1}x_{10}^{-1}x_3x_{10}x_9 = x_9^{-1}x_{10}^{-1}x_3x_{10}x_9x_3). \tag{4.17}$$

We may use this relation to isolate and eliminate x_1, yielding the free group on three generators, $G(K_3) \cong F_3$.

We conclude that $G(K_1) \cong G(K_3) \cong F_3$ and that $G(K_2) \cong G(\text{trefoil}) * F_2$. Now, the factors of a free product are subgroups of the product and by the Nielsen-Schreier theorem [69] any subgroup of a free group is free. Since $G(\text{trefoil})$ is not free, the groups $G(\text{trefoil}) * F_2$ and F_3 are not isomorphic, and we may conclude that the graphs K_1 and K_3 are distinct from K_2.

On the other hand, since K_1 and K_3 have the same groups, we cannot yet decide whether or not they are equivalent. In this case, the groups come out equivalent because the graph embeddings are homotopy equivalent. A sequence of homotopies taking K_3 into K_1 is demonstrated in Fig. 4.14. Notice that this sequence of homotopies involves sliding one branch along another. This homotopy is *not* an isotopy since the sliding operation does not preserve vertex number or valences. The two graphs are in fact inequivalent, since periodic orbits that pass through the branch with the trefoil generally have non-trivial knot types. In particular, the periodic orbit following the outer cycle of the graph is itself a trefoil.

We have given in Thm.4.2 a presentation for the fundamental group of a graph complement by generalizing the Wirtinger presentation for knot groups. As we have seen, computing and comparing the fundamental

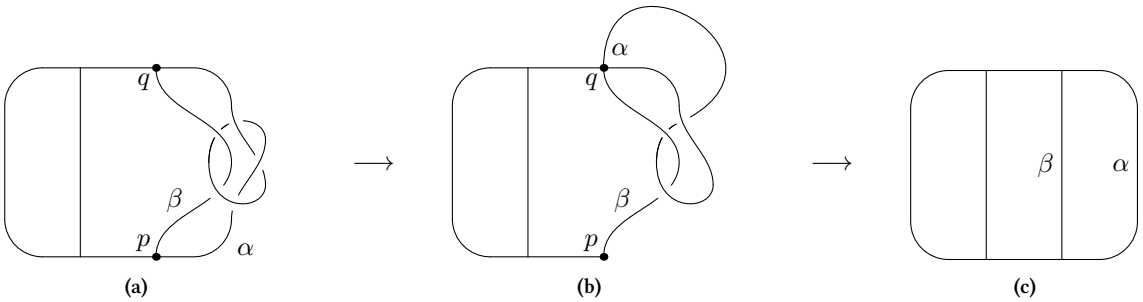

Figure 4.14: Sequence of homotopies from K_3 to K_1. From (a) to (b) the end of the knotted branch α is slid along branch β from point p to point q. From (b) to (c) the loop α above point q is rotated about point q (back to front), α is then slid back from q to p along β, and then everything is straightened out.

groups of graphs is a non-trivial process. One may suggest passing to the abelianization, H_1. However, this invariant is not much use as it is sensitive only to the genus of the graph, and not at all to its knot type. First, extend $\mathbb{R}^3$ to S^3 by adding a point at infinity[1] We then have

$$H_1(S^3 - K) \cong H_1(K) \cong \mathbb{Z}^g. \tag{4.18}$$

The first isomorphism is known as Alexander duality [7]. The second isomorphism follows at once from the Mayer-Vietoris sequence, noting that a genus g graph has the homotopy type of a one point union of g circles.

4.5 Covers and Images

In this section we make a few comments concerning cover and image systems. Let (X, ϕ) and (Y, ψ) be two manifolds with flows. A (topological) conjugacy between X and Y is a diffeomorphism $f : X \to Y$ that commutes the flows, $\psi(f(x), t) = f(\phi(x), t)$ for all points $x \in X$ and times $t \in \mathbb{R}$. If we drop injectivity, then f is a semi-conjugacy. Since the mapping f is surjective, it may be thought of as a covering map. If the covering is even, that is, if $\operatorname{card} f^{-1}(p)$ is independent of $p \in Y$, we will refer to $f : X \to Y$ as a *cover-image* relation between X and Y. X is the cover, Y the image, and f the covering map. An important instance of this relation is when X is equivariant[2] under some symmetry group G, f is a symmetry modding map, and the image system Y possess less or even no symmetry. In such cases f is necessarily non-injective since f

[1] The is called the one-point compactification.

[2] A dynamical system is equivariant if the vector field possesses a symmetry. Such systems are studied more extensively in Chaps. 5 and 6.

reduces the degree of symmetry by identifying symmetry related domains.

A simple, but important, example is provided by the Lorenz and proto-Lorenz systems (see Fig. 4.15). The cover is the Lorenz system, which has a two-fold rotational symmetry. The image is the proto-Lorenz system, which is obtained by identifying the two symmetry related domains in the cover. Since the cover has rotational symmetry, the image system is obtained by applying the local diffeomorphism [26]

$$\begin{aligned} u_1 &= x^2 - y^2 \\ u_2 &= 2xy \\ u_3 &= z, \end{aligned} \tag{4.19}$$

to the cover system. Equivalently, an image without symmetry is obtained by a differential embedding based on a symmetry-invariant observation function, such as z (see Chap. 5).

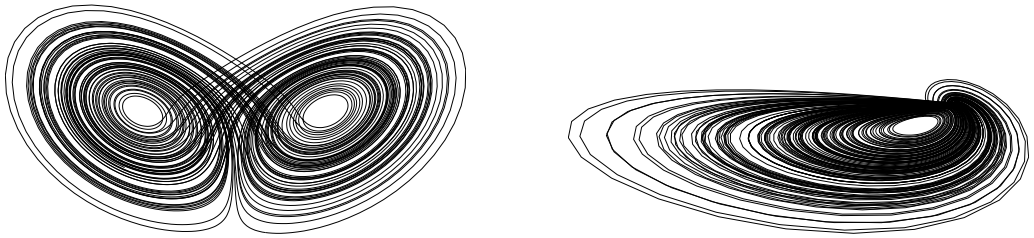

(a) (b)

Figure 4.15: The Lorenz system (a) with a two-fold rotation symmetry, and the proto-Lorenz system (b) without symmetry.

Conversely, an image Y may be *lifted* to a cover X, often with symmetry, through a local diffeomorphism g. Given a covering map $f : X \to Y$, g is constructed from the local inverses of f. Of course, g cannot be a mapping, since if f is $n \to 1$, then g must be $1 \to n$. It is perhaps better to think of using f to pull back the dynamical system on Y to X.

In three dimensions, cover and image systems will often possess phase spaces of different genus. Recall that a handlebody of genus g may be constructed as the connected sum of g solid tori. We expect an $n \to 1$ image map f to identify n of these tori summands to one in the image. However, this is not the only behavior possible. More generally, some tori may be identified with themselves in an $n \to 1$ fashion. Thus, the image handlebody need not have genus g/n if the cover has genus g.

For example, the Lorenz dynamical system is contained in a bounding torus of genus $g = 3$. The central hole is centered at the origin, which belongs to the fixed point set of the equivariance group. Equation 4.19 provides a $2 \to 1$ covering map from the genus three Lorenz system to the genus one proto-Lorenz system, modding out the symmetry. The outer two solid tori of the Lorenz system are symmetry related, so become identified in the image. The central torus is symmetry related to itself, so becomes identified with itself in a $2 \to 1$ manner. This suggests the image should have genus two, although no dynamical system lives in a genus two handlebody (see Chap. 1). In fact, the flow does not go "around" this torus at all. This hole is spurious and may be "sewn up", resulting in an image system with genus one. This is most apparent at the level of the branched manifolds [26].

The relation that exists between the phase spaces of cover-image systems suggests an investigation from the point of view of representation theory. Let (X, ϕ) and (Y, ψ) be two handlebodies with flows, denote by h_X and h_Y diffeomorphisms of X and Y respectively, and let ϕ' and ψ' be the image flows. Then consider the diagram

$$\begin{array}{ccc} (X,\phi) & \xrightarrow{h_X} & (X',\phi') \\ {\scriptstyle f_1}\big\downarrow & & {\scriptstyle f_2}\big\downarrow \\ (Y,\psi) & \xrightarrow{h_Y} & (Y',\psi') \end{array} , \tag{4.20}$$

where f_1 and f_2 are two covering maps. A fundamental question is: given any three maps in Eq. (4.20), can the fourth be found so as to complete the diagram?

The simplest case is when all maps except one of the covering maps are given, which we take to be f_2. In this case, we may simply take $f_2 = h_Y f_1 h_X^{-1}$. This works since h_X and h_Y are diffeomorphisms preserving flows and f_1 is an image map. This says that given a cover-image relation $f_1 : X \to Y$, arbitrary diffeomorphic copies X' of X and Y' of Y also possess a cover-image relation. In particular, X' and Y' may be representations that are not equivalent to X and Y, that is, h_X and h_Y need not be trivially isotopic.

However, even if $f_1 : X \to Y$ is a symmetry reducing cover, it does not follows that f_2 is as well. This is because (geometrical) symmetry is not a diffeomorphism invariant and need not be preserved by h_X. Consider again the Lorenz system. We can create new representations by applying Dehn twists along any of the six curves in Fig. 4.6. However, in order for symmetry to be maintained, we must apply twists simultaneously along symmetry related curves, e.g. e and f. So, if (X, ϕ) is equivariant under a group G, equivariance is

preserved by applying simultaneous Dehn twists to symmetry related ports between trinions. If Dehn twists are added asymmetrically, then (X, ϕ') will not generally be equivariant at all, so there is no symmetry for f_2 to mod out.

Suppose now that both covering maps f_i are given, so that we have two distinct cover-image pairs, and one of h_X or h_Y. An immediate necessary condition is that f_1 and f_2 must both be $n \to 1$ with the same n. However, this is not sufficient. The group $G \cong \mathbb{Z}_2$ can act in many ways on three dimensional systems. One is through π rotations in the xy-plane; another is reflection about this plane. A dynamical system equivariant under the first action, such as the Lorenz system, is connected, whereas it is clear that a system equivariant under the second is disconnected (the xy-plane is an invariant set that disconnects the phase space). Systems of both types can be obtained from lifts of the proto-Lorenz system, but are obviously not diffeomorphic because of their different connectedness properties [26].

However, it is not necessary for X and X' to be equivariant under the same representation of the same group. For instance, take X to be the rotationally equivariant Lorenz system, and take X' to be the parity equivariant induced Lorenz system. We saw in Chap. 5 that while the induced system is not even a representation in three dimensions, it is in four dimensions, and is in fact isotopic to the inclusion of the Lorenz system there. Hence, though f_1 and f_2 mod different symmetries, the two systems are diffeomorphic, in fact isotopic.

Two different lifts of the same image are locally diffeomorphic to each other. Consider two lifts X_1 and X_2 of the same image Y. We obtain the diagram

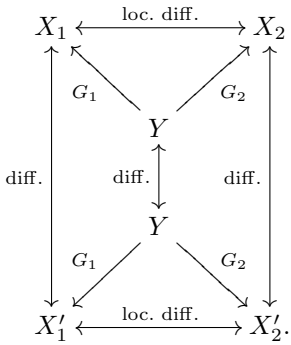

(4.21)

Here, the arrows from Y to X_1 and X_2 represents lifts with symmetries G_1 and G_2, respectively. The vertical arrows are diffeomorphisms giving changes in representation, and the horizontal arrows are local

diffeomorphisms.

4.6 Résumé

We have successfully extended representation theory from the three dimensional dynamical systems of genus one considered in the previous chapter to systems of arbitrary genus $g \geq 3$. For three-dimensional embeddings, three topological indices are required to distinguish inequivalent representations. Two of these indices are extrinsic: parity and oriented knot type, and one is intrinsic: a spectrum of $3(g-1)$ local torsions. In four dimensions, the two extrinsic indices fall away as the extra dimension allows sufficient room for isotopy. The intrinsic index is also affected, suffering a reduction $\mathbb{Z} \to \mathbb{Z}_2$. The number of independent local torsions is also reduced $3(g-1) \to 2(g-1)$. All labels fall away in five dimensions. There is therefore a universal embedding in $\mathbb{R}^5$ for every three dimensional dynamical system of any genus, and all lower dimensional representations are projections of this universal embedding. These results are summarized in Tab. 4.1.

We conclude that some of the information obtained by analyzing any three-dimensional embedding of a three dimensional dynamical system depends on the embedding (knot type, parity, and global/local torsion), while the rest is embedding independent. However, since the universal embedding exists in $\mathbb{R}^5$ (or higher), any information extracted from a five-dimensional embedding must be intrinsic – it depends on the dynamics alone and not at all on the embedding.

Chapter 5: The Lorenz system - A Case Study

Ideally an embedding of an N-dimensional dynamical system is N-dimensional. Ideally, an embedding of a dynamical system with symmetry is symmetric. Ideally, the symmetry of the embedding is the same as the symmetry of the original system. Differential embeddings of the Lorenz system, which possesses a two-fold rotation symmetry, are not ideal. The presence of symmetry poses a significant constraint on the embedding problem for dynamical systems. In this chapter we examine the Lorenz system in detail. Some of the conclusions of this chapter will be generalized in the following chapter.

The motivation for a detailed study of this system is as follows. In Chap. 4 we identified all inequivalent representations of the Lorenz system in $\mathbb{R}^3$. The standard differential embedding of the Lorenz attractor based on the x (the "induced" Lorenz system) or y coordinate produces a system not included in this list of inequivalent representations. Specifically, there is no embedding of the Lorenz phase space into $\mathbb{R}^3$ whose attracting set is homeomorphic to the attracting set of the induced system. We sought to determine how this could be possible. This is a non-trivial question. The answer to this question and more is provided below.

In general, reconstructions of dynamical systems with symmetry pose a special problem. According to Takens' theorem it is necessary to use a generic observation function for a reconstruction. However, generic functions are not symmetric, and an embedding made using a non-symmetric observable also lacks symmetry. Worse, King and Stewart [38] showed that while an observable with some symmetry can be used for an embedding, the embedding typically does not possess the same symmetry as the original dynamical system. This was shown explicitly by Letellier and his colleagues [43] for the Lorenz dynamical system. In particular, they showed that using an observation function that is odd under the two-fold rotation symmetry of the Lorenz attractor will result in a dynamical system with inversion rather than rotation symmetry.

In Sec. 5.1 we introduce the Lorenz ($\mathcal{L}$) and induced Lorenz ($\mathcal{L}_i$) systems. In Sec. 5.2 we examine in detail the differential mappings constructed from the x-coordinate of $\mathcal{L}$ and decide when they furnish embeddings. Singularities found to be present in these mappings are analyzed in Sec. 5.3 where they are shown to be consequences of the different symmetries of $\mathcal{L}$ and $\mathcal{L}_i$. This shows that a three-dimensional reconstruction

of the Lorenz system with parity symmetry is never an embedding. In Sec. 5.4 we show that $\mathcal{L}$ and $\mathcal{L}_i$ are related by a "local reflection" of $\mathbb{R}^3$ and are in fact isotopic in $\mathbb{R}^4$. We extend this analysis in Sec. 5.5 to the bounding tori and branched manifolds of the two systems. In Sec. 5.6 we generalize the observation in [43] that equivariant embeddings of the Lorenz system are parity symmetric to arbitrary dynamical systems with a two-fold symmetry. We also demonstrate how reconstructions with arbitrary two-fold symmetry may be recovered from a generic observation function. Finally, we state our conclusions in Sec. 5.7.

5.1 The Lorenz and Induced Lorenz Systems

The Lorenz dynamical system $\mathcal{L}$ is a flow on $\mathbb{R}^3$ defined by the equations

$$\dot{x} = \sigma(y - x) \tag{5.1a}$$

$$\dot{y} = Rx - y - xz \tag{5.1b}$$

$$\dot{z} = -bz + xy, \tag{5.1c}$$

where σ, R, and b are control parameters. We make no assumptions on the values of these parameters other than $\sigma \neq 0$. A dynamical system $\dot{x} = v(x)$ is said to be equivariant under a linear transformation M if $M\dot{x} = v(Mx)$. The Lorenz system is equivariant under the transformation $R_z(\pi) : (x, y, z) \mapsto (-x, -y, z)$, which is a π rotation about the z-axis. We say that $\mathcal{L}$ possesses rotation symmetry or is rotationally equivariant. The Lorenz branched manifold [3, 4, 43] is shown in Fig. 5.1. It too is rotationally symmetric. This template is obtained from the standard "mask" by rotating each of the two lobes of the mask through 90 degrees in opposite directions, and then viewing the attractor from above. This template transformation procedure preserves the topological organization of the periodic orbits and the symmetry of the system. This transformation is described in more detail in [26, 42].

A differential embedding of the Lorenz system based on the x-coordinate constructs the so-called "induced Lorenz system", $\mathcal{L}_i$. Unlike the original system $\mathcal{L}$, the induced system is equivariant under the transformation $P : (X, Y, Z) \mapsto (-X, -Y, -Z)$, which is an inversion. We say that $\mathcal{L}_i$ possesses parity symmetry or is parity equivariant. The induced Lorenz branched manifold [43], which is also parity symmetric, is shown in Fig. 5.2. The explicit equations describing this embedding are given in the next section.

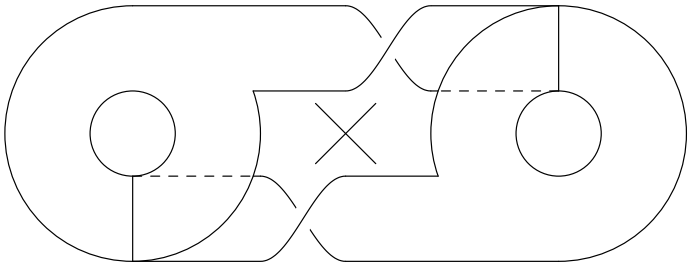

Figure 5.1: Template for the Lorenz system $\mathcal{L}$ with rotation symmetry, $R_z(\pi)$. The "$\times$" denotes the central saddle fixed point. The x and y directions are in the page, horizontal and vertical respectively. The z direction is out of the page.

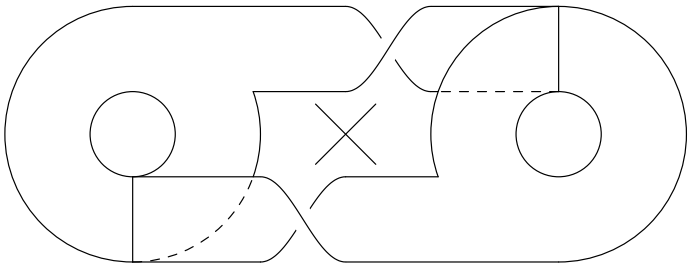

Figure 5.2: Template for the induced Lorenz system $\mathcal{L}_i$ with parity symmetry, P. The "$\times$" denotes the central saddle fixed point. The coordinate axes are the same as Fig. 5.1.

The induced system passes the usual embedding tests and is regarded as an embedding of the original dynamical system into $\mathbb{R}^3$ [67]. While this is essentially true on the attracting set, we claim that the mapping giving rise to this "embedding" is in fact not an embedding on any open subset containing the attractor and therefore does not truly represent the entire original flow. We prove this claim in the next section. The attracting sets of both the Lorenz and the induced Lorenz system are shown in Fig. 5.3.

5.2 Differential Mappings

Recall that if M is an m-dimensional manifold with flow φ_t, and if $f : M \to \mathbb{R}$ is a real-valued observation function on M, then Takens' theorem (Thm. 1.40) states that generically the map $M \to \mathbb{R}^{2m+1}$ given by

$$x \mapsto \left(f(x), \left.\frac{d}{dt}\right|_0 f(\varphi_t(x)), \ldots, \left.\frac{d^{2m}}{dt^{2m}}\right|_0 f(\varphi_t(x)) \right), \tag{5.2}$$

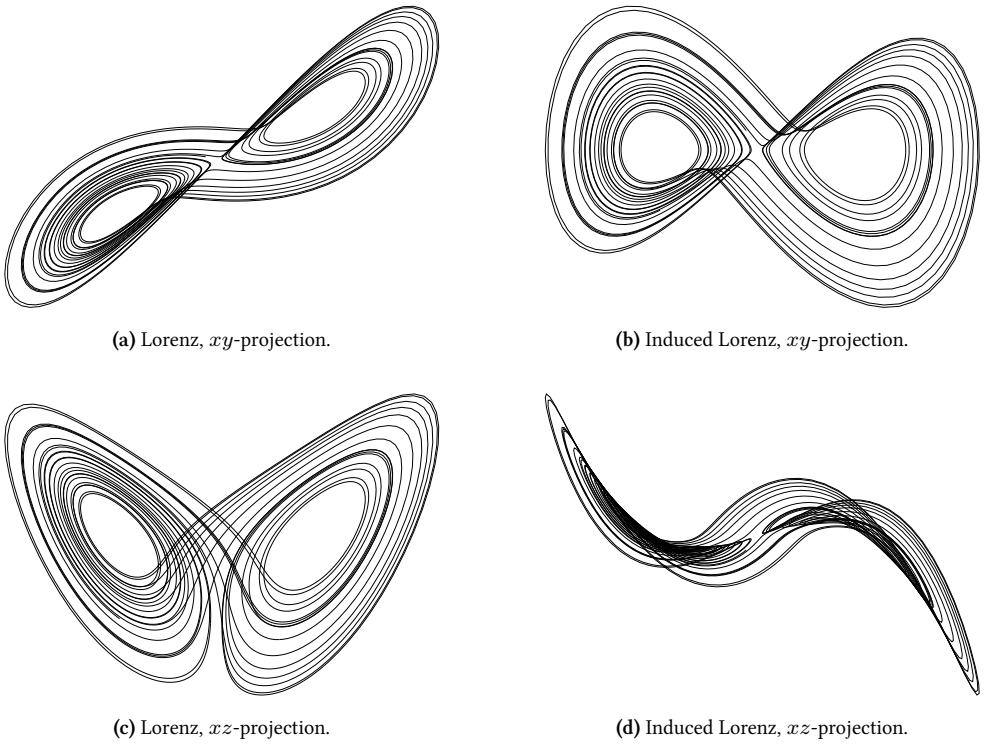

(a) Lorenz, xy-projection.

(b) Induced Lorenz, xy-projection.

(c) Lorenz, xz-projection.

(d) Induced Lorenz, xz-projection.

Figure 5.3: Projections of the Lorenz and induced Lorenz attractors. The first row shows that both attractors possess $(x, y) \to -(x, y)$ symmetry. The bottom row shows that the Lorenz system has no z symmetry while the induced system has $(x, z) \to -(x, z)$ symmetry.

is an embedding. This theorem all but guarantees that the differential embedding of $\mathcal{L}$ constructed from x and its first six derivatives is an embedding into $\mathbb{R}^7$. This leaves open the question of whether an embedding may be found in lower dimensions, which ought to be the case since $\mathcal{L}$ was originally defined in $\mathbb{R}^3$.

Consider $\mathcal{L}$ with observation function $f(x) = x$ and define the series of differential mappings

$$F_n(x) = \left(x, \frac{dx}{dt}, \ldots, \frac{d^{n-1}x}{dt^{n-1}} \right), \tag{5.3}$$

for each $n \geq 3$. The mapping F_3, which gives rise to the system $\mathcal{L}_i$ in $\mathbb{R}^3$, is explicitly given by

$$\begin{pmatrix} X \\ Y \\ Z \end{pmatrix} = \begin{pmatrix} x \\ \sigma(y - x) \\ \sigma(R + \sigma - z)x - \sigma(1 + \sigma)y. \end{pmatrix}. \tag{5.4}$$

Note that F_3 is antisymmetric under $R_z(\pi)$: $F_3(-x,-y,z) = -F_3(x,y,z)$. The Jacobian of the transformation is

$$J_3 = \begin{pmatrix} 1 & 0 & 0 \\ -\sigma & \sigma & 0 \\ \sigma(R+\sigma-z) & -\sigma(1+\sigma) & -\sigma x \end{pmatrix}. \tag{5.5}$$

The Jacobian determinant is $-\sigma^2 x$, so the mapping is singular on the entire yz-plane. By setting $x = 0$ in F_3 one sees that the mapping collapses lines of constant y onto points in the yz-plane, and this is the only set where F_3 fails to be injective. This demonstrates that F_3 is not a diffeomorphism on any open set intersecting the yz-plane ($x = 0$). Since the attractor cuts this plane, we conclude that F_3 fails to be a diffeomorphism on any neighborhood containing the attractor.

The existence of these singularities has been known [43, 44, 45]. In these references, the singularities are interpreted as obstructions to an observation function well-sampling an attractor, a property called observability. However, since the set of singularities has measure zero it has been tacitly assumed that that they do not affect whether or not one actually obtains an embedding of the phase space. In other words, obtaining an embedding of the attractor is distinct from and less restrictive than obtaining an embedding of the entire phase space. A three-dimensional differential embedding of the Lorenz system based on the x coordinate accomplishes the former task, but not the latter. This is why the induced Lorenz system does not appear on the list of inequivalent representations of the Lorenz system – in $\mathbb{R}^3$ it is not a representation at all.

It is straightforward to derive the equations describing the image flow under F_3 expressed in the new variables (X, Y, Z). We include them for completeness. They are

$$\dot{X} = Y \tag{5.6a}$$

$$\dot{Y} = Z \tag{5.6b}$$

$$\begin{aligned} \dot{Z} = {} & b\sigma(R-1)X - b(1+\sigma)Y - (1+b+\sigma)Z \\ & - X^2 Y - \sigma X^3 + \frac{Y}{X}\left(Z + (1+\sigma)Y\right), \end{aligned} \tag{5.6c}$$

and the parity symmetry is apparent [28, 29]. Notice the $1/X$ behavior in the $\dot{Z}$ equation. The behavior of

the vector field as $X \to 0$ is direction dependent. In particular, if $Z = -(1+\sigma)Y$ then the last term in $\dot{Z}$ vanishes for every X. Notice that according to Eq. (5.4) $X = 0$ exactly when $x = 0$, but then $Y = \sigma y$ and $Z = -\sigma(1+\sigma)y$, or equivalently $Z = -(1+\sigma)Y$, which is precisely the condition that the image vector field be well behaved (cf. Eq. (5.6c)).

Before moving on we give the LU-decomposition of $J_3 = L_3U_3$ which will be useful in the sequel. We have

$$U_3 = \begin{pmatrix} 1 & 0 & 0 \\ 0 & \sigma & 0 \\ 0 & 0 & -\sigma x \end{pmatrix} \quad \text{and} \quad L_3 = \begin{pmatrix} 1 & 0 & 0 \\ -\sigma & 1 & 0 \\ \sigma(R+\sigma-z) & -1-\sigma & 1 \end{pmatrix}. \tag{5.7}$$

In this case singularities in U_3 (when $x = 0$) correspond to singularities in J_3.

Now consider the differential mapping F_4 into $\mathbb{R}^4$. We will show that this mapping *does* provide an embedding of $\mathcal{L}$. To simplify formulas we introduce the abbreviations $A = 1+b+2\sigma$, $B = \sigma(R+\sigma+1)+1$, and $C = R+2R\sigma+\sigma^2$, which are constants depending only on the control parameters. The map F_4 is given by

$$\begin{pmatrix} X \\ Y \\ Z \\ W \end{pmatrix} = \begin{pmatrix} x \\ \sigma(y-x) \\ \sigma(R+\sigma-z)x - \sigma(1+\sigma)y \\ \sigma z(Ax-\sigma y) + \sigma y(B-x^2) - \sigma Cx. \end{pmatrix}, \tag{5.8}$$

where the first three coordinate are of course the same as F_3, given in Eq. (5.4).

The top 3×3 sub-matrix of the Jacobian J_4 is J_3, so that in the LU-decomposition $J_4 = L_4U_4$, U_4 has main diagonal[1] equal to that of U_3 and the top-left 3×3 block of L_4 is L_3. In full, we have

$$U_4 = \begin{pmatrix} 1 & 0 & 0 & 0 \\ 0 & \sigma & 0 & 0 \\ 0 & 0 & -\sigma x & 0 \end{pmatrix} \quad \text{and} \quad L_4 = \begin{pmatrix} 1 & 0 & 0 & 0 \\ -\sigma & 1 & 0 & 0 \\ \sigma(R+\sigma-z) & -1-\sigma & 1 & 0 \\ \sigma Az - \sigma(2xy+C) & B-\sigma z-x^2 & \sigma\dfrac{y}{x} - A & 1 \end{pmatrix}. \tag{5.9}$$

It is apparent that U_4 can fail to have maximal rank only if $x = 0$. However, L_4 contains a term propor-

[1] The main diagonal of a non-rectangular matrix is the diagonal starting from the upper left entry.

tional to $1/x$, and so the rank of U_4 does not indicate the rank of J_4 in this limit. If one first sets $x = 0$ in J_4, in the new LU-decomposition $L_4'U_4'$ we obtain

$$U_4' = \begin{pmatrix} 1 & 0 & 0 & 0 \\ 0 & \sigma & 0 & 0 \\ 0 & 0 & -\sigma^2 y & 0 \end{pmatrix} \quad \text{and} \quad L_4' = \begin{pmatrix} 1 & 0 & 0 & 0 \\ -\sigma & 1 & 0 & 0 \\ \sigma A z - \sigma C & B - \sigma z & 1 & 0 \\ \sigma(R + \sigma - z) & -(1+\sigma) & 0 & 1 \end{pmatrix}. \tag{5.10}$$

The matrix U_4' has maximal rank unless $y = 0$, and L_4' is regular for all (x, y, z). We conclude that F_4 is singular only along the z-axis, which is disjoint from the Lorenz flow (it is the stable manifold of the central fixed point). We conclude that F_4 provides an embedding of $\mathcal{L}$ into $\mathbb{R}^4$. In fact, F_4 provides an embedding of $\mathcal{L}$ onto a three dimensional submanifold M of $\mathbb{R}^4$. This manifold is disjoint from origin in $\mathbb{R}^4$, which is the image of the z-axis under F_4. This situation is described further in Sec. 5.4.

The differential mappings F_n for $n > 4$ may be analyzed analogously. They all share a similar LU-decomposition such that U_n has the same main diagonal as U_3 and L_n possesses a $1/x$ singularity. Setting $x = 0$ in J_n gives a U_n' with main diagonal $\mathrm{diag}(1, \sigma, -\sigma^2 y)$, the same as U_4', and an L_n' which is regular on $\mathbb{R}^3$, so that the singular set consists of exactly the z-axis in each case. We conclude that the differential mapping F_n is an embedding into $\mathbb{R}^n$ for $n \geq 4$.

5.3 Symmetry

In this section we show that the singular sets of the mappings F_n are symmetry-induced, that is, they exist because of the symmetry properties of the original flow and of the chosen observation function.

We have seen that the Lorenz system is equivariant under the diffeomorphism $R_z(\pi) : (x, y, z) \mapsto (-x, -y, z)$. On the other hand, each mapping F_n is antisymmetric under $R_z(\pi) : F_n(-x, -y, z) = -F_n(x, y, z)$. We then have the commutative diagram

$$\begin{array}{ccc} (x, y, z) & \xrightarrow{F_n} & (X_1, \ldots, X_n) \\ {\scriptstyle R_z(\pi)}\downarrow & & \downarrow{\scriptstyle P} \\ (-x, -y, z) & \xrightarrow{F_n} & -(X_1, \ldots, X_n), \end{array} \tag{5.11}$$

where the map P is inversion. It follows that each induced flow in $\mathbb{R}^n$ is parity or P equivariant. In particular this holds for $\mathcal{L}_i$ in $\mathbb{R}^3$. This change of symmetry is a result of the original system and the observation function together with its derivatives transforming differently under the equivariance group.

The difference of symmetry between the Lorenz flow and the induced flows forces the existence of the singularities in the mappings F_n, independent of the particular details of how the mappings are constructed. Note that the z-axis is pointwise invariant under $R_z(\pi)$ while its image is inverted under P. Eq. (5.11) demands that $F_n(0,0,z) = -F_n(0,0,z)$, which is only satisfied if the z-axis is mapped to the origin. However, since the z-axis is disjoint from the Lorenz flow this singularity poses no obstruction to obtaining an embedding.

More can be said when $n = 3$. We will assume that the z-axis is the only singularity of F_3 and show that this leads to a contradiction. Under this assumption F_3 is a diffeomorphism on $\mathbb{R}^3 - \{z\text{-axis}\}$. Now the rotation $R_z(\pi)$ is isotopic (isotopy will be defined in the next section) to the identity through rotations $R_z(\theta)$ for $0 \leq \theta \leq \pi$. It follows that the composition $F_3 \circ R_z(\theta) \circ F_3^{-1}$ is an isotopy from the map P to the identity. However, P is orientation reversing in $\mathbb{R}^3$ and cannot be isotopic to the identity. Therefore F_3 must have additional singularities. The mildest form this singularity can take is the collapsing of some plane containing the z-axis onto a line (which is parity symmetric).

The preceding argument is no restriction on F_n for $n > 3$ since embeddings of $\mathbb{R}^3$ with different orientation are isotopic in this case (see Chap. 3). In both of these arguments the essential feature is that the original system is equivariant under an order two symmetry which the observation function is antisymmetric under. This forces the image system to have a different order two symmetry than the original which in turn forces the existence of singularities. This theme is taken up again in Sec. 5.6.

5.4 $\mathcal{L}$, $\mathcal{L}_i$, and Local Reflections

This section specifies how the systems $\mathcal{L}$ and $\mathcal{L}_i$ are related in $\mathbb{R}^3$ and in $\mathbb{R}^4$. The mappings F_3 and F_4 seem rather complicated, but their complexity is almost entirely superficial. By allowing smooth deformations the mappings may be brought into simpler forms. Specifically, in $\mathbb{R}^3$ the two systems differ by a simple mapping called a "local reflection," which we define below, while in $\mathbb{R}^4$ the two systems are in fact identical.

The coordinate reflection of $\mathbb{R}^3$, $(x, y, z) \mapsto (x, y, -z)$ cannot be smoothly deformed in to the identity in $\mathbb{R}^3$ because it reverses orientation. However, such a smooth deformation is possible in $\mathbb{R}^4$. If we consider

$\mathbb{R}^3 \subset \mathbb{R}^4$ as the subspace spanned by the first three coordinates, $(x, y, z) \mapsto (x, y, z, 0)$, a deformation (parametrized by s) is given by

$$(x, y, z, 0) \to (x, y, -z \sin s, z \cos s) \to (x, y, -z, 0), \tag{5.12}$$

by rotating from $s = -\pi/2$ to $\pi/2$. Notice that this rotation leaves the xy-plane ($z = 0$) pointwise invariant.

From this deformation we can obtain a twisted embedding of $\mathbb{R}^3$ into $\mathbb{R}^4$ by allowing the rotation to depend on coordinates of $\mathbb{R}^3$. Setting $s = \arctan x$, the explicit form of this embedding is then

$$F : (x, y, z) \mapsto \left(x, y, \frac{-xz}{\sqrt{1+x^2}}, \frac{z}{\sqrt{1+x^2}} \right). \tag{5.13}$$

The projection of this embedding back into $\mathbb{R}^3$ is singular: it sends the yz-plane onto the y-axis. We call this mapping a *local reflection* since it reflects only half of $\mathbb{R}^3$. Fig. 5.4 illustrates this phenomenon by demonstrating a twisted embedding of $\mathbb{R}^2$ into $\mathbb{R}^3$. This lower dimensional example may be obtained from Eq. (5.13) by ignoring the y coordinate. Any projection of this twisted embedding back into $\mathbb{R}^2$ results in a singularity.

The denominators in the last two coordinates of Eq. (5.13) normalize them so that the embedding approaches inclusion as $x \to \pm\infty$ (that is, for $|x|$ large, $F(x, y, z) \approx (x, y, -z \operatorname{sgn} x, 0)$, which is the inclusion $\mathbb{R}^3 \hookrightarrow \mathbb{R}^4$, at least up to a coordinate reflection).

Through a sequence of deformations, one can show[2] that the mapping F_3 is equivalent to a local reflection. This relation will be explored further in the following section. In a similar manner one can show that F_4 is equivalent to the standard inclusion $\mathbb{R}^3 \hookrightarrow \mathbb{R}^4$. Thus in $\mathbb{R}^4$ the two systems $\mathcal{L}$ and $\mathcal{L}_i$ are the same - one can be smoothly deformed into the other. The systems provide identical *representations* of the Lorenz dynamical system in $\mathbb{R}^4$. We remark that since the two systems possess different symmetry, the smooth deformation between them cannot be done in a symmetry preserving fashion.

Moreover, we may regard the induced system as providing a three dimensional embedding contained in a three dimensional submanifold $M \subset \mathbb{R}^4$. The manifold M is not $\mathbb{R}^3$. Since F_4 is a diffeomorphism away from the z-axis, M is diffeomorphic to $\mathbb{R}^3 - \{z\text{−axis}\}$.

[2] See Appendix B.

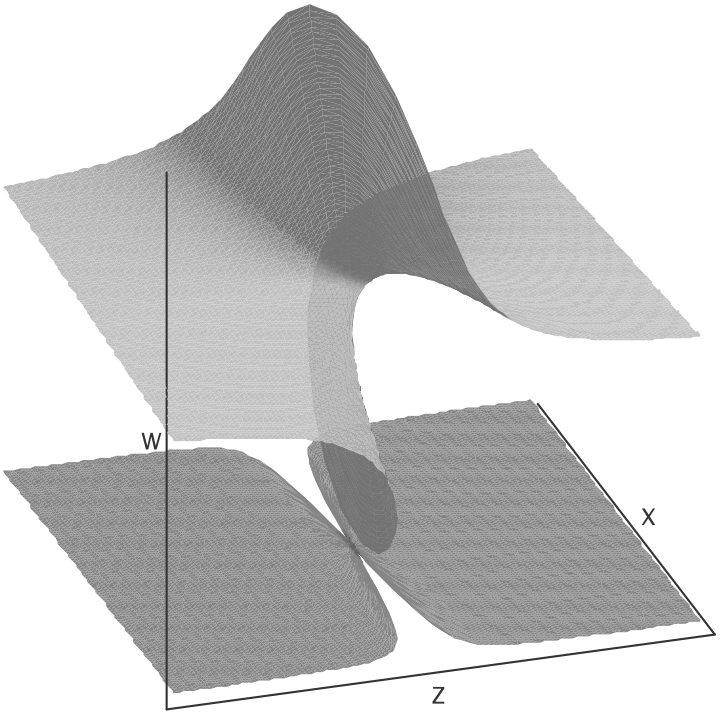

Figure 5.4: Twisted embedding of $\mathbb{R}^2$ in $\mathbb{R}^3$ and projection onto a local reflection. This is equivalent to the mapping F in Eq. (5.13) by ignoring y.

5.5 $\mathcal{L}$, $\mathcal{L}_i$, and Branched Manifolds

In the previous section we explored the relationship between the Lorenz and induced Lorenz systems at the level of the differential equations. In this section we consider how the conclusions of that section apply to the branched manifolds of the two systems, Figs. 5.1 and 5.2. Both the Lorenz and induced Lorenz systems possess branched manifolds constructed from two joining and two splitting charts. Both systems live inside a genus three handlebody built up from four trinions. The handlebody together with its trinion decomposition is shown in Fig. 5.5.

A visual inspection of the branched manifolds for $\mathcal{L}$ (Fig. 5.1) and $\mathcal{L}_i$ (Fig. 5.2) shows that, though they are similar, they differ in two important respects. Both of these differences are in the "bottom" branches that flow from the bottom right trinion to the bottom left one. First, in the Lorenz system this branch twists counter clockwise with respect to the flow direction (cf. Fig. 5.1), while in the induced system it twists clockwise (cf.

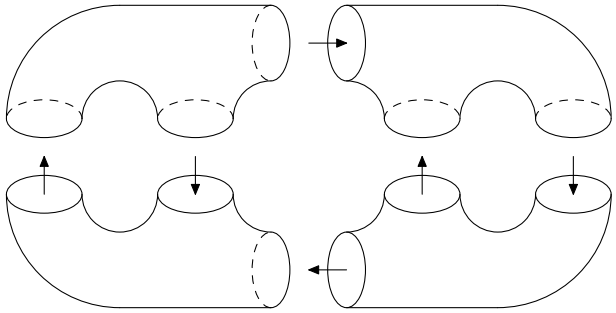

Figure 5.5: Genus three handlebody with trinion decomposition. Arrows indicate flow direction between trinions. The branched manifolds of the Lorenz and induced Lorenz systems may be naturally embedded within this handlebody.

Fig. 5.2). Second, in the Lorenz system this branch attaches from below while in the induced system it attaches from above. Both of these differences are demanded by the different symmetries of the two systems. The two distinct joining trinions differing in attaching order are shown in Fig. 5.6.

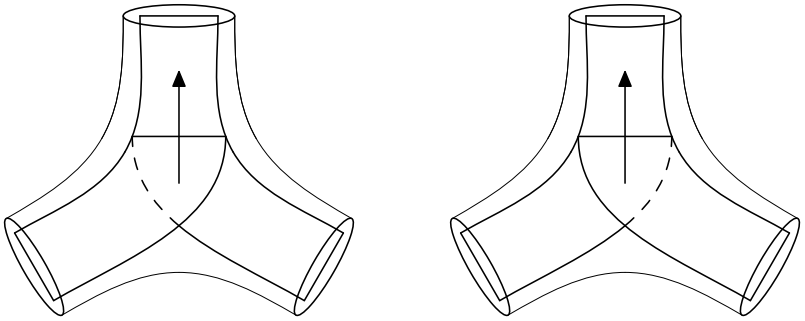

Figure 5.6: The two types of joining trinion related by a reflection in the z-direction (out of the page). The top exit branch is a subset of the xy-plane, which is invariant under reflections

In Sec. 5.4 we saw that up to isotopy $\mathcal{L}$ and $\mathcal{L}_i$ differ by a local reflection of $\mathbb{R}^3$. The local reflection collapses vertical lines in the yz-plane to points along the y-axis. The handlebody carrying $\mathcal{L}$ intersects the yz-plane twice, once on each side of the z-axis. Each intersection is a disk whose image under the local reflection is a line segment (the disk is collapsed onto a diameter). Therefore each of these two branches of the handlebody is "pinched " by the local reflection as they pass through the yz-plane. We conclude that in $\mathbb{R}^3$ the natural handlebody containing $\mathcal{L}_i$ is *not* the image of the handlebody containing $\mathcal{L}$. This is a reflection of the fact established in Sec. 5.2 that F_3 is not a diffeomorphism on any neighborhood of the attractor and therefore does not represent the entire Lorenz flow. The image handlebody is however well defined in $\mathbb{R}^4$ but has a singular projection in $\mathbb{R}^3$.

Next, consider the effect of the local reflection on the Lorenz branched manifold. The two horizontal branches that run through the horizontal tubes of the handlebody each cut the yz-plane in a horizontal line segment. However, this line segment is *invariant* under the action of the local reflection; no two points are identified. Recall that the local reflection preserves the orientation of $\mathbb{R}^3$ on one side of the singular set and reverses it on the other by sending $z \to -z$. The effect of this reversal on half of the branched manifold is shown in Fig. 5.7 [26]. This is precisely the operation that takes the Lorenz branched manifold onto the induced Lorenz branched manifold.

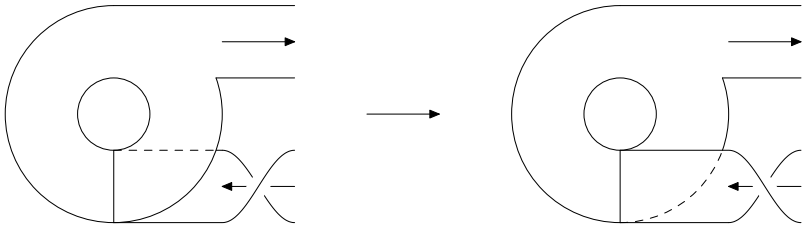

Figure 5.7: Effect of the change of orientation $z \to -z$ (out of the page) induced by the local reflection on half of the Lorenz branched manifold. Arrows indicate the flow direction.

In general, if a dynamical system and its image under some mapping into $\mathbb{R}^3$ have branched manifolds that are the same except for a pair of joining charts that are of opposite type the mapping cannot be a diffeomorphism of the flow. The two joining charts are related by a reflection, but the other charts are related without reflection, so a local reflection is required somewhere for the corresponding handlebody and trinions to match up correctly. Since a local reflection is the singular projected image into $\mathbb{R}^3$ of a smooth embedding into $\mathbb{R}^4$, there is no distinction between the two joining trinions in $\mathbb{R}^4$.

Finally, that the two branched manifolds are diffeomorphic can also be seen by considering the mapping F_3. Recall that the singularity along the yz-plane collapses the lines $y = \text{const}$. By applying the Birman-Williams projection on the Lorenz flow one obtains a branched two-manifold that cuts the yz-plane transversely in the form of a graph over y (see Fig. 5.8). Therefore, no two points of the branched manifolds are identified by F_3 and the Birman-Williams projection commutes with this mapping and the two branched manifolds are diffeomorphic.

In [24] it was found that, neglecting knot type, inequivalent representations of *attractors* differ by local rotation and local reflection operations. A local rotation is equivalent to a Dehn twist at glued trinion ports.

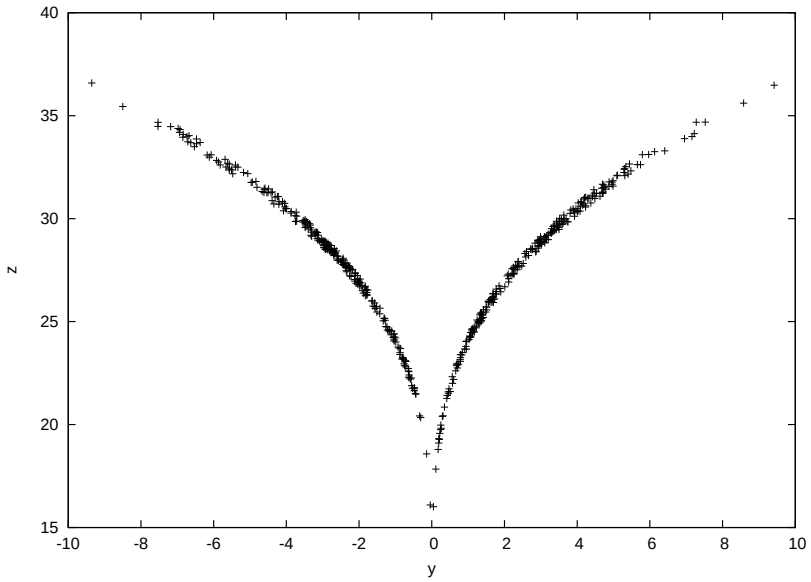

Figure 5.8: Intersection of the Lorenz flow with the yz-plane. The fuzziness of this intersection is in the stable direction of the flow. Since the Birman-Williams projection collapses orbits along the stable direction the fuzziness disappears, resulting in a set describable as a graph over y.

A local reflection has the form shown in Fig. 5.7. There are $g-1$ regions in the decomposition of a genus-g handlebody that can be subjected to local reflections. The foregoing discussion clarifies that local reflections are the result of projections of local rotations from higher dimensional embeddings. In three dimensions, local reflections describe embeddings of the branched manifold, not the flow whose projection is the branched manifold. In order to construct embeddings for the flow, the mapping must be into one higher dimension.

5.6 $R_z(\pi)$ Equivariant Embeddings

It has been observed [43] that one cannot obtain a rotationally equivariant embedding of the Lorenz system from a differential embedding based on a single observable. It is the purpose of this section to demonstrate this explicitly. More generally, we show that if a differential embedding of a dynamical system with an order two symmetry possesses symmetry, it is necessarily parity symmetry. Of course, embeddings with the original symmetry do exist (e.g. the identity map), therefore such embeddings cannot be constructed through successive derivatives of any single observation function, that is, they are not differential embeddings in the

usual sense.

Suppose that a dynamical system $\dot{x} = v(x)$ is equivariant under a mapping (group operation) g, so that $v(gx) = gv(x)$. Let f be an eigenfunction of g satisfying $f(gx) = \pm f(x)$. This is equivalent to saying that f has definite parity (either even or odd) under g. We show that if f is an eigenfunction then $d/dt|_0 f(\varphi_t(x))$ is an eigenfunction of the same parity, where φ_t is the flow associated to v.

By definition of derivative

$$\begin{aligned} \left.\frac{d}{dt}\right|_0 f(\varphi_t(x)) &= \lim_{t=0} \frac{f(\varphi_t(x)) - f(x)}{t} \\ &= \lim_{t=0} \frac{f(x + tv_x) - f(x)}{t}. \end{aligned} \tag{5.14}$$

Now by transforming $x \mapsto gx$ we have

$$\begin{aligned} \left.\frac{d}{dt}\right|_0 f(\varphi_t(gx)) &= \lim_{t=0} \frac{f(gx + tv_{gx}) - f(gx)}{t} \\ &= \lim_{t=0} \frac{f(g(x + tv_x)) - f(gx)}{t} \\ &= \left.\frac{d}{dt}\right|_0 f(g(\varphi_t(x))), \end{aligned} \tag{5.15}$$

where in the second line we used the assumption of equivariance. It is now apparent that this expression is an eigenfunction of the same parity as f under g. By induction the higher derivatives are eigenfunctions of the same parity. Now a differential mapping F_n constructed from f is given by $F_n = (f_1, f_2, \ldots, f_n)$. Here $f_1 \equiv f$ and for $i > 1$ f_i is the time derivative of f_{i-1}. It follows that when f has definite parity that F_n has the same definite parity.

Therefore if f is odd under g then the corresponding differential mapping F_n will be odd and the image system will be parity equivariant. If on the other hand f is even then the differential mapping F_n will be even and thus necessarily two-to-one since $F_n(x) = F_n(gx)$. The image is therefore trivially equivariant or invariant. For example, z is even, and a differential mapping based on z yields a two-to-one mapping onto the proto-Lorenz system. Explicit equations may be found in [29].

Now let f be any observation function and make an eigen-decomposition of f as $f = f^+ + f^-$, where $f^\pm$ are the even $(+)$ and odd $(-)$ parts of f under g. Since the derivative is linear, the components f_i of

the differential mapping F_n split into even and odd parts $f_i^{\pm}$, which are just the even and odd parts of i-th derivative of f.

Now suppose that $g = R_z(\pi)$. We show that equivariance of the image under g leads to a contradiction. In order for the image to be g equivariant F_3 must be g equivariant. Suppose first that the principal directions of g align with the components of F_3. Since up to a permutation of the axes $g = \mathrm{diag}(-1, -1, 1)$, every component function f_i must be an eigenfunction, two with eigenvalue -1 (odd) and one with eigenvalue $+1$ (even). In any case the component $f_1 = f$ is an eigenfunction, but we have seen that its derivatives are necessarily eigenfunctions of the same parity which yields a contradiction. Thus F_3 cannot be equivariant under g.

More generally, suppose that y_i are equivariant coordinates linearly related to the f_j by $y_i = M_i{}^j f_j$. Assume without loss of generality that y_1 is even. Then we must have $M_1{}^j f_j^- = 0$, which says that the f_j^- are linearly dependent. In the same way y_2 and y_3 being odd force the f_j^+ to be linearly dependent. Therefore all f_j are linearly dependent, but then F_3 cannot be an embedding. We therefore conclude that no differential embedding of a $R_z(\pi)$ equivariant dynamical system can be $R_z(\pi)$ equivariant, the Lorenz system in particular.

The general case follows at once. The generator of any order two symmetry acting in $\mathbb{R}^n$ is given in the appropriate basis by $g = \mathrm{diag}(\pm 1, \pm 1, \ldots, \pm 1)$, where the signs are incoherent, and we have $g^2 = I_n$. The previous considerations show a differential embedding will not be equivariant under g, but rather I_n or $-I_n$. In the first case the image is invariant, and in the second case it is parity equivariant. However, as we have seen, it is possible for a system and its parity equivariant image to be diffeomorphic, even isotopic. Finally, we note that in the spirit of [38], a pair of observation functions, one even under g and the other odd, may be used to reconstruct any order two symmetry. In particular, the projection of a generic (non-symmetric) observation function onto the even and odd eigen-directions suffices.

5.7 Résumé

We have analyzed differential mappings of the rotationally equivariant Lorenz dynamical system $\mathcal{L}$ in some detail. While the mapping constructed from the x coordinate and its first two derivatives is one-to-one on the attractor of $\mathcal{L}$, it does not provide a diffeomorphism of the flow. The induced Lorenz system $\mathcal{L}_i$ is not

diffeomorphic to the Lorenz system in $\mathbb{R}^3$. This is consistent with our findings from representation theory. However, the differential mappings of $\mathcal{L}$ into $\mathbb{R}^n$ for $n \geq 4$ do yield embeddings. We saw that the failure to achieve an embedding in $\mathbb{R}^3$ was related to the different symmetry properties of $\mathcal{L}$ and $\mathcal{L}_i$: the former is rotationally equivariant and the latter is parity equivariant. We then showed that the two systems are actually isotopic in $\mathbb{R}^4$ and showed how their associated bounding tori and branched manifolds are related. Finally, we worked out the details of the observation made in [43] that no differential mapping of the Lorenz system is rotationally equivariant; any equivariant image of such a system is either invariant, possessing no non-trivial symmetry, or else is parity equivariant with a two-fold symmetry. We then generalized this result to show that an equivariant reconstruction of any system with a two-fold symmetry is parity symmetric. Finally, we showed how to recover an arbitrary two-fold symmetry from a generic observation function.

While it is not possible to obtain a differentiable embedding of the Lorenz system in the three dimensional manifold $\mathbb{R}^3$, it *is* possible to embed it into a three dimensional twisted submanifold M of $\mathbb{R}^4$. The projection of this manifold into $\mathbb{R}^3$ possesses singularities. In particular, the projection induces a local reflection. This solves the mystery revealed by representation theory. The standard "differentiable embedding" of the Lorenz system into $\mathbb{R}^3$ is not an embedding at all. It fails to be a representation.

Chapter 6: Equivariant Dynamical Systems

The analysis of the previous chapter was prompted by a specific problem – why is the induced Lorenz system not in the list of representations indicated by representation theory. The answer is that this system is not actually a representation. It was seen that the symmetry of the Lorenz system was responsible for the peculiar behavior of its differential mappings and embeddings. This suggests a more general analysis of equivariant systems. This analysis is presented here.

Symmetry is an important property enjoyed by many equations describing physical phenomena. Common examples include the Lorenz [47], Burke and Shaw [41, 72], Kremliovsky [40], and Thomas [81] dynamical systems. We are interested in determining what constraints the symmetry of a non-linear dynamical system imposes on this reconstruction process. Specifically, the questions this chapter addresses are the following: for a differential embedding constructed from a single observation function, 1) is the reconstructed dynamics equivariant; 2) if yes, under which group is it equivariant; and 3) under which representation of that group?

In short, equivariance provides an extremely tight constraint on the embedding problem. Specifically, we shall show that only two possibilities exist when attempting to reconstruct an equivariant dynamics, either 1) the reconstruction has no symmetry; or 2) the reconstruction is equivariant under the parity representation of $\mathbb{Z}_2$, the cyclic group of order two. In other words, regardless of the symmetry of the original system, the construction possesses at most a two-fold symmetry. It most cases this precludes the possibility of an actual embedding since the loss of symmetry prevents the reconstruction from being one-to-one. That is not to say that embeddings do not exist; they just cannot preserve symmetry.

In Sec. 6.1 we provide background material and motivation. In Sec. 6.2 we review the structure theory for equivariant dynamical systems, while in Sec. 6.3 we introduce a structure theory for differential mappings (dynamical system reconstructions). We work out the structure of equivariant reconstructions in Secs. 6.4 and 6.5. We provide the implications of this theory for the embedding problem in Sec. 6.6. Finally, we state our conclusions in Sec. 6.7.

6.1 Dynamics, Groups, and Representations

Consider a dynamical system v on $\mathbb{R}^n$, $v : \mathbb{R}^n \to \mathbb{R}^n$, with flow φ_t. A group G may act on $\mathbb{R}^n$ as a set of linear transformations. Such an action is through a *representation* Γ of G. A dynamical system $\dot{x} = v(x)$ is said to be symmetric or *equivariant* under G if there exists a *faithful* representation Γ of G acting on $\mathbb{R}^n$ such that the following diagram commutes for every $g \in G$

$$\begin{array}{ccc} \mathbb{R}^n & \xrightarrow{v} & \mathbb{R}^n \\ {\scriptstyle \Gamma(g)}\downarrow & & \downarrow{\scriptstyle \Gamma(g)} \\ \mathbb{R}^n & \xrightarrow{v} & \mathbb{R}^n. \end{array} \tag{6.1}$$

This relation states the the vector field "looks the same" when viewed from a point x as is does from any symmetry related point $\Gamma(g)(x)$. The representation is required to be faithful to eliminate trivial equivariance, which is simply invariance.

The Lorenz and Kremliovsky dynamical systems are both equivariant under $\mathbb{Z}_2$, the cyclic group of order two. The Lorenz system is given by the equations

$$\begin{aligned} \dot{x} &= \sigma(y - x) \\ \dot{y} &= Rx - y - xz \\ \dot{z} &= -bz + xy, \end{aligned} \tag{6.2}$$

which are equivariant under the transformation $R_z(\pi) : (x, y, z) \mapsto (-x, -y, z)$, equivalent to a π rotation about the z-axis. We say that the Lorenz system is rotationally equivariant. The Lorenz attractor, which is also rotationally equivariant, was shown in Fig. 5.3. The Kremliovsky system is given by the equations

$$\begin{aligned} \dot{x} &= -y - z \\ \dot{y} &= x + ay \\ \dot{z} &= bx + z(x^2 - c), \end{aligned} \tag{6.3}$$

which are equivariant under the transformation $P : (x, y, z) \mapsto (-x, -y, -z)$, which is a spatial inversion. We say that the Kremliovsky system is parity equivariant. The Kremliovsky attractor, which is also parity

equivariant, is shown in Fig. 6.1. The representations $R_z(\pi)$ and P are inequivalent in $\mathbb{R}^3$. The two systems therefore possess distinct symmetries even though they are both equivariant under faithful representations of the same group, $\mathbb{Z}_2$.

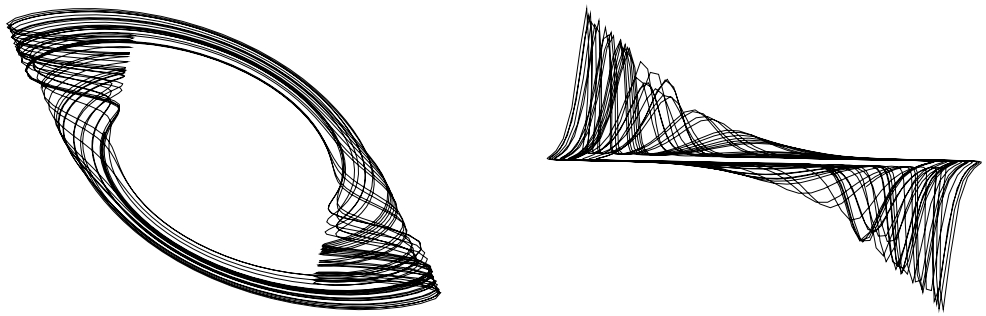

(a) xy-projection. **(b)** xz-projection.

Figure 6.1: The Kremliovsky attractor.

The structure of equivariant dynamical systems and their differential embeddings depends on the structure of the underlying equivariance group, G. We will assume that G is a finite group. Let Γ be a representation of G acting on the linear space V. Then Γ is said to be reducible if there exists a proper subspace $U \subset V$ that is invariant under Γ, that is $\Gamma(g)(u) \in U$ for every $u \in U$. If V has no proper invariant subspaces then Γ is said to be irreducible. Thus, the only subspaces of V invariant under Γ in an irreducible representation are $\emptyset$ and V.

A representation Γ is said to be fully reducible if whenever U is a proper invariant subspace, there exists a complementary subspace which is also invariant. This means that in the proper basis the matrices $\Gamma(g)$ are simultaneously block diagonal. It is a fundamental fact that representations of finite groups are always fully reducible [32]. In this case every representation is a direct sum of irreducibles.

When speaking of irreducibility it is important to specify the field. A representation that is irreducible over $\mathbb{R}$ may be reducible over $\mathbb{C}$. Examples are provided by the representations of the cyclic groups $\mathbb{Z}_p$ for $p > 2$ as planar rotations through angle $2\pi/p$ (this is discussed further in Sec. 6.2). As we are concerned with real representations on real vector spaces ($\mathbb{R}^n$), irreducibility will be understood over $\mathbb{R}$ unless otherwise noted.

Two more fundamental results that are instrumental to the following analysis are Schur's lemmas, which

describe the structure of homomorphisms between irreducible representations. Though applicable in more general settings, in the context of group representations they take the following form [32].

Lemma 6.1 (Schur's First). *Suppose that Γ is an irreducible representation of a group G acting on a vector space V. If there exists a linear map $M : V \to V$ that commutes with Γ for every $g \in G$,*

$$\begin{array}{ccc} V & \xrightarrow{M} & V \\ {\scriptstyle \Gamma(g)}\downarrow & & \downarrow{\scriptstyle \Gamma(g)} \\ V & \xrightarrow{M} & V, \end{array} \tag{6.4}$$

then M is a multiple of the identity, $M = \lambda I$.

Lemma 6.2 (Schur's Second). *Suppose that Γ^1 is an irreducible representation of a group G acting on a vector space V^1 and that Γ^2 is an irreducible representation of G acting on V^2. If there exists a linear map $M : V^1 \to V^2$ that commutes with Γ^i for every $g \in G$,*

$$\begin{array}{ccc} V^1 & \xrightarrow{M} & V^2 \\ {\scriptstyle \Gamma^1(g)}\downarrow & & \downarrow{\scriptstyle \Gamma^2(g)} \\ V^1 & \xrightarrow{M} & V^2, \end{array} \tag{6.5}$$

then either M is zero or an isomorphism. In the latter case the two representations Γ^1 and Γ^2 are equivalent.

6.2 The Structure of Equivariant Dynamical Systems

This section reviews the structure theory of equivariant dynamical systems [26]. Let the representation Γ^D define an action of the group G on $\mathbb{R}^n$. Then Γ^D acts on the coordinate functions x^i of $\mathbb{R}^n$. Denote by $\mathbb{R}[x]$ the set of all polynomials in variables $x^1, \ldots, x^n$. This set is a ring under the operations of polynomial addition and multiplication. The action of Γ^D on the monomials x^i induces an action on all of $\mathbb{R}[x]$ in a natural way. This representation is denoted by Γ^R.

Let $p \in \mathbb{R}[x]$ be a polynomial. If p is invariant under Γ, $p(\Gamma x) = p(x)$, then p is said to be an invariant polynomial. Otherwise p is said to be covariant. Since Γ^R is fully reducible, each polynomial p can be decomposed into components, each belonging to an invariant subspace transforming under a particular irreducible representation. The invariant polynomials all belong to the same subspace, which transforms under the trivial

representation $\Gamma(g) = I_n$. The sets of invariant and covariant polynomials each possess a basis set of polynomials from which all others may be constructed through the ring operations [12]. They are called an integrity basis and a ring basis, respectively.

An arbitrary function f on $\mathbb{R}^n$ may be decomposed with respect to the action Γ^D of G on $\mathbb{R}^n$ into a sum of an invariant and a covariant function. The invariant part may be written as $h_0(p)$, where h_0 is a (not necessarily polynomial) function of the integrity basis polynomials, p. The covariant part may be further decomposed as $\sum_r h_r(p)q^r$, where $r \geq 1$, the q^r are polynomials in the ring basis, and the h_r are functions of the invariant polynomials. If we define $q^0 \equiv 1$ as a ring basis polynomial representing the invariant irreducible subspace, an arbitrary function f may be written as $f = h_r(p)q^r$, where $r \geq 0$ and summation is implicit over the repeated index.

Now consider a dynamical system $\dot{x}^i = v^i$ equivariant under the representation Γ^D of G. Each component of the vector field may be expanded in the ring basis as $v^i = h^i{}_r(p)q^r$. The behavior of the dynamical system under the group operation g is determined by

$$\begin{aligned} gv^i &= gh^i{}_r(p)q^r \\ gv^i &= h^i{}_r(p)gq^r \\ \Gamma^D(g^{-1})^i{}_j v^j &= h^i{}_r(p)\Gamma^R(g^{-1})^r{}_s q^s \\ \Gamma^D(g^{-1})^i{}_j h^j{}_s q^s &= h^i{}_r(p)\Gamma^R(g^{-1})^r{}_s q^s, \end{aligned} \tag{6.6}$$

where in the second line we used invariance of the $h^i{}_r$, in the third the definitions of the representations Γ^D and Γ^R, and in the last the expansion of v^j in the ring basis.

The last line must hold for each basis element q^s in the ring basis separately. The resulting equation may be expressed as the commutative diagram

$$\begin{array}{ccc} \mathbb{R}[x] & \xrightarrow{h} & \mathbb{R}^n \\ {\scriptstyle \Gamma^R(g)}\downarrow & & \downarrow{\scriptstyle \Gamma^D(g)} \\ \mathbb{R}[x] & \xrightarrow{h} & \mathbb{R}^n, \end{array} \tag{6.7}$$

demonstrating that h intertwines the two representations Γ^D and Γ^R. We may regard $\mathbb{R}^n$ as a subspace

of $\mathbb{R}[x]$ spanned by the monomials x^i. Since both Γ^D and Γ^R are fully reducible, Schur's first lemma may be applied to the restriction of h to the irreducible subspaces. The conclusion is that h is multiplication by a constant (that is, an invariant polynomial) between equivalent representations and zero otherwise. This severely restricts the structure of the functions $h^i{}_j$ that define an equivariant dynamical system.

For example, consider the representation $\Gamma^D = R_z(\pi)$ of $\mathbb{Z}_2$, the equivariance group of the Lorenz system. The invariant polynomials z, x^2, xy, and y^2 span an integrity basis. The ring basis polynomials x and y each transform under the non-trivial one dimensional representation $\mathbb{Z}_2 \to \{1, -1\}$. The most general form of a three dimensional dynamical system equivariant under $\Gamma^D = R_z(\pi)$ is given by

$$\frac{d}{dt}\begin{pmatrix} x \\ y \\ z \end{pmatrix} = \begin{pmatrix} 0 & h^1{}_2 & h^1{}_3 \\ 0 & h^2{}_2 & h^2{}_3 \\ h^3{}_1 & 0 & 0 \end{pmatrix} \begin{pmatrix} 1 \\ x \\ y \end{pmatrix}, \tag{6.8}$$

where each $h^i{}_j$ is an arbitrary function of the invariant polynomials. The Lorenz system is defined by the choices $h^1{}_3 = -h^1{}_2 = \sigma$, $h^2{}_2 = R - z$, $h^2{}_3 = -1$, and $h^3{}_1 = -bz + xy$.

6.3 The Structure of Differential Mappings

This section describes two properties of differential mappings that restrict the structure of equivariant embeddings of dynamical systems. These are 1) the canonical form of the image dynamical equations; and 2) the preservation of transformation properties under differentiation.

Differential mappings were introduced in Sec. 1.3.4. A differential mapping F is constructed from the consecutive derivatives of a single observation function f. When the image dynamical system is well defined (for example, when the mapping is an embedding) the new vector field V at $F(x)$ is given by

$$\begin{aligned} V^i &= \frac{\partial F^i}{\partial x^j} v^j \\ &= \left.\frac{d}{dt}\right|_0 F^i(\varphi_t(x)) \end{aligned} \tag{6.9}$$

It is immediate from the definition that $V^1 = F^2$. For V^2 we have

$$\begin{aligned}
\left.\frac{d}{dt}\right|_0 F^2(\varphi_t(x)) &= \left.\frac{d}{dt}\right|_0 \left.\frac{d}{ds}\right|_0 f(\varphi_s(\varphi_t(x))) \\
&= \left.\frac{d}{dt}\right|_0 \left.\frac{d}{ds}\right|_0 f(\varphi_{s+t}(x)) \\
&= \left.\frac{d}{dt}\right|_0 \left.\frac{d}{ds'}\right|_t f(\varphi_{s'}(x)) \\
&= \left.\frac{d^2}{dt^2}\right|_0 f(\varphi_t(x)) \\
&= F^3(x),
\end{aligned} \tag{6.10}$$

where $s' = s + t$. By induction we have the general rule that $V^i = F^{i+1}$ for $i < m$.

Therefore the image dynamical system always has the canonical form

$$\begin{aligned}
\dot{F}^1 &= F^2 \\
\dot{F}^2 &= F^3 \\
&\vdots \\
\dot{F}^{m-1} &= F^m \\
\dot{F}^m &= h(F^1, \ldots, F^m),
\end{aligned} \tag{6.11}$$

for some function h. We can express this canonical form by $\dot{F}^i = M^i{}_j F^j + \delta^i{}_m h(F)$, where above the last row M is an upper shift matrix (unit super-diagonal) and the bottom row is zero,

$$M = \left(\begin{array}{cccc} 0 & 1 & 0 & \ldots \\ 0 & 0 & 1 & \ldots \\ \vdots & \vdots & \vdots & \ddots \\ \hline & & 0 & \end{array}\right). \tag{6.12}$$

Next we consider how the derivatives of the observation function f transform under a group operation g.

By repeating the calculation in Eq. 5.15 we see that

$$\left.\frac{d}{dt}\right|_0 f(\varphi_t(gx)) = \left.\frac{d}{dt}\right|_0 f(g(\varphi_t(x))). \tag{6.13}$$

It follows that if f is invariant under g then so is its time derivative since $f \circ g = f$. Suppose $f = q^i$ is a ring basis polynomial. In this case

$$\left.\frac{d}{dt}\right|_0 q^i(g\varphi_t(x)) = \Gamma^i{}_j(g) \left.\frac{d}{dt}\right|_0 q^j(\varphi_t(x)), \tag{6.14}$$

which just says the derivative of q^i transforms under the same representation as q^i. In the general case of a linear combination of covariant polynomials multiplied by arbitrary invariant polynomials, the derivative of f transforms the same as f, that is, it is composed of the same representations. This follows at once from the linearity of the derivative, the chain rule, and the special cases already considered.

Consider again the Lorenz system with observation function x, which transforms under the parity representation of $\mathbb{Z}_2$. The differential mapping $F(x, y, z) = (X, Y, Z)$ of the Lorenz system into $\mathbb{R}^3$ constructed using x is given by

$$\begin{aligned} X &= x \\ Y &= \sigma(y - x) \\ Z &= \sigma(R + \sigma - z)x - \sigma(1 + \sigma)y, \end{aligned} \tag{6.15}$$

and it is apparent that the coordinate functions (X, Y, Z) transform under the P representation of $\mathbb{Z}_2$. The canonical equations of motion are satisfied with h given by [28, 29]

$$\begin{aligned} &b\sigma(R-1)X - b(1+\sigma)Y - (1+b+\sigma)Z \\ &- X^2Y - \sigma X^3 + \frac{Y}{X}\left(Z + (1+\sigma)Y\right). \end{aligned} \tag{6.16}$$

The canonical equations are also equivariant under P.

6.4 The Structure of Equivariant Representations

This section applies the structure built up in the past two sections to constrain the symmetry of equivariant dynamical systems under differential mappings. First, we demonstrate that equivariance requires that an observation function be composed of polynomials transforming under a single representation. Next, we demonstrate that this representation is necessarily abelian, in fact cyclic. Finally, we show that this representation is one dimensional. We conclude that if the image of an equivariant dynamical system is itself equivariant, the equivariance group representation is necessarily one dimensional.

Suppose that $f = F^1$ is an observation function and that $F = (F^1, \dots, F^m)$ is the corresponding differential mapping. Since the original dynamical system is equivariant, the image system will be equivariant under G if the following diagram commutes

$$\begin{array}{ccc} \mathbb{R}^n & \xrightarrow{F} & \mathbb{R}^m \\ {\scriptstyle \Gamma^D(g)}\downarrow & & \downarrow{\scriptstyle \Gamma^{D'}(g)} \\ \mathbb{R}^n & \xrightarrow{F} & \mathbb{R}^m. \end{array} \tag{6.17}$$

Recall that the definition of equivariance requires that $\Gamma^{D'}$ be faithful. As we shall see, Eq. (6.17) is often satisfied by an unfaithful representation $\Gamma^{D'}$. In this case $\Gamma^{D'}$ provides a faithful representation of some group G' homomorphic to G. Specifically, if $\rho : G \to \Gamma^{D'}$ is the homomorphism defining the representation, then $G' \cong G/\ker\phi$. We say that the image system is equivariant under G' rather than G.

For instance, the Lorenz system is equivariant under $\mathbb{Z}_2$ acting as π rotations around the z-axis. The coordinate function z is invariant under this action and a differential mapping constructed using this function results in a dynamical system without symmetry. It is equivariant under the identity representation $\rho : \mathbb{Z}_2 \to I_3$. We will return to this example in Sec. 6.5.

As in Sec. 6.2 we expand each component F^i in the ring basis of $\mathbb{R}^n$ as $F^i = h^i{}_j(p)q^j$. By essentially the same reasoning that led to Eq. (6.7) we obtain the diagram

$$\begin{array}{ccc} \mathbb{R}[x] & \xrightarrow{h} & \mathbb{R}^m \\ {\scriptstyle \Gamma^R(g)}\downarrow & & \downarrow{\scriptstyle \Gamma^{D'}(g)} \\ \mathbb{R}[x] & \xrightarrow{h} & \mathbb{R}^m, \end{array} \tag{6.18}$$

showing that h intertwines Γ^R and $\Gamma^{D'}$, that is $h\Gamma^R = \Gamma^{D'}h$.

Using full reducibility, decompose Γ^R and $\Gamma^{D'}$ into a direct sum of irreducible representations, $\Gamma^R = \operatorname{diag}\left(\Gamma^{(l_1)}, \ldots, \Gamma^{(l_s)}\right)$, and $\Gamma^{D'} = \operatorname{diag}\left(\Gamma^{(k_1)}, \ldots, \Gamma^{(k_r)}\right)$. Similarly decompose $\mathbb{R}[x]$ and $\mathbb{R}^m$ into the corresponding invariant subspaces on which the irreducible representations act, $\mathbb{R}[x] = U_1 \oplus \cdots \oplus U_s$ and $\mathbb{R}^m = V_1 \oplus \cdots \oplus V_r$. Let the indices of $h^i{}_j$ refer now to invariant subspaces rather than matrix elements so that $h^i{}_j : U_j \to V_i$ is a linear map for each i, j. Schur's second lemma requires that each $h^i{}_j$ be an isomorphism when non-zero, in particular U_j and V_i have the same dimension. We obtain the commutative diagram

$$\begin{array}{ccc} U_j & \xrightarrow{h^i{}_j} & V_i \\ {\scriptstyle \Gamma^{(l_j)}}\downarrow & & \downarrow{\scriptstyle \Gamma^{(k_i)}} \\ U_j & \xrightarrow{h^i{}_j} & V_i, \end{array} \tag{6.19}$$

for each pair of indices (i, j).

Using the decompositions given by the previous paragraph, Eq. (6.18) can be written in the block form

$$\begin{pmatrix} h^1{}_1\Gamma^{(l_1)} & h^1{}_2\Gamma^{(l_2)} & \cdots \\ h^2{}_1\Gamma^{(l_1)} & h^2{}_2\Gamma^{(l_2)} & \cdots \\ \vdots & \vdots & \ddots \end{pmatrix} = \begin{pmatrix} \Gamma^{(k_1)}h^1{}_1 & \Gamma^{(k_1)}h^1{}_2 & \cdots \\ \Gamma^{(k_2)}h^2{}_1 & \Gamma^{(k_2)}h^2{}_2 & \cdots \\ \vdots & \vdots & \ddots \end{pmatrix}. \tag{6.20}$$

The components of F are built from covariant polynomials. Suppose that $f = F^1$ contains a polynomial q^r transforming under some representation, which we assume to be $\Gamma^{(l_1)}$ without loss of generality. Then some $h^i{}_1$ is non-zero and therefore an isomorphism. Assume without loss of generality that $i = 1$. We then have $h^1{}_1\Gamma^{(l_1)} = \Gamma^{(k_1)}h^1{}_1$, which shows that $\Gamma^{(l_1)}$ and $\Gamma^{(k_1)}$ are isomorphic and therefore the same representation.

Now, by the results of Sec. 6.2 every component of F must contain a covariant polynomial transforming under the same representation $\Gamma^{(l_1)}$. This in turn requires that $h^i{}_1$ is non-zero (and therefore an isomorphism) for every value of i. The first column of Eq. (6.20) then yields the equation $h^i{}_1\Gamma^{(l_1)} = \Gamma^{(k_i)}h^i{}_1$ for every i, which shows that *every* irreducible representation $\Gamma^{(k_i)}$ appearing in $\Gamma^{D'}$ is the same and equal to the representation $\Gamma^{(l_1)}$. In the same way, comparing the remaining columns shows that every representation of Γ^R is equal to $\Gamma^{(l_1)}$ as well. A very strong result follows: each component of F must be composed of

polynomials transforming under a *single* irreducible representation.

It turns out that this representation cannot be arbitrary; it is necessarily abelian as we now show. Recall the canonical form $\dot{F}^i = M^i{}_j F^j + \delta^i{}_m h(F)$ of the image differential equations, where M is given by Eq. (6.12). Equivariance under Γ yields the equation

$$\left(\Gamma^i{}_j M^j{}_k - M^i{}_j \Gamma^j{}_k\right) F^k = \delta^i{}_m h(\Gamma F) - \Gamma^i{}_m h(F). \tag{6.21}$$

The LHS is manifestly linear in F and the RHS must be linear in F as well. When $i \neq m$ the delta vanishes and we must have $\Gamma^i{}_m h(F)$ be linear in F. Since h is always non-linear in cases of interest (we are studying non-linear dynamical systems) we see that $\Gamma^i{}_m = 0$ and therefore $\Gamma^i{}_j M^j{}_k = M^i{}_j \Gamma^j{}_k$ when $i \neq m$. By writing $M^i{}_j = \delta^{i+1}{}_j$, it follows immediately that $\Gamma^i{}_j = \Gamma^{i+1}{}_{j+1}$, which says that Γ is Toeplitz in the basis spanned by the F^i.

That every matrix in Γ is simultaneously Toeplitz implies that Γ is an abelian representation. The components of an $n \times n$ Toeplitz matrix A are completely determined by the values along the anti-diagonal, which can be considered as a vector of length $2n-1$. In index notation we may write $A_{ij} = a_{i-j+n}$, in terms of the vector a. Similarly let $B_{ij} = b_{i-j+n}$. If A and B belong to Γ then both products AB and BA belong to Γ and must be Toeplitz.

Now the components AB and BA are given in terms of the vectors a and b by

$$\begin{aligned}(AB)_{ij} &= \sum_{k=1}^{n} a_{n+i-k} b_{n-j+k} \\ (BA)_{ij} &= \sum_{l=1}^{n} b_{n+i-l} a_{n-j+l}.\end{aligned} \tag{6.22}$$

In the expression for BA, the sum over l may be rewritten as a sum over k by setting $l = n+1-k$. A term from this sum is now given by $a_{2n+1-k-j} b_{k+i-1}$. The anti-diagonal of a matrix is specified by the index condition $i + j = n + 1$. This relation can be used to swap i and j in the terms giving BA, yielding $a_{2n+1-k-j} b_{k+i-1} \to a_{n+i-k} b_{n-j+k}$, which is exactly the form of the terms giving AB. Thus the two matrices have identical anti-diagonals. But since the anti-diagonal determines the entire matrix, the two matrices are identical. We conclude that A and B commute.

Thus the representation Γ is necessarily abelian for *any* equivariance group G. In particular, if a dynamical system is equivariant under a non-abelian group G, the largest equivariance group of any image system constructed by a differential mapping is the abelianization $\tilde{G} = G/G^{(1)}$, which is the quotient of the group by its commutator subgroup $G^{(1)} = [G, G]$. This is because if $G' = G/N$ is any abelian quotient of G then $G^{(1)} \leq N$. In other words, $\tilde{G}$ is the largest abelian homomorphic image of G. It follows that a differential mapping for a non-abelian G cannot provide an embedding equivariant under G since group elements representing non-trivial commutators are mapped to the identity.

For example, the alternating group A_4 (the group of all even permutations on four objects) is a non-abelian group of order twelve. The commutator subgroup is isomorphic to the *vierergruppe* V_4 and the abelianization is $\tilde{A}_4 \cong A_4/V_4 \cong \mathbb{Z}_3$, the cyclic group of order three [70]. Therefore a differential mapping of a dynamical system equivariant under A_4 will have at most a three-fold symmetry. For $n \geq 5$ A_n is non-abelian and simple [70]. Since A_n is non-abelian, $A_n^{(1)}$ is not trivial. Since A_n is simple $A_n^{(1)}$ must then be equal to all of A_n, and the abelianization $\tilde{A}_n \cong A_n/A_n$ is trivial. A differential mapping of a dynamical system equivariant under A_n for $n \geq 5$ never has symmetry. Remarkably, we will see that differential mappings for A_4 and $A_3 \cong \mathbb{Z}_3$ equivariant dynamical systems never have symmetry either.

Finally, we show that Γ must be one dimensional. To this end we momentarily extend to the complex plane. Schur's first lemma implies that every irreducible representation of an abelian group is one dimensional over $\mathbb{C}$. There are thus two possibilities for Γ. Either the representation is one dimensional over $\mathbb{R}$ and therefore irreducible over $\mathbb{C}$, or two dimensional over $\mathbb{R}$ and expressible as the direct sum of a one dimensional complex representation and its complex conjugate, $\Gamma = \Gamma^{(i)} \oplus \bar{\Gamma}^{(i)}$.

We now suppose that Γ is two dimensional. In the decomposition $\Gamma = \Gamma^{(j)} \oplus \bar{\Gamma}^{(j)}$, the complex irreducible representation $\Gamma^{(j)}$ is one dimensional and unitary and therefore a complex number of modulus one, which can be written $\Gamma^{(j)}(g) = \exp i\phi(j, g)$. It follows that Γ is similar to a real 2×2 rotation matrix

$$\Gamma = \begin{pmatrix} \exp i\phi & 0 \\ 0 & \exp -i\phi \end{pmatrix} \simeq \begin{pmatrix} \cos\phi & \sin\phi \\ -\sin\phi & \cos\phi \end{pmatrix}. \tag{6.23}$$

Note that every 2×2 rotation matrix is manifestly Toeplitz. We may think of Γ as providing a homomorphism

of G onto a finite subgroup of $SO(2)$. Such a subgroup is not only abelian, it is necessarily cyclic.

All of the irreducible representations of cyclic groups are known [32]. If we let g denote the generator of the cyclic group of order p then there are exactly p inequivalent irreducible representations of $\mathbb{Z}_p$ over $\mathbb{C}$. They are given by

$$\Gamma^{(q)}(g^m) = \epsilon^{mq}, \tag{6.24}$$

where ϵ is a primitive p-th root of unity and $0 \leq q < p$. The representation $q = 0$ is always the identity. Setting $z = x + iy$, the invariant basis polynomials for $\Gamma^{(0)}$ are $\bar{z}z$, z^p, and $\bar{z}^p$. The covariant polynomials for $\Gamma^{(j)}$, $j > 1$, are z^j and $\bar{z}^{p-j}$. Since real representations are formed by the direct sum of a complex representation and its complex conjugate, q and $p - q$, the real basis polynomials are the real and imaginary parts of the corresponding complex polynomials.

In the defining representation on $\mathbb{R}^2$, the x and y coordinates transform under the $\Gamma = \Gamma^{(1)} \oplus \bar{\Gamma}^{(1)}$ representation. The only other polynomials that transform under this representation are the real and imaginary parts of $\bar{z}^{p-1}$. If a dynamical system is equivariant under Γ then in a two dimensional subspace on which Γ acts the equations of motion have the complex form $\dot{z} = \xi z + \zeta \bar{z}^{p-1}$, with ξ and ζ functions of invariant polynomials. In terms of the real variables we have

$$\frac{d}{dt}\begin{pmatrix} x \\ y \end{pmatrix} = \begin{pmatrix} \xi_1 & \xi_2 \\ -\xi_2 & \xi_1 \end{pmatrix}\begin{pmatrix} x \\ y \end{pmatrix} + \begin{pmatrix} \zeta_1 & \zeta_2 \\ -\zeta_2 & \zeta_1 \end{pmatrix}\begin{pmatrix} \Re(\bar{z}^{p-1}) \\ \Im(\bar{z}^{p-1}) \end{pmatrix}. \tag{6.25}$$

Notice that the real an imaginary parts of $\bar{z}^{p-1}$ are non-linear in x and y when $p > 2$.

Now if the image of a dynamical system under a differential mapping is equivariant under Γ, then as was shown in Sec. 6.4 the image phase space $\mathbb{R}^m$ must decompose as $\mathbb{R}^m = \mathbb{R}^2 \oplus \cdots \oplus \mathbb{R}^2$ with the same representation Γ of $\mathbb{Z}_p$ acting on each factor $\mathbb{R}^2$. In each subspace the equations of motion must have the form of Eq. (6.25). This is a second canonical form for the equations of motion (Eq. (6.11) being the first).

Denote by Y the coordinates defining this decomposition so that (Y^{2k-1}, Y^{2k}) spans the k-th subspace. These coordinates are related to the canonical coordinates F by some invertible linear transformation, $Y^i = P^i_{\ j} F^j$. We wish to show that the two canonical forms of the equations are consistent only when h is linear.

The differential equations in the Y coordinates are given by

$$\begin{aligned}\dot{Y}^i &= P^i_{\ j}\,\dot{F}^j \\ &= P^i_{\ j}\,M^j_{\ k}\,F^k + P^i_{\ m}\,h(F) \\ &= P^i_{\ j}\,M^j_{\ k}\,(P^{-1})^k_l Y^l + P^i_{\ m}\,h(P^{-1}Y) \\ &= N^i_{\ j}\,Y^j + C^i\tilde{h}(Y),\end{aligned} \tag{6.26}$$

where $N^i_{\ j}$ and C^i are constants and $\tilde{h} = h\circ P^{-1}$ is a non-linear function of Y. For simplicity in the following we will drop the tilde and write h for $\tilde{h}$.

The function h may be uniquely written as $h = h_r(p)q^r$ in terms of invariant and covariant polynomials. If we identify $(Y^{2i-1}, Y^{2i}) = (x, y)$ for any i, then the most general form of h consistent with Eq. (6.25) is

$$h = h_1 x + h_2 y + h_3\Re(\bar{z}^{p-1}) + h_4\Im(\bar{z}^{p-1}), \tag{6.27}$$

where the h_i are functions of invariant polynomials. Using this decomposition of h, Eq. (6.26) becomes in the $(Y^{2i-1}, Y^{2i}) = (x, y)$ subspace

$$\begin{aligned}\frac{d}{dt}\begin{pmatrix}x\\y\end{pmatrix} &= \begin{pmatrix}N_{11}+C_1h_1 & N_{12}+C_1h_2\\ N_{21}+C_2h_1 & N_{22}+C_2h_2\end{pmatrix}\begin{pmatrix}x\\y\end{pmatrix} \\ &\quad + \begin{pmatrix}C_1h_3 & C_1h_4\\ C_2h_3 & C_2h_4\end{pmatrix}\begin{pmatrix}\Re(\bar{z}^{p-1})\\ \Im(\bar{z}^{p-1})\end{pmatrix}.\end{aligned} \tag{6.28}$$

Comparing this to Eq. (6.25) leads to the equations $\zeta_1 = C_1h_3 = C_2h_4$ and $\zeta_2 = C_1h_4 = -C_2h_3$. These equations require that $C_1^2 = -C_2^2$, or $C_1 = C_2 = 0$, which in turn implies that $\zeta_1 = \zeta_2 = 0$. We conclude that this equation is satisfied only if h is linear. But if h is linear then the image dynamical system is linear and uninteresting. We therefore conclude that for non-linear systems the representation Γ must be one dimensional.

For completeness, we note that in the linear case two dimensional equivariant embeddings do exist. Con-

sider the simple two dimensional dynamical system

$$\begin{aligned} \dot{x} &= y \\ \dot{y} &= -x, \end{aligned} \tag{6.29}$$

which is equivariant under $SO(2)$ and therefore every $\mathbb{Z}_p$ acting as rotations through angle $2\pi/p$. For $p > 2$ the complex representation $\Gamma^1 = \{1, \epsilon, \epsilon^2, \ldots, \epsilon^{p-1}\}$ is faithful. The complex basis polynomial is $z = x + iy$, and the monomials x and y form a basis for the two dimensional real representation. Suppose that x is chosen as the observation function. Then since $\dot{x} = y$ the differential mapping is $F = (x, y)$ which is just the identity. The image system is in this case identical to the original system and manifestly equivariant under the same representation of the same symmetry group.

As an application of the results of this section, consider the Thomas system [81], which is defined by the differential equations

$$\begin{aligned} \dot{x} &= -bx + ay - y^3 \\ \dot{y} &= -by + az - z^3 \\ \dot{z} &= -bz + ax - x^3. \end{aligned} \tag{6.30}$$

These equations have a six-fold symmetry. They are equivariant under the parity representation P of $\mathbb{Z}_2$ with generator $g_2 = -I_3$ as well as the $C_3 = R_{\mathbf{u}}(2\pi/3)$ representation of $\mathbb{Z}_3$, where $\mathbf{u} = (1, 1, 1)$. The generator of C_3 is the cyclic permutation matrix

$$g_3 = \begin{pmatrix} 0 & 1 & 0 \\ 0 & 0 & 1 \\ 1 & 0 & 0 \end{pmatrix}. \tag{6.31}$$

Since the Thomas system is equivariant under both $\mathbb{Z}_2$ and $\mathbb{Z}_3$ it is equivariant under their direct product $\mathbb{Z}_6 \simeq \mathbb{Z}_2 \otimes \mathbb{Z}_3$ with generator $g_6 \equiv g_2 g_3 = g_3 g_2$. This generator can also be described by a $2\pi/6$ rotation about $\mathbf{u}$ followed by a reflection in the plane perpendicular to $\mathbf{u}$. The generators of the two subgroups are recovered as $C_3 = g_6^2$ and $P = g_6^3$. Projections of the Thomas attractor are shown in Fig. 6.2.

A more convenient representation of the system is given by transforming to new variables defined by the

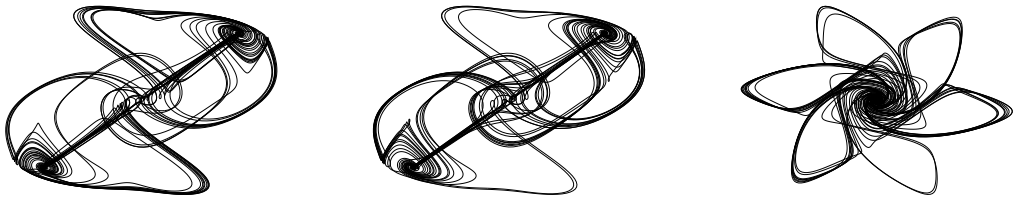

(a) xy-projection. **(b)** xz-projection. **(c)** XY-projection.

Figure 6.2: The Thomas attractor. The six-fold symmetry is evident in the XY-projection of the new coordinates, Eq. 6.32 (c).

linear transformation [26]

$$\begin{pmatrix} X \\ Y \\ Z \end{pmatrix} = \begin{pmatrix} -\frac{\sqrt{3}}{2} & \frac{\sqrt{3}}{2} & 0 \\ -\frac{1}{2} & -\frac{1}{2} & 1 \\ 1 & 1 & 1 \end{pmatrix} \begin{pmatrix} x \\ y \\ z \end{pmatrix}, \tag{6.32}$$

which makes Z the new rotation axis so that projection onto the XY-plane exhibits the six-fold symmetry. Basis polynomials for both subgroups can be constructed and have degree at most three. Each basis polynomial has definite transformation properties under the two generators C_3 and P. The transformation properties of these polynomials and the equivariance properties of the images constructed from them are summarized in Table 6.1.

Table 6.1: Transformation properties for basis polynomials of degree at most two for the symmetries of the Thomas system, P and C_3. Cov and Inv denote covariance and invariance respectively. The final column gives the symmetry of the image system using the corresponding basis polynomial as observation function. An I denotes the identity representation or invariance.

Polynomial	P	C_3	Image
X, Y	Cov	Cov	P
Z	Cov	Inv	P
$X^2 + Y^2$	Inv	Inv	I
$X^2 - Y^2, 2XY$	Inv	Cov	I

All four combinations of invariance and covariance between the two subgroups exist. The coordinate functions X and Y are covariant polynomials of both symmetries and are therefore covariant polynomials of the complete symmetry group $\mathbb{Z}_6$. However, in accordance with the results of this section, no differential mapping constructed from any of these functions can possess more than the $\mathbb{Z}_2$ symmetry. A direct calculation shows that differential mappings constructed from X or Y have parity symmetry, and visual inspection shows

no apparent rotational symmetry.

6.5 The Structure of One Dimensional Representations

The previous section demonstrated that the only non-trivial equivariance group representations for differential mappings are one dimensional. In this case every basis polynomial must be an eigenvector with eigenvalue $\lambda = \pm 1$. Since all components of the mapping F transform under the same representation, each component is a simultaneous eigenvector with the same eigenvalue. If $\lambda = 1$ then the image is equivariant under the trivial representation $\Gamma(g) = I_m$ for every g. The image system is no longer equivariant under G, but rather invariant. We say that F has modded out the symmetry of the dynamical system. In this case, the nicest possible behavior for F is providing a $|G| \to 1$ local diffeomorphism [26]. We noted in Sec. 6.4 that constructing a differential mapping of the Lorenz system using the z coordinate results in an image without symmetry. This mapping is in fact a $2 \to 1$ local diffeomorphism [26].

On the other hand if $\lambda = -1$ then the image coordinates transform under a representation satisfying $\Gamma(g) = \pm I_n$ and $\Gamma(g^2) = I_n$ for every g. In this case Γ furnishes the parity representation of $G \cong \mathbb{Z}_2$ in $\mathbb{R}^m$. This representation defines a group homomorphism $G \to \mathbb{Z}_2$.

The necessary and sufficient condition for the existence of such a homomorphism is the existence of a normal subgroup $N \triangleleft G$ with $|N| = |G|/2$, since by Lagrange's Theorem we have $|G/N||N| = |G|$ and $\mathbb{Z}_2$ is the unique group of order two. We see immediately that when the order of G is odd that no such homomorphism can exist. In particular, if a dynamical system is equivariant under $\mathbb{Z}_p$, p odd, its image under any differential mapping cannot be equivariant.

When $|G|$ is even such a homomorphism may or may not exist, depending on the group. For example the alternating group A_4 has order twelve but has no subgroup of order six [70], so possesses no homomorphism onto $\mathbb{Z}_2$. One could also note that the abelianization is $\tilde{A}_4 \cong \mathbb{Z}_3$, which possesses no homomorphism onto $\mathbb{Z}_2$. Since there is no homomorphism of A_4 onto $\mathbb{Z}_2$, the image of an A_4 equivariant dynamical system under any differential mapping cannot have symmetry.

Notice that A_4 is non-abelian. Abelian groups of even order always possess a normal subgroup of half the group order, which we now show. By the fundamental theorem of finite abelian groups we can write G as a direct product of cyclic groups. Since the order of a direct product is the product of the orders, at least one

summand $\mathbb{Z}_r$ must have even order. If the generator of this subgroup is h, then h^2 generates a cyclic subgroup of order $r/2$. But every subgroup of an abelian group is normal, which establishes the claim.

Consider again the Lorenz system, equivariant under the representation $\Gamma = R_z(\pi)$ of $\mathbb{Z}_2$. The basis set of invariant polynomials is given by z, x^2, xy, and y^2, while the basis set of covariant polynomials, which transform under P, is given by x and y. Constructing a differential mapping using an invariant polynomial results in an image without symmetry. For instance, using z results in a $2 \to 1$ local diffeomorphism onto the proto-Lorenz system [26]. On the other hand, using a covariant function such as x results in a parity equivariant image, the induced Lorenz system. In no case is it possible to construct an image transforming under the same representation as the original Lorenz system, $R_z(\pi)$. This agrees with the results of the previous chapter, obtained using different techniques. Similar remarks would hold for any $R_z(\pi)$ equivariant dynamical system, such as the Burke and Shaw system.

It is worth stressing this last observation. If one constructs a differential mapping of *any* equivariant dynamical system and the image system is equivariant, it is necessarily *parity* equivariant, regardless of the original symmetry. This is congruent with the results of the Thomas system in Sec. 6.4. In particular this means that a differential *embedding* of a system equivariant under a group of order greater than two cannot be equivariant under a faithful representation of the symmetry group. In general, symmetries are not preserved by differential embeddings constructed from a single observation function.

6.6 Implications for Embeddings

An important consequence of the foregoing analysis is that in almost all cases equivariant differential mappings of equivariant systems are not embeddings. This is immediate if the symmetry of the original system has order $|G| > 2$. Specifically, the action of G partitions the original phase space into $|G|$ symmetry related domains. Since the image system has only two symmetry related domains, the original domains are mapped onto the image domains in a $|G|/2 \to 1$ fashion. If the image system is invariant, these domains are mapped in a $|G| \to 1$ fashion.

Even when $|G| = 2$ one may fail to obtain an embedding when the original representation of $\mathbb{Z}_2$ is not the parity representation. Every representation of $\mathbb{Z}_2$ acting in $\mathbb{R}^n$ is given in the appropriate basis by $\Gamma = \mathrm{diag}(1, \cdots, 1, -1, \cdots, -1)$. Representations are distinguished by their signature, that is, the number

of $+$ signs in this matrix. Since the coordinate directions corresponding to the $+$ signs are left invariant (and those corresponding to the $-$ signs covariant), representations are distinguished by the dimension of their invariant subspace. The parity representation leaves only the origin (zero dimensional subspace) invariant.

A differential mapping must map the symmetry invariant set (not to be confused with the dynamical invariant set) of the original system onto that of the image system. When the original invariant set has non-zero dimension, this identification obviously precludes an embedding. However, in many cases this invariant set may be considered disjoint from the flow. In the case of the Lorenz system, the z-axis is the stable manifold of the central fixed point and is generally ignored (excised) when discussing embeddings.

Even with this understanding trouble still arises. Let $z = (x, y)$, where x and y the invariant and covariant coordinates, respectively, so that $\Gamma(x, y) = (x, -y)$. Let F be the differential mapping between spaces of the same dimension which satisfies $F(\Gamma z) = -F(z)$. Note that $\Gamma^2 = I$ and that by the chain rule we have

$$\frac{\partial F(\Gamma z)}{\partial z} = \left.\frac{\partial F}{\partial z}\right|_{\Gamma z} \Gamma. \tag{6.33}$$

Thus the Jacobian at Γz is

$$\begin{aligned} JF(\Gamma z) &= \left.\frac{\partial F}{\partial z}\right|_{\Gamma z} \\ &= \frac{\partial F(\Gamma z)}{\partial z}\Gamma \\ &= -\frac{\partial F(z)}{\partial z}\Gamma \\ &= -JF(z)\Gamma, \end{aligned} \tag{6.34}$$

and the Jacobian determinants are related by

$$|JF(\Gamma z)| = |-JF(z)||\Gamma| = (-1)^n |JF(z)| \cdot (-1)^{\#y}, \tag{6.35}$$

where n is the total number of coordinates and $\#y$ denotes the number of covariant coordinates. Since $n = \#x + \#y$, we have

$$|JF(\Gamma z)| = (-1)^{\#x} |JF(z)|. \tag{6.36}$$

We see that if $\#x$ is odd, the Jacobian determinants at (x, y) and at $\Gamma(x, y)$ have opposite sign, and so the Jacobian must become degenerate somewhere along any curve connecting these two points. This presents an obstruction to obtaining an embedding into a space of the same dimension as the original system. We note, however, that this condition on the Jacobian is not an obstruction to finding an embedding in higher dimensions.

For example, the Lorenz system has the z-axis as a one-dimensional invariant subspace. Therefore no equivariant differential mapping of Lorenz into $\mathbb{R}^3$ can be an embedding. This is true for any $R_z(\pi)$ equivariant dynamical system. However, for the Lorenz system, a differential mapping constructed from the x coordinate does provide an embedding into $\mathbb{R}^4$ and higher dimensions. This was worked out explicitly in the previous chapter.

The general theory presented here provides the following implications for the four dynamical systems listed in the introduction: an equivariant embedding of the Kremliovsky system Eq. (6.3) is possible that preserves the parity symmetry; an equivariant embedding of the Lorenz system Eq. (6.2) or the Burke and Shaw system is possible, but the symmetry necessarily changes from rotation to parity; an equivariant embedding of the Thomas system Eq. (6.30) is not possible.

Finally, we note that while differential mappings typically destroy symmetry, it is sometimes possible to recover the lost symmetry. If one has an invariant (non-equivariant) image it is possible to construct a lift of the image system to a covering system with any prescribed symmetry. If the original symmetry group and representation are known, then a lift to a system equivariant under this symmetry is possible. This two part process of generating an invariant image and lifting to an equivariant system yields an embedding of the original system which preserves symmetry. For details of this construction, see [42, 23, 26].

6.7 Résumé

This chapter has considered the embedding problem for equivariant dynamical systems. Equivariant dynamical systems possess a rather rigid structure that constrains this problem. We have shown that for any dynamical system equivariant under any representation of any discrete equivariance group, there are only two possibilities when attempting to construct equivariant images under differential mappings: either 1) the image is invariant; or 2) the image is equivariant under the parity representation of $\mathbb{Z}_2$. An immediate corollary is

that the only symmetry that can be preserved under a differential mapping is parity symmetry.

It follows that in almost all cases differential mappings are not embeddings. This is always the case if the original symmetry has order $|G| > 2$, since symmetry related domains in the original system are mapped onto symmetry domains in the image in a $|G| \to 2$ or $|G| \to 1$ fashion. Even if $|G| = 2$, an equivariant differential mapping of an n-dimensional system into $\mathbb{R}^n$ will fail to be an embedding if the dimension of the symmetry invariant subspace is odd. Embeddings in the same dimension are only possible when the symmetry invariant subspace has even dimension, such as when the original system is already parity equivariant. The symmetry of an equivariant dynamical system typically cannot be preserved under differential embedding.

Chapter 7: Towards Higher Dimensional Systems

The theory developed in the preceding chapters may be regarded as a capstone on the well developed and essentially completed topological classification of three dimensional chaotic dynamical systems. On the other hand, precious little is known about the topological structure of chaotic dynamical systems in dimensions greater than three. At the very least, the embeddings of three dimensional systems into three dimensional submanifolds of higher dimensional Euclidean spaces studied in previous chapters is a starting point. This, of course, does not address systems that are inherently higher dimensional. Nevertheless, the program of representation theory can be carried out in isolated cases and introduces a fresh perspective from which to study the problem.

While the general structure of dynamical phase spaces in higher dimensions is not yet well understood, there is an easily defined and important class of systems in every dimension. This class generalizes the genus one dynamical systems in three dimensions. Recall that in three dimensions a genus one system has as its phase space the three dimensional solid torus $D^2 \times S^1$. Systems of this type are readily created by periodically driving (S^1) a two dimensional oscillator (D^2). Equivalently, they are suspensions of two dimensional maps. In direct analogy, one may periodically drive or suspend an oscillator on D^n for any $n \geq 3$, obtaining a flow with phase space $D^n \times S^1$. We will refer to such a system as a *toral system* and the phase space as a *solid n-torus*. Note that the solid n-torus is $n+1$ dimensional.

We begin in Sec. 7.1 by determining the mapping class group of $\mathcal{T}^n$, since this is how we began with the three dimensional systems considered earlier. However, we ignore smoothness and compute this group in the topological category, obtaining a straightforward generalization of the result obtained for $D^2 \times S^1$. The result is $\mathrm{MCG}(D^n \times S^1) \cong \mathbb{Z}_2 \oplus \pi_1 SO(n)$. The factor $\pi_1 SO(n)$ has to do with the twisting available in D^n and gives the usual $\mathbb{Z}$ for $n = 2$. The methods used to obtain this result break down in the smooth case. We spend some time in Sec. 7.2 to attempt to understand the nature and extent of this failure. This failures prevents use from computing the smooth mapping class group. However, we bypass this difficulty in Sec. 7.3 by computing the spectrum of embeddings directly. This happy occurrence is possible due to the fiber bundle structure of

$\mathcal{T}^n$. The results are summarized in Tab. 7.1. Finally, we conclude in Sec. 7.4.

Table 7.1: Representation labels for solid torus systems, $D^n \times S^1$. For parity $\mathbb{Z}_2 = \{\pm 1\}$, while for global torsion $\mathbb{Z}_2 = \{0, 1\}$.

Representation	Obstructions to Isotopy		
Labels	$\mathbb{R}^{n+1}$	$\mathbb{R}^{n+2}$	$\mathbb{R}^{n+3}$
Global Torsion	$\mathbb{Z}_2$	$\mathbb{Z}_2$	-
Parity	$\mathbb{Z}_2$	-	-
Knot Type	-	-	-

7.1 Mapping Class Groups of Solid Tori

The n-torus is the n-fold Cartesian product of S^1 with itself, $T^n = S^1 \times \cdots \times S^1$, while the solid n-torus is $\mathcal{T}^n = D^n \times S^1$. Topologically, this is the same as "filling in" the first $n-1$ factors of S^1 to D^2 and taking the product. However, this does not immediately yield a smooth manifold, but rather a manifold with corners. The boundary of $\mathcal{T}^n$ is the manifold $\partial\mathcal{T}^n = \partial D^n \times S^1 \cong S^{n-1} \times S^1$, and is *not* an n-torus except when $n = 2$.

We wish to determine the mapping class group of $\mathcal{T}^n$, the group of diffeomorphisms of $\mathcal{T}^n$ modulo (smooth) isotopy. However, for the present we will work in the topological category, meaning we replace *smooth* by *continuous*. Thus $\mathrm{MCG}(\mathcal{T}^n)$ will denote the group of orientation preserving homeomorphisms modulo (continuous) isotopy. In analogy with with usual solid torus $D^2 \times S^1$, we wish to define a meridional disk as a properly embedded ball $D^n \to \mathcal{T}$ whose removal does not disconnect $\mathcal{T}$. Proper means that the embedding take boundaries into boundaries, $\partial D^n \to \partial\mathcal{T}$. For the removal of the disk to not disconnect $\mathcal{T}$ requires that the image of the boundary S^{n-1} not be contractible in $\partial\mathcal{T}$, that is, does not represent the trivial element in $\pi_{n-1}(\partial\mathcal{T})$.

However, this is not quite enough. We require the embedded ball and boundary sphere to be embedded "nicely". In a classic paper, Alexander [2, 64] constructed a topological two sphere embedded so badly in S^3 that the complement was not simply connected on either side. In particular, the embedding could not be extended to the three ball (which is simply connected). Due to the details of its construction it is known as Alexander's horned sphere. A caricature of its appearance in $\mathbb{R}^3$ is given in Fig. 7.1.

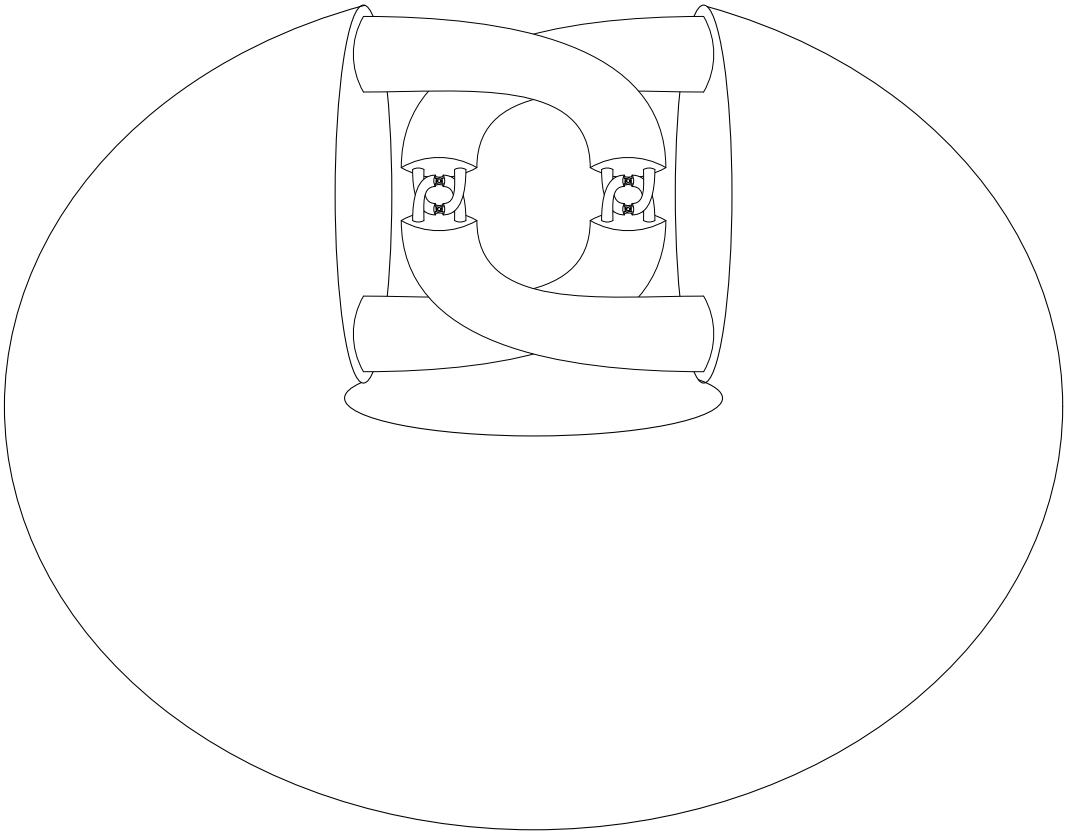

Figure 7.1: First few iterations in the construction of Alexander's horned sphere, which is an infinite construction. As presented, this solid object is homeomorphic to D^3 but its exterior is not simply connected. Thus, to obtain obtain an embedding of S^2 that does not extend to D^3 one simply turns this object "inside-out".

In order to rule out such pathological meridians a niceness condition is required. Requiring the embedding to be smooth would suffice, however that would be inappropriate in the topological category. An appropriate condition is that the embedding be bicollared. An embedding $f : M \to N$ of a topological space is said to be *bicollared* if it extends to an embedding $F : M \times [-1, 1] \to N$ with $F|_{M\times\{0\}} = f$. In other words, this guarantees that M has a nice collar neighborhood in N. If M has codimension one in N, the bicollar is just a tubular neighborhood. This condition is sufficient to eliminate pathologies such as the horned sphere [8]:

Theorem 7.1 (Generalized Schönflies). *A bicollared $(n-1)$-sphere in $\mathbb{R}^n$ bounds a ball. More specifically, the closure of the bounded complementary domain is homeomorphic with D^n.*

We may now define a *meridional disk* of $\mathcal{T}$ as a bicollared, properly embedded D^n such that the image of the boundary S^{n-1} is not contractible in $\partial\mathcal{T}$. The image of the boundary sphere is called a *meridian.* Thus

a meridian is a bicollared sphere S^{n-1} embedded in but not contractible in $\partial\mathcal{T}$. A standard or prototype meridional disk is $D^n \times \{p\} \subset \mathcal{T}$, where $p \in S^1$, and the corresponding meridian is its boundary. We now establish that meridians and meridional disks are essentially unique.

Lemma 7.2. *Meridians and meridional disks are unique up to isotopy.*

Proof. Let $f : D^n \to D \subset ST^n$ be a meridional disk with meridian $S = \partial D$. It suffices to bring D to a standard form. Since D^n is contractible, f lifts to an embedding $\tilde{f}$ into the covering space $D^n \times \mathbb{R}$ of $D^n \times S^1$. Since D^n is compact, the lift $\tilde{f}$ descends to an embedding into the two-point compactification $C \cong D^{n+1}$ of $D^n \times \mathbb{R}$. As a subset of $\partial C \cong S^n$, S is bicollared and hence bounds disks on both sides. There is thus a homeomorphism of S to the standard $S^{n-1} \hookrightarrow S^n$ which extends over S^n (it extends over each bounded disk by Lemma 7.3). Let D_1 be one of the two disks. Since the union $D \cup D_1$ is a collared sphere in D^{n+1} it bounds a ball, thus there is an isotopy taking D to D_1 by pushing across the ball. □

Note that this uniqueness is up to orientation, depending on whether the map sending S to the standard sphere preserves or reverses orientation.

The following two lemmas as each referred to as the Alexander trick. The first lemma was used in the preceding proof. The second lemma will be essential in the sequel. It says that any two homeomorphisms between disks D^n that agree on their boundaries are isotopic.

Lemma 7.3. *A homeomorphism f of ∂D^n extends over D^n.*

Proof. By applying a homeomorphism we may assume D^n is the unit disk in $\mathbb{R}^n$, so that a point in D^n may be written as xt where $x \in S^{n-1}$, the unit sphere, and $t \in [0, 1]$. Define the extension $\tilde{f}$ by $\tilde{f}(tx) = tf(x)$. □

Lemma 7.4. $\mathrm{MCG}(D^n; \partial D^n) \cong 0$.

Proof. Let $f : D^n \to D^n$ be a homeomorphism satisfying $f|_{\partial D^n} = \mathrm{id}$ and let $x \in D^n$. Define the isotopy from the identity to f by

$$h_t(x) = \begin{cases} tf(x/t) & 0 \leq ||x|| < t \\ x & t \leq ||x|| \leq 1 \end{cases}.$$

□

There is a standard embedding of the solid n-torus $\mathcal{T}^n$ into $\mathbb{R}^{n+1}$ analogous to the embedding of $D^2 \times S^1$ into $\mathbb{R}^3$ as a solid of revolution (see Fig. 7.2). Embed the disk D^n into the hyperplane $\{0\} \times \mathbb{R}^n$ as the unit disk but with the origin translated to $x^2 = 2$ so that the disk is disjoint from the $x^3 \cdots x^{n+1}$-hyperplane complementary to the x^1x^2-hyperplane. Then revolve this disk in a circle through the x^1x^2-plane. By construction $\mathcal{T}$ has a rotational symmetry in the x^1x^2-plane, but it also possesses a reflection symmetry in every coordinate.

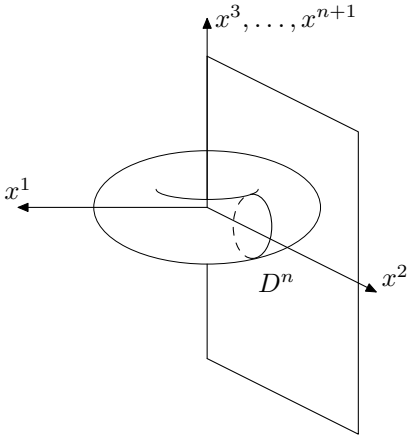

Figure 7.2: Illustration of the embedding $\mathcal{T}^n \to \mathbb{R}^{n+1}$ as a "solid" of revolution.

Consider a π rotation of $\mathbb{R}^{n+1}$ in the x^1x^3-plane (or any coordinate plane other than the rotational symmetry plane). This rotation maps $x^i \to \pm x^i$, where the sign is $-$ for $i = 1, 3$ and $+$ otherwise. By the reflection symmetry of $\mathcal{T}^n$, this operation maps the solid torus to itself, so its restriction to $\mathcal{T}^n$ defines a map we call the *inversion map* z_π (see Fig. 7.3). This map preserves orientation of $\mathcal{T}^n$, but reverses the orientation of each factor (since it reverses one coordinate function belonging to each factor – x^1 of S^1 and x^3 of D^n).

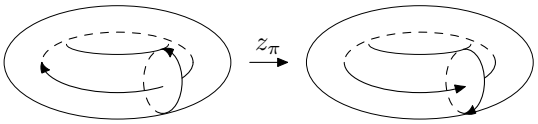

Figure 7.3: The inversion map $z_\pi : \mathcal{T}^n \to \mathcal{T}^n$. The arrowheads indicate orientations in the tangent spaces to the two factors S^1 and D^n. Both tangent spaces change orientation under z_π, thus $\mathcal{T}^n$ retains its orientation.

We can now state and prove the main result of this section,

Theorem 7.5. $\mathrm{MCG}(\mathcal{T}^n) \cong Z_2 \oplus \pi_1 SO(n)$, *where the first factor is generated by the inversion map* z_π *and the second by a "twist" along a meridional disk.*

Proof. (Consult Fig. 7.4.) Let D be a meridional disk with $\partial D = S$, and let $f : \mathcal{T}^n \to \mathcal{T}^n$ be an orientation preserving homeomorphism. It follows from Lemma 7.2 that either f or $z_\pi \circ f$ is isotopic to the identity on D. Assume that it is f. By applying an isotopy we may assume that f fixes D. We can then cut $\mathcal{T}^n$ open along D to obtain a homeomorphism on the "cylinder" $\overline{\mathcal{T}^n - D} \cong D^n \times [0,1]$, which is fixed on the "ends" $D^n \times \{0,1\}$. From this we obtain a homeomorphism f' by restricting to the "rim" of the cylinder $N \equiv \partial D^n \times [0,1] \cong S^{n-1} \times [0,1]$. The mapping f' is fixed on boundary of N, $\partial N = S^{n-1} \times \{0,1\}$.

Fix a point $p \in S^{n-1}$ and let $\gamma = \{p\} \times [0,1]$ be a simple curve in N (think of γ as a seam). Suppose first that f' fixes γ up to isotopy. Isotope f' to a new map fixing γ. We may then cut N open along γ and obtain a new homeomorphism on $\overline{(S^{n-1} \times [0,1]) - \gamma} \cong D^{n-1} \times [0,1] \cong D^n$ (unroll the "cylinder" by removing the seam). This homeomorphism is fixed on the boundary. Thus, by the Alexander trick (Lem. 7.4), this homeomorphism is isotopic to the identity on all of $\overline{(S^{n-1} \times [0,1]) - \gamma}$ and thus on all of N. Now, the boundary of our "cylinder" is $\partial(\overline{\mathcal{T}^n - D}) \cong N \cup D^n \times \{0,1\}$. We already had f fixed on the ends, and we have just shown that it is fixed on N, so f is fixed on all the boundary. So, by Alexander, f is isotopic to the identity on all of $\overline{\mathcal{T}^n - D}$. But it is then isotopic to the identity on all of $\mathcal{T}^n$.

It remains to consider the case that $\gamma' = f'(\gamma)$ is not isotopic to γ. Since γ is compact, so is γ'. Using compactness, the curve γ' may be isotoped until it has the form of a graph. That is, if we write $(s,t) \in S^{n-1} \times [0,1]$, then γ' will have the form $(s'(t'), t'))$. If we compose γ' with the projection $\pi : N \to S^{n-1}$, we obtain a loop in S^{n-1}. The point $\pi\gamma'(t)$ may be obtained from the initial point $\pi\gamma'(0)$ by a rotation of the sphere. By choosing this rotation to vary continuously with t, we obtain a loop in $\pi_1 SO(n)$. This loop depends only on the isotopy class of γ'. This fundamental group element can be represented by a power of a Dehn twist. By composing f' with the inverse of these twists, the image of γ' determines the trivial loop in $\pi_1 SO(n)$, and is therefore isotopic to γ. We then proceed as in the previous paragraph.

We see that the only non-trivial operations are the inversion z_π and powers of Dehn twists coming from $\pi_1 SO(n)$. Finally, z_π and the generator of $\pi_1 SO(n)$ commute. □

The fundamental group of every special orthogonal group is known. Since $\pi_1 SO(2) \cong \mathbb{Z}$ this reproduces the earlier result that $\mathrm{MCG}(D^2 \times S^1) \cong \mathbb{Z}_2 \oplus \mathbb{Z}$. On the other hand, we have $\pi_1 SO(n) \cong \mathbb{Z}_2$ when $n > 2$. Thus obtain the following

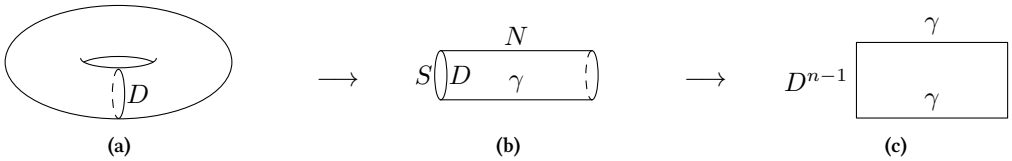

Figure 7.4: Illustration of the steps in the proof of Thm. 7.5. The initial solid torus (a) is cut along meridional disk D to produce the "cylinder" (b). N is the outer boundary of this cylinder (not including the ends). The cylinder is cut open along the seam γ to produce a disk (c).

Corollary 7.6. *For $n > 2$, $\mathrm{MCG}(\mathcal{T}^n) \cong \mathbb{Z}_2 \oplus \mathbb{Z}_2$.*

7.2 The Smooth Case

One would like to substitute "smooth" for "continuous" in Thm. 7.5 and have the proof go through *mutatis mutandis*, but this will not work. The main problem is that the Alexander trick, which the proof invokes repeatedly, is a continuous and not a smooth construction. In the proof of the lemma, the mapping f is "squeezed" down to the origin. For every $t \neq 0$ we have

$$\left.\frac{\partial}{\partial x}\right|_0 tf(x/t) = f'(0),$$

whereas as $t = 0$ the derivative is the identity. The germ of f changes abruptly at zero and the isotopy is not immediately smoothable.

It turns out that there is no smooth analogue of the Alexander trick in general. In particular, in certain dimensions there are diffeomorphisms of the disk that are not isotopic to the identity modulo the boundary. Similarly, there are diffeomorphisms of the sphere which do not extend to the disk. The remainder of this section is a detailed account of this failure and may be regarded as cultural information. We consider the extension problem first.

First, we require a result that basically says that embeddings of disks are nice [52].

Theorem 7.7 (Disk Theorem). *Let f and g be two embeddings of D^k into the interior of a (connected) manifold M^n. If $k = n$, then assume that f and g are equioriented. Then f is isotopic to g. If f and g agree on some $D^m \subset D^k$, the isotopy may be assumed stationary on D^m.*

Consider two orientation preserving diffeomorphisms f and g of S^{n-1}. By the disk theorem, f is isotopic to a map fixed on the northern hemisphere (a disk) and g is isotopic to one fixed on the southern hemisphere. Denote these maps by f' and g' respectively. The commutator $[f,g] \equiv fgf^{-1}g^{-1}$ is isotopic to the commutator $[f',g']$, but this latter commutator vanishes by the construction of f' and g'. It follows that the commutator of any two orientation preserving diffeomorphisms is isotopic to the identity, hence the commutator subgroup of $\mathrm{Diff}(S^{n-1})$ is contained in $\mathrm{Diff}_0(S^{n-1})$, the subgroup of diffeomorphisms isotopic to the identity. Any subgroup containing the commutator subgroup is normal and its quotient is abelian. This implies that $\mathrm{MCG}(S^n) = \mathrm{Diff}(S^{n-1})/\mathrm{Diff}_0(S^{n-1})$ is an abelian group.

Now consider those diffeomorphisms of S^{n-1} that extend over D^n. This may be thought of as the image of $\mathrm{Diff}(D^n)$ under the restriction to the boundary, $\partial : \mathrm{Diff}(D^n) \to \mathrm{Diff}(S^{n-1})$. Since any diffeomorphism of the sphere which is isotopic to the identity extends over the disk (since the identity extends) we have $\mathrm{Diff}_0 S^{n-1} \subset \mathrm{Diff}(D^n)$, hence the latter contains the commutator subgroup of $\mathrm{Diff}(S^{n-1})$ and is normal. We then have

Proposition 7.8. *The group $\Gamma_n \equiv \mathrm{Diff}(S^{n-1})/\partial\,\mathrm{Diff}(D^n)$ of diffeomorphisms of S^{n-1} modulo those that extend over D^n is an abelian group.*

Thus Γ_n measures the failure of diffeomorphisms of S^{n-1} to extend over D^n. Triviality of Γ_n is thus equivalent to the extension form of the Alexander trick (Lem. 7.3).

A *twisted sphere* is the manifold that results from gluing two disks together along their common boundary by some diffeomorphism, $\Sigma(h) = D^n \cup_h D^n$, where $h : S^{n-1} \to S^{n-1}$ an orientation preserving diffeomorphism. This procedure does not immediately yield a smooth manifold. A smooth pasting procedure can be defined as follows (see Fig. 7.5). Start with two copies of $\mathbb{R}^n$ and identify the interiors $\mathbb{R}^n - \{0\}$ by means of the diffeomorphism

$$x \to \frac{1}{||x||} h\left(\frac{x}{||x||}\right), \tag{7.1}$$

where $||x||$ is the usual Euclidean norm. Considering $D^n \subset \mathbb{R}^n$ as the unit disk this procedure glues the two unit disks by h on the boundary. This procedure yields a smooth manifold since by construction we have two charts with transition function given by Eq. 7.1 which is smooth in the overlap $\mathbb{R}^n - \{0\}$. This is directly

analogous to smoothing the connected sum.

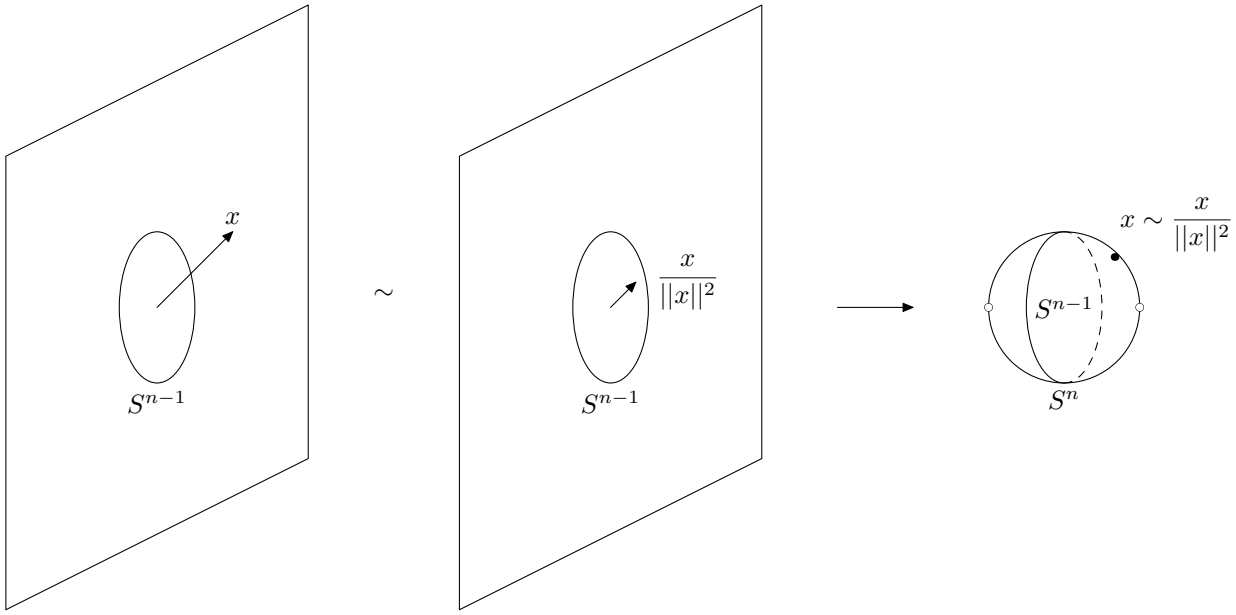

Figure 7.5: Constructed of twisted sphere. Here, $h = \mathrm{id}$ for illustration. Each copy of $\mathbb{R}^n$ gets wrapped over the resulting topological sphere S^n, the "left" copy of $\mathbb{R}^n$ missing only the "right" pole of S^n and the "right" copy of $\mathbb{R}^n$ missing only the "left" pole. The unit spheres S^{n-1} in each copy of $\mathbb{R}^n$ are identified yielding the "equator" of S^n.

Since h is a diffeomorphism it is in particular a homeomorphism, and thus it extends to the disk by Lem. 7.3, and it follows that Σ is homeomorphic to S^n. However, though h is a diffeomorphism, Σ is not necessarily diffeomorphic to S^n. In particular we have the following [39]

Proposition 7.9. *$\Sigma(h)$ is diffeomorphic to S^n if and only if h extends over D^n.*

This remarkable result relates Γ_n to smooth structures on spheres. In fact, Smale has shown [39, 77] in his proof of the generalized Poincaré conjecture that for $n \geq 5$, not only is every homotopy sphere[1] homeomorphic to S^n, each is actually diffeomorphic to a twisted sphere! Thus we have the following

Proposition 7.10. *For $n \geq 5$ there is an isomorphism $\Gamma_n \cong A_n$, where A_n is the group of smooth structures on the topological n-sphere.*

Therefore the extension version of the Alexander trick fails if there exist manifolds homeomorphic but not diffeomorphic to the standard sphere, i.e. if *exotic spheres* exist. The first result of this type was given by Milnor [48] who showed that $\Gamma_7 \cong \mathbb{Z}_{28}$. Seven is in fact the first value of n for which Γ_n is non-trivial.

[1] A *homotopy sphere* is any n-manifold that is homotopy equivalent to S^n.

Showing that $\Gamma_1 \cong 0$ is trivial, and showing that $\Gamma_2 \cong 0$ is straight-forward. That $\Gamma_3 \cong 1$ was proved by Smale [76] and Munkres [51] and that $\Gamma_4 \cong 1$ was proved in a lengthy paper of Cerf [10]. For $n \leq 3$ it is known that A_n is trivial[2], so we have $\Gamma_n \cong A_n$ in these cases as well. Essentially nothing is known about the group A_4 (this is perhaps related to the fact that $\mathbb{R}^4$ admits $2^{\aleph_0}$ smooth structures). The order[3] of the first eighteen groups A_n, which appear to be rather erratic, are indicated in Tab. 7.2.

Table 7.2: Order of the group A_n ($= |\Gamma^n|$, $n \neq 4$) of smooth structures on the n-sphere for n from one to eighteen. This information is taken from integer sequence A001676 in [73].

n	1	2	3	4	5	6	7	8	9	10	11	12	13	14	15	16	17	18
$\lvert A_n \rvert$	1	1	1	?	1	1	28	2	8	6	992	1	3	2	16256	2	16	16

We know turn our attention to the mapping class version of the Alexander trick. It is known [85] that $\mathrm{Diff}(S^n)$ has the homotopy type of $SO(n+1) \times \mathrm{Diff}(D^n; \partial D^n)$ from which if follows immediately that $\mathrm{MCG}(D^n; \partial D^n) \cong \mathrm{MCG}(S^n)$, since the special orthogonal groups are connected (π_0 is trivial). However, it is not difficult to prove this fact directly.

Proposition 7.11. $\mathrm{MCG}(D^n; \partial D^n) \cong \mathrm{MCG}(S^n)$.

Proof. First consider a diffeomorphism f of S^n fixing the north pole N. By the disk theorem, f is isotopic to a map f' fixing the northern hemisphere D_N, which is diffeomorphic to D^n. But the southern hemisphere D_S is also diffeomorphic to D^n, and the restriction $f'|_{D_S}$ yields a diffeomorphism of D^n which is fixed on the boundary. This diffeomorphism is well-defined up to isotopy so yields an element of $\mathrm{MCG}(D^n; \partial D^n)$.

If however f does not fix N there is an arc in S^n connecting N and $f(N)$ and an isotopy of f taking $f(N)$ back to N. Thus we may in fact assume that f fixes N and we obtain a map $\mathrm{MCG}(S^n) \to \mathrm{MCG}(D^n; \partial D^n)$. This mapping is in fact a group homomorphism. To see this let f_1 and f_2 be two diffeomorphisms of S^n. There are isotopies h_i, $i = 1, 2$, taking f_i to f_i' fixed on D_N. We need to show that $f_2 f_1$ is isotopic to $f_2' f_1'$. But the latter map is given in terms of the isotopies by $h_2(h_1(x, 1), 1)$, which suggests the mapping $h_2(h_1(x, t), t)$ as a possible isotopy. This mapping is smooth, is a diffeomorphism for each fixed t, and when $t = 0$ it is equal to $f_2 f_1$, thus it is the isotopy we sought.

[2] That $A_3 \cong 0$ follows from Perelman's proof [55, 56, 57] of the Poincaré conjecture in dimension three.
[3] The order of a group is the number of elements or its cardinality as a set.

Finally, it is clear that the kernel of this homomorphism is trivial. For if $f \mapsto g$ and g is isotopic to the identity on D^n then thinking of D^n as D_S this isotopy extends to an isotopy of f on S^n to the identity by defining it to be the identity on D_N. □

Now a failure of the Alexander trick will follow from the failure of a diffeomorphism of the sphere to be isotopic to the identity. Recall the construction of $\Sigma(f)$ (see Pg. 136). One can show [39] that if f and g are isotopic, then $\Sigma(f)$ and $\Sigma(g)$ are diffeomorphic. If f is isotopic to the identity, then $\Sigma(f) \cong \Sigma(\mathrm{id}) \cong S^n$. For $n \geq 5$, going back to Smale, every exotic sphere is diffeomorphic to $\Sigma(f)$ for some f. Thus if $\Sigma(f)$ has a non-standard differentiable structure, then f cannot be isotopic to the identity.

This concludes our diversion into some very interesting arcana of differential topology. Not only does the Alexander trick fail in many higher dimensions, the extent of the failure is very different from one dimension to the next. In some it actually holds. One the face of things, one may be led to expect that the number of distinct embeddings of solid tori into various Euclidean spaces would be similarly erratic. As we shall see in the next section, this is not the case.

7.3 Embeddings of Solid Tori

While there are isolated cases where Γ_n is trivial and Thm. 7.5 could be extended, in the majority of cases trouble remains. We seek a more systematic approach. In the case of solid tori we may actually bypass the mapping class group and determine the set of all embeddings into various $\mathbb{R}^m$ directly. This happy occurrence is somewhat peculiar to solid tori and rests on their bundle structure. Remarkably, the results are consonant with the continuous mapping class group (Thm. 7.5).

For any submanifold $M \subset N$, a *tubular neighborhood* T of M is any codimension zero submanifold of N that has the structure of a vector bundle over M, $\pi : T \to M$, with M identified with the zero section of the bundle. If T has a (closed) disk bundle structure instead of a vector bundle structure (open disk) it is called a *closed tubular neighborhood*. The solid torus $D^n \times S^1$ is a trivial disk bundle over S^1, and we may identify S^1 with the zero section $\{0\} \times S^1$.

A vector bundle, as a smooth manifold, may always be equipped with a Riemannian metric (by stitching together local metrics with a partition of unity). This allows the structure group of the bundle to be reduced

from $GL(n)$ to $O(n)$. With respect to this metric a disk bundle may be considered as the unit disk subbundle (the set of all vectors with length ≤ 1 with respect to the Riemannian metric). In particular, the disk bundle inherits the $O(n)$ structure group and it makes sense to consider orthogonal maps on fibers since these preserve vector length and thus map the unit disk to itself.

Vector bundle neighborhoods are essentially unique according to the following theorem [39]

Theorem 7.12. *Let M be a closed submanifold of N with F_0 a vector bundle of any dimension over M and F_1 a tubular neighborhood of M. Then there exists an isotopy of the inclusion $F_0 \hookrightarrow N$, fixed on M, to a map taking $F_0 \to F_1$, which has maximal rank on each fiber.*

We are however interested in closed tubular neighborhoods of compact manifolds. In this case the isotopy extension theorem [39] guarantees that the isotopy in the previous theorem can be taken to be ambient.

First consider the codimension zero case where F_0 and F_1 are both tubular neighborhoods of S^1 in any manifold N. That is, we are considering each F_i as embeddings of $D^n \times S^1 \to N$, where $\dim N = n + 1$. Suppose for the moment that there exists an isotopy taking $F_0|_{S^1} \to F_1|_{S^1}$ pointwise. Then there is an ambient isotopy taking $F_0 \to F_1$ and which has full rank on each fiber. This means that the difference between F_0 and F_1 is characterized by a smooth map $f : S^1 \to O(n)$ giving the linear map on each fiber.

If we assume that F_0 and F_1 share the same orientation then we have $\gamma : S^1 \to SO(n)$. The embeddings F_0 and F_1 are now isotopic precisely when f is homotopic to the identity in $SO(n)$. This is because by considering F_0 fixed, the path γ determines how rotated each fiber of F_1 is with respect to F_0. A homotopy of γ alters this rotation in a continuous fashion. If γ is null homotopic, then the rotation on each fiber can be continuously brought to the identity, aligning F_0 with F_1. We conclude that the isotopy classes of orientation preserving embeddings of $D^n \times S^1 \to N$ are in bijective correspondence with $\pi_1 SO(n)$.

In the $n = 2$ case ($D^2 \times S^1$) this reproduces our previously stated results. When the two knots (images of S^1) are isotopic, classifying the embeddings reduces to an element of $\pi_1 SO(2) \cong \mathbb{Z}$ and can be understood as the number of Dehn twists. Now, when $n > 2$ any two embeddings of S^1 are automatically isotopic in $\mathbb{R}^{n+1}$. Thus we have

Theorem 7.13 (Codimension zero). *For $n \geq 3$ the embeddings of the solid torus $D^n \times S^1$ into $\mathbb{R}^{n+1}$ are in bijective correspondence with $\mathbb{Z}_2 \oplus \pi_1 SO(n) \cong \mathbb{Z}_2 \oplus \mathbb{Z}_2$. The first factor of $\mathbb{Z}_2$ is orientation or parity.*

This theorem may be understood much as in the classical $D^2 \times S^1$ case. We can define a Dehn twist for $D^n \times S^1$ as follows. Cut open $D^n \times S^1$ about a meridional disk $D \cong D^n$. Rotate one side 2π in some fixed plane and then reattach the two sides of the disk[4] (see Fig. 7.6). The connectivity properties of $SO(n)$ show that this procedure defines a homotopically non-trivial loop whose class is independent of the rotation plane chosen. Furthermore, applying a second Dehn twist results in a contractible loop resulting in an embedding indistinguishable from one with no applied Dehn twists.

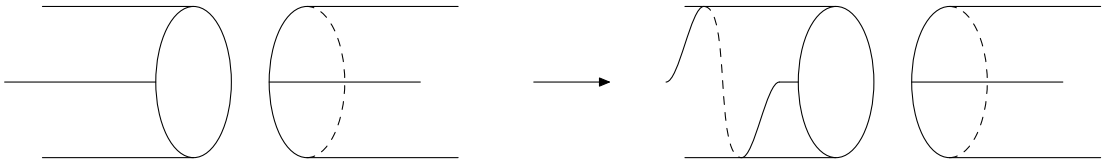

Figure 7.6: Application of a "Dehn twist" to $\mathcal{T}^n$.

We now consider embeddings of $D^n \times S^1$ into $\mathbb{R}^{m+1}$ with codimension $k = m - n = 1$. The immediate difficulty is that the image F_1 of $\mathcal{T}^n$ is no longer a tubular neighborhood, though of course it is still a disk-bundle neighborhood of S^1. If F_0 is a tubular neighborhood of S^1, Thm. 7.12 yields an ambient isotopy taking F_1 to a linear sub-bundle of F_0 of codimension 1. Let ξ_1 denote a one dimensional complementary bundle (which may be chosen uniquely using the Riemannian structure on the tubular neighborhood) so that $F_1 \oplus \xi_1 = F_0$.

Now, embeddings of F_0 are characterized by $\pi_1(SO(n+1))$. We now show that this information is contained in the sub-bundle F_1. That is, any pair of one dimensional bundles ξ are isotopic when $n \geq 2$. Since ξ is a one-dimensional sub-bundle of F_0, it is fully specified by a choice of unit vector at every point along S^1. In other words, it is equivalent to a section σ of the unit normal bundle $UN(S^1)$ in $\mathbb{R}^{m+1}$, which is a product bundle $S^1 \times S^m$. Letting π denote projection onto the second factor we have the diagram

$$\begin{array}{ccc} S^1 & \xrightarrow{\sigma} & S^1 \times S^m \\ & \searrow & \downarrow \pi \\ & & S^m \end{array} \tag{7.2}$$

The projection π sends the section σ to a closed path $\pi \circ \sigma$ in S^m. Since S^m is simply connected for $m \geq 2$, there is a homotopy h_t of $\pi \circ \sigma$ to a constant path. Since product spaces possess the homotopy lifting property

[4] This procedure may be done smoothly by damping out he rotation using a smooth bump function.

[7], there is a lifted homotopy H_t of σ such that $\pi \circ H_t = h_t$. Thus σ is isotopic to a constant section. But any two constant sections are isotopic by an obvious simultaneous rotation of each S^m factor. We have thus proven that

Theorem 7.14 (Codimension one). *For $n \geq 2$, the embeddings of the solid torus $D^n \times S^1$ into $\mathbb{R}^{n+2}$ are in bijective correspondence with $\pi_1 SO(n+1) \cong \mathbb{Z}_2$.*

We next consider codimension $k = m - n = 2$. In Sec. 3.5 we constructed an explicit isotopy from a single Dehn twist to the identity, showing that codimension two realizes the universal embedding type for the solid torus. The idea was to embed both the twisted and untwisted versions simultaneously, and the isotopy transitioned from projecting one embedding to projecting the other. The analogous procedure for a general solid torus $D^n \times S^1$ seems to require dimension $2n+1$, or codimension $(2n+1) - (n+1) = n$. However, recall that the Dehn twist in the general case involves only a single two dimensional subspace of the fiber D^n. This suggests the same isotopy may work by singling out this two dimensional subspace where the rotation takes places, since this will only require codimension two.

To this end we write $x \in D^n$ in the polar form $x = ru$, where $r \in [0,1]$ and $u \in S^{n-1} = \partial D^n$. We then introduce hyperspherical coordinates [35] on the sphere S^{n-1} by

$$u_1 = \cos\phi_1 \tag{7.3}$$

$$u_2 = \sin\phi_1 \cos\phi_2 \tag{7.4}$$

$$\vdots \tag{7.5}$$

$$u_k = \sin\phi_1 \cdots \sin\phi_{k-1} \cos\phi_k \tag{7.6}$$

$$\vdots \tag{7.7}$$

$$u_{n-1} = \sin\phi_1 \cdots \sin\phi_{n-2} \cos\theta \tag{7.8}$$

$$u_n = \sin\phi_1 \cdots \sin\phi_{n-2} \sin\theta, \tag{7.9}$$

where $\phi_k \in [0,\pi]$ are polar angles and $\theta \in [0, 2\pi)$ is the azimuthal angle. The final two coordinates, which

include the azimuthal angle, may be conveniently expressed in the complex form

$$z = u_{n-1} + iu_n = \sin\phi_1 \cdots \sin\phi_{n-2} e^{i\theta}. \tag{7.10}$$

If we parametrize S^1 by $s \in [0, 2\pi)$, then using these coordinates a Dehn twist may be written without loss of generality as

$$z \to ze^{is}, \tag{7.11}$$

and is constant on all other coordinates. By an abuse of notation we let u refer only to the coordinate $u_1, \ldots, u_{n-2}$, or all coordinates on the sphere except the last two, which are covered by z. In direct analogy with Sec. 3.5 we define the embedding

$$\begin{pmatrix} s \\ ru \\ rz \end{pmatrix} \mapsto \begin{pmatrix} s \\ ru \\ rz \\ rze^{is} \end{pmatrix}, \tag{7.12}$$

and the isotopy

$$\left(\begin{array}{c|cc} 1 & 0 & \\ \hline 0 & \cos\theta & \sin\theta \\ & -\sin\theta & \cos\theta \end{array}\right) \left(\begin{array}{c} s \\ ru \\ \hline rz \\ rze^{is} \end{array}\right), \tag{7.13}$$

which exchanges the two complex factors between $\theta = 0$ and $\theta = \pi/2$. Thus we have established that

Theorem 7.15 (Codimension two). *For $n \geq 2$, the embeddings of the solid torus $D^n \times S^1$ into $\mathbb{R}^{n+3}$ are all isotopic.*

Finally, since the same trick works for higher codimension, we have the following

Theorem 7.16 (Universality). *Any two embeddings of $D^n \times S^1$ into $\mathbb{R}^{n+1+k}$ for $k \geq 2$ are isotopic, i.e. there exists a universal embedding of solid tori in codimension at least two.*

7.4 Résumé

While a there exists a well understood theory for three dimensional dynamical systems, much less is known in higher dimensions. The present chapter uses the perspective of representation theory to gain some insight into their structure. In particular, the spectrum of embeddings for dynamical systems that live in $\mathcal{T}^n \cong D^n \times S^1$ has been completely worked out for every n. The $n > 2$ case is quite unlike the $n = 2$ case in that the "extrinsic" part of the problem is quite trivial. There are no non-trivial knot types to consider since $\mathcal{T}^n$ is just a thickened circle, and embeddings of this circle will always have codimension at least three. For $\mathcal{T}^n$ in codimension zero and one there are two distinct representations, which are quite analogous to the two classes obtained for the $n = 2$ case in $\mathbb{R}^4$. The universal embeddings is obtained in codimension two. These results are summarized in Tab. 7.1.

The results of the present chapter highlight some of the problems involved in working with higher dimensional systems. There are many pathologies one encounters, and more advanced techniques and imagination are required to make progress than were necessary in dimension three. Nevertheless, progress indeed has been made. While a complete understanding of higher dimensional systems remains elusive, and might forever remain so, we are still one step closer than we were previously.

Chapter 8: Conclusions and Outlook

We have taken the first steps in creating a representation theory for dynamical systems. On the theoretical level, these steps have been motivated by and guided to some extent by an analogy with the representation theory of groups. On the practical level, these steps have been motivated by recognizing the non-uniqueness of the reconstruction phase of any data analysis. Representations are embeddings (reconstructions) of an n-dimensional dynamical system into $\mathbb{R}^k$, $k \geq n$. Equivalence of representations is by isotopy. We have carried this program out for (almost) all three dimensional dynamical systems and for a restricted class of systems in arbitrary dimension.

The general program is as follows. Identify all the labels necessary to distinguish among inequivalent representations of the n-dimensional dynamical system when mapped into $\mathbb{R}^k$ for $k = n$. These labels are obstructions to isotopy. When inequivalent representations are mapped into a Euclidean space of one higher dimension, some may become equivalent because there is more room to "move around" and so avoid certain obstructions. As a result, some representation labels are no longer necessary. This process continues until all representations are isotopic and all obstructions have vanished. Then there is only one "universal" representation. According to a result of Wu, this universal representation definitely exists in $\mathbb{R}^{2n+1}$. For all systems considered presently, the universal representation always exists in codimension two: five for three-dimensional systems, and more generally in dimension $n + 2$ for n dimensional systems.

We developed the representation theory for three dimensional dynamical systems in two stages. The first stage was the representation theory of dynamical systems of "genus one" type. Such systems have the solid torus $\mathcal{T}$ as phase space, and their chaotic dynamics is generated by "stretching and folding" only. There are three representations labels in $\mathbb{R}^3$: knot type, parity, and global torsion; one in $\mathbb{R}^4$: global torsion (mod 2); and none in $\mathbb{R}^5$. The universal representation exists in $\mathbb{R}^k$, $k \geq 5$. This information is summarized in Tab. 3.1.

The second stage was extending this analysis to all "genus-g dynamical systems," $g \geq 3$. These systems have genus-g handlebodies as phase space and their chaotic dynamics are generated by "tearing and squeezing". There are three representations labels in $\mathbb{R}^3$: knot type, parity, and a spectrum of local torsions; one in

$\mathbb{R}^4$: a reduced spectrum of local torsions (mod 2); and none in $\mathbb{R}^5$. The universal representation exists in $\mathbb{R}^k$, $k \geq 5$. This information is summarized in Tab. 4.1.

Next we took a break from representation theory proper to consider in some detail the embeddings of the Lorenz dynamical system, which has genus three. We sought to understand how the standard differential mapping could yield an embedding not on our list of representations. We found that, in fact, this embedding was not an embedding at all, and thus not a true representation. In particular, this mapping is the singular projection into three-space of an embedding into four-space. This phenomenon is known as local reflection.

We then generalized those results for the Lorenz system concerning its symmetry to arbitrary equivariant dynamical systems. We were able to show that differential mappings are unable to retain more than a two-fold symmetry. This implies that such mappings are rarely embeddings.

Finally, we returned to our main theme and worked out the representation theory for toral systems of arbitrary dimension. These systems generalize the three dimensional genus one systems. We demonstrated many of the pitfalls that exist in higher dimensions which frustrate a straight-forward and intuitive understanding. Nevertheless, we were able to make progress and complete the theory for these systems.

We have considered representation theory at the level of phase spaces. We saw in Chap. 5 that the standard differential embedding of the Lorenz system is not actually a phase space embedding since it fails to be injective. However, it is essentially injective on the attracting set. More specifically, it is injective on the branched two-manifold. This suggests an extension of representation theory from phase spaces to templates for three dimensional dynamical systems. In general, local reflections of phase spaces lead to new and distinct representations for templates. It is unknown whether or not this is the only new way to create new representations. Since the reconstruction of a template rather than a full phase space is more natural when working with experimental data, it is worthwhile to consider and work out this extension.

The theory worked out in this thesis is in some sense the pinnacle of the topological theory for three dimensional systems, while it is only the beginning of the topological theory for higher dimensional systems. We hope that this fresh perspective will allow new insights into the structure of these systems. Ideally, this will eventually lead to a satisfying topological theory in higher dimensions.

The current impediments to such a theory are the want of an extension of the Birman-Williams theorem

and, more seriously, the want of appropriate topological invariants. We discussed the first in Chap. 1. We discuss the second here. For three-dimensional representations, the main calculational tool was the linking number (and more generally the link-type) of periodic orbits in the flow. Since copies of the circle never non-trivially link in dimensions beyond three, this tool is no longer available. Nevertheless, we have seen that there are non-trivial representations of three-dimensional systems in four dimensions. While the orbits do not link considered as curves in four-space, there is some non-trivial relation among them within the embedded phase space. While we have only detected this relationship at the level of the whole phase space embedding, there may be some way to extract this information more directly. Success on this point may lead to finding appropriate topological invariants for general higher-dimensional systems.

Having appropriate invariants at our disposal will lead to a better understanding of the structure of these systems and the mechanisms that generate chaos. This is precisely our goal: an understanding of the phase space mechanisms that underlie any physical system. This will lead to a better understanding of the data generated by these systems, then to a better understanding of the systems themselves, and ultimately to a better understanding of the physics they describe.

Bibliography

[1] Roy Adler, Tomasz Downarowicz, and Michal Misiurewicz, *Topological entropy*, Scholarpedia **3** (2008), no. 2, 2200.

[2] J. W. Alexander, *An example of a simply-connected surface bounding a region which is not simply-connected*, Proc. Nat. Acad. Sci. **10** (1924), 8–10.

[3] J. S. Birman and R. F. Williams, *Knotted periodic orbits in dynamical systems-I: Lorenz's equations*, Topology **22** (1983), no. 1, 47–82.

[4] _____, *Knotted periodic orbits in dynamical systems-II: Knot holders for fibered knots*, Contemp. Math. **20** (1983), 1–60.

[5] R. Bowen, *One-dimensional hyperbolic sets for flows*, J. Diff. Eq. **12** (1972), 173–179.

[6] _____, *On axiom A diffeomorphisms*, Regional Conference Series in Mathematics, vol. 35, National Science Foundation, American Mathematical Society, 1978, pp. 1–45.

[7] Glen E. Bredon, *Topology and geometry*, Graduate Texts in Mathematics, vol. 139, Springer, New York, NY, 1993.

[8] Morton Brown, *A proof of the generalized Schönflies theorem*, Bull. A. M. S. **66** (1960), 74–76.

[9] J. Cerf, *Topologie des certains espaces de plongements*, Bull. Soc. Math. France **89** (1961), 227–380.

[10] _____, *Sur les difféomorphismes de la sphère de dimension trois*, Lecture Notes in Mathematics, vol. 53, Springer, Berlin, 1968.

[11] Y. Coudene, *Pictures of hyperbolic dynamical systems*, Notices of the AMS **53** (2006), no. 1, 8–13.

[12] D. Cox, J. Little, and D. O'Shea, *Ideals, varieties, and algorithms*, Springer-Verlag, New York, NY, 1996.

[13] P. Cromwell, *Knots and links*, Cambridge Univ. Press, Cambridge, UK, 2004.

[14] Stefano Demichelis and Michael H. Freedman, *Uncountably many exotic $\mathbb{R}^4$'s in standard 4-space*, J. Diff. Geom. **35** (1992), 219–254.

[15] R. L. Devaney, *An introduction to chaotic dynamical systems*, second ed., Westview Press, Cambridge, MA, 2003.

[16] Richard P. Feynman and Steven Weinberg, *Elementary particles and the laws of physics: The 1986 Dirac memorial lectures*, Cambridge University Press, New York, NY, 1987.

[17] T. Frankel, *The geometry of physics*, Cambridge Univ. Press, New York, NY, 2006.

[18] Michael H. Freedman, *The topology of four-dimensional manifolds*, J. Diff. Geom. **17** (1982), 357–453.

[19] G Frobenius, *Über matrizen aus nicht negativen elementen*, Sitzungsberichte der Preussischen Akademie der Wissenschaften zu Berlin, 1912, pp. 456–477.

[20] R. W. Ghrist, P. J. Holmes, and M. C. Sullivan, *Knots and links in three-dimensional flows*, Lecture Notes in Mathematics, vol. 1654, Springer-Verlag, Berlin, 1997.

[21] R. Gilmore, *Topological analysis of chaotic dynamical systems*, Revs. Mod. Phys. **70** (1998), 1455–1530.

[22] R. Gilmore, Jean-Marc Ginoux, Timothy Jones, C. Letellier, and U. S. Freitas, *Connecting curves for dynamical systems*, J. Phys. A **43** (2010), no. 25, 255101.

[23] R. Gilmore and C. Letellier, *Dressed symbolic dynamics*, Phys. Rev. E **67** (2003), no. 3, 036205.

[24] R. Gilmore, C. Letellier, and N. Romanazzi, *Global topology from an embedding*, J. Phys. A: Math. Theor. **40** (2007), 13291–13297.

[25] Robert Gilmore and Mark Lefranc, *The topology of chaos: Alice in stretch and squeezeland*, Wiley, New York, NY, 2002.

[26] Robert Gilmore and Christophe Letellier, *The symmetry of chaos*, Oxford University Press, New York, NY, 2007.

[27] C. McA. Gordon and J. Luecke, *Knots are determined by their complements*, J. Amer. Math. Soc. **2** (1989), no. 2, 371âĂŞ415.

[28] G. Gouesbet, *Reconstruction of vector fields: the case of the Lorenz system*, Phys. Rev. A **46** (1992), no. 4, 1784–1796.

[29] G. Gouesbet and C. Letellier, *Global vector field reconstruction by using a multivariate polynomial $L2$-approximation on nets*, Phys. Rev. E **49** (1994), no. 6, 4955–4972.

[30] J. Guckenheimer and P. Holmes, *Nonlinear oscillations, dynamical systems, and bifurcations of vector fields*, Applied Mathematical Sciences, vol. 42, Springer-Verlag, New York, NY, 1983.

[31] Victor Guillemin and Alan Pollack, *Differential geometry*, Prentice Hall, Inc., Englewood Cliffs, NJ, 1974.

[32] Morton Hamermesh, *Group theory and its applications to physical problems*, Dover, Mineola, NY, 1962.

[33] Allen Hatcher, *Algebraic topology*, Cambridge Univ. Press, Cambridge, UK, 2001.

[34] H. Hirsch, C. Pugh, and M. Schub, *Invariant manifolds*, Springer Lecture Notes in Mathematics, vol. 583, Springer-Verlag, New York, 1970.

[35] Kiyoshi Itō (ed.), *Encyclopedic dictionary of mathematics*, second ed., MIT Press, Cambridge, MA, 2000.

[36] Jürgen Jost, *Riemannian geometry and geometric analysis*, Springer, New York, NY, 2000.

[37] Ittai Kan, *Open sets of diffeomorphisms having two attractors each with an everywhere dense basin*, Bull. Amer. Math. Soc **31** (1994), no. 1, 68–74.

[38] G. P. King and Ian Stewart, *Phase space reconstruction for symmetric dynamical systems*, Physica D **58** (1992), 216–228.

[39] Antoni A. Kosinski, *Differential manifolds*, Dover Publications, Inc, Mineola, NY, 1993.

[40] M. Kremliovsky, *Can we understand time scales of solar activity?*, Solar Physics **151** (1994), 351–370.

[41] C. Letellier, P. Dutertre, J. Reizner, and G. Gousbet, *Evolution of a multimodal map induced by an equivariant vector field*, J Phys A: Math Gen **29** (1996), 5359âĂŞ5373.

[42] C. Letellier and R. Gilmore, *Covering dynamical systems: Two-fold covers*, Phys. Rev. E **63** (2000), 016206.

[43] C. Letellier and G. Gouesbet, *Topological characterization of reconstructed attractors modding out symmeetries*, J. Phys. II France **6** (1996), 1615–1638.

[44] Christophe Letellier and Luis A. Aguirre, *Investigating nonlinear dynamics from time series: The influence of symmetries and the choice of observables*, Chaos **12** (2002), no. 3, 549.

[45] _____, *Symbolic observability coefficients for univariate and multivariate analysis*, Phys. Rev. E **79** (2009), 066210.

[46] Christophe Letellier, Luis A. Aguirre, and U. S. Freitas, *Frequently asked questions about global modeling*, Chaos **19** (2009), 023103.

[47] E. N. Lorenz, *Deterministic nonperiodic flow*, Journal of Atmospheric Science **20** (1963), 130–141.

[48] John W. Milnor, *Differentiable structures on spheres*, Americal Journal of Mathematics **81** (1959), no. 4, 962–972.

[49] ———, *Attractor*, Scholarpedia **1** (2006), no. 11, 1815.

[50] G. B. Mindlin, H. G. Solari, M. A. Natiello, R. Gilmore, and X.-J. Hou, *Topological analysis of chaotic time series data from the Belousov-Zhabotinskii reaction*, J. Nonlinear Science **1** (1991), 147–173.

[51] J. Munkres, *Differentiable isotopies of the 2-sphere*, Mich. Math. J. **7** (1960), 193–197.

[52] R Palais, *Extending diffeomorphisms*, Proc. Amer. Math. Soc. **11** (1960), 274–277.

[53] R. Palais, *Local triviality of the restriction map for embeddings*, Comment. Math. Helv. **34** (1960), 305–312.

[54] C. Wayne Patty, *Foundations of topology*, Waveland Press, Prospect Heights, Il, 1993.

[55] Grisha Perelman, *The entropy formula for the Ricci flow and its geometric applications*, arXiv:math/0211159, 2002.

[56] ———, *Finite extinction time for the solutions to the Ricci flow on certain three-manifolds*, arXiv:math/0307245, 2003.

[57] ———, *Ricci flow with surgery on three-manifolds*, arXiv:math/0303109, 2003.

[58] Oskar Perron, *Zur theorie der matrices*, Mathematische Annalen **64** (1907), no. 2, 248–263.

[59] H. Poincaré, *Les méthodes nouvelles de la mécanique céleste*, Gauthier-Villars, Paris, 1892.

[60] William H. Press, Saul A. Teukolsky, William T. Vetterling, and Brian P. Flannery, *Numerical recipes in C*, second ed., Cambridge University Press, New York, NY, 1992.

[61] Charles C. Pugh, *A generalized Poincaré index formula*, Topology **7** (1968), no. 3, 217–226.

[62] J. Robbins, *A structural stability theorem*, Ann. Math. **94** (1971), 447–493.

[63] C. Robinson, *Structural stability of vector fields*, Invent. Math. **99** (1974), 154–175.

[64] D. Rolfsen, *Knots and links*, American Mathematical Society, Providence, RI, 2003.

[65] N. Romanazzi, M. Lefranc, and R. Gilmore, *Embeddings of low-dimensional strange attractors: Topological invariants and degrees of freedom*, Phys. Rev. E **75** (2007), 066214.

[66] O. E. Rössler, *An equation for continuous chaos*, Phys. Lett. A **57** (1976), no. 5, 397–398.

[67] T. D. Sauer, *Attractor reconstruction*, Scholarpedia **1** (2006), no. 10, 1727.

[68] Timothy D. Sauer, Joshua A. Tempkin, and James A. Yorke, *Spurious lyapunov exponenets in attractor reconstruction*, Phys. Rev. Lett. **81** (1998), no. 20, 4341–4344.

[69] Otto Schreier, *Die untergruppen der freien gruppen*, Abhandlungen aus dem Mathematischen Seminar der Universität Hamburg **5** (1929), 161–183.

[70] W. R. Scott, *Group theory*, Dover, New York, NY, 1987.

[71] Herbert Seifert, *über das geschlecht von knoten*, Math. Annalen **110** (1934), 571–592.

[72] R. Shaw, *Strange attractor, chaotic behavior and information flow*, Zeitschrift für Naturforschung **36** (1981), no. a, 80–112.

[73] N. J. A. Sloane, *The on-line encyclopedia of integer sequences*, Published electronically at http://www.research.att.com/~njas/sequences/.

[74] S. Smale, *Differentiable dynamical systems*, Bull. Am. Math. Soc. **73** (1967), 747–817.

[75] Stephen Smale, *Differentiable and combinatorial structures on manifolds*, Annals of Mathematics, Second Series **74** (1961), no. 3, 498–502.

[76] Steven Smale, *Diffeomorphisms of the 2-sphere*, Proc. Amer. Math. Soc. **10** (1959), 621–626.

[77] ———, *Generalized Poincaré's conjecture in dimensions greater than four*, Ann. of Math **74** (1961), no. 2, 485–488.

[78] H. G. Solari and R. Gilmore, *Relative rotation rates for driven dynamical systems*, Phys. Rev. A **37** (1988), 3096–3109.

[79] F. Takens, *Detecting strange attractors in turbulence*, Dynamical Systems and Turbulence, Lecture Notes in Mathematics (D. A. Rand and L. S. Young, eds.), vol. 898, Springer-Verlag, New York, NY, 1981, pp. 366–381.

[80] Clifford Henry Taubes, *Gauge theory on asymptotically periodic 4-manifolds*, J. Diff. Geom. **25** (1987), 363–430.

[81] R. Thomas, *Deterministic chaos seen in terms of feedback circuits: Analysis, synthesis, "labyrinth chaos"*, International Journal of Bifurcations and Chaos **9** (1999), no. 10, 366–381.

[82] Tsvetelin D. Tsankov, *Topological aspects of the structure of chaotic attractors in* $\mathbb{R}^3$, Ph.D. thesis, Drexel University, 2004.

[83] Tsvetelin D. Tsankov and Robert Gilmore, *Topological aspects of the structure of chaotic attractors in* $\mathbb{R}^3$, Phys. Rev. E **69** (2004), no. 5, 056206.

[84] N. B. Tufillaro, T. A. Abbott, and J. P. Reilly, *An experimental approach to nonlinear dynamics and chaos*, Addison-Wesley, New York, NY, 1992.

[85] Edward C. Turner, *A survey of diffeomorphisms groups*, Algebraic and Geometrical Methods in Topology, Lecture Notes in Mathematics, vol. 428, Springer, Berlin, 1974, pp. 200–218.

[86] B. Wajnryb, *Mapping class group of a handlebody*, Fundamenta Mathematicae **158** (1998), 195–228.

[87] H. Whitney, *Differentiable manifolds*, Ann. Math. **37** (1936), 645.

[88] W. Wu, *On the isotopy of* C^r*-manifolds of dimension* n *in Euclidean* $(2n+1)$*-space*, Sci. Rec. N. S. **II** (1958), 271–275.

Appendix A: Homology of Connected Sums

It is the purpose of this appendix to calculate the homology groups and Euler characteristic of a connected sum of manifolds. Suppose that M and N are compact, closed, and oriented n-manifolds with homology groups $H_p(M)$ and $H_p(N)$, respectively. We wish to calculate the homology groups $H_p(M\#N)$. The result is

Theorem A.1. *The homology groups of the connected sum of two compact, closed, and oriented n-manifolds M and N is the direct sum of the homology groups $H_p(M\#N) = H_p(M) \oplus H_p(N)$ for every $p \neq 0, n$. In the last two cases, $H_p(M\#N) \cong \mathbb{Z}$.*

The rest of this appendix presents a proof of this fact.

Since homology groups are homeomorphism invariants, it suffices to use the topological definition of connected sum. Thus, we take embeddings D and D' of D^n into M and N respectively, remove the interiors, and then identify the boundaries, which are copies of S^{n-1}. We may therefore write $M\#N = (M - D) \cup (N - D')$ with $(M - D) \cap (N - D') \cong S^{n-1}$.

We must first determine the homology of $M - D$ and $N - D'$. This is the hardest computation, though the result is quite simple. The arguments are typical of algebraic topology.

Lemma A.2. *For an embedding $D : D^n \to M$ of an n-disk into a manifold, $H_n(M - D) \cong 0$ and $H_p(M - D) \cong H_p(N)$ for $p \neq n$.*

Proof. Because D^n is contractible, the embedding D is homotopic to a constant map. By homotopy invariance we have $H_p(M - D) \cong H_p(M - x)$, where $x \in M$ is a point. Consider the pair of spaces $(M, M - x)$ and the corresponding long exact sequence (see Eq. 1.13)

$$\cdots \to H_p(M - x) \to H_p(M) \to H_p(M, M - x) \to H_{p-1}(M - x) \to \cdots . \tag{A.1}$$

Since M is a manifold, x has a neighborhood U homeomorphic to $\mathbb{R}^n$. We may assume the homeomorphism takes x to the origin. If we remove the complement U^c of U from M, then by the excision property [7], we

obtain homeomorphisms

$$H_p(M, x) \cong H_p(M - U^c, (M - x) - U^c) \cong H_p(U, U - x) \cong H_p(\mathbb{R}^n, \mathbb{R}^n - 0), \tag{A.2}$$

where the first homeomorphism is excision, the second is just the definition of the spaces, and the third is induced by homeomorphism.

Now, for the new pair $(\mathbb{R}^n, \mathbb{R}^n - 0)$ we have the long exact sequence

$$\cdots \to H_p(\mathbb{R}^n - 0) \to H_p(\mathbb{R}^n) \to H_p(\mathbb{R}^n, \mathbb{R}^n - 0) \to H_{p-1}(\mathbb{R}^n - 0) \to \cdots . \tag{A.3}$$

Since $\mathbb{R}^n$ is contractible, its only non-zero homology group is $H_0 \cong \mathbb{Z}$. Putting in these trivial groups, for $p > 1$ we obtain the sequences

$$0 \to H_p(\mathbb{R}^n, \mathbb{R}^n - 0) \to H_{p-1}(\mathbb{R}^n - 0) \to 0, \tag{A.4}$$

which implies that the middle map as an isomorphism. Now, consider $H_0(\mathbb{R}^n, \mathbb{R}^n - 0)$. A relative 0-cycle is just a finite linear combination of points of $\mathbb{R}^n$ with integer coefficients. Let $x \in \mathbb{R}^n$. Choose a path γ such that $\gamma(1) = x$ and $\gamma(0) \neq 0$. Then $x = \partial\gamma \mod \mathbb{R}^n - 0$, hence x is a relative boundary. We conclude that $H_0(\mathbb{R}^n, \mathbb{R}^n - 0) \cong 0$. Since $\mathbb{R}^n - 0$ is connected, $H_0(\mathbb{R}^n - 0) \cong \mathbb{Z}$. Thus, for $p = 1$ we obtain the sequence

$$0 \to H_1(\mathbb{R}^n, \mathbb{R}^n - 0) \to \mathbb{Z} \to \mathbb{Z} \to 0. \tag{A.5}$$

By exactness, the homomorphism $\mathbb{Z} \to \mathbb{Z}$ is surjective, hence an isomorphism. This implies that $H_1(\mathbb{R}^n, \mathbb{R}^n - 0) \cong 0$.

Now, the space $\mathbb{R}^n - 0$ is homotopic to S^{n-1}, which has non-trivial homology groups $H_0 \cong H_{n-1} \cong \mathbb{Z}$. We conclude that the pair $(\mathbb{R}^n, \mathbb{R}^n - 0)$ has only one non-trivial homology group: $H_n \cong \mathbb{Z}$. By Eq. (A.2), the same is true for the homology groups of the pair $(M, M - x)$. By placing these zero groups into Eq. (A.1) we

immediately obtain, for $p < n-1$, isomorphisms

$$H_p(M-x) \cong H_p(M). \tag{A.6}$$

For the top two dimensions we have the sequence

$$0 \to H_n(M-x) \to H_n(M) \xrightarrow{f} H_n(M, M-x) \cong \mathbb{Z} \to H_{n-1}(M-x) \to H_{n-1}(M) \to 0. \tag{A.7}$$

Since we have assumed M to be compact, closed, and oriented, $H_n(M) \cong \mathbb{Z}$ and is generated by M. But M also generates $H_n(M, M-q)$, hence the map f above is an isomorphism. This forces the map into $H_n(M)$ and the map out of $H_n(M, M-q)$ to both be zero. It immediately follows that $H_n(M-q) \cong 0$ and $H_{n-1}(M-q) \cong H_{n-1}(M)$. We conclude that $H_p(M-D) \cong H_p(M)$ for $p \neq n$ and that $H_n(M-D) \cong 0$. □

We now have the homology groups of $M-D$ and of $N-D'$ in terms of those of M and N respectively. We have written the connected sum as the union of these two subspaces. Whenever a space X may be written as a union $X = A \cup B$, the homology of X, A, B, and of $A \cap B$ fit into a long exact sequence called the Mayer-Vietoris sequence [7]:

$$\cdots \to H_p(A \cap B) \to H_p(A) \oplus H_p(B) \to H_p(X) \to H_{p-1}(A \cap B) \to \cdots, \tag{A.8}$$

which in the present case is

$$\cdots \to H_p(S^{n-1}) \to H_p(M-D) \oplus H_p(N-D') \to H_p(M\#N) \to H_{p-1}(S^{n-1}) \to \cdots. \tag{A.9}$$

Since $H_p(S^{n-1})$ is trivial unless $p = 0, n-1$, we immediately obtain isomorphisms $H_p(M\#N) \cong H_p(M) \oplus H_p(N)$ for $p = 2, \ldots, n-2$. Since all spaces are connected, every $H_0 \cong \mathbb{Z}$, and we obtain the isomorphism $H_1(M\#N) \cong H_1(M) \oplus H_1(N)$.

In the top two dimensions we have the sequence

$$0 \to H_n(M\#N) \to \mathbb{Z} \to H_{n-1}(M) \oplus H_{n-1}(N) \to H_{n-1}(M\#N) \to 0. \tag{A.10}$$

Since M and N are compact, closed, and oriented, so is $M\#N$. Thus $H_n(M\#N) \cong \mathbb{Z}$, the map from this group to $\mathbb{Z}$ is an isomorphism, and thus the map out of $\mathbb{Z}$ is zero. We therefore obtain an isomorphism $H_{n-1}(M\#N) \cong H_{n-1}(M) \oplus H_{n-1}(N)$. Putting this together we have

$$H_p(M\#N) \cong \begin{cases} \mathbb{Z}, & p = 0, n \\ H_p(M) \oplus H_p(N), & \text{otherwise} \end{cases} \tag{A.11}$$

Finally, we compare the Euler characteristic. If we write $b_i = \operatorname{rank} H_i$ for the Betti numbers, then for $i \neq 0, n$ we have $b_i(M\#N) = b_i(M) + b_i(N)$. When $i = 0, n$ we may write $b_i(M\#N) = 1 = b_i(M) + b_i(N) - 1$. We therefore have

$$\begin{aligned} \chi(M\#N) &= \sum_{i=0}^{n} (-1)^i b_i(M\#N) \\ &= \big(b_0(M) + b_0(N) - 1\big) - \big(b_1(M) + b_1(N)\big) + \cdots + (-1)^n \big(b_n(M) + b_n(N) - 1\big) \\ &= \chi(M) + \chi(M) - (1 + (-1)^n) \\ &= \chi(M) + \chi(M) - \chi(S^n). \end{aligned} \tag{A.12}$$

Note the strange even/odd dependence on the manifold dimension.

When $n = 2$ these results are particularly simple. Two homology groups are trivial to compute: $H_0(M\#N) \cong H_2(M\#N) \cong \mathbb{Z}$. This leaves only $H_1(M\#N) = H_1(M) \oplus H_1(N)$. The Euler characteristic is given by $\chi(M\#N) = \chi(M) + \chi(N) - 2$.

Appendix B: Local Reflection Isotopy

The purpose of this appendix is to fill in the technical details of Sec. 5.4 by constructing explicit deformations of the mappings F_3 and F_4 to a local reflection and inclusion respectively. The idea of a smooth deformation of an embedding is made precise through the notion of *isotopy*. Two embeddings f and g are isotopic if there is a smooth map $h(x,s)$, $s \in [0,1]$, that satisfies the following three properties: 1) for every fixed s, $h_s(x) \equiv h(x,s)$ is an embedding; 2) $h_0 = f$; and 3) $h_1 = g$. We will refer to either $h(x,s)$ or $h_s(x)$ as the isotopy. Thinking of s as time, the isotopy smoothly transforms the embedding f at time zero to the embedding g at time one through a sequence of embeddings. It is natural to regard isotopic embedding's as the same or equivalent. We note that it will often be convenient to define an isotopy over an interval other than $[0,1]$. In all cases the isotopies defined will be obviously smooth, so one need only check that they are one-to-one for each s.

Recall the twisted embedding Eq. (5.13), and the denominators of the last two coordinate which normalized them to approach inclusion as $|x| \to \infty$. This embedding is isotopic to the un-normalized mapping

$$G : (x,y,z) \mapsto (x,y,-xz,z). \tag{B.1}$$

One can take for the deformation $(1-s)F + sG$ with $s \in [0,1]$ and check that this is one-to-one for each s. We may also refer to the first three coordinates of this mapping as a local reflection of $\mathbb{R}^3$.

The mapping F_3 defines a rather complicated embedding of $\mathbb{R}^3 - \{yz\text{-plane}\}$ into $\mathbb{R}^3$. Denote the image of (x,y,z) by $(X,Y,Z) = F_3(x,y,z)$ and recall that these coordinates are given by Eq. (5.4). We will now simplify F_3 through a sequence of isotopies. We note that the isotopies need only be one-to-one away from the yz-plane since F_3 is singular there. In each case $s \in [0,1]$. Our goal is to show that F_3 is isotopic to a local reflection.

First note that the first coordinate is already $X = x$. Next, by smoothly rescaling the axes, the overall factor of σ on the last two components may be set to one. The second coordinate is now given by $Y = y - x$.

By defining $Y_s = y + (s-1)x$ this coordinate can be smoothly changed to $Y = y$. One can check that this is one-to-one for every s. For the third coordinate define $Z_s = Z(1-s) - szx$ to smoothly deform it to $-zx$. In this case points with different z coordinate are identified when $x = 0$. In fact, when $x = 0$, $Z_s = (s-1)(1+\sigma)y$, so for every s the yz-plane is taken to a line. The form of the singularity is preserved during this deformation and Z_s defines an isotopy of F_3 away from its singular set. We have thus succeeded in bring F_3 to the form of (the first three coordinates of) Eq. (B.1) through a sequence of deformations. This proves the claim in Sec. 5.4 that the attractors $\mathcal{L}_i$ and $\mathcal{L}$ differ by a local reflection in $\mathbb{R}^3$.

Now we consider the embedding F_4 into $\mathbb{R}^4$. Since the first three coordinate of F_4 are given by F_3, the above isotopies apply to F_4 as well. However, the isotopy Z_t was singular for F_3 along $x = 0$. By checking the fourth coordinate W of F_4 given in Eq. (5.8) we see that points are identified only when $y = 0$ as well. But this defines the z-axis, which is the singular set of F_4. We conclude that Z_t is an isotopy away from the singular set of F_4.

It remains only to transform the final coordinate W to z to arrive at the twisted embedding Eq. (B.1). This can be done through a sequence of deformations, $W \to z(x-y) \to zx \to z$. At each step the deformation is linear: $f \to g$ by $sg + (1-s)f$. It is tedious but straightforward to check that each deformation is one-to-one away from the z-axis and so completes the isotopy of F_4 to the twisted embedding. Finally, the twisted embedding is isotopic to the standard inclusion $\mathbb{R}^3 \hookrightarrow \mathbb{R}^4$. This can be achieved by the isotopy

$$(x, y, z, s) \to (x, y, -z\sin\xi, z\cos\xi), \tag{B.2}$$

where we set

$$\xi = s\arctan x + (s-1)\pi/2, \tag{B.3}$$

and $s \in [0, 1]$. We conclude that F_4 is isotopic to the inclusion $\mathbb{R}^3 \hookrightarrow \mathbb{R}^4$. This proves the claim in Sec. 5.4 that the attractors $\mathcal{L}_i$ and $\mathcal{L}$ are identical in $\mathbb{R}^4$.

Appendix C: Linking Integral Projection

The linking integral is an invariant of the link-type of two manifolds immersed in a Euclidean space. It is shown that the ordinary Gauss integral in three dimensions may be simplified to a winding number integral in two dimensions. This result is then generalized to show that in certain circumstances the linking integral between arbitrary manifolds may be similarly reduced to a lower dimensional integral. This procedure simplifies practical calculations and may prove useful in investigating the topological structure of higher dimensional dynamical systems. We include it here for completeness.

C.1 Reduction of the Gauss Integral to the Winding Number Integral

The linking number of two disjoint oriented closed curves in $\mathbb{R}^3$ is an integer invariant that in some sense measures the extent of linking between the curves. While there are many equivalent ways to compute this number [64], the most well-known is the linking integral of Gauss. In this section we show that this integral in 3-space may always be simplified to an integral in 2-space which is equivalent to a winding number integral.

Proposition C.1. *Given two disjoint immersed closed curves $s \mapsto \gamma_1(s)$ and $t \mapsto \gamma_2(t)$ in $\mathbb{R}^3$, the Gauss linking integral of the pair reduces to a sum of winding numbers of one curve about a sequence of points determined by the other, contained in some 2-dimensional hyperplane (see Fig. C.1).*

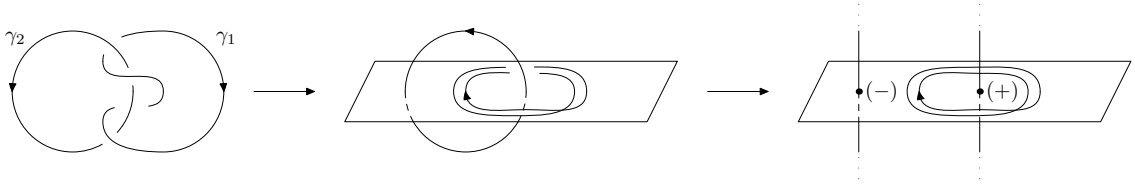

Figure C.1: Reduction of linking number to winding number. Curve γ_1 is projected into a plane, and we calculate the sum of its winding numbers about the intersection points of γ_2 with this plane. The sum of winding numbers is -2, which is equal to the linking number of the two curves.

Proof. The link of γ_1 and γ_2, $\mathrm{lk}(\gamma_1, \gamma_2)$, is given by the Gauss integral,

$$\mathrm{lk}(\gamma_1, \gamma_2) = \frac{1}{4\pi} \int \det\left(r, \frac{\partial \gamma_1}{\partial s}, \frac{\partial \gamma_2}{\partial t}\right) \frac{ds dt}{r^3},$$

where each term in the determinant is a column vector and $r = \gamma_2 - \gamma_1$ is the relative position vector. Through a homotopy of the maps we may arrange γ_1 to lie in the plane $x_3 = 0$ with γ_2 intersecting the plane perpendicularly in a finite number of points p_i. This may be done so that γ_1 and γ_2 remain disjoint throughout. Since the Gauss integral is a homotopy invariant, $\mathrm{lk}(\gamma_1, \gamma_2)$ is preserved through this deformation. If the homotopy was merely continuous we may replace it with an arbitrarily close smooth homotopic approximation.

Next, deform γ_2 near the intersection with the plane so that it becomes a straight line segment perpendicular to the plane in a neighborhood of each intersection point. Now deform it further by "stretching" it away from the plane so that the straight line segments are extended further away from the plane and the rest of γ_2 is pushed further away from the plane. In the limit that the stretching goes off to infinity, the denominator of the integral falls off sufficiently fast that its contribution goes to zero. We are left with a finite number of infinite line segments perpendicular to the plane and disjoint from γ_1. We assume each line is parametrized in the standard way, $t \mapsto \pm x_3$.

We will now assume each line parametrized by $t \mapsto x_3$ so that $\partial\gamma_2/\partial t = e_3$, but introduce an orientation to each point $o(p_i)$ which is ± 1 depending on the original parameterization of the corresponding line in an obvious way. We then see that the linking integral becomes

$$\sum_i o(p_i) \frac{1}{4\pi} \int \det\left(r, \frac{\partial\gamma_2}{\partial s}, e_3\right) \frac{ds dt}{(\rho^2 + t^2)^{3/2}},$$

where ρ is the restriction of r to the plane $x_3 = 0$.

Notice that since $e_3 = (0, 0, 1)^t$ the determinant reduces to that of the upper-left block, which is $\det(\rho_{12}, \partial\gamma_2/\partial s))$ and is independent of t. Thus we may evaluate the integral

$$\int_{\mathbb{R}} \frac{dt}{(\rho^2 + t^2)^{3/2}} = \frac{2}{\rho^2},$$

and the linking integral becomes

$$\sum_i o(p_i) \frac{1}{2\pi} \int \det\left(\rho, \frac{\partial\gamma_2}{\partial s}\right) \frac{ds}{\rho^2},$$

which is easily seen to be the sum of the winding numbers of γ_2 about each point p_i times the orientation of p_i. □

The construction in the proof also allows one to show the linking integral may also be given as an intersection number of γ_1 with a surface spanned by γ_2. Indeed, perturb γ_2 to an embedding and let S be a Seifert surface constructed by Seifert's algorithm [64, 71]. The number of Seifert disks above a p_i is precisely the winding number of γ_1 about p_i and the induced orientation of each Seifert disk is given by the orientation of the bounding curve. Finally, with $o(p_i)$ we have the signed intersection number of γ_2 with the Seifert disk, and the sum over all gives the signed intersection number of γ_2 with S.

C.2 The General Linking Integral Projection

In this section the proposition of Sec. C.1 is generalized from curves to arbitrary compact boundaryless oriented manifolds M^n and N^n mapped disjointly into $\mathbb{R}^{p+1}$, $p = m + n$. In this case one may define a linking number by $\mathrm{lk}(M, N) = (-1)^m \deg \hat{r}$, where $\hat{r}$ is the unit relative position vector defined by

$$\begin{aligned} \hat{r} : M \times N &\to S^p \\ (x, y) &\mapsto \frac{r}{||r||} = \frac{x - y}{||x - y||}, \end{aligned}$$

where x and y are points in the images of M and N in $\mathbb{R}^{p+1}$ respectively. We will show that under certain conditions the linking number calculation reduces to a calculation in a hyperplane. We note that these expressions may be defined with differing sign conventions in which case the conclusion of the theorem will hold up to a sign. The present convention is most convenient for expressing the present result.

Theorem C.2. *Given M and N as above, suppose that there exists smooth homotopies of M and N maintaining disjointness and taking M into an $m + n' + 1$-dimensional hyperplane H, $0 \leq n' \leq n$, and that N intersects H transversely in the submanifold N'. Then $\mathrm{lk}(M, N) = \mathrm{lk}(M, N')$, where the first linking integral is taken in $\mathbb{R}^{p+1}$ and the second in $H \cong \mathbb{R}^{p'+1}$, where $p = m + n$ and $p' = m + n'$.*

Proof. It is straightforward to show [17] that the degree of this map may be written explicitly as

$$\deg \hat{r} = \frac{(-1)^m}{\mathrm{vol}S^p} \int_{M\times N} \det\left(r, \frac{\partial x}{\partial s}, \frac{\partial y}{\partial t}\right) \frac{dsdt}{||r||^{p+1}}, \tag{C.1}$$

where s and t represent oriented local coordinates s_i and t_j on M and N respectively, and the quantities in the determinant are column vectors.

We now deform (homotopy) M into $H \simeq \mathbb{R}^{p'+1}$ and deform N so that it intersects H transversely. The intersection $N' = \cup N'_i$ will be a finite disjoint union of closed oriented manifolds of dimension n' (the codimension of the transverse intersection of two manifolds is the sum of their codimensions). We may actually assume that $N \perp H$ (in the Euclidean metric of $\mathbb{R}^{p+1}$) so that N is locally of the form $N' \times \mathbb{R}^{n-n'}$ in some neighborhood of H. Now extend this local product decomposition by pushing the rest of N off to ∞ as was done in Sec. C.1. Since the integrand in Eq. C.1 falls off sufficiently fast with distance, this contribution to the integral goes to zero, so we may make the replacement $N \to N' \times \mathbb{R}^{n-n'}$.

Adapt the coordinates on N with respect to the product decomposition so that the last $n - n'$ coordinates are Euclidean coordinates on $\mathbb{R}^{n-n'}$. The partial derivatives $\partial y/\partial t_i$ with respect to these coordinates are just $\pm e_i$, the i-th unit vector, but the signs may vary on different N'_i. We may absorb these signs into the orientation of the components, considering their orientations reversed if necessary (rather than explicitly introducing an orientation function as was done in Sec. C.1).

The matrix in the integrand has a block structure with an $n - n'$ unit matrix in the lower right block and zero in the upper right block. Thus the determinant may be replaced with just that of the upper left block. Since this matrix is independent of the last $n - n'$ coordinates the distance function r reduces to $\rho = r|_H$. It remains to evaluate the integral

$$I = \int_{-\infty}^{\infty} \cdots \int_{-\infty}^{\infty} \frac{dt_{q+1} \cdots dt_n}{(\rho^2 + \sum t_i^2)^{(p+1)/2}},$$

for $i = q+1, \ldots, n$. Write $t_n = z$ and $a = \rho^2 + \sum t_i^2$, $i \neq n$ and then

$$\int_{-\infty}^{\infty} \frac{dz}{(a+z^2)^{(p+1)/2}} = \frac{\sqrt{\pi}}{a^{p/2}} \frac{\Gamma(\frac{p}{2})}{\Gamma(\frac{p+1}{2})} = \frac{1}{a^{p/2}} \frac{\mathrm{vol}_{S^p}}{\mathrm{vol}_{S^{p-1}}},$$

using the well-known expression for the volume of a sphere. By progressively isolating the variables t_i we obtain an integral of the same form but with p decreasing by one each time. Proceeding by induction we obtain

$$I = \frac{1}{||\rho||^{p'+1}} \frac{\mathrm{vol}_{S^p}}{\mathrm{vol}_{S^{p'}}},$$

where $p' = p - n + n' = m + n'$. Hence Eq. C.1 becomes

$$\begin{aligned} \deg \hat{r} &= \frac{(-1)^m}{\mathrm{vol} S^{p'}} \int_{M \times N'} \det\left(\rho, \frac{\partial x}{\partial t}, \frac{\partial y}{\partial s}\right) \frac{dsdt}{||\rho||^{p'+1}} \\ &= (-1)^m \deg \hat{\rho}, \end{aligned}$$

which is $\mathrm{lk}(M, N')$. □

Appendix D: Thesis Defense Slides

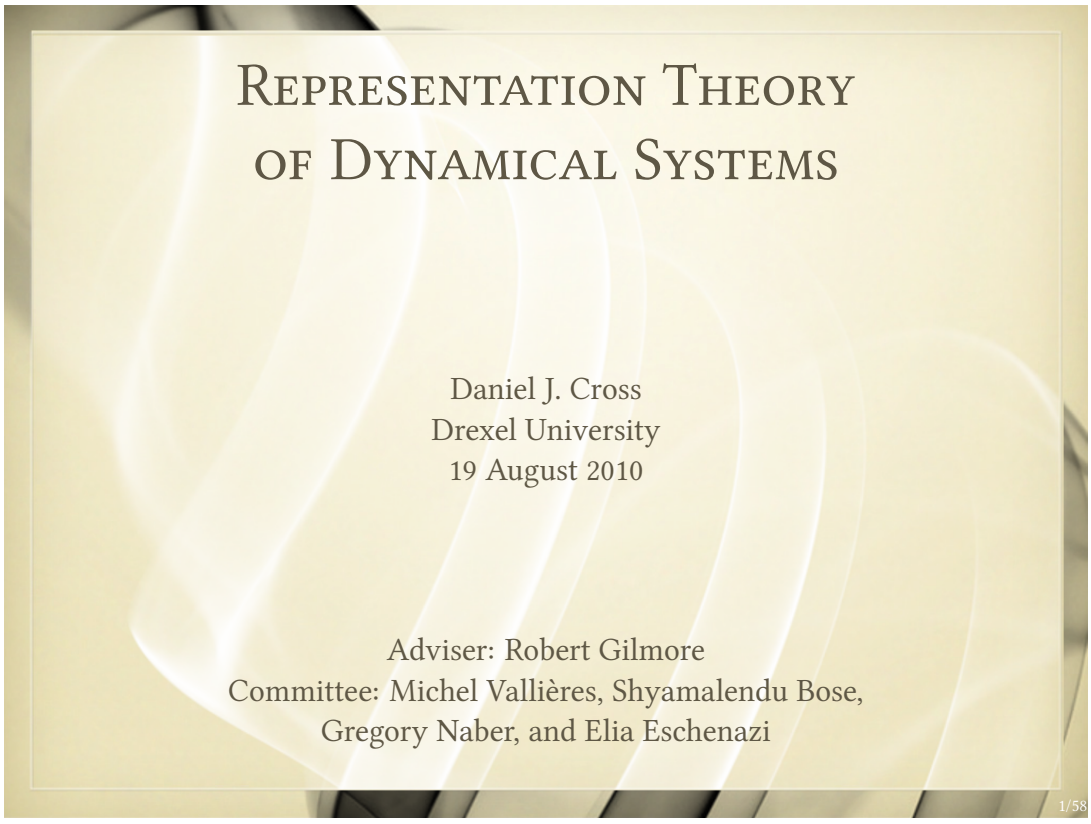

An Experimental Problem

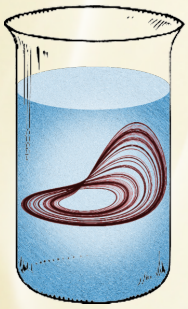

observable

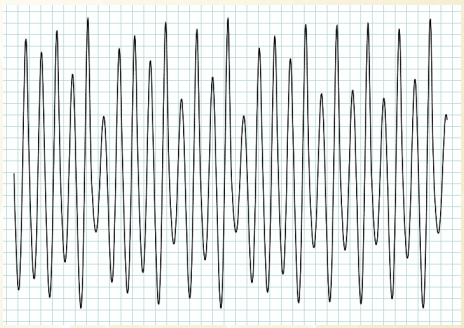

reconstruction

$(x(t), x(t-\tau), x(t-2\tau))$

$(x(t), \dot{x}(t), \ddot{x}(t))$

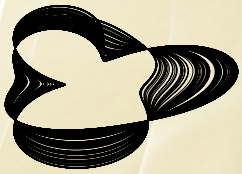

The Questions

"When you perform an analysis on a reconstruction, are you studying the original dynamical system or are you studying the reconstruction?"

(Anonymous) Referee to Bob

i. For any analysis methodology, which results depend on the reconstruction and which are reconstruction independent?

ii. For data taken from a given dynamical system, what is its spectrum of inequivalent reconstructions and how are they distinguished?

iii. As the dimension of the reconstruction increases, do reconstructions remain inequivalent?

The Answers

i. For any analysis methodology, which results depend on the reconstruction and which are reconstruction independent?

Measure	Example	Independent
Geometrical	Fractal Dimensions	Y

Fractal Dimension:

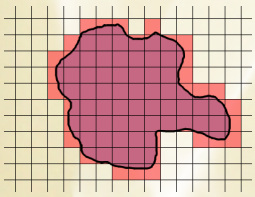

Cover object with ϵ-sized boxes: $N(\epsilon) \sim \left(\frac{1}{\epsilon}\right)^{\dim}$.

Rearranging, $\dim = -\lim_{\epsilon \to 0} \frac{\ln N(\epsilon)}{\ln \epsilon}$.

The Answers

i. For any analysis methodology, which results depend on the reconstruction and which are reconstruction independent?

Measure	Example	Independent
Geometrical	Fractal Dimensions	Y

Fractal Dimension:

Define $\dim = -\lim_{\epsilon \to 0} \frac{\ln N(\epsilon)}{\ln \epsilon}$.

Iteration	$N(\epsilon)$	ϵ
	1	1
	2	1/4
	2^2	$1/4^2$
	2^3	$1/4^3$

$$\dim = -\lim_{n \to \infty} \frac{\ln 2^n}{1/4^n} = \frac{\ln 2}{2 \ln 2} = \frac{1}{2}.$$

The Answers

i. For any analysis methodology, which results depend on the reconstruction and which are reconstruction independent?

Measure	Example	Independent
Geometrical	Fractal Dimensions	Y
Dynamical	Lyapunov Exponents	Y*

Lyapunov Exponents:

$\lambda_1 = 0$

$\lambda_2 > 0$

$\lambda_3 < 0$

$$d(t) \sim e^{\lambda t}$$

The Answers

i. For any analysis methodology, which results depend on the reconstruction and which are reconstruction independent?

Measure	Example	Independent
Geometrical	Fractal Dimensions	Y
Dynamical	Lyapunov Exponents	Y*
Topological	Linking Numbers of UPOs	N

Linking Numbers:

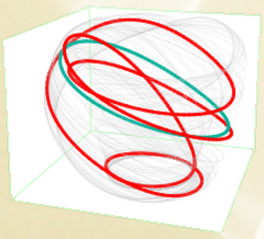

$$\mathrm{lk}(\gamma_1, \gamma_2) = \frac{1}{4\pi} \oint_{\gamma_1} \oint_{\gamma_2} \frac{\gamma_2 - \gamma_1}{||\gamma_2 - \gamma_1||^3} \cdot (d\gamma_1 \times d\gamma_2)$$

The Answers

ii. For data taken from a given dynamical system, what is its spectrum of inequivalent reconstructions and how are they distinguished?

iii. As the dimension of the reconstruction increases, do reconstructions remain inequivalent?

Representation theory …

Representation Theory: The Idea

Regard reconstructions as *representations* of the original dynamics.

Consider two representations equivalent if they are smoothly deformable into each other.

"Topological obstructions" prevent deformations.

Representation Theory: The Program

i. Determine a Euclidean space of minimum dimension in which to reconstruct the system.

ii. Compute the complete set of inequivalent representations (and topological indices) in this space.

iii. Reconstruct in a Euclidean space of one higher dimension. Determine which representations remain inequivalent and which become equivalent because of the additional room available for deformations.

iv. Repeat until all representations become equivalent.

Dynamical Systems

Definition

A **dynamical system** (M, φ) on a manifold M is a flow, $\varphi_t : M \to M$. Equivalently, one may specify the vector field v generating φ_t. In coordinates, $\dot{x} = v(x)$.

Example: The Rössler System

$$\begin{aligned}\dot{x} &= -y - z\\ \dot{y} &= x + ay\\ \dot{z} &= b + z(x - c)\end{aligned}$$

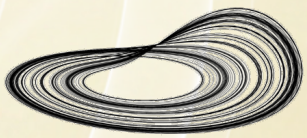

Dynamical Systems

Definition

A **dynamical system** (M, φ) on a manifold M is a flow, $\varphi_t : M \to M$. Equivalently, one may specify the vector field v generating φ_t. In coordinates, $\dot{x} = v(x)$.

Example: The Rössler System

$$\begin{aligned}\dot{x} &= -y - z\\ \dot{y} &= x + ay\\ \dot{z} &= b + z(x - c)\end{aligned}$$

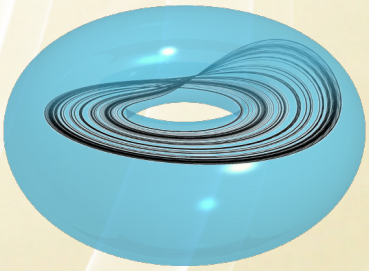

Dynamical Representations

Definition

A **representation** of the dynamical system (M, φ) is an embedding (diffeomorphism) $f : M \to \mathbb{R}^n$ (that preserves the flow):

$$\begin{array}{ccc} M & \xrightarrow{f} & \mathbb{R}^n \\ {\scriptstyle \varphi_t}\downarrow & & \downarrow{\scriptstyle \psi_t} \\ M & \xrightarrow{f} & \mathbb{R}^n. \end{array}$$

Definition

Two representations f_0 and f_1 are **equivalent** if f_1 is isotopic (smoothly deformable) to f_2. That is, if there is a smooth map $F : M \times [0, 1] \to N$ with

- $F_s(x) = F(x, s)$ is an embedding for each fixed s;
- $F_0(x) = f_0(x)$ and $F_1(x) = f_1(x)$.

A Few Good Theorems

Whitney (1936)

Generically, $F : M^n \to \mathbb{R}^N$ is an embedding, $N \geq 2n + 1$.

Takens (1981)

If M has a flow φ, generically it suffices to take $F(x) = f(x), \frac{d}{dt}f(\varphi_t(x)), \frac{d^2}{dt^2}f(\varphi_t(x)), \ldots, \frac{d^{2n}}{dt^{2n}}f(\varphi_t(x)), N \geq 2n + 1$.

Wu (1958)

If $F, G : M^n \to \mathbb{R}^N$ are embeddings, they are isotopic if $N \geq 2n + 1$ $(n > 1)$.

What if $N < 2n + 1$?

10/58

A Few Good Theorems

	Manifolds	Dynamical Systems
Embeddings	Whitney (1936)	Takens (1981)
Isotopy	Wu (1958)	

11/58

Three Dimensional Systems

"Every" three-dimensional dynamical system "lives" inside a genus-g handlebody, M_g:

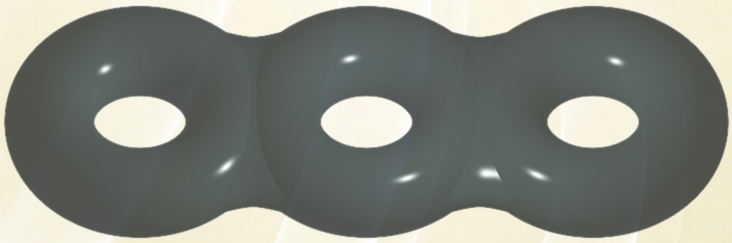

Find embeddings of $M_g \to \mathbb{R}^3, \mathbb{R}^4, \ldots$

Genus One Systems

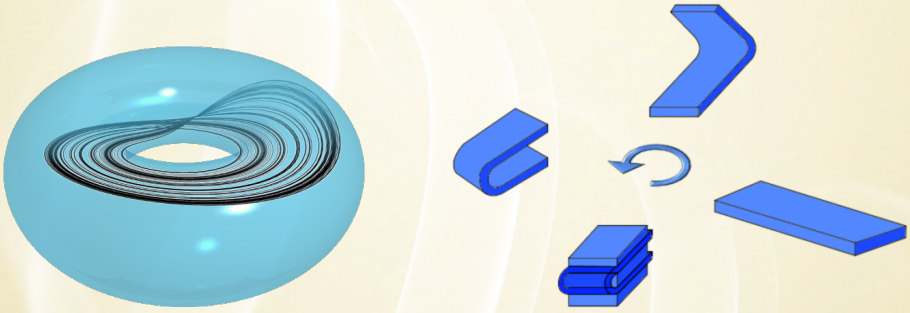

Continuous "stretch and fold" mechanisms.

Solid torus $\mathcal{T} = D^2 \times S^1$ phasespace.

Embeddings of $\mathcal{T} \to \mathbb{R}^3, \mathbb{R}^4, \ldots$

Genus One Representations

Representation Labels	Obstructions to Isotopy				
	$\mathbb{R}^3$	$\mathbb{R}^4$	$\mathbb{R}^5$	$\mathbb{R}^6$	$\mathbb{R}^7$
?	?	?	?	?	-
?	?	?	?	?	-
?	?	?	?	?	-
⋮	⋮	⋮	⋮	⋮	⋮

The Mapping Class Group

Classify diffeomorphisms $\mathcal{T} \to \mathcal{T}$ up to isotopy.

Dehn Twist:

Inversion:

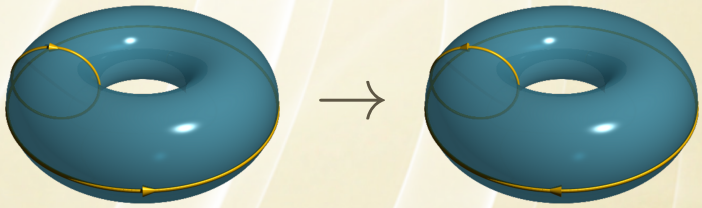

$\mathrm{MCG}(\mathcal{T}) = \mathbb{Z} \oplus \mathbb{Z}_2 \oplus \mathbb{Z}_2$

Genus One: $\mathbb{R}^3$

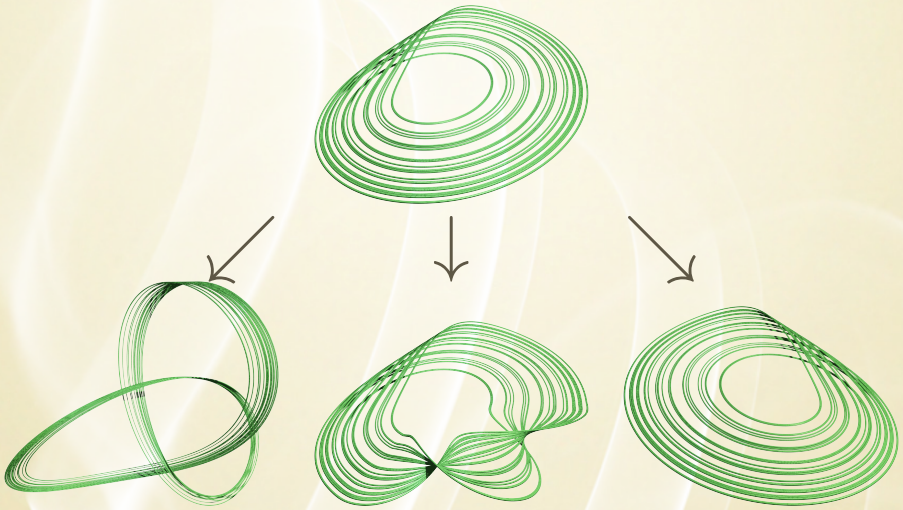

Inversion?

Inversion defined by an isotopy on the trivial embedding.
What about non-trivial knot-types?

If we give K an orientation, then $Inv : K \to -K$, (orientation reversed)
So consider oriented knot-type.

If $K = -K$, K is inversion-symmetric.
'Simplest" inversion-asymmetric knot, 8_{17}:

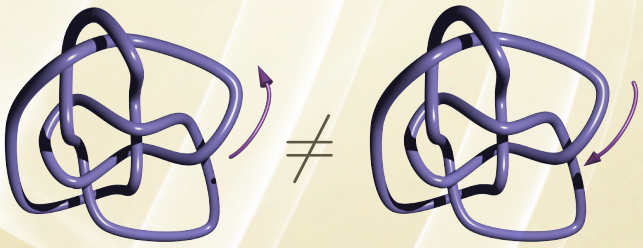

Genus One Representations

Representation	Obstructions to Isotopy				
Labels	$\mathbb{R}^3$	$\mathbb{R}^4$	$\mathbb{R}^5$	$\mathbb{R}^6$	$\mathbb{R}^7$
Global Torsion	$\mathbb{Z}$	?	?	?	-
Parity	$\mathbb{Z}_2$	?	?	?	-
Oriented Knot-Type	$\mathcal{K}$	?	?	?	-

Parity in $\mathbb{R}^4$

Parity becomes trivial:

$$\begin{pmatrix} x^1 \\ x^2 \\ x^3 \end{pmatrix} \xrightarrow{\text{Inject}} \begin{pmatrix} x^1 \\ x^2 \\ x^3 \\ 0 \end{pmatrix} \xrightarrow{\text{Isotopy}} \begin{pmatrix} x^1 \\ x^2 \\ x^3\cos\theta \\ x^3\sin\theta \end{pmatrix} \xrightarrow[\theta=\pi]{\text{Project}} \begin{pmatrix} x^1 \\ x^2 \\ -x^3 \end{pmatrix}$$

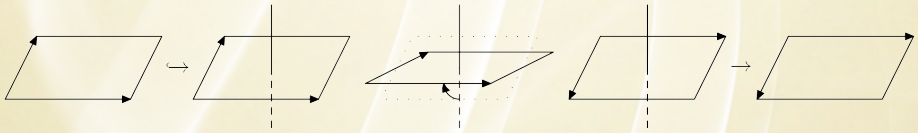

Genus One Representations

Representation	Obstructions to Isotopy				
Labels	$\mathbb{R}^3$	$\mathbb{R}^4$	$\mathbb{R}^5$	$\mathbb{R}^6$	$\mathbb{R}^7$
Global Torsion	$\mathbb{Z}$	?	?	?	-
Parity	$\mathbb{Z}_2$	-	-	-	-
Oriented Knot-Type	$\mathcal{K}$	?	?	?	-

Knot-Type in $\mathbb{R}^4$

Knot-type becomes trivial (x^4 =color):

Any knot may be changed into any other by flipping crossings.

Genus One Representations

Representation	Obstructions to Isotopy				
Labels	$\mathbb{R}^3$	$\mathbb{R}^4$	$\mathbb{R}^5$	$\mathbb{R}^6$	$\mathbb{R}^7$
Global Torsion	$\mathbb{Z}$	?	?	?	-
Parity	$\mathbb{Z}_2$	-	-	-	-
Oriented Knot-Type	$\mathcal{K}$	-	-	-	-

Global Torsion in $\mathbb{R}^3$ (Again)

Consider how to detect global torsion in $\mathbb{R}^3$:

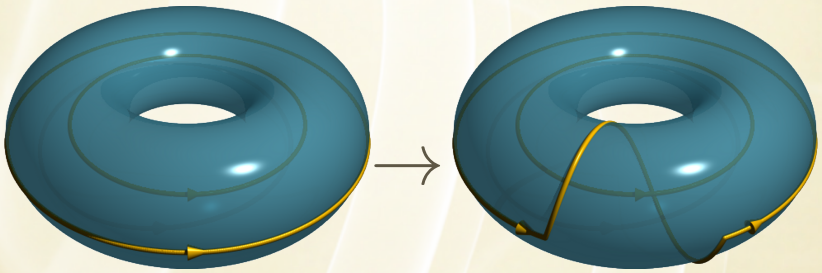

Twists change the linking number of these two curves.

But curves don't link in $\mathbb{R}^4 \rightarrow$ no global torsion?

Global Torsion in $\mathbb{R}^3$ (Again)

Frame (t, u, v) along torus core:

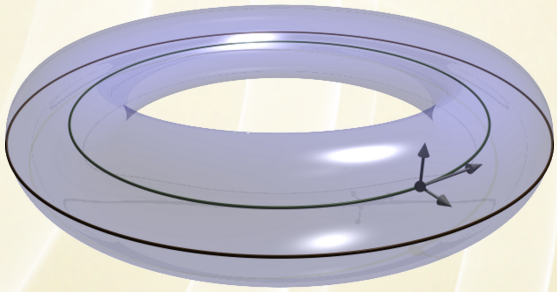

t is tangent, u point toward the longitude, and $v = u \times t$.

As we go along core, the pair (u, v) determines a sequence of frames of $\mathbb{R}^2$, or a sequence of rotations. This determines a closed loop in $SO(2)$.

Global Torsion in $\mathbb{R}^3$ (Again)

Smooth deformations of the embedding $\rightarrow$ smooth deformations of the loop.

The set of all loops in a space M up to deformation is the fundamental group $\pi_1 M$.

$\pi_1 SO(2) = \mathbb{Z} \leftrightarrow$ global torsion in $\mathbb{R}^3$.

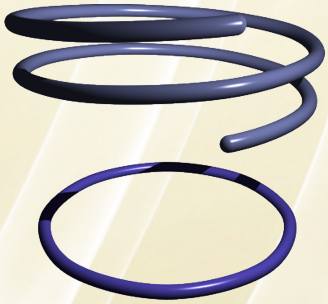

Global Torsion in $\mathbb{R}^4$

Frame (t, u, v, w) along core.

As we go along core, the triple (u, v, w) determines a sequence of frames of $\mathbb{R}^3$, or a sequence of rotations. This determines a closed loop in $SO(3)$.

Smooth deformations of the embedding $\rightarrow$ smooth deformations of the loop.

$\pi_1 SO(3) = \mathbb{Z}_2 \leftrightarrow$ global torsion in $\mathbb{R}^4$.

Genus One Representations

Representation	Obstructions to Isotopy				
Labels	$\mathbb{R}^3$	$\mathbb{R}^4$	$\mathbb{R}^5$	$\mathbb{R}^6$	$\mathbb{R}^7$
Global Torsion	$\mathbb{Z}$	$\mathbb{Z}_2$	?	?	-
Parity	$\mathbb{Z}_2$	-	-	-	-
Oriented Knot-Type	$\mathcal{K}$	-	-	-	-

Global Torsion in $\mathbb{R}^5$

Parametrize $\mathcal{T} = S^1 \times D^2$ by $(s, re^{i\phi})$.

If $s \in S^1$, twist: $z \to ze^{is}$.

Embed in $S^1 \times D^4 \subset \mathbb{R}^5$

$$\begin{pmatrix} s \\ re^{i\phi} \end{pmatrix} \mapsto \begin{pmatrix} s \\ re^{i\phi} \\ re^{i(\phi+s)} \end{pmatrix}$$

Define the isotopy by

$$\left(\begin{array}{c|cc} 1 & 0 & \\ \hline 0 & \cos\theta & \sin\theta \\ & -\sin\theta & \cos\theta \end{array}\right) \begin{pmatrix} s \\ re^{i\phi} \\ re^{i(\phi+s)} \end{pmatrix},$$

which exchanges the two complex factors between $\theta = 0$ and $\theta = \pi/2$.

Genus One: Summary

Complete representations for genus one, $D^2 \times S^1$.

Representation	Obstructions to Isotopy		
Labels	$\mathbb{R}^3$	$\mathbb{R}^4$	$\mathbb{R}^5$
Global Torsion	$\mathbb{Z}$	$\mathbb{Z}_2$	-
Parity	$\mathbb{Z}_2$	-	-
Oriented Knot-Type	$\mathcal{K}$	-	-

Phys. Rev. E, **80**, 056207 (2009).

Higher Genus Systems

Lorenz System:

$$\dot{x} = \sigma(y - x)$$
$$\dot{y} = x(R - z) - y$$
$$\dot{z} = xy - \beta z$$

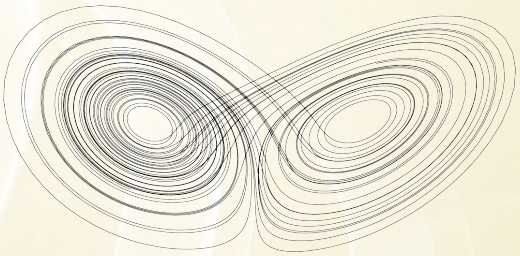

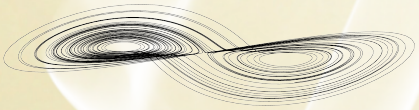

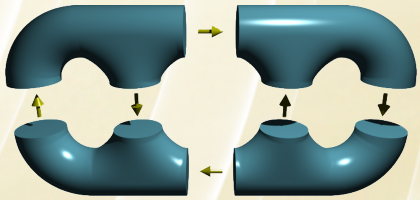

30/58

Trinions, Dreibeins, and Graphs

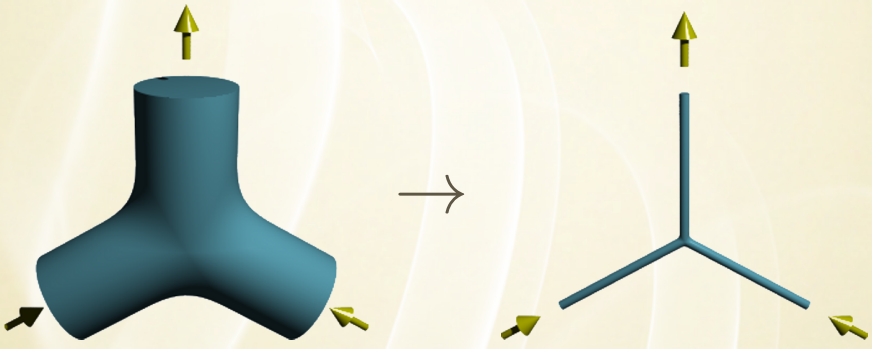

Graph Embeddings:

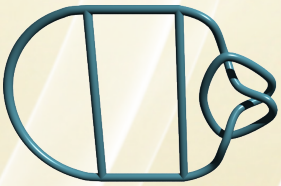

31/58

Local Torsion

A genus-g handlebody decomposes into $2(g-1)$ trinions:

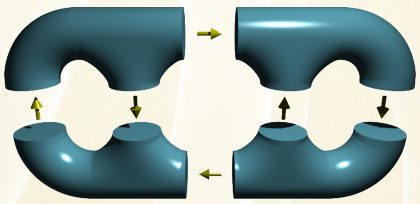

Add a twist on each "port" of the trinion $\rightarrow 6(g-1)$ twists.

Ports identified pairwise $\rightarrow 3(g-1)$ twists.

$\mathbb{Z}^{3(g-1)} \leftrightarrow$ local torsion in $\mathbb{R}^3$.

32/58

Higher Genus Representations

Representation	Obstructions to Isotopy		
Labels	$\mathbb{R}^3$	$\mathbb{R}^4$	$\mathbb{R}^5$
Local Torsion	$\mathbb{Z}^{3(g-1)}$	?	?
Parity	$\mathbb{Z}_2$	?	?
Oriented "Knot"-Type	$\mathcal{K}_g$	?	?

33/58

Representations in $\mathbb{R}^4$

Parity becomes trivial as before.

Graph "knots" become trivial as before.

Local Torsion reduced $\mathbb{Z} \to \mathbb{Z}_2$ as before, but . . .

Local Torsion in $\mathbb{R}^4$

Twist exchange:

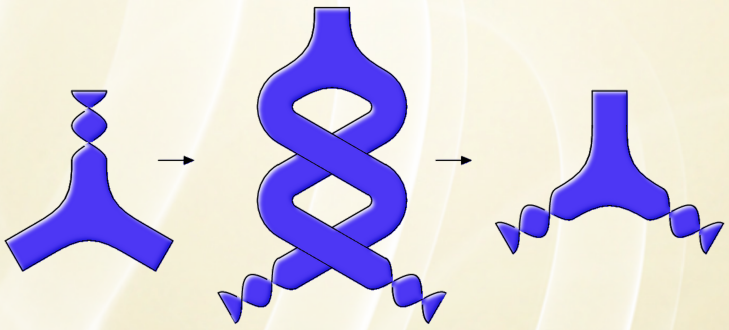

So. One twist is redundant: $\mathbb{Z}^3 \to \mathbb{Z}^2$.

Thus $\mathbb{Z}^{3(g-1)} \to \mathbb{Z}_2^{2(g-1)}$.

Higher Genus Representations

Representation	Obstructions to Isotopy		
Labels	$\mathbb{R}^3$	$\mathbb{R}^4$	$\mathbb{R}^5$
Local Torsion	$\mathbb{Z}^{3(g-1)}$	$\mathbb{Z}_2^{2(g-1)}$	?
Parity	$\mathbb{Z}_2$	-	-
Oriented "Knot"-Type	$\mathcal{K}_g$	-	-

Local Torsion in $\mathbb{R}^5$

Remaining twists become trivial as before.

All embeddings isotopic.

Higher Genus Systems: Summary

Complete representations for genus-g.

Representation	Obstructions to Isotopy		
Labels	$\mathbb{R}^3$	$\mathbb{R}^4$	$\mathbb{R}^5$
Local Torsion	$\mathbb{Z}^{3(g-1)}$	$\mathbb{Z}_2^{2(g-1)}$	-
Parity	$\mathbb{Z}_2$	-	-
Oriented "Knot"-Type	$\mathcal{K}_g$	-	-

Phys. Rev. E, (submitted).

38/58

Interim Summary

"When you perform an analysis on a reconstruction, are you studying the original dynamical system or are you studying the reconstruction?"

Until now, a framework for answering this questions did not exist.

I have addressed it by introducing a Representation Theory for Dynamical Systems.

Based on the topological theory for three dimensional systems, I have completely worked out this theory for these systems.

When performing an analysis of data from three-dimensional systems, we know what depends on the physical mechanism and what depends on the reconstruction (knot-type, torsion, parity).

39/58

Extensions

i. Representations of the Lorenz System.

ii. Pushing into higher dimensions.

Lorenz

Perform a differential "embedding" of the Lorenz system using $x(t)$:

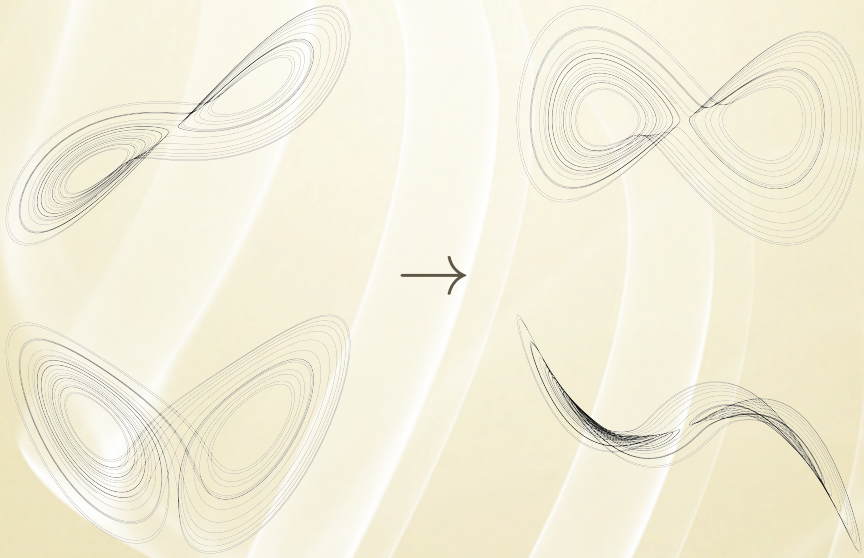

Branched Manifolds

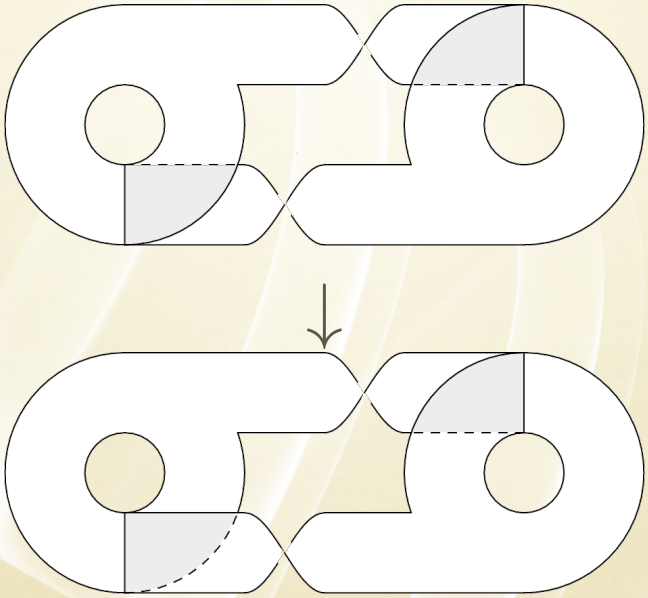

Differential Mapping into $\mathbb{R}^3$

$$F_3 = \begin{pmatrix} X \\ Y \\ Z \end{pmatrix} = \begin{pmatrix} x \\ \sigma(y-x) \\ \sigma(R+\sigma-z)x - \sigma(1+\sigma)y \end{pmatrix}$$

This mapping is singular on yz-plane:

$$F_3(0,y,z) = \begin{pmatrix} 0 \\ \sigma y \\ -\sigma(1+\sigma)y \end{pmatrix}$$

This plane cuts the attractor, so is not an embedding into $\mathbb{R}^3$.

Differential Mappings into $\mathbb{R}^4$

$$F_4 = \begin{pmatrix} X \\ Y \\ Z \\ W \end{pmatrix} = \begin{pmatrix} x \\ \sigma(y-x) \\ \sigma(R+\sigma-z)x - \sigma(1+\sigma)y \\ \sigma z(Ax - \sigma y) + \sigma y(B - x^2) - \sigma Cx \end{pmatrix}$$

where $A = 1 + b + 2\sigma$, $B = \sigma(R + \sigma + 1) + 1$, and $C = R + 2R\sigma + \sigma^2$.

F_4 is not singular and provides an embedding into $\mathbb{R}^4$.

Moreover, this embedding is isotopic to the standard one.

We conclude that F_3 is a "bad" projection of F_4 into $\mathbb{R}^3$.

Local Reflection

$$F : (x, y, z) \mapsto \left(x, y, \frac{-xz}{\sqrt{1+x^2}}, \frac{z}{\sqrt{1+x^2}} \right).$$

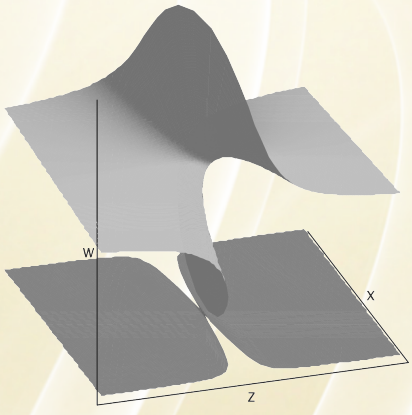

Lorenz: Conclusion

Representation theory shows that the standard "differential embedding" of the Lorenz system into $\mathbb{R}^3$ cannot actually be an embedding.

However, the differential mapping F_4 embeds the Lorenz system into $\mathbb{R}^4$.

This embeddings is the trivial representation, though "twisted".

The mapping F_3 is a singular projection of this twisted embedding into $\mathbb{R}^3$.

Phys. Rev. E, **81**, 066220 (2010).

46/58

Towards Higher Dimensions

Solid n-torus: $\mathcal{T}^n = D^n \times S^1$.

Problem: find $\mathrm{MCG}(\mathcal{T}^n)$.

Dehn Twist:

Inversion:

47/58

Mapping Class Group

If smoothness is dropped, then $\mathrm{MCG}(\mathcal{T}^n) = \pi_1 SO(n) \oplus \mathbb{Z}_2 \oplus \mathbb{Z}_2$.

A "Dehn twist" yields a loop in $SO(n)$ (amount of rotation along S^1).

$\pi_1 SO(2) = \mathbb{Z}$ and $\pi_1 SO(n) = \mathbb{Z}_2$ for $n > 2$.

Smooth case = ?

Smooth Mapping Class Group

The problem is Alexander's Lemmas:

Lemma 1: Any homeomorphism $f : S^n \to S^n$ extends to a homeomorphism $F : D^n \to D^n$.

$$F(rx) = rf(x)$$

Lemma 2: Any homeomorphism $f : D^n \to D^n$ which is the identity on S^n is isotopic to the identity on all of D^n.

$$h_t(x) = \begin{cases} tf(x/t) & 0 \leq ||x|| < t \\ x & t \leq ||x|| \leq 1 \end{cases}.$$

Problem: these are not smooth procedures!

Twisted Spheres

Construct a sphere Σ by glue disks along their boundaries.

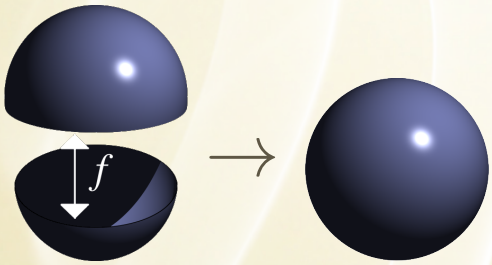

$\Sigma \cong S^n$ iff f extends over D^n.

n	1	2	3	4	5	6	7	8	9	10	11	12	13	14	15	16	17	18
$\lvert A_n \rvert$	1	1	1	?	1	1	28	2	8	6	992	1	3	2	16256	2	16	16

Working Around

Solution: Determine spectrum of embeddings directly.

$\mathcal{T}^n = D^n \times S^1 \to \mathbb{R}^{n+1+c}$, $c = 0, 1, 2, \ldots$

$\mathcal{T}^n$ is a "thickened" circle or knot.

If $n \geq 3$ then $n + 1 \geq 4$ and no non-trivial knot-type.

Parity ($\mathbb{Z}_2$) only in $\mathbb{R}^{n+1}$ ($c = 0$).

Global Torsion in $\mathbb{R}^{n+1}$ and $\mathbb{R}^{n+2}$

Determine twisting by "frames long the core" as for $\mathcal{T}^2$.

$\mathbb{R}^{n+1} \to \pi_1 SO(n) \cong \mathbb{Z}_2$.

$\mathbb{R}^{n+2} \to \pi_1 SO(n+1) \cong \mathbb{Z}_2$.

Global Torsion in $\mathbb{R}^{n+3}$

Write x in "polar" form $x = ru$ and use hyperspherical coordinates

$$u_k = \sin\phi_1 \cdots \sin\phi_{k-1} \cos\phi_k$$
$$z = u_{n-1} + iu_n = \sin\phi_1 \cdots \sin\phi_{n-2} e^{i\theta}.$$

If $s \in S^1$, twist: $z \to ze^{is}$.

$$\begin{pmatrix} s \\ ru \\ rz \end{pmatrix} \mapsto \begin{pmatrix} s \\ ru \\ rz \\ rze^{is} \end{pmatrix} \to \left(\begin{array}{c|cc} 1 & 0 & \\ \hline 0 & \cos t & \sin t \\ & -\sin t & \cos t \end{array}\right) \begin{pmatrix} s \\ ru \\ rz \\ rze^{is} \end{pmatrix},$$

which exchanges the two complex factors between $t = 0$ and $t = \pi/2$.

Higher Dimensions: Summary

Complete representations of $\mathcal{T}^n = D^n \times S^1$.

Representation	Obstructions to Isotopy		
Labels	$\mathbb{R}^{n+1}$	$\mathbb{R}^{n+2}$	$\mathbb{R}^{n+3}$
Global Torsion	$\mathbb{Z}_2$	$\mathbb{Z}_2$	-
Parity	$\mathbb{Z}_2$	-	-
Oriented Knot-Type	-	-	-

Conclusions

The analysis of data from complex dynamical systems relies on reconstructions of the original phase space.

Methods of analysis may in principle depend on the choice of reconstruction.

We have introduced a representation theory to classify these reconstructions.

This representation theory has been worked out for three-dimensional dynamical systems and a class of higher dimensional systems.

Outlook

A topological understanding of dynamical systems exists in three dimensions.

Representation theory provides a capstone to this theory.

A topological understanding of dynamical systems in higher dimensions is lacking.

Representation theory provides a cornerstone on which to build this theory.

This will lead to a better understanding of the phasespace mechanisms that generate chaos and ultimately to a better understanding of the underlying physics.

Fin

Vita

Daniel James Cross was born in Long Beach, California, on 10 March 1980. From 1998 to 2002 he attended Cedarville University in Cedarville, Ohio, graduating *cum laude* with a *scientiarum baccalaureus* in mathematics and a *artium baccalaureus* in physics. In September of 2002 he began his graduate studies at Drexel University in Philadelphia, Pennsylvania. He obtained his *scientiarum magister* in physics in 2005, and he completed his *philosophiae doctor* in physics in 2010 under the direction of Robert Gilmore.

His publications during his graduate student tenure include:

1. *Representation Theory for Strange Attractors*, with R. Gilmore, Phys. Rev. E, **80**, 056207 (2009).
2. *Representations of Dynamical Systems*, with R. Gilmore, IEEE ICCSA Proceedings, Le Havre, France (2009).
3. *A Biological Algorithm for Data Reconstruction*, with Ryan Michaluk and R. Gilmore, Phys. Rev. E, **81**, 036217 (2010).
4. *Concerning the Differential Embedding of the Lorenz Attractor*, with R. Gilmore, Phys. Rev. E, **81**, 066220 (2010).
5. *A Schwinger Disentangling Theorem*, with R. Gilmore, J. Math. Phys, (to appear).
6. *Equivariant Differential Embeddings*, with R. Gilmore, J. Math. Phys, (to appear).
7. *Complete Set of Representations for Three Dimensional Dynamical Systems*, with R. Gilmore, Phys. Rev. E, (submitted).
8. *Comments on the Cooperstock-Tieu Galaxy Model*, astro-ph/0601191 (2006).

His Erdős Number is three.

Soli Deo Gloria